BIOMECHANICS OF THE UPPER LIMB: APPLICATIONS OF MOTION ANALYSIS AND FORCE MEASUREMENT TECHNIQUES

EDWARD K. J. CHADWICK, BEng (Hons)

This thesis is presented in partial fulfilment of the requirements for the degree of Doctor of Philosophy from the Bioengineering Unit, University of Strathclyde, Glasgow, January 1999.

ACKNOWLEDGEMENTS

My sincerest thanks go to the following people:

Professor Barbenel for providing the opportunity to study in the Bioengineering Unit;
The Medical Research Council, the Scottish Office and various police authorities for funding the work;
Sandy Nicol for his thorough supervision and support;
Judith Lane and Sheryl Goldie for their invaluable help with testing and data processing;
Luigi Lucchetti for his contribution to the experimental protocol;
Robert Hay, Davie Robb, Willie Tierney, Stevie Miller and John Wilson from the mechanical workshop;
John Maclean and Stan Floyd from the electronics workshop;
All other staff and students who have given their time and skill;
My friends and family for their support and encouragement.

ABSTRACT

Two studies involving different applications of motion analysis and force measurement techniques are presented. The first study provides data on typical loads on the upper limb, and the muscle and joint forces which oppose them. The second presents parameters defining the biomechanics of knife stab attacks in order to specify standards for the testing of stab resistant body armour.

A three dimensional, mathematical model of the elbow and wrist joints, including 15 muscle units, 3 ligaments and 4 joint forces, has been developed. A new strain gauge transducer has been developed to measure functional grip forces. The device measures radial forces divided into six components and forces of up to 250N per segment can be measured with an accuracy of ±1%. Ten normal volunteers from within the Bioengineering Unit were asked to complete four tasks representing occupational activities, during which time their grip force was monitored. Together with kinematic information from the six-camera Vicon data, the moment effect of these loads at the joints was calculated. These external moments are assumed to be balanced by the internal moments, generated by the muscles, passive soft tissue and bone contact. The effectiveness of the body's internal structures in generating joint moments was assessed by studying the geometry of a simplified model of the structures, where information about the lines of action and moment arms of muscles, tendons and ligaments is contained. The assumption of equilibrium between these external and internal joint moments allows formulation of a set of equations from which muscle and joint forces can be calculated. A two stage, linear optimisation routine minimising the overall muscle stress and the sum of the joint forces has been used to overcome the force sharing problem. Humero-ulnar forces of up to 1600N, humero-radial forces of up to 800N and wrist joint forces of up to 2800N were found for moderate level activity. The model was validated by comparison with other studies.

A wide range of parameters defining the biomechanics of knife stab attacks has been measured in order to specify standards for the testing of stab resistant body armour. Stab styles based on reported incidents provided more realistic data than had previously existed. A six camera Vicon motion analysis system and specially developed force measuring knife were used to measure the parameters. Twenty volunteers were asked to stab a target with near maximal effort. Three styles of stab were used: a short thrust forward, a horizontal style sweep around the body and an overhand stab. The body holding the knife was modelled as a series of rigid segments: trunk, upper arm, forearm and hand, and knife. The calculation of the velocities of these segments, and knowledge of the mass distribution from biomechanical tables, allowed the calculation of the segment energy and momentum values. The knife measured four components of load: axial force (along the length of the blade), cutting force (parallel to the breadth of the blade), lateral force (across the blade) and torque (twisting action) using foil strain gauges. The 95th percentile values for axial force and energy were 1885N and 69J respectively.

TABLE OF ABBREVIATIONS

Abbreviation	Full Name
FPL	Flexor pollicis longus
FDS	Flexor digitorum superficialis
FDP	Flexor digitorum profundus
FCR	Flexor carpi radialis
FCU	Flexor carpi ulnaris
ECU	Extensor carpi ulnaris
ECRB	Extensor carpi radialis brevis
ECRL	Extensor carpi radialis longus
BIC	Biceps brachii
BRA	Brachialis
BRD	Brachioradialis
PRT	Pronator teres
TRI	Triceps brachii
ANC	Anconeus
PRQ	Pronator quadratus
SUP	Supinator
MCLA	Medial collateral ligament (anterior band)
MCLP	Medial collateral ligament (posterior band)
LCL	Lateral collateral ligament
JLAT	Lateral trochlear joint force
JMED	Medial trochlear joint force
JR	Radial head joint force
JW	Wrist joint force

CONTENTS

PART A

CALCULATION OF ELBOW AND WRIST JOINT FORCES DURING OCCUPATIONAL ACTIVITIES

PART B

INVESTIGATION OF KNIFE STAB CHARACTERISTICS

PART A

BIOMECHANICS OF THE UPPER LIMB: CALCULATION OF ELBOW AND WRIST JOINT FORCES DURING OCCUPATIONAL ACTIVITIES

CHAPTER 1 INTRODUCTION

1.1 BACKGROUND

The early 1980s saw a steep rise in the number of cases of work related upper limb disorders (WRULD) coming before the Australian courts. The term repetitive strain injury was at that time applied to the conditions, but was felt by many to be unhelpful as it pointed to a discernible biological pathology or lesion, which was not always seen. The conditions described by this term covered a broad range, including not only the diffuse pain syndrome for which no pathology could be identified, but also tendonitis, tenosynovitis and carpal tunnel syndrome (Quintner (1991), Barker (1995)). Other terms avoiding reference to specific pathology have been used since then, including cumulative trauma disorder (CTD) and occupational overuse syndrome (OOS). The former of these has been favoured as it declines to associate the syndrome with occupational factors, thereby reducing the number of worker compensation claims (Brooks (1993)).

The incidence of CTD has a high social and economic cost, with it now accounting for 56% of all occupational injuries in the United States (Melhorn (1998)) and yet little is known about the aetiology of the disorders. Some authors claim that no association between arm pain and type of work has been shown (Brooks (1993)), that psychosocial factors are paramount (Ireland (1998)) and that concurrent diseases such as diabetes mellitus and hypothyroidism are causative factors (Atcheson *et. al.* (1998)). These authors make a definite distinction between easily identifiable pathologies and diffuse pain syndromes.

A number of studies have been conducted, however, examining the link between occupational tasks and CTD. Several risk factors have been identified by these studies, including repetition, poor posture, insufficient recovery periods and high force (Bacis *et. al.* (1996), Occhipinti and Colombini (1996)) and prolonged muscle fibre activity (Sjogaard and Sjogaard (1998)).

1.2 BIOMECHANICAL ANALYSES

A comprehensive analysis of the effect of work activity on the structures of the upper limb would be a valuable source in the understanding of upper limb disorders. A number of models of the upper limb reporting forces in the structures can be found in the literature. Models of the elbow joint have been reported by An *et. al.* (1984), Amis (1978), Nicol (1977), Seireg and Arvikar (1989) and others, with varying degrees of complexity. There have also been models of the wrist joint, though these are fewer, including those of Buchanan *et. al.* (1992) and Seireg and Arvikar (1989). Many of these types of models have been limited by their simplicity, being either non-three dimensional or with inclusion of too few muscle units. In addition to a valid model, to produce useful data one must also have realistic input data. There is a lack of analyses in the literature where occupational tasks have been studied to provide input data for the models. In many cases, unloaded motions have been studied in the form of activities of daily living, and in other cases simple planar movements have been examined.

1.3 OBJECTIVES

The objective of the current study is to develop a mathematical model of the elbow and wrist joints, which may be used to predict the contact forces in the joints and the forces in the muscles and ligaments which control their motion. A biomechanical analysis of occupational lifting motions, including the measurement of grip force, will be undertaken in order to provide the model with realistic input data. The forces in the structures during these activities, calculated by the model, will be presented and discussed.

CHAPTER 2 STAGES IN THE DEVELOPMENT OF A MODEL

2.1 JOINT MODELLING OVERVIEW

Joint modelling may best be described as the application of mathematical modelling techniques to the analysis of the loads on the structures of the human body and the body's response. This study provides data on typical loads on the upper limb, the muscle forces that oppose them, and the effect these actions have on the joints of the elbow and wrist.

In order for the model to be useful, a realistic estimate is needed of the values of the loads to which the body is exposed; hence this study uses, as input to the model, directly measured loads encountered during simulated occupational activities. Together with kinematic information from video analysis, the moment effect of these loads at the joints can be calculated.

These so-called external moments are assumed to be balanced by the internal moments, generated by the muscles, passive soft tissue and bone contact, in the application of Newton's Laws. The effectiveness of the body's internal structures in generating joint moments can be assessed by studying the geometry of a simplified model of the structures, where information about the lines of action and moment arms of muscles, tendons and ligaments is contained; this is referred to as an anatomical model.

The assumption of equilibrium between these external and internal joint moments allows formulation of a set of equations from which muscle and joint forces can be calculated. The number of unknown quantities contained in this model far exceeds the number of independent equations relating them, making the solution indeterminate. This has been overcome with linear optimisation using the Simplex algorithm.

One of the most important aspects of joint modelling is validation of the model. Currently, *in vivo* measurements of upper limb joint contact forces or muscle forces are not feasible and so other methods of validation must be sought, such as the use of electromyography (EMG) and, simply, comparison with other studies.

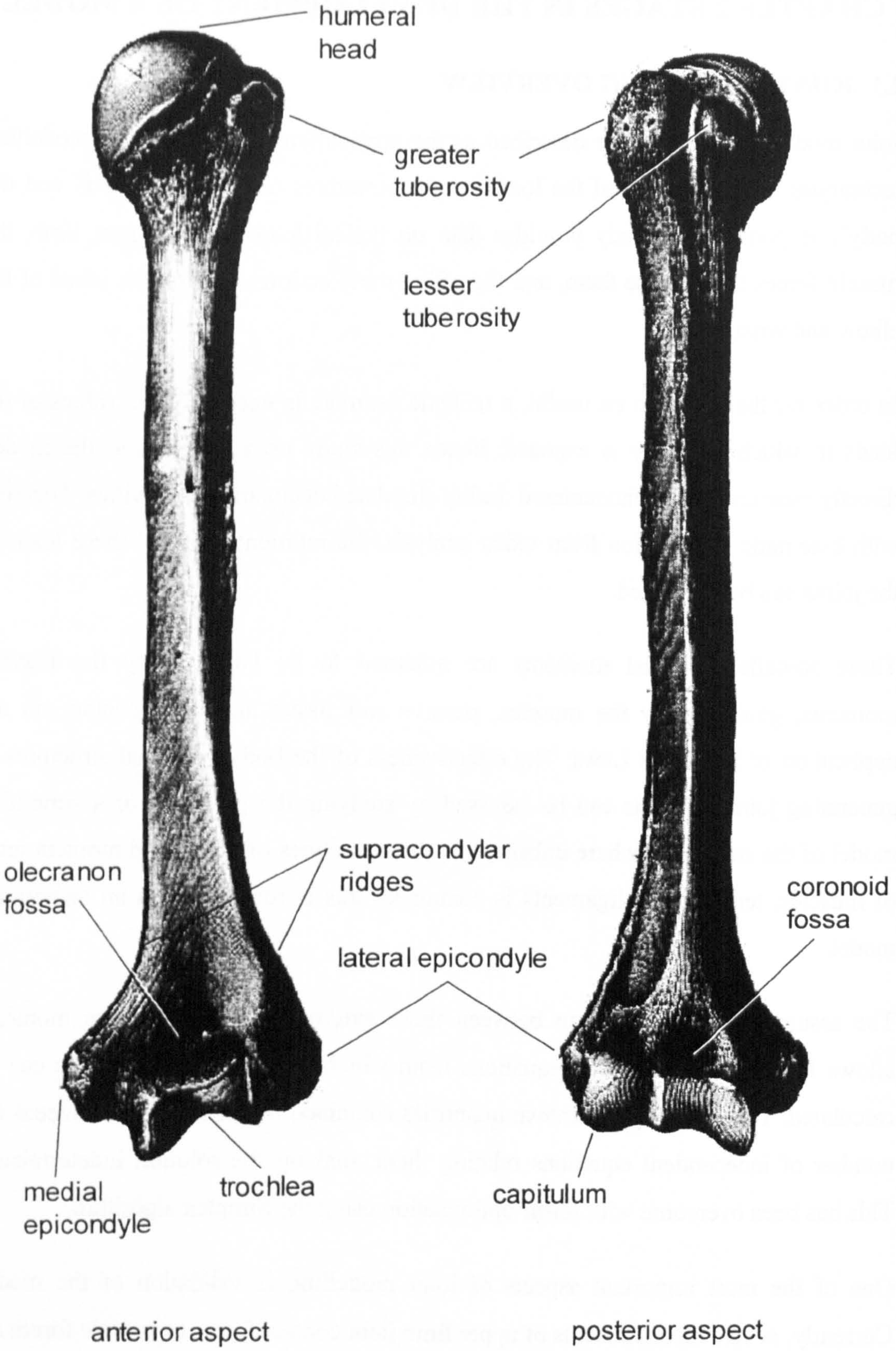

Figure 2.1 Anatomy of the humerus (adapted from Wheeless (1996)).

2.2 KINEMATICS

2.2.1 TECHNIQUES FOR DESCRIPTION

2.2.1.1 Bony anatomy

To define fully the elbow and wrist joint kinematics using bone-embedded axis systems, some description of the bones involved must be given. The elbow joint complex involves three bone articulations: the humero-ulnar, humero-radial and proximal radio-ulnar joints. Similarly, the wrist joint involves the radio-carpal, ulno-carpal and distal radio-ulnar joints. A brief guide to the anatomy of the articulating bones is presented below. As some of the muscles used in the model originate from the bones of the shoulder other than the humerus, some detail of the shoulder joint will be given.

The long bone forming the upper arm is the **humerus**, its proximal end forming the humeral part of the shoulder joint and its distal end articulating with the radius and ulna to form the elbow joint. The head of the humerus is directed proximally, posteriorly and medially and is part spherical. Below the head are the *greater* and *lesser tuberosities*, which serve as sites for muscle attachment. The lesser tuberosity projects anteriorly and the greater antero-laterally. At the distal end the shaft widens to form the *epicondyles*, above which are the *supracondylar ridges*, and the articulating surfaces of the *trochlea* and *capitulum*. The trochlea is the 'bobbin' shaped surface which forms the medial part of the joint and articulates with the ulna. The capitulum is partially spherical to articulate with the dished proximal end of the radius and lies lateral to the trochlea. Above the trochlea are the *coronoid fossa* anteriorly and the *olecranon fossa* posteriorly which receive the coronoid process of the ulna in full flexion and the olecranon process in full extension respectively. The bone with its main features is shown in Figure 2.1.

Distal to the elbow joint, the ulna and radius are the bones of the forearm. The **ulna** is the medial of the two (in the anatomical position) and has an articulating surface that fits that of the trochlea on the humerus at its proximal end. Two prominent features seen in Figure 2.2 are the *coronoid process* and the *olecranon process*. On the lateral side of the coronoid process is seen the *radial notch*, in which the head of the radius

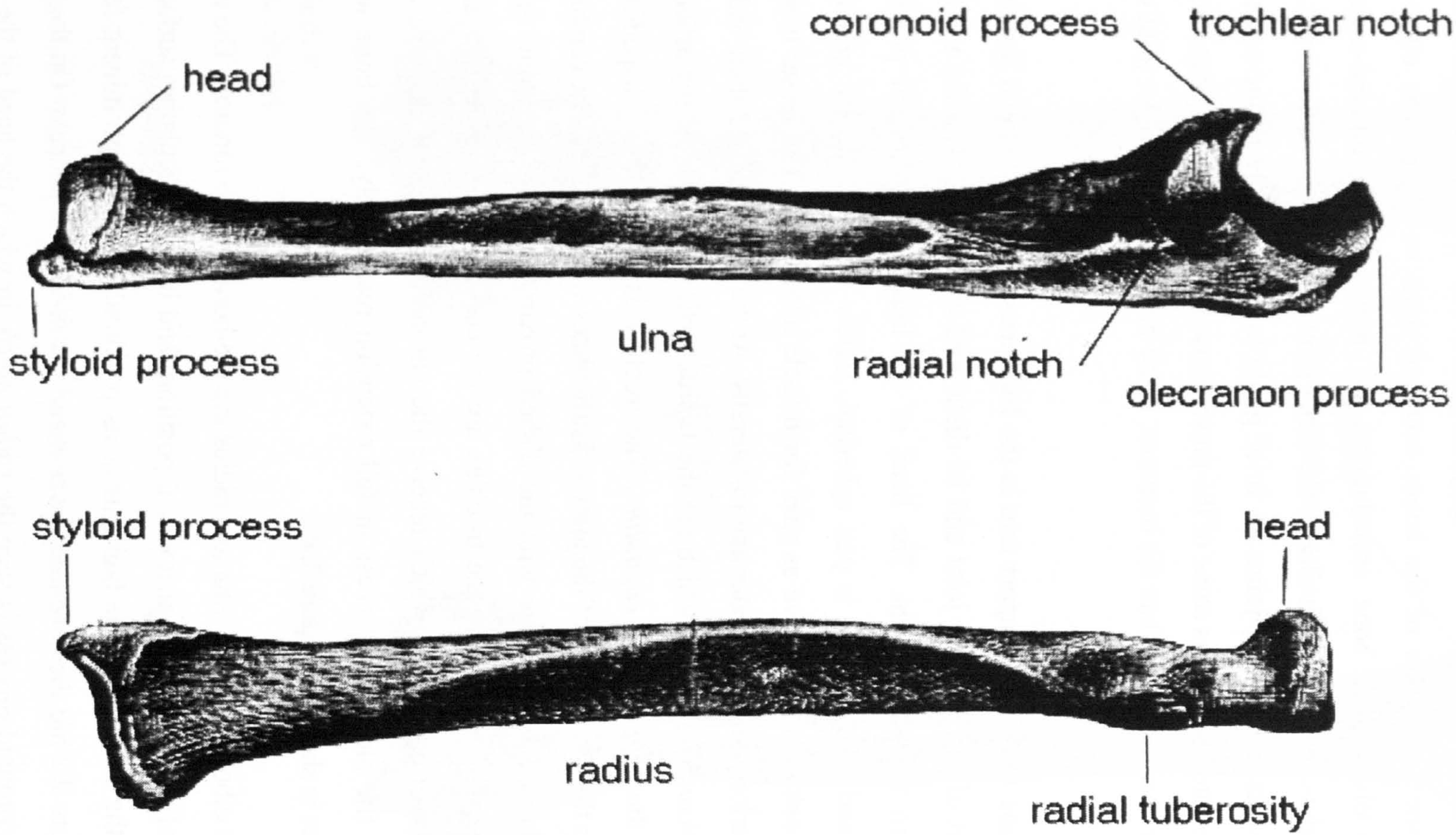

Figure 2.2 Anatomy of the radius and ulna. (Adapted from Wheeless (1996))

rotates. At the distal end the ulnar shaft widens into the ulnar head, around which the distal radius rotates, with the styloid process being the most distal part.

The **radius** lies lateral to the ulna, and rotates around it during pronation and supination. Proximally, the head of the radius is dished to receive the capitulum of the humerus, narrowing into a shaft distally. At the distal end, the shaft widens again into the styloid process as the most distal point. The end is concave and articulates with the carpal bones of the wrist. The medial border of the distal radius articulates with ulna in the distal radio-ulnar joint. The radius is also shown in Figure 2.2.

The distal radius and ulna articulate with proximal row of **carpal** bones. The wrist joint consists of eight bones, whose movement is subject to discussion. Anatomically, they are arranged in two rows of four: scaphoid, lunate, triquetrum and pisiform proximally and trapezium, trapezoid, capitate and hamate distally. This is shown in Figure 2.3. Functionally, they are not always considered in two rows, but moving in a columnar arrangement. Navarro first proposed the idea of a columnar carpus in 1919 (Taleisnik (1976) and Sennwald (1987)); this view was modified by Taleisnik (1976) to consist of a central column comprising the lunate and distal carpal row, a medial column comprising the triquetrum and a lateral column consisting of the scaphoid. The pisiform is not considered functionally to be part of the carpus but as a sesamoid bone in the tendon of flexor carpi ulnaris. The detailed study of carpal bone motion is outwith the scope of this study and only the interaction of the proximal row with the radius and ulna will be considered.

Returning to the shoulder joint, the part spherical humeral head articulates with the *glenoid fossa* of the **scapula**, the wing shaped bone of the shoulder complex, forming a ball-and-socket joint. There is a prominent projection arising from the antero-lateral border of the scapula above the gleno-humeral joint known as the *acromion process*, which will be used in axis definition. The *spine of the scapula* is what forms the 'shoulder blade'. The bone running from the sternum to the scapula is the **clavicle**, or collarbone.

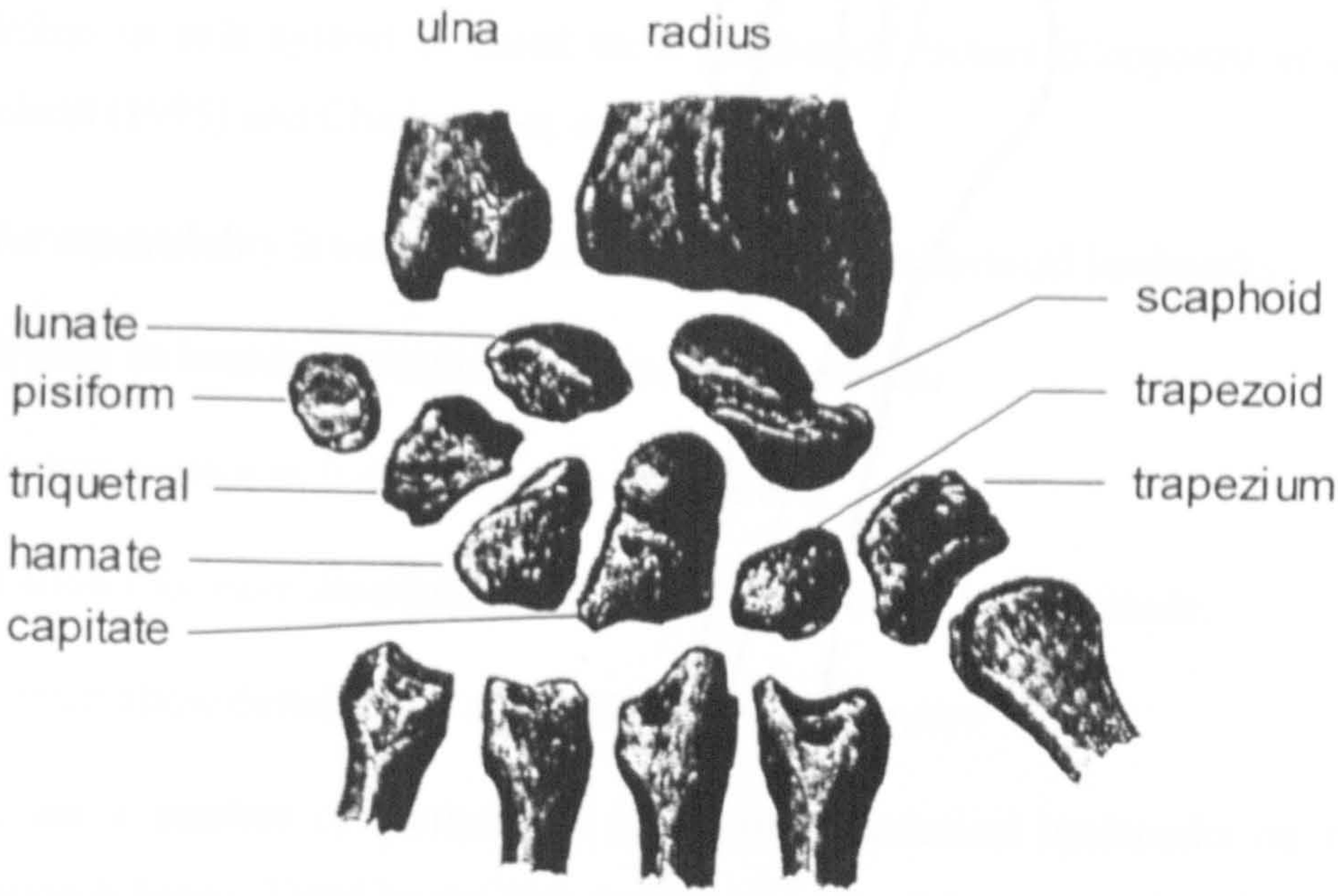

Figure 2.3 Anatomy of the carpus (adapted from Lockhart et. al. (1959)).

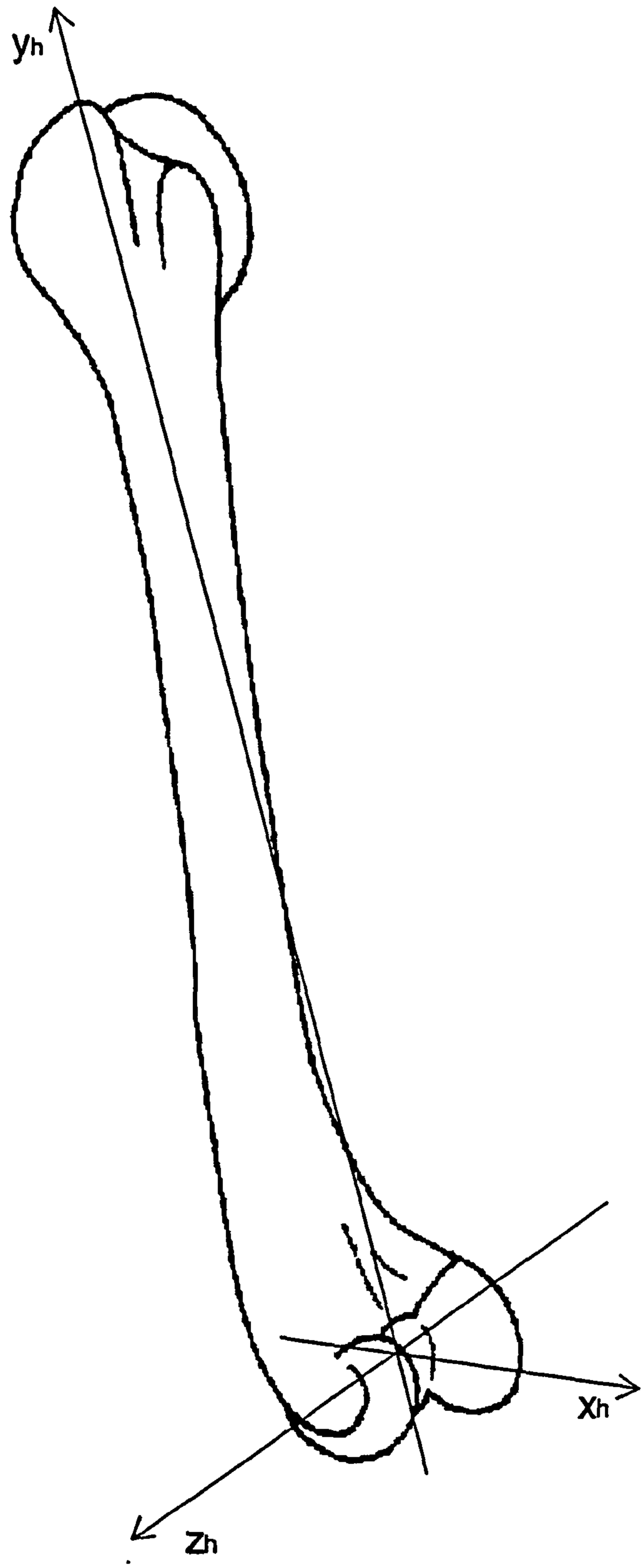

Figure 2.4 The bone-embedded axis system for the humerus.

2.2.1.2 Axis definitions

The joint kinematics are taken to be the change in the relative position and orientation of two rigid body segments, usually referred to as proximal and distal, mathematically described by the relative positions of bone embedded axis systems. The choice of how to define an axis system is based on a number of factors (Cappozzo *et al.* (1995), Lucchetti (1995) and Chadwick *et. al.* (1996)):

for repeatability it must be based on recognised anatomical landmarks;

it must be based on practical experimental methods;

it must contain as few parameters as possible;

it allows for easy description and visualisation of the bone attitude;

it must allow definition to a suitable level of accuracy.

There are a number of methods to locate the anatomical landmarks on which the definition is based (listed by the ISB document) and, of these, there is only one that is a possibility for this study: palpation. It is recognised that other methods such as x-ray computed tomography and bone-embedded markers are more accurate, but the ethical implications make these untenable.

The axis system for each bone is given below, based on a right limb.

The Humerus

The axis system is shown in Figure 2.4.

The origin is defined as the mid-point between the lateral and medial epicondyles.

The y-axis is along a line from the origin to the greater tuberosity; its positive direction is distal to proximal.

A temporary axis, z', is defined as the line passing through the epicondyles with its positive direction from medial to lateral.

The x-axis is orthogonal to y and z' and is positively directed anteriorly.

The z-axis is then defined as being orthogonal to x and y.

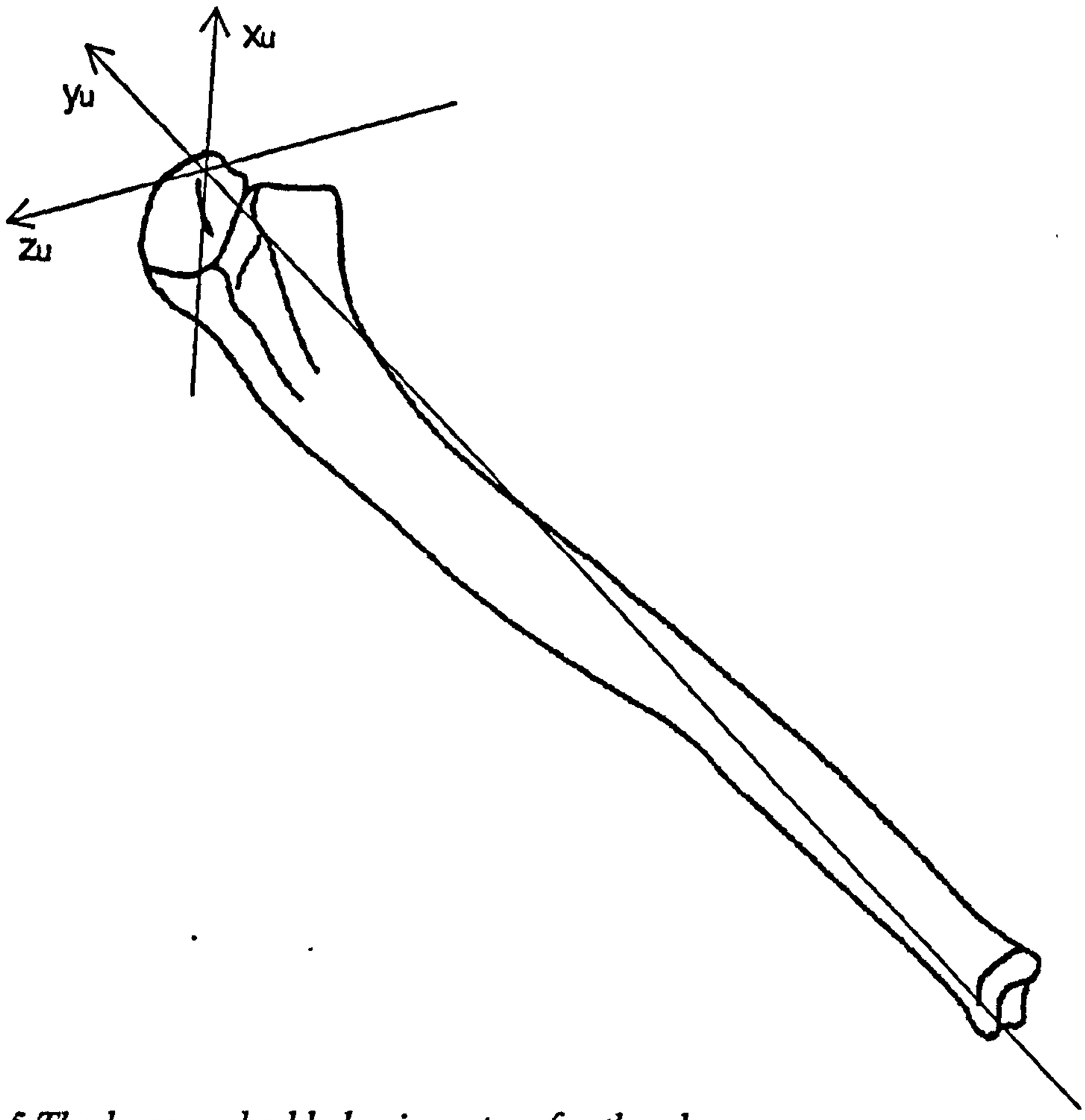

Figure 2.5 The bone-embedded axis system for the ulna.

The Ulna

The axes for the ulna are shown in Figure 2.5.

The origin and temporary *z*-axis, *z'*, are coincident with those of the humerus.

The *y*-axis is the line joining the styloid process of the ulna to the origin and its positive direction is distal to proximal.

The *x*-axis is orthogonal to *y* and *z'* and its positive direction is posterior to anterior.

The *z*-axis is orthogonal to *x* and *y*.

The Radius

The radial axes are shown in Figure 2.6.

The origin is the mid point of the radial and ulnar styloids.

The *y*-axis is along a line joining the origin to the centre of the capitulum, defined in terms of the humeral epicondyles. Its positive direction is distal to proximal.

A temporary *z*-axis, *z'*, is defined as the line joining the radial and ulnar styloids with its positive direction from ulnar to radial.

The *x*-axis is orthogonal to *y* and *z'* and it is positively directed posterior to anterior.

The *z*-axis is orthogonal to *x* and *y*.

The Hand

The hand axes are shown in Figure 2.7.

The origin is located midway along the length of the third metacarpal, at the posterior surface.

The *y*-axis runs along the length of the dorsal surface of the third metacarpal; its positive direction is distal to proximal.

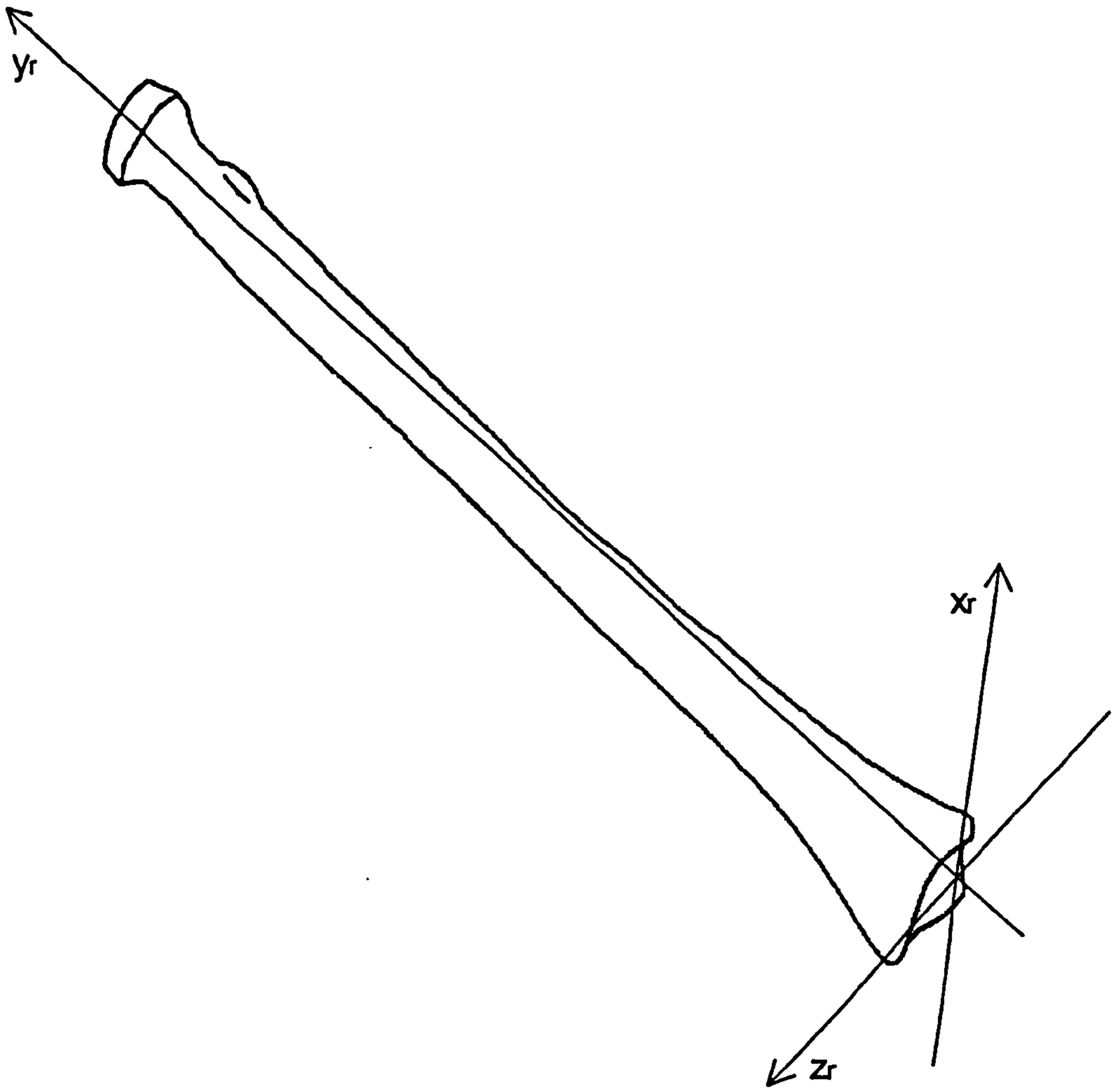

Figure 2.6 The bone-embedded axis system for the radius.

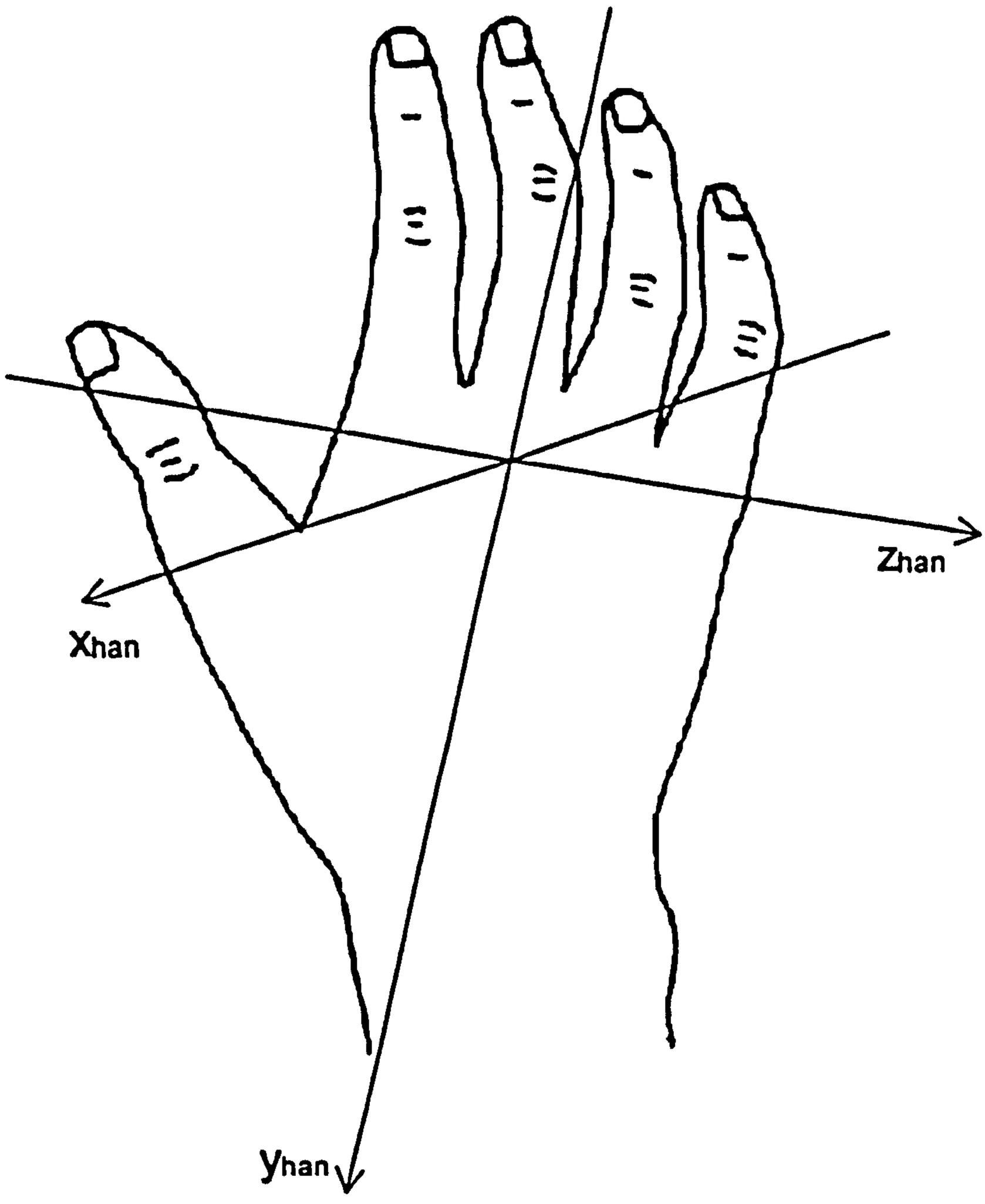

Figure 2.7 The bone-embedded axis system for the hand.

A temporary z axis, z', is defined as the line joining the posterior surfaces of the third and fifth metacarpal heads and its positive direction is fifth to third.

The x-axis is orthogonal to y and z' and its positive direction is posterior to anterior.

The z-axis is orthogonal to x and y.

2.2.1.3 Joint Co-ordinate Systems

There are three commonly used techniques to describe joint kinematics and they are the Euler angle, screw displacement axis (SDA) and floating axis techniques.

The Euler angle technique involves specifying three ordered rotations about orthogonal axes to define a direction cosine matrix relating one co-ordinate system to another. These axes are based on the clinical axes of flexion/extension, abduction/adduction and internal/external rotation, which makes for easy description in clinical terms. A disadvantage, however, is that the result is dependant on the order in which the rotations are performed. As this is not standardised in the literature, this can lead to confusion and difficulty in making comparisons between studies.

The SDA or helical axis technique is based on the principle that any relative movement between two rigid bodies can be described by a rotation about an axis and a displacement along that axis. Although uniquely defined, use of the SDA does not allow easy description of three-dimensional motion in clinical terms and is unduly sensitive to noise for small rotation angles.

The floating axis technique is also one where the relative orientation of the segments is described in terms of three rotations, but the axes are not necessarily orthogonal. One axis is defined to be fixed in each segment and a third `floating axis', orthogonal to these, is found. This technique was chosen because it is felt to be more clinically useful and allows easy comparison between studies as it gives flexion/extension, abduction/adduction and rotation angles directly. The technique applied to the knee joint is described in Grood and Suntay (1983) and is generalised by Cole *et al.* (1993).

Definitions

Axis $\hat{\mathbf{e}}_1$ is fixed in the reference (proximal) segment and is the axis of flexion/extension. Axis $\hat{\mathbf{e}}_3$ is fixed in the target (distal) segment and represents rotation about the long axis of the segment. Axis $\hat{\mathbf{e}}_2$ is the floating axis and is perpendicular to axes $\hat{\mathbf{e}}_1$ and $\hat{\mathbf{e}}_3$, and represents abduction/adduction movement of the joint.

The orthogonal axis sets representing each segment are defined by *x* postero-anterior, *y* disto-proximal and *z* medio-lateral (for a right limb). The unit vectors $\hat{\mathbf{i}},\hat{\mathbf{j}},\hat{\mathbf{k}}$ describe the attitude of the *x*, *y*, *z* axes with respect to the ground axis system.

ϕ_x angle of rotation about *x* axis

ϕ_y angle of rotation about *y* axis

ϕ_z angle of rotation about *z* axis

Cole *et al.* made four modifications to the system reported in Grood and Suntay to ensure complete generality:

- Renamed segment axes with F (axis of flexion, $\hat{\mathbf{f}}$), L (longitudinal axis, $\hat{\mathbf{l}}$), T (third axis, $\hat{\mathbf{t}}$, cross product of $\hat{\mathbf{f}}$ and $\hat{\mathbf{l}}$) so that a right handed joint co-ordinate system always results;
- Included a factor A (=1 or -1) in the definition of $\hat{\mathbf{e}}_2$ to ensure that it is continuous throughout the range $-\pi \le \phi \le \pi$;
- Sign of the rotation angle is determined from one equation;
- Introduced a vector, $\hat{\mathbf{r}}$, so that the sign of the angle always matches the direction of rotation, where $\hat{\mathbf{r}} = \dfrac{\hat{\mathbf{f}}_1 \wedge \hat{\mathbf{e}}_{2y}}{\left|\hat{\mathbf{f}}_1 \wedge \hat{\mathbf{e}}_{2y}\right|}$.

If the proximal segment has axes $(\hat{\mathbf{f}}_i, \hat{\mathbf{l}}_i, \hat{\mathbf{t}}_i)$ and the distal segment has axes $(\hat{\mathbf{f}}_j, \hat{\mathbf{l}}_j, \hat{\mathbf{t}}_j)$ then the joint co-ordinate system is given by $(\hat{\mathbf{e}}_{1ij}, \hat{\mathbf{e}}_{2ij}, \hat{\mathbf{e}}_{3ij})$ where

$$\hat{\mathbf{e}}_{1ij} = \hat{\mathbf{f}}_i \tag{2.1}$$

$$\hat{\mathbf{e}}_{3ij} = \hat{\mathbf{l}}_j \tag{2.2}$$

$$\hat{\mathbf{e}}_{2ij} = \frac{\hat{\mathbf{e}}_{3ij} \wedge \hat{\mathbf{e}}_{1ij}}{\left|\hat{\mathbf{e}}_{3ij} \wedge \hat{\mathbf{e}}_{1ij}\right|} * A \tag{2.3}$$

where
$$A = \begin{cases} -1 & \text{if } \left(\hat{\mathbf{e}}_{3ij} \wedge \hat{\mathbf{e}}_{1ij}\right) \cdot \hat{\mathbf{t}}_j < 0 \text{ and } \left(\left(\hat{\mathbf{e}}_{3ij} \wedge \hat{\mathbf{e}}_{1ij}\right) \wedge \hat{\mathbf{e}}_{3ij}\right) \cdot \hat{\mathbf{f}}_j > 0 \\ +1 & \text{otherwise} \end{cases} \tag{2.4}$$

The three angles describing the joint attitude can now be calculated from:

$$\phi_{1ij} = \cos^{-1}\left(\hat{\mathbf{e}}_{2ij} \cdot \hat{\mathbf{t}}_i\right) * sign\left(\hat{\mathbf{e}}_{2ij} \cdot \hat{\mathbf{l}}_i\right) \tag{2.5}$$

$$\phi_{2ij} = \cos^{-1}\left(\hat{\mathbf{r}} \cdot \hat{\mathbf{l}}_j\right) * sign\left(\hat{\mathbf{f}}_i \cdot \hat{\mathbf{l}}_j\right) \tag{2.6}$$

$$\phi_{3ij} = \cos^{-1}\left(\hat{\mathbf{e}}_{2ij} \cdot \hat{\mathbf{t}}_j\right) * sign\left(\hat{\mathbf{e}}_{2ij} \cdot \hat{\mathbf{f}}_j\right) \tag{2.7}$$

A vector, H, is defined by Grood and Suntay to describe joint translation where each component of H is a translation along one of the joint co-ordinate axes:

$$\mathbf{H} = S_1\hat{\mathbf{e}}_{1ij} + S_2\hat{\mathbf{e}}_{2ij} + S_3\hat{\mathbf{e}}_{3ij} \tag{2.8}$$

In clinical terms, the three displacements of interest are medio-lateral draw (positive to the right), antero-posterior draw (positive anterior) and joint compression/distraction

(distraction positive). These distances are given by projection of the vector **H** onto the joint co-ordinate axes such that:

$$\begin{aligned} q_1 &= \mathbf{H} \cdot \hat{\mathbf{e}}_{1y} \\ q_2 &= \mathbf{H} \cdot \hat{\mathbf{e}}_{2y} \\ q_3 &= -\mathbf{H} \cdot \hat{\mathbf{e}}_{3y} \end{aligned} \tag{2.9}$$

For the elbow joint the flexion axis, $\hat{\mathbf{f}}$, is the humeral z axis and the longitudinal axis, $\hat{\mathbf{l}}$, is the ulnar y axis. For the wrist joint the flexion axis is the radial z axis and the longitudinal axis is the hand y axis.

2.2.2 TECHNIQUES FOR MEASUREMENT

2.2.2.1 The Vicon System

The Oxford Metrics VICON motion analysis system was used for the collection of kinematic data. The system consists of six charge-coupled device (CCD) video cameras, a data-station and a PC. The cameras emit pulsed infrared light at 50Hz from an array of light emitting diodes (LEDs) positioned in a ring around the lens. Light reflected back from markers placed on the subject then forms an image in the camera's field of view. This produces a two-dimensional image of a given marker, allowing the calculation of the centre of the marker from the leading and trailing edges. If the images from two or more cameras are combined, the three dimensional position of the marker in the laboratory space can be reconstructed.

The pulsed nature of the light gives rise to consecutive frames of 'static' positions, which must be converted into a continuous trajectory for the marker. This process is carried out automatically by the software by calculation of the expected position of the marker in the next frame; governed by a set of reconstruction parameters defining the possible path of the marker. If the marker falls outwith the volume of the expected position, as can happen repeatedly with 'difficult' data, a new trajectory is started and the trajectories must be manually linked by the user. The final stage, giving 3D co-ordinates for each marker, is to label each trajectory.

Calibration of the system is carried out to define the position of the cameras relative to the laboratory and to each other. Two techniques are possible: static and dynamic. The first of these uses a 3D array of fixed markers whose positions in the laboratory are accurately known and the images of which are used to calculate the 3D positions of the cameras. In the second method, a rod, on which two markers are mounted with a known separation, is waved around the workspace volume. Three markers hanging on a wire from a tripod mark the position of the origin and the direction of the forward axis, x, is defined as a line from the origin to another marker placed on the floor. The dynamic method of calibration was used in this study and its accuracy determined by inspection of the residuals calculated by the Vicon software. The residuals are described as the average of distances between a reconstructed point and the rays used

for its reconstruction. An average value of 1.6mm (±0.63) was recorded for 20 randomly selected trajectories.

Markers are passive, and consist of 25mm polystyrene spheres covered with retro-reflective tape. The retro-reflective tape causes light falling on the markers to be reflected back along the path by which it came. This helps to ensure that the cameras see the marker as a circle with a well-defined edge, allowing non-circular markers to be rejected, thus minimising reflections, and improving the accuracy with which the marker centre is calculated.

2.2.2.2 The Marker Set

To fully describe the motion of a rigid body, it is necessary to track the motion of at least three points on the body. If the subject can be modelled as a series of rigid segments, then there must be at least three markers on each segment to fully describe the 3D kinematics. Traditionally, markers have been placed directly onto the skin over either relevant anatomical points or experimentally convenient points, but, more recently by Cappozzo *et al.* (1995), by mounting markers on rigid cuffs and strapping these to the segments.

In the case of upper limb analysis, it was felt by the author that skin movement would be excessive if markers were placed directly onto the skin, particularly with regard to forearm pronation/supination. Work was carried out with Lucchetti (1995), as part of a CAMARC project, to develop a marker system using cuffs and to determine the optimum marker configuration.

The marker set consists of three fixtures upon which the markers are mounted, one each for the upper arm, forearm and hand. Lucchetti originally used four markers per segment, thus allowing noise reduction in the marker position data by means of a least squares algorithm. Due to the close proximity of the markers on the fixtures of the (distal) forearm and hand, there was the problem of either trajectory crossover or broken trajectories occurring. It was decided, therefore, to use only three markers per segment. Lucchetti reported standard deviations of less than 1° in joint angle calculations using three markers per segment.

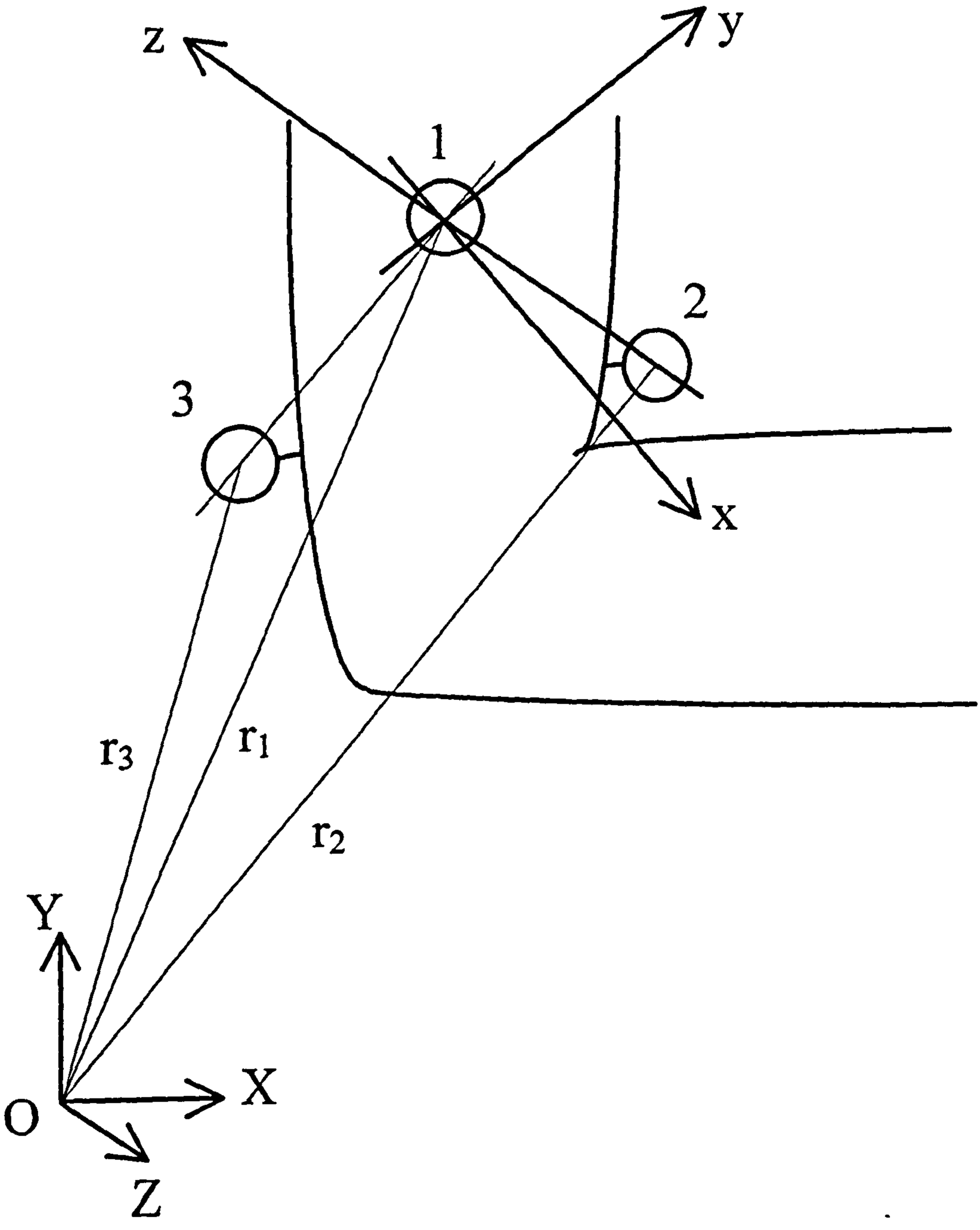

Figure 2.8 Technical frame definition for the upper arm.

2.2.2.3 Technical Frames of Reference

The three markers on each segment are used to define a right-handed, orthogonal axis system, known as a 'technical frame', which is assumed to be fixed relative to the underlying bone. To illustrate this, the example of the upper arm is shown in Figure 2.8.

Let the markers be 1, 2, 3 as shown. If the position vector of marker i is $\mathbf{r}_i$ in the laboratory, or global, axis system then the three markers have position vectors $\mathbf{r}_1$, $\mathbf{r}_2$, $\mathbf{r}_3$.

The three axes are then defined by three unit vectors as follows:

$$\mathbf{z} = (z_1, z_2, z_3) = (\mathbf{r}_1 - \mathbf{r}_2)/|\mathbf{r}_1 - \mathbf{r}_2| \tag{2.10}$$

$$\mathbf{x} = (x_1, x_2, x_3) = \mathbf{z} \wedge (\mathbf{r}_3 - \mathbf{r}_1)/|\mathbf{r}_3 - \mathbf{r}_1| \tag{2.11}$$

$$\mathbf{y} = (y_1, y_2, y_3) = \mathbf{z} \wedge \mathbf{x} \tag{2.12}$$

The origin is taken as the position of marker number one, $\mathbf{r}_1$.

A rotation matrix, R, can be defined to allow transformation from global to technical co-ordinates where

$$\mathbf{R} = \begin{bmatrix} x_1 & y_1 & z_1 \\ x_2 & y_2 & z_2 \\ x_3 & y_3 & z_3 \end{bmatrix} \tag{2.13}$$

The position of any point in the global system, $\mathbf{r}_i$, can then be expressed in the technical system by

$$\mathbf{r}_{ti} = \mathbf{R}(\mathbf{r}_i - \mathbf{r}_1). \tag{2.14}$$

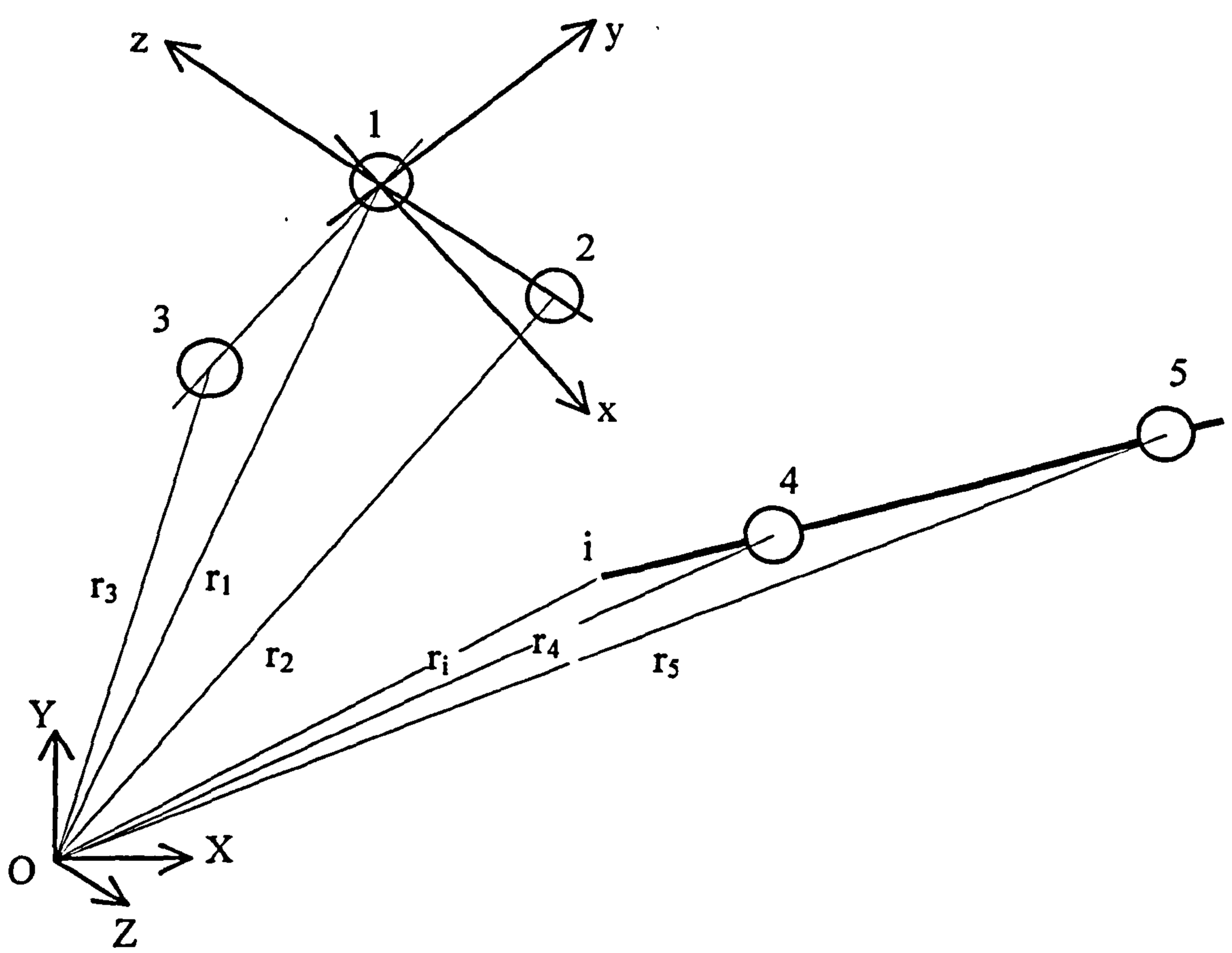

Figure 2.9 Anatomical point calibration technique

2.2.2.4 Anatomical Point Calibration Technique

The marker cuffs are placed on the subject in experimentally convenient, rather than anatomically significant, places; based on a number of criteria:

- the subject should be comfortable;
- the markers must be visible to as many cameras as possible;
- the markers must not obstruct movement of the subject;
- the cuff must be secure, i.e. it must not move after calibration;
- the movement of the cuff must follow as closely as possible the movement of the limb segment;
- the markers should not be collinear and the separation should be sufficient to minimise any errors.

At the start of each session, when the cuffs have been fitted according to the criteria above, their positions must be recorded. This process is known as anatomical point calibration and allows the bone-embedded axes to be defined from the technical frames. A pointer, containing two markers, is held against each anatomical point in turn while a short data sequence is captured.

If the pointer tip and the two markers have position vectors $\mathbf{r}_i$, $\mathbf{r}_4$ and $\mathbf{r}_5$ respectively, the tip position, and hence the anatomical landmark position in the global system is given by (See Figure 2.9):

$$\mathbf{r}_i = (\mathbf{r}_4 - \mathbf{r}_5)/|\mathbf{r}_4 - \mathbf{r}_5| * d + \mathbf{r}_4 \qquad (2.15)$$

where d is the distance from marker number 4 to the pointer tip.

From Equation 2.14 the position of the anatomical point in the technical frame may be determined, thus allowing, by the inverse transformation, the positioning of the anatomical point in the global system during a dynamic trial.

To allow the definition of bone embedded axis systems, the following anatomical landmarks need to be identified:

Humerus	greater tuberosity
	lateral epicondyle
	medial epicondyle
Ulna	styloid process
Radius	styloid process
Hand	base of 3rd metacarpal
	3rd metacarpal head
	5th metacarpal head.

2.3 FORCE MEASUREMENT

The external loads on the limb can conveniently be divided into three groups: gravitational, inertial and contact. Although the effect of a load action is the same, to produce moments and forces at the joint, it is useful to consider its origin.

2.3.1 GRAVITATIONAL

The weight of the limb segments themselves, as well any apparatus that is being held, will contribute to the loading on each joint. The weight of a limb segment can be calculated from other information about the subject, such as height and weight, by using published tables of body segment parameters (BSP).

2.3.1.1 Body Segment Parameters

A review of techniques for the determination of body segment parameters is found in Pearsall and Reid (1994). They highlight three main shortcomings of existing data: standards based on small-sample studies, the use of cadavers instead of live subjects, and a lack of information on diverse populations. In the present study, the sample of subjects consists of students of both sexes from within the Bioengineering Unit, and the choice of data for BSP should reflect this. Only data drawn from similar populations and where a significant number of living subjects was used were considered.

Drillis and Contini (1966) measured anthropometric data in twenty North American male students between the ages of 20 and 40. They found segment mass, volume, centre of mass and moment of inertia using reaction board, water displacement, pendulum swing and photogrammetry techniques. Zatsiorsky and Seluyanov (1983) published one of the most comprehensive sets of data on the mass and inertial characteristics of human body segments, based on a study of 100 young, male Russians. The subjects were scanned on a γ-scanner and the absorption of γ-rays used to calculate segment properties. Each of the properties is scaled according to the subject's height and body mass.

BSP data for females are less common in the literature, but two studies are relevant. Young *et al.* (1983) reported data on a sample of 46 females between the ages of 21 and 45 and Finch (1985) used a sample of 15 females between the ages of 20 and 29. Both studies made use of photogrammetry techniques.

2.3.2 INERTIAL

2.3.2.1 D'Alembert's Principle

D'Alembert's Principle allows a dynamic problem to be reduced to a static one by application of Newton's Laws, thus rendering solution and visualisation simpler. If one imagines a body of mass m accelerating with acceleration **a**, then the force producing that must be ma. If the term ma is now replaced with a force **F** acting in the opposite direction from **a**, the problem can be considered to be one involving static equilibrium, where **F** is the *inertial* force. The same logic applies to angular acceleration and torque.

2.3.2.2 Inverse Dynamics

The method taken to calculate inertial loads on a limb segment is one of inverse dynamics. That is, starting with information about the velocities and accelerations of the segment, the loads that produced these can be calculated. This is the application of D'Alembert's Principle.

Inertial force is given by

$$\mathbf{F} = m_i \mathbf{a} \tag{2.16}$$

where m_i is the segment mass and **a** is the linear acceleration of the centre of mass.

The linear acceleration of the centre of mass can be thought of as being made up of three components: overall linear acceleration of the body, tangential acceleration $r_i\alpha$ and centripetal acceleration $r_i\omega^2$ due to rotation of the body about a point offset from the centre of mass, where ω and α are the angular velocity and acceleration of the segment respectively.

Inertial torque is given by

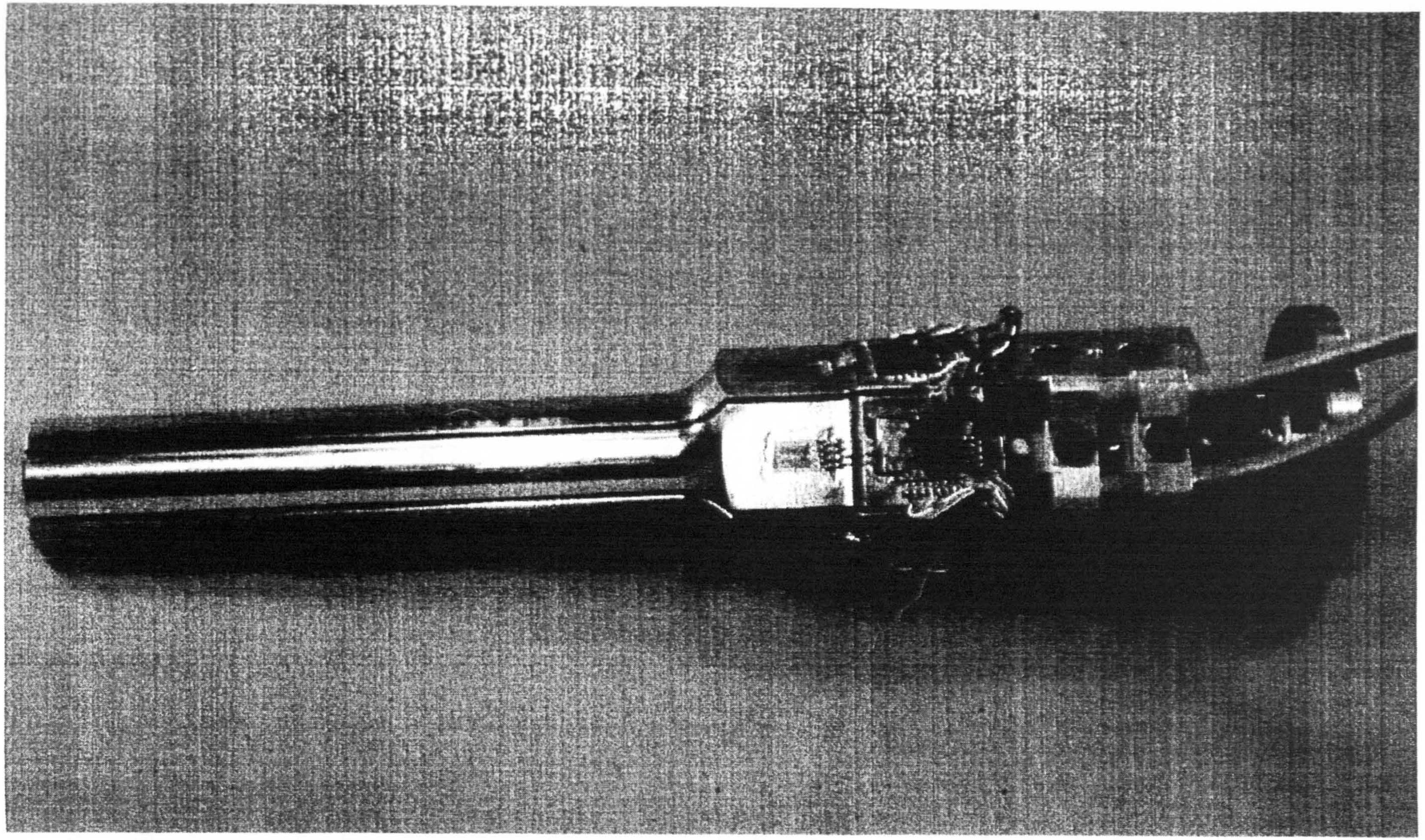

Figure 2.10 The grip force transducer after final assembly.

$$T = I_i \alpha = m_i k_i^2 \alpha \qquad (2.17)$$

where I_i is the principal segment mass moment of inertia, k_i is the segment radius of gyration.

2.3.3 Contact

Contact force between a body and an object in its environment is often the largest contributor of the three types of force mentioned here. In the current study, which involves manipulating objects in the hand, the force of interest is grip.

2.3.3.1 Grip Force Measurement

Although there were a number of existing devices for measuring grip strength reported in the literature, none was suitable for measuring functional grip. Richards and Palmiter-Thomas (1996) describe several devices falling into four groups: hydraulic, pneumatic, mechanical and strain gauge. Most of these are designed to measure maximal, not functional, forces, have only one degree of freedom, and are of more use in the clinic than in research.

Strain gauge devices are the obvious choice for this type of study as they allow the recording of force variation with time, are sensitive and accurate (Richards and Palmiter-Thomas (1996)). An *et. al.* (1980) described two strain gauge grip measuring devices: one was uni-axial only, the other measured the force on each phalanx but only for one finger. Pronk and Niesing (1981) described a uni-axial device with a range of 0 - 900N and an accuracy of better than 5%.

For this study, a new device was needed that would allow the measurement of the distribution of grip force during functional activities, and thus enable MCP joint moments to be calculated.

Design of a New Device

A force transducer has been specially designed to measure hand grip forces during functional activities (see Figure 2.10). It consists of six active beams (Figure 2.11), mounted as cantilevers on a hexagonal core so as to form a cylinder of diameter 30mm, thus allowing the device to form the handle of a piece of equipment. The forces

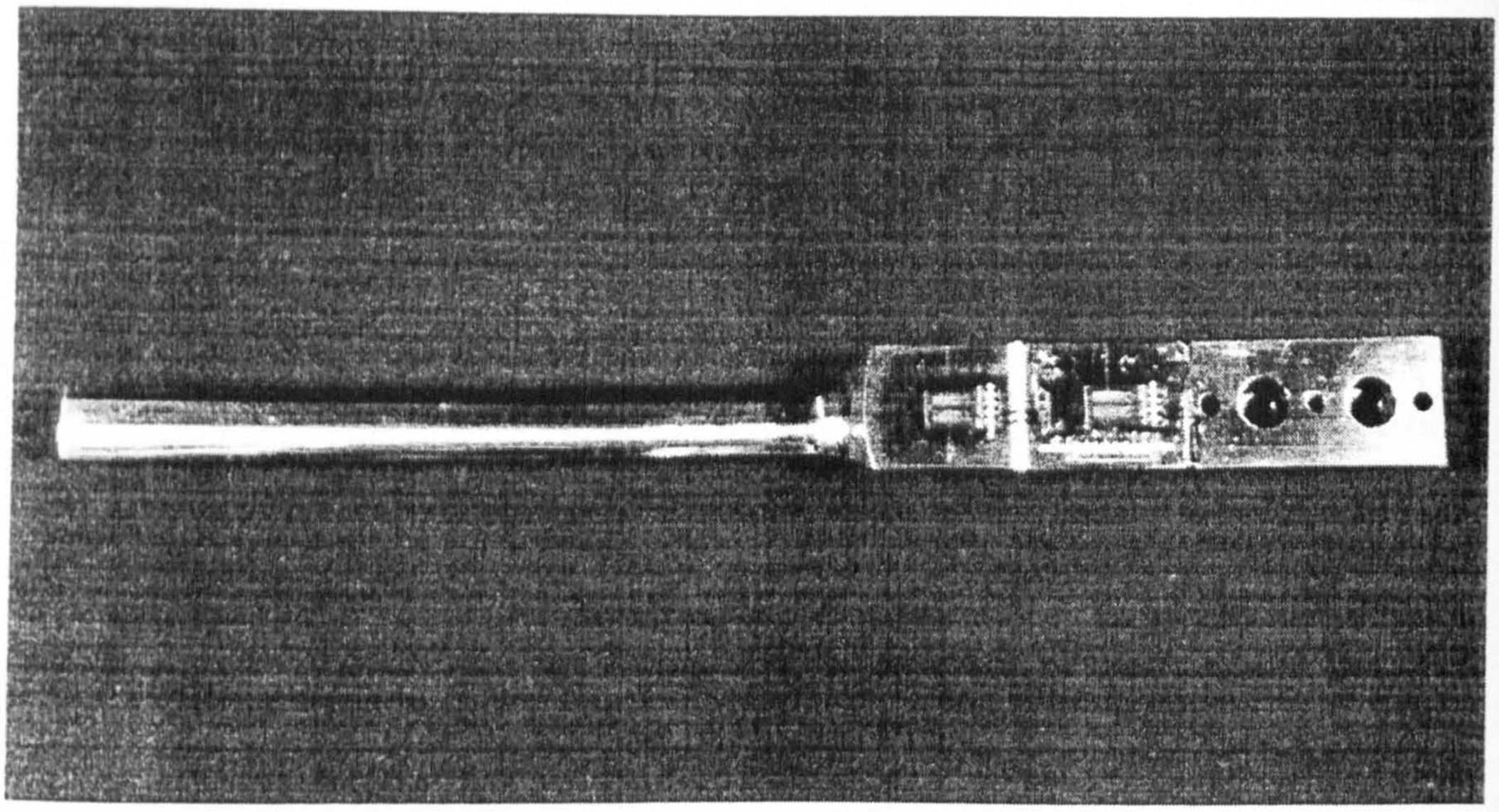

Figure 2.11 One beam of the transducer ready for calibration.

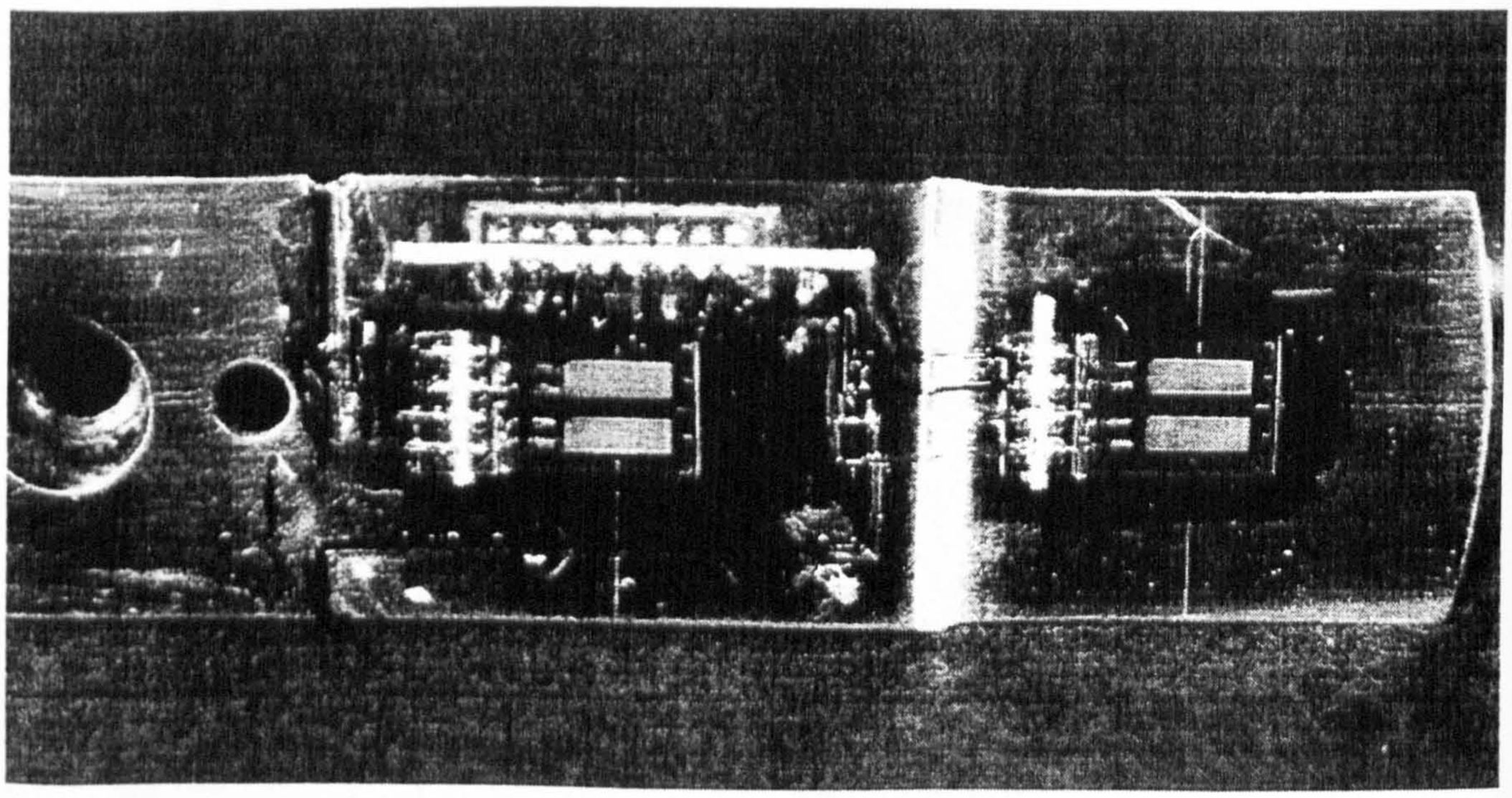

Figure 2.12 Detail of the gauge sites on one beam of the transducer.

being measured are assumed to be radial. Six beams were incorporated into the device to gain the maximum amount of information, whilst ensuring that the design was feasible and the number of electrical output channels reasonable.

Foil strain gauges are applied to the top and bottom surfaces of the beams at two cross-sections (Figure 2.12), giving two channels of strain output on each arm so that the magnitude and position along the arm of the applied force may be calculated. The shape of the cross-section at the gauge sites was that of a trapezium, formulae for the calculation of bending stress for which are given in Roark's Formulas for Stress and Strain (Young (1989)).

Data on functional grip force is very scarce in the literature, but some studies of maximal grip force have been reported. Ejeskar *et al.* (1981) gave values for the flexion force produced by individual fingers of between 78N and 104N for men. Swanson *et al.* (1970) quoted an average hand grip force, measured on a Jamar dynamometer, of 467N and Lee and Rim (1991) found a grip force of 600N for a cylinder of 30mm diameter. In light of this, the choice was made to allow 250N per segment to be measured. In terms of the design of transducer, the limiting factor was the bending moment at the gauge sites, not the shear force, thus the rated load was 250N applied at the ends of the beams. Under these conditions, the strain gauges would be subjected to approximately 500με. To protect against overloading the device, the design is such that all six beams come together at a load of about 250N per beam.

The shape of the cross-section at the gauge sites and along the gripping area allows the maximum amount of material to be included in the smallest overall size, whilst allowing a flat surface for gauge mounting and a cylinder for gripping, thus minimising the deflection at the ends of the beams.

If the measured bending moments at the two gauge sites are $\mathbf{M}_a$ and $\mathbf{M}_b$ and a and b are the respective distances from the point of application of the load, F, to the sites then

$$\mathbf{M}_a = \mathbf{F}a \quad \text{and} \quad \mathbf{M}_b = \mathbf{F}b$$

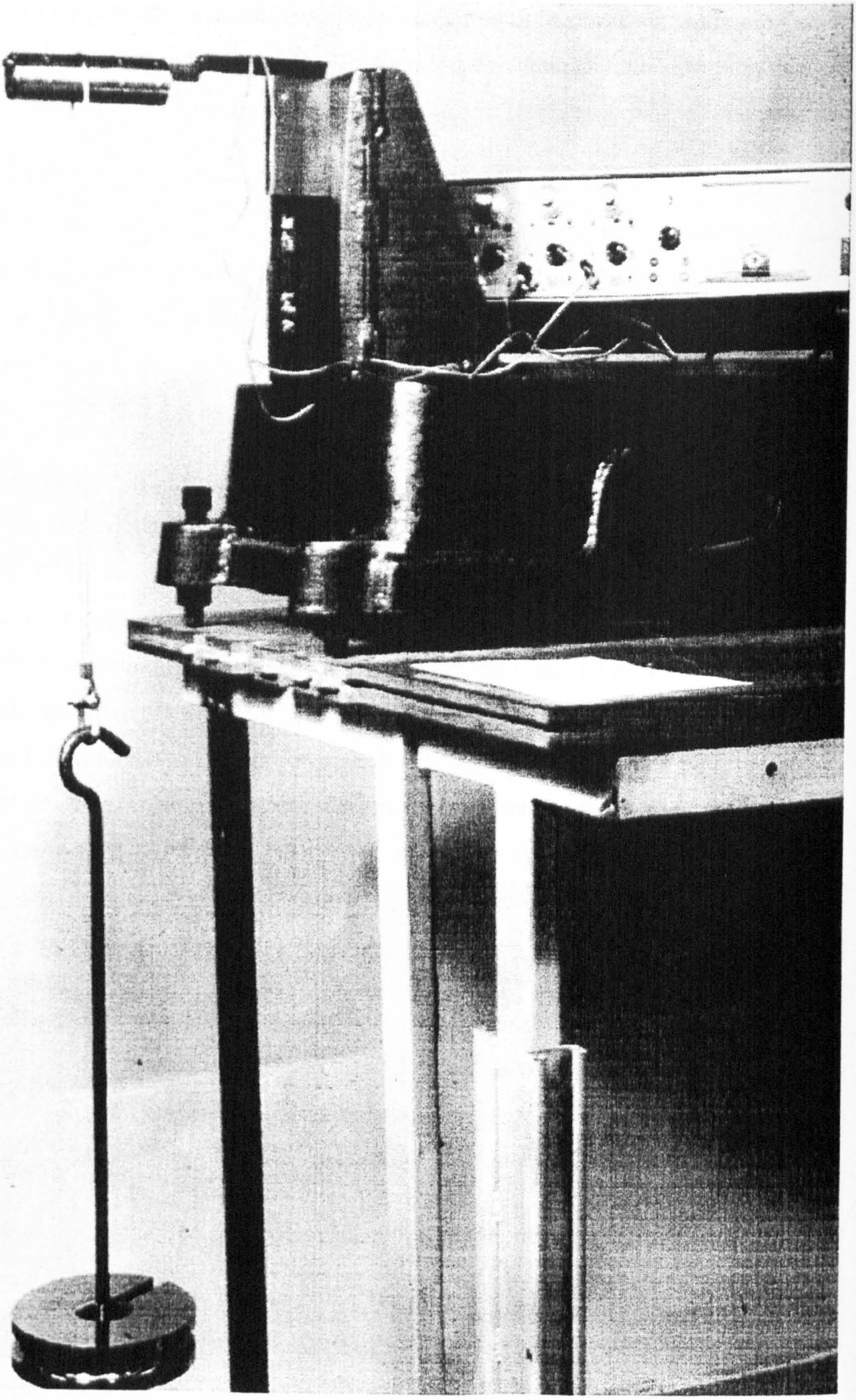

Figure 2.13 Calibration of one of the transducer beams.

$$\Rightarrow M_a - M_b = F(a-b)$$

$$\Rightarrow F = \frac{M_a - M_b}{a-b} \tag{2.18}$$

$$\Rightarrow a = \frac{M_a}{F} \tag{2.19}$$

Each arm is calibrated individually up to 250N by the application of dead weights in four different positions along the arm, as shown in Figure 2.13. The results of this calibration, along with design drawings, may be seen in Appendix B.

2.3.3.2 The Calculation of Moments about the Metacarpophalangeal Joints

The force values measured during activity are produced by forces in the tendons crossing the wrist joint, and thus must be calculated for inclusion in the model. These forces were calculated by consideration of moment equilibrium at the MCP joints. Due to the diversity of the grips used in the tests, a different scheme for calculation of MCP moments was needed for each one. The scale of the movements involved in the activities required a workspace volume that was too large to allow accurate measurement of the position of individual fingers, therefore a number of assumptions had to be made about the position of the hand and fingers with respect to the transducer.

Power Grip (transducer handle vertical)

Figure 2.14 shows the position of the forces with respect to the MCP joints for the vertical power grip. As there is no way of measuring the distribution between the digits, the analysis is treated as planar and load sharing is based on data from the literature. The potential moment contribution of each digit to the total moment was based on the product of muscle physiological cross sectional area (PCSA) and moment arm of the MCP joint. Data from Brand and Hollister (1993) gave the relative tension of finger flexors, based on PCSA, split into individual finger components for both superficialis and profundus muscles. Any force produced by the thumb and thenar eminence was transferred to the fingers for the analysis. Although this may give rise to

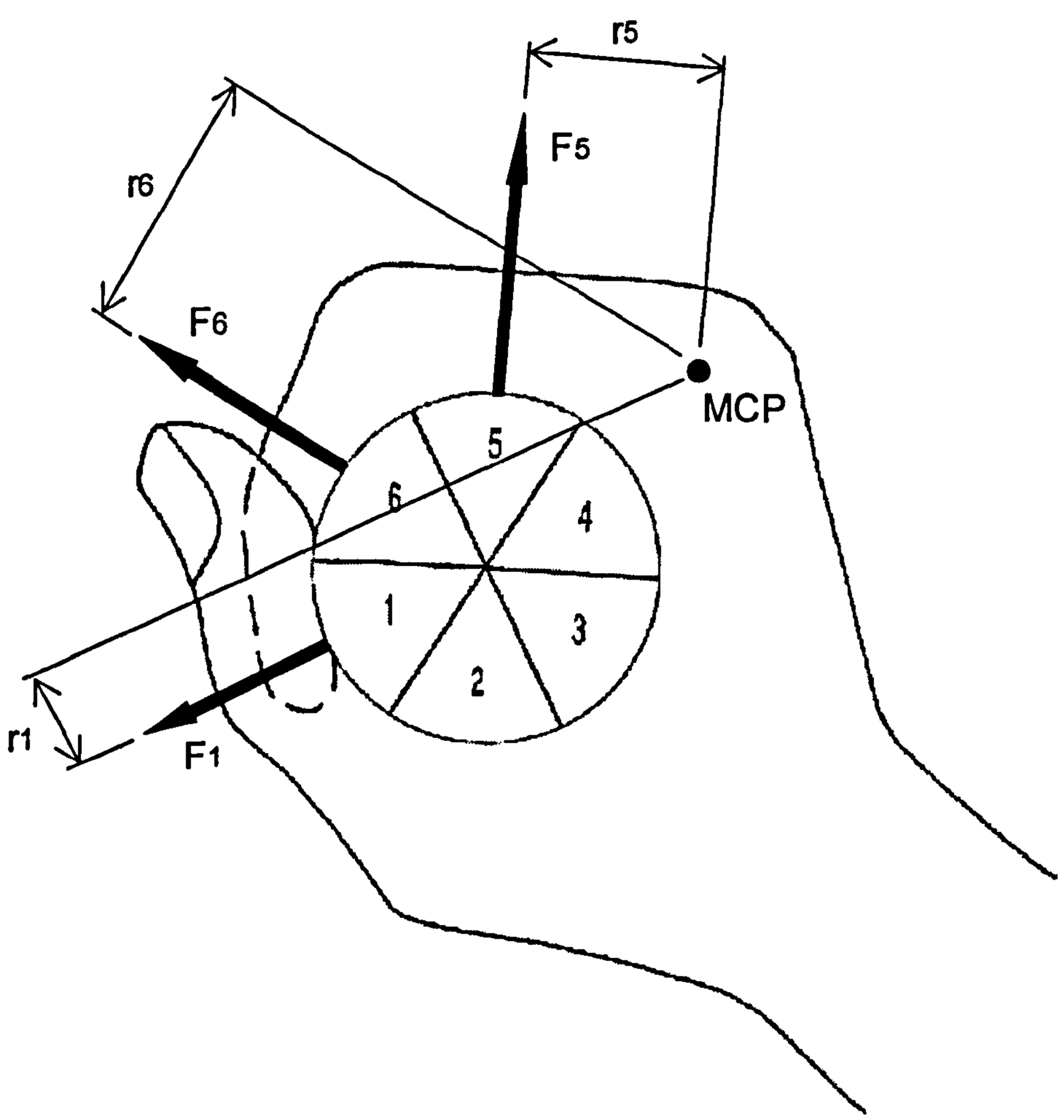

Figure 2.14 Schematic representation of forces acting on the hand during the vertical power grip.

errors in the individual tendon forces at the MCP joints, the total tendon force crossing the wrist and elbow joints, the main interest of this study, should be affected to a much lesser extent.

The positions of the forces and the MCP joint were calculated in the transducer axis system and the moments calculated from

$$\mathbf{M} = \sum_{i=k+1}^{n} F_i \times r_i \qquad (n = k+1+m) \tag{2.20}$$

and $\quad if \quad i > 6 \quad then \quad i = i - 6$

where F_i is the force on beam i

r_i is the lever arm of each force with respect to the MCP joint

k is the number of the beam over which the MCP joint rests

m is the number of beams covered by the fingers.

The segment number over which the MCP joints lay was calculated from the Vicon data and the number of beams covered by the fingers was recorded manually. This was done at the start of the session by asking the volunteer to grasp the device and counting the number of segments covered by the digits.

Power Grip (transducer handle horizontal)

The analysis for this grip was similar in concept to that for the vertical power grip, except that the transducer axis ran in the opposite direction, so that the numbering order for the beams was reversed. The distribution of moments between the digits was based on the same assumptions as for the vertical power grip.

Hook Grip (transducer handle horizontal)

The transducer was held in a very similar way for this activity to the way it was held for the horizontal power grip activity. The analysis in terms of the calculation of MCP joint moments was the same as for the horizontal power grip.

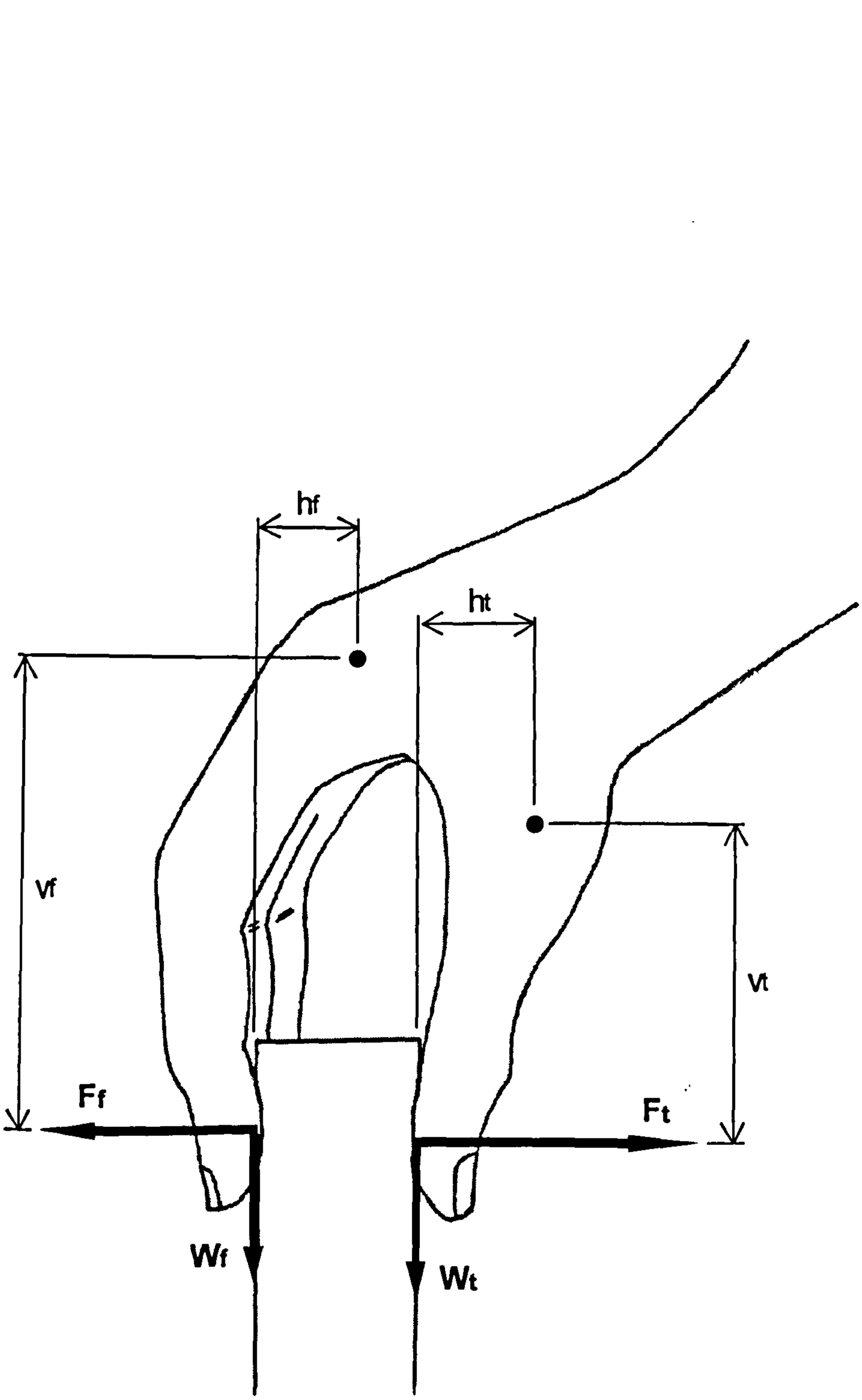

Figure 2.15 Schematic representation of the forces acting on the hand during the chuck grip.

Chuck Grip (transducer handle vertical)

In the chuck grip, the transducer was gripped by three fingers (first, middle and ring) and the thumb. The calculation of the position of the forces on the transducer was a one-dimensional problem, being simply the position of the force along the length of the beam. The analysis is depicted in Figure 2.15.

The position of the third MCP joint was obtained from the Vicon motion analysis data. Only the distance along the transducer long axis was found, and the positions of the second and fourth MCP joints were assumed to be the same as the third in this dimension. The position of the thumb MCP joint relative to the third MCP joint was measured statically for each subject and assumed to be the same for each trial. Any error introduced by this as a result of variability in the subject's technique would affect the moments at the thumb MCP joint only, and would be a maximum of 15%.

The moments were given by

$$M_{MPC1} = F_t \times v_t + W_t \times h_t \tag{2.21}$$

$$M_{MCPf} = F_f \times v_f + W_f \times h_f \qquad (f = 2, 3, 4) \tag{2.22}$$

The weight forces, W_t, were calculated to be the total weight of the transducer, divided in the proportion of the normal forces, F_t.

2.4 OPTIMISATION

2.4.1 PREVIOUS WORK

Biomechanical analyses of joints result in sets of indeterminate equations as there are many more load bearing structures crossing a joint than are necessary to satisfy the equilibrium conditions. Therefore, a method of deciding how the body will distribute the load between these structures is needed. This has often been done by simplifying the model to the point where the equation set is statically determinate (Nicol (1977), Amis (1978)), or by implementing some form of optimisation routine. Optimisation involves the minimisation of an objective function subject to a set of constraint equations. The constraint equations not only define the equilibrium conditions which must be satisfied, but can also introduce additional constraints such as non-negativity, limits on the relative values and maximum bounds for the forces. A variety of objective functions has been used in previous studies to produce physiologically realistic force-sharing models. If the objective function and the constraint equations feature only linear combinations of the variables then the solution procedure is readily implemented using the linear programming method. A number of studies using linear optimisation techniques have been published.

Linear optimisation routines have the advantages of being readily implemented and producing stable solutions but do not always lead to physiologically reasonable results. Barbenel (1972) and Yeo (1976) tested the minimisation of total muscular force as an objective function and found their results were not verified by comparison with EMG studies. Such simple criteria, particularly when used with simple, planar models, often fail to predict co-activation of synergistic muscles as the number of non-zero variables in the solution is limited to being, at most, the same as the number of constraint equations (Tsirakos *et. al.* (1997)). In these simple models, the muscle with the largest moment arm will be recruited first and, if the muscle force is unbounded, will be required to do all the work.

In an attempt to produce more realistic muscle force sharing, An *et. al.* (1984) minimised maximum muscle stress, σ, in their sagittal-plane model of the humero-

ulnar joint, which included nine muscle units. For each muscle, *i*, an additional constraint was introduced such that

$$F_i \leq PCSA_i \times \sigma \tag{2.23}$$

where F is the force, PCSA is the physiological cross sectional area and σ is the upper limit on muscle stress. The results from this method were compared to those from previous studies using linear and non-linear optimisation criteria and to studies using EMG comparison with favourable agreement.

Bean *et. al.* (1986), however, suggested that the minimisation of maximum muscle stress as used by An *et. al.* might not lead to unique solutions. To overcome this they presented a two-stage optimisation, the first of which minimised the maximum muscle stress and the second minimised the joint compression force, using this muscle stress value as a constraint. They showed how the method could be applied to a simple model of the lumbar spine and compared their results favourably to those using different optimisation criteria.

In more complex models, where there is more than one degree of freedom at a joint, muscle co-activation is naturally predicted as muscles which are agonists in one plane behave as antagonists in another. This increases still further as two joint muscles are introduced and, in fact, the combination of a comprehensive three dimensional model with additional physiologically based constraints can "overcome the limitations of a basic linear programming approach" (Tsirakos *et. al.* (1997)).

As a further improvement on the linear programming technique, some authors have introduced limits on the muscle force based on force-length, force-velocity and muscle activation (number of active motor units and their firing frequencies), whilst minimising the activation. An *et. al.* (1989) applied the technique to the elbow and Kaufman *et. al.* (1991) applied it to the lower limb. The technique was shown to produce muscle co-activation in a realistic manner, but was not validated with direct comparison to EMG studies.

Other authors have tried to produce more realistic results by increasing the complexity of the solution algorithm, and implementing non-linear techniques. Crowninshield and Brand (1981) and Dul (1986) used a physiologically based method by considering the inverse relationship between muscle force and endurance, and maximising the latter. Both sets of authors found reasonable agreement between predicted force activation and actual EMG measurements, the former in a human gait study and the latter in a cat study. The minimum fatigue criterion may be a reasonable hypothesis for a repetitive activity such as gait, and indeed their results show good agreement between the model and recorded EMG patterns during gait, but is not necessarily so for the higher exertion activities under consideration in this study.

Several studies utilising non-linear, dynamic, neurophysiologically-based and EMG-assisted solution algorithms have been published (Pandy *et. al.* (1992), Davy and Audu (1987), Raschke *et. al.* (1996), Buchanan *et. al.* (1996) and Cholewicki and McGill (1994)). In light of the decreasing stability and increasing complexity of these techniques, it was decided to base the optimisation chosen for this study on that of Bean *et. al.* (1986), which has been shown to combine simplicity with realistic muscle force prediction, when used in a highly constrained linear system.

2.4.2 DEVELOPMENT OF THE OPTIMISATION ROUTINE

The optimisation technique used to overcome the indeterminate problem in this study was a two stage technique, also known as sequential programming (Bean *et. al.* (1986)). It uses the Simplex routine and is based on code written by Press *et. al.* (1992). Fitzsimmons (1995) and Runciman (1993) have previously described a similar technique.

The first stage was to minimise the overall maximum muscle stress, σ, subject to the constraints comprising force and moment equilibrium equations and joint stability conditions. The primary constraint that all variables must be non-negative is implicit in the routine. The Simplex algorithm may be formulated thus (for input to the tableau, each variable must be expressed):

Minimise z, where

$$z = 0 \times F_1 + 0 \times F_2 + \ldots + 0 \times F_{n-1} + \sigma \tag{2.24}$$

subject to

$$F_i - PCSA_i \times \sigma \leq 0 \qquad (1 \leq i \leq m) \tag{2.25}$$

and

$$\sum r_i \times F_i d_i - \sum M_E = 0 \tag{2.26}$$

$$\sum F_i \times f_i - \sum F_E = 0 \tag{2.27}$$

$$J_{lateral} - kJ_{axial} \leq 0 \tag{2.28}$$

where $PCSA_i$ is the physiological cross sectional area of the i^{th} muscle

n is the number of variables

m is the number of stress-limited variables (muscle and ligament)

F_i is the force in the i^{th} structure

M_E, F_E are the external moments and forces about and along a given axis

r_i is the moment arm of the i^{th} structure about the given axis

d_i is the component of the i^{th} structure normal to the given axis

f_i is the component of the i^{th} structure along a given axis

$J_{lateral}$, J_{axial} are joint forces

k is a constant

There are 16 equations of the type of Equation 2.25 (13 muscles and 3 ligaments), 5 of type 2.26 (3 at the elbow and 2 at the wrist), 6 of type 2.27 (3 at the elbow and 3 at the wrist) and 4 of type 2.28 (2 at the elbow and 2 at the wrist). These are explained more fully in the Section 2.5: Anatomical model.

There is no precedent in the literature for the inclusion of ligament forces in the minimisation criteria, because in previous studies where ligaments have been included in the model, their force has been determined statically. The inclusion of ligaments which were not stress-limited, initially led to their extensive recruitment, as they have no 'cost' implication in the optimisation, and have large moment arms. This was felt to be unrealistic and so the ligaments have been stress-limited in the same way as the muscles by the allocation of a pseudo cross-sectional area. The choice of this cross-sectional area was made on the basis that the primary function of ligaments is to constrain the motion of the joint and their role as load bearing structures is secondary, and thus the ligament force should be kept to a minimum. It was found that if very small cross-sectional areas were allocated to the ligaments, and insufficient force was allowed to develop in them, the model became unstable. There was an optimum range between the ligament force being over restricted and unrestricted that produced mathematically stable solutions. The ligaments were allocated the minimum cross sectional area within this range.

In the second stage the sum of the joint and ligament forces was minimised, with the same constraints as the first stage, and the additional constraint that the muscle stress was limited to σ. Bean *et. al.* (1986) minimised the joint force as their second stage, but in this case the inclusion of ligament force was found to be necessary to produce mathematical stability.

2.5 ANATOMICAL MODEL

2.5.1 AXES OF ROTATION

2.5.1.1 Elbow Flexion/Extension

Although several studies on elbow rotation have been carried out, the data are not comprehensive. This is due to non-standardisation of techniques for measurement and description and the fact that the studies inevitably involve small sample sizes. Chao and Morrey (1978) studied the three dimensional rotation of the elbow in cadaveric specimens using orthogonal X-rays and found variations in both the carrying angle and forearm rotation angle with elbow flexion. This is in contrast to the work of London (1981) and Shiba *et. al.* (1988), who maintained that the elbow is a uni-axial joint. The carrying angle is generally thought of as the adduction/abduction angle of the elbow, although precise definitions vary, and here difficulty is experienced trying to compare studies of elbow joint motion.

Chao and Morrey defined elbow motion based on the relative motion of the humerus and a single axis for the forearm, passing from the centre of the radial head through the ulnar styloid, whereas London described elbow flexion in terms of the relative motion of the humerus and ulna. Another difficulty is that it is not clear exactly how Chao and Morrey defined their humeral axis system. The *y*-axis was taken as the long axis of the humerus; the *z*-axis described as being normal to the *y*-axis and through the centre of the trochlea; and the *x*-axis as the common perpendicular. Presumably, the *z*-axis was also restricted to being in the plane of the x-ray image in the anteroposterior view, thus making it dependent on the positioning of the humerus for the x-ray.

London (1981) studied the motion of eight normal elbows (four living, four cadaveric) using lateral roentgenograms, demonstrating that motion occurs about a single axis, except at the extremes of motion. London's technique differed from previous authors in that he took the x-rays with the plane of the trochlear sulcus perpendicular to the x-ray beam. He concluded that the single axis of flexion for the elbow joint passes through the centre of the arcs formed by the trochlear sulcus and the capitellum; that the direction of the axis is between 3° and 8° internally rotated with respect to the humeral epicondyles; and 4° to 8° inverted in the frontal plane with respect to a line

perpendicular to the long axis of the humerus. He also reported that the carrying angle of the forearm does not vary with elbow flexion, remaining between 9° and 14° (mean 12°).

Shiba *et. al.* (1988) measured the geometry of the humero-ulnar articulation of four human cadaveric elbows, using a sectioning and photographing method. They found that through the capitellum and trochlea, the centres of curvature for superimposed sections did not deviate by more than 1mm. The medio-lateral axis (in this case *x*) was accurately defined, using the outermost tips of the medial and lateral epicondyles in both the coronal and transverse planes, and the axis of flexion related to this.

In light of these studies it was decided, for this study, to treat the elbow joint as uni-axial in the development of the model with the axis of rotation lying along the centres of curvature of the trochlear sulcus and capitellum.

2.5.1.2 Wrist Flexion/Extension and Radio-Ulnar Deviation

The wrist joint is sometimes described as a universal, or condyloid, joint, having two degrees of freedom: flexion-extension (F-E) and radio-ulnar (R-U) deviation (An *et. al.* (1991)). This was experimentally demonstrated by Moore *et. al.* (1993) in a paper describing a technique whereby the *minimum* number of degrees of freedom (DOF) for a joint could be determined. The technique was based around the concept of the *joint configuration space*, which is the set of all points that the parameters describing the joint attitude can attain, and the number of parameters is the number of DOF of the joint. Any point in the configuration space then fully defines the joint attitude and the number of dimensions of the space is equal to the number of DOF of the joint. Thus, a single DOF joint can be described by one parameter and the resulting configuration space plot is a line; a two DOF joint is represented by a surface and a three DOF joint by a volume. The technique was applied to six normal volunteers whose wrist motion was tracked during specified motions using an opto-electronic motion analysis system. The configuration space was then plotted and a parameterised surface fitted to establish whether the motion was two DOF. The low residual indicated that the data were described satisfactorily by the assumed number of DOF. Moore *et. al.* concluded that

the wrist joint consists of two stationary axes of motion, which may be non-intersecting and non-orthogonal.

Sarrafian *et. al.* (1976) investigated the flexion-extension motion in 55 living wrists using x-rays taken in three positions: neutral, full flexion and full extension. They found that in extension 66% of the motion occurred at the radio-carpal joint and 34% at the mid-carpal and in flexion 40% occurred at the radio-carpal and 60% at the mid-carpal, implying that two centres of rotation may exist for F-E motion.

A study of wrist motion in F-E and R-U deviation, made by Youm *et. al.* (1978) and Youm and Flatt (1979), found that the centres of rotation in both planes lay in the head of the capitate, with the axis for F-E being more proximal. This is in general agreement with the work of several other investigators, such as Andrews and Youm (1979), Volz *et. al.* (1980), Brumbaugh *et. al.* (1982) and Jackson *et. al.* (1994), although there is controversy over the exact positioning and direction of the axes and, in particular, whether or not they intersect. Andrews and Youm state that the axes are offset by approximately 5mm whereas Brumbaugh *et. al.* conclude that the axes, to all intents and purposes, intersect. It must be noted here that the latter study involved 15 normal subjects; the former only one. Brumbaugh *et. al.* also quoted the direction of the screw displacement axes, being 10° dorsal to the positive z axis in the xz plane for F-E and 12° proximal to the positive x axis in the xy plane for R-U deviation. Jackson *et. al.* used a magnetic tracking device to determine the three dimensional kinematics of two cadaver wrists and used screw displacement axes to describe the motion. Tests were carried out under simulated physiological loading by the application of forces to the main flexor and extensor tendons of the wrist.

2.5.2 MUSCULAR AND LIGAMENTOUS ANATOMY

Before a detailed description of the anatomical data used can be given, a brief introduction to the anatomy is needed. The muscles described below have been classified according to their function; inevitably, there is some overlap. Anatomy of the upper limb is shown in Figures 2.16 to 2.19.

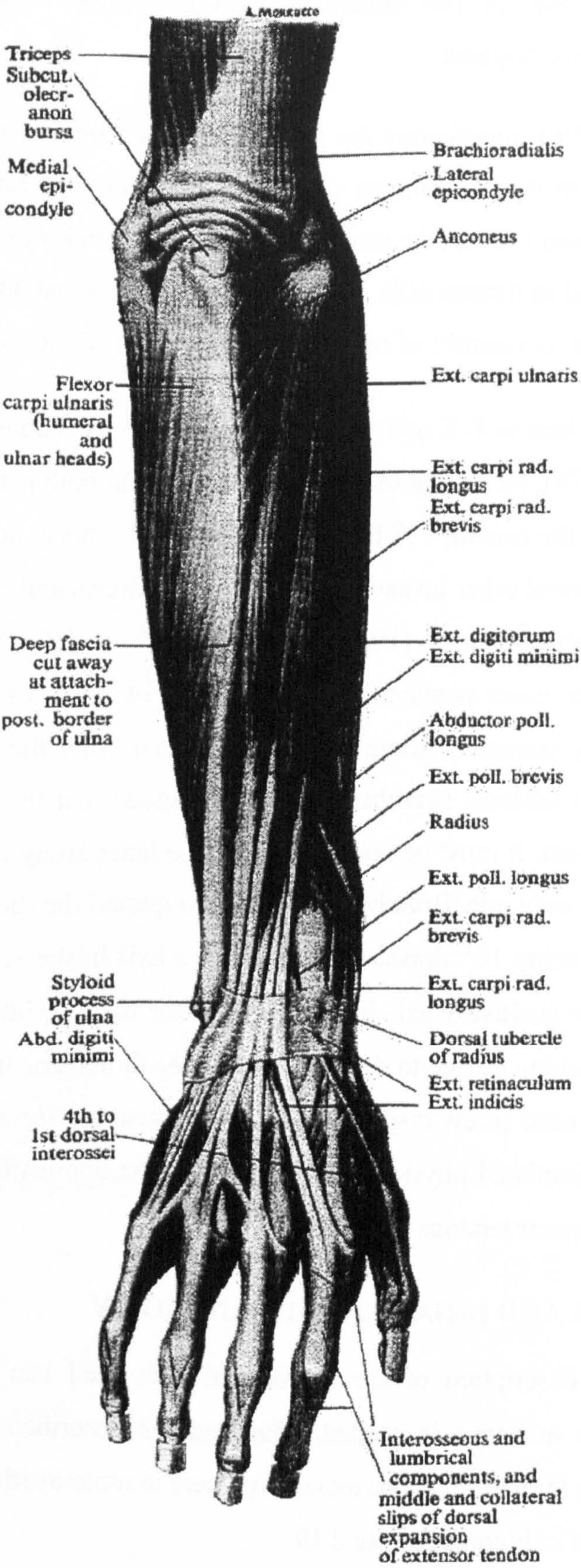

Figure 2.16 Superficial dissection of forearm - dorsal aspect (from Lockhart (1959)).

2.5.2.1 Muscles Moving the Elbow

Biceps Brachii - Divided into two heads, the long head originating from the supra-glenoid tuberosity of the scapula, the short head from the coracoid process of the scapula, the muscle's tendon passes anterior to the elbow joint in the cubital fossa to insert into the posterior border of the radial tuberosity and the fascia of proximal forearm muscles. This muscle is a powerful supinator of the forearm as well as a major flexor.

Brachialis - Originating from the anterior aspect of the distal two thirds of the humerus and medial inter-muscular septum, the muscle belly passes across the elbow joint to insert by mixed tendon and muscle fibre into the coronoid process and ulnar tuberosity. It is a major elbow flexor.

Brachioradialis - This muscle originates from the lateral supracondylar ridge of the humerus and inserts with a flat tendon into the lateral radius just proximal to the styloid process. It is primarily an elbow flexor.

Triceps Brachii - The major muscle for extension of the elbow, triceps is divided into three heads. The long head originates from the infra-glenoid tuberosity of the scapula, the lateral head from the lateral side of the humerus above the deltoid tuberosity and the medial head from the medial side of the humerus. Insertion is by a broad, flat tendon into the olecranon process.

Anconeus - A much weaker elbow extensor than triceps, anconeus originates from the posterior aspect of the lateral epicondyle and inserts on the lateral border of the olecranon process.

Pronator Teres - This muscle is divided into two heads, the superficial head originating from the common origin of the medial epicondyle and the medial supracondylar ridge and the deep head originating from the medial side of the coronoid process. The muscle inserts by a flat tendon into the lateral surface of the radius about half way along its length. Although primarily a pronator of the forearm, this muscle is also a flexor of the elbow.

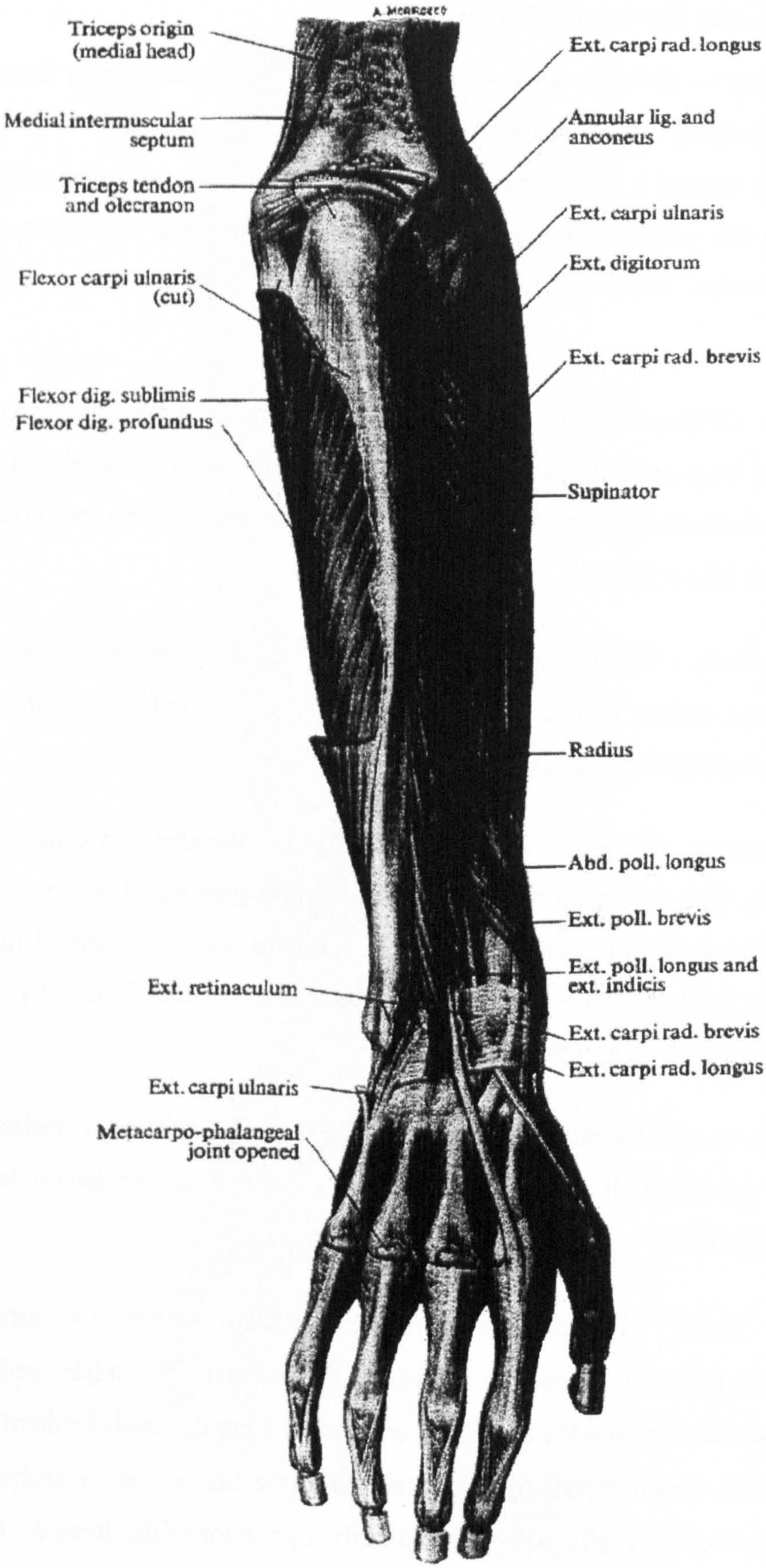

Figure 2.17 Deep dissection of forearm - dorsal aspect (from Lockhart (1959)).

Supinator - This is a broad, flat muscle passing from an extensive origin including the lateral epicondyle, the lateral ligament of the elbow, the annular ligament of the proximal radio ulnar joint and the lateral border of the ulna, posterior to the radius to insert on the lateral aspect of the radius.

Pronator quadratus - This is a small muscle located in the distal quarter of the forearm, passing from the anterior surface of the radius to the anterior surface of the ulna, which, as its name suggests, pronates the forearm.

2.5.2.2 Muscles Moving the Wrist

Flexor carpi radialis - This muscle originates from the common origin on the anterior aspect of the medial epicondyle of the humerus and inserts into the bases of metacarpals II and III and, sometimes, the scaphoid, passing through a groove in the trapezium bone. As well as flexing the wrist, this muscle also abducts the joint radially.

Flexor carpi ulnaris - Originating from the common origin, as well as the aponeurosis attached to the medial border of the olecranon and the upper two thirds of the posterior surface of the ulna, the muscle inserts into the carpus via the pisiform, a sesamoid bone. This muscle is also an ulnar adductor of the wrist.

Although these two muscles are the only muscles whose prime function is wrist flexion, many of the muscles controlling grip are also wrist flexors. These will be discussed later.

Extensor carpi radialis brevis - This muscle originates from the common extensor tendon from the lateral epicondyle and the lateral ligament of the elbow and inserts into the dorsal aspects of the base of the third metacarpal .

Extensor carpi radialis longus - Originating from the lateral supracondylar ridge of the humerus, this muscle inserts into the dorsal aspect of the base of the second metacarpal. The tendons of brevis and longus run side by side in the distal half of the forearm. As well as extending the wrist, both muscles radially abduct the joint.

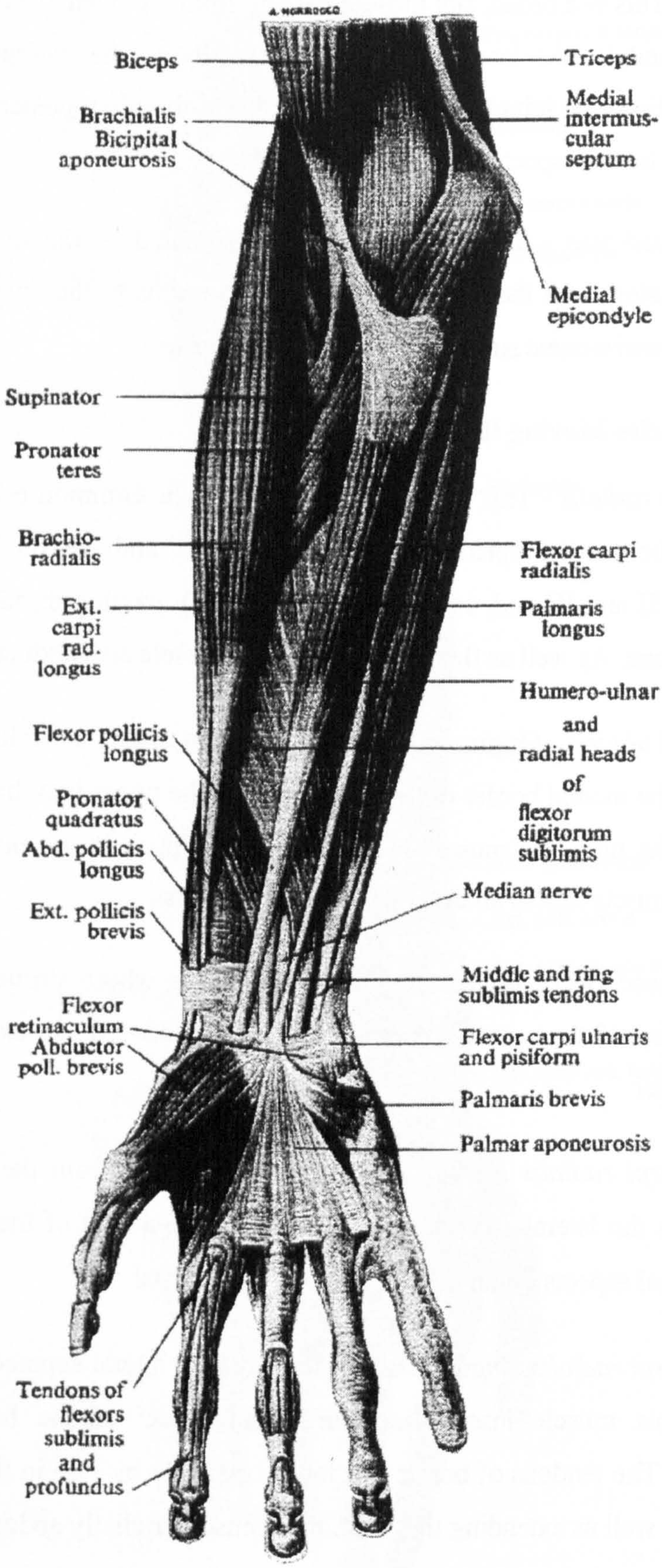

Figure 2.18 Superficial dissection of forearm - anterior aspect (from Lockhart (1959)).

Extensor carpi ulnaris - This muscle originates from the common extensor origin and the posterior border of the ulna and inserts into the medial aspect of the base of the fifth metacarpal, causing ulnar deviation as well as wrist extension.

2.5.2.3 The Muscles Controlling Grip

Flexor digitorum profundus - This muscle originates from the medial surface of the olecranon, the upper two thirds of the medial and anterior surfaces of the ulna and the adjacent interosseous membrane. The tendon for the index finger separates in the forearm, with the remaining tendon splitting into three for the other three fingers just above the flexor retinaculum. The four tendons then pass through the carpal tunnel and insert into the distal phalanges. The primary action of flexor digitorum profundus is flexion of the distal interphalangeal (DIP) joint, although inevitably it also produces flexion of the proximal interphalangeal (PIP), metacarpophalangeal (MCP) and wrist joints.

Flexor digitorum superficialis - Arising from the common flexor origin, the medial ligament of the elbow joint, the medial border of the coronoid process and the anterior oblique line of the radius, the muscle gives rise to four independent tendons crossing the wrist joint in the carpal tunnel superficial to those of profundus and inserting into the palmar aspect of the middle phalanx of each of the four digits. Its primary action is to flex the PIP, although a tendency to flex the MCP and wrist joints also results.

Flexor pollicis longus - The origin of this muscle is the anterior surface of the radius, between the insertions of *biceps* and *pronator quadratus* and the adjacent interosseous membrane. It passes deep to the flexor retinaculum along the medial side of the thenar eminence and inserts on the base of the distal phalanx of the thumb, being a flexor of the thumb interphalangeal (IP) and MCP joints.

Extensors digitorum communis, digiti minimi and indicis - The first two of these muscles originate from the common extensor origin on the lateral epicondyle of the humerus, the *communis* splitting into four tendons just proximal to the wrist and inserting into the bases of the middle phalanges, and *digiti minimi* providing a separate tendon for insertion into the little finger. The latter, *extensor indicis* arises from the

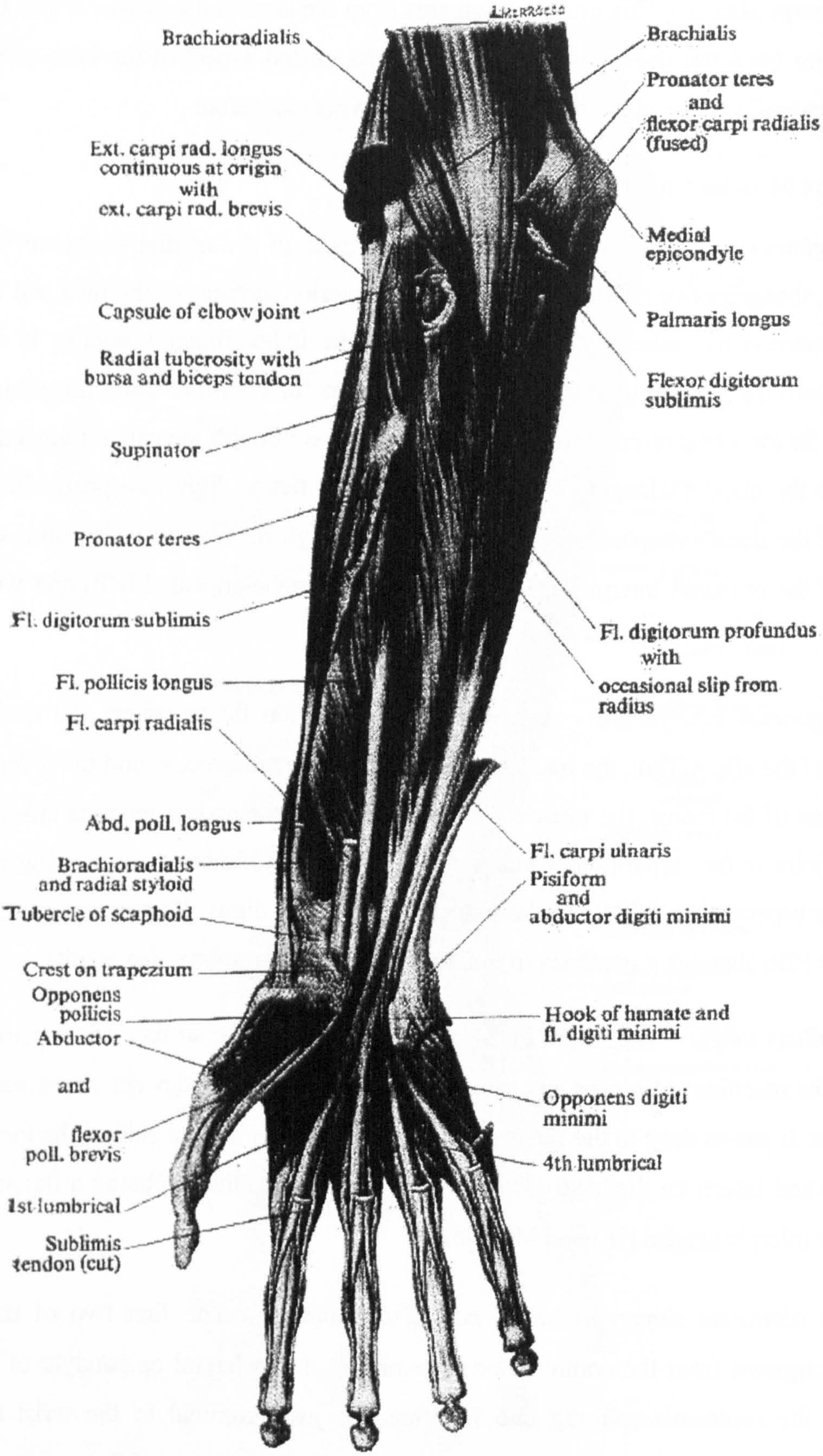

Figure 2.19 Deep dissection of forearm - anterior aspect (from Lockhart (1959)).

posterior ulna and interosseous membrane and inserts into the middle phalanx of the index finger. All these tendons except digiti minimi pass through a common synovial sheath. Arising from the insertion of these tendons is the dorsal digital expansion, which inserts into the distal phalanges.

Extensor pollicis longus - Originating from the back of the ulna, this muscle passes deep to the extensor retinaculum and inserts into the base of the distal phalanx. As well as extending the IP and MCP joints of the thumb, the muscle also tends to oppose the action of *opponens pollicis.*

Extensor pollicis brevis - This muscle arises from the radius and the interosseous membrane and inserts into the base of the first phalanx of the thumb.

Abductor pollicis longus - Arising from the posterior surface of the ulna, the interosseous membrane and the posterior radius, just above the origin of extensor pollicis brevis, this muscle inserts into the lateral aspect of the base of the metacarpal of the thumb.

2.5.2.4 The Ligaments of the Elbow

Radial (lateral) ligament complex – Figure 2.20 shows the lateral ligament complex, which comprises four parts. The lateral ulnar collateral ligament is the only true collateral ligament (that is, one which originates directly from and inserts directly into bone) and passes from the lateral epicondyle of the humerus to the lateral border of the ulnar. This ligament has been shown by O'Driscoll *et. al.* (1991) to be a prime stabiliser of the elbow under varus loading. The *annular ligament* is attached to the margins of the radial notch of the ulna, and surrounds the radial head, which rotates in it. The *radial collateral ligament* is a flattened band attached to the humerus just below the common extensor origin and inserting into the *annular ligament*. The *accessory collateral ligament* passes from the annular ligament to the insertion of the *lateral ulnar collateral ligament*, but is not always present.

Ulnar (medial) ligament complex – Figure 2.21 shows the three bands of the medial ligament complex. The strongest of these, the *anterior* band, runs from the medial

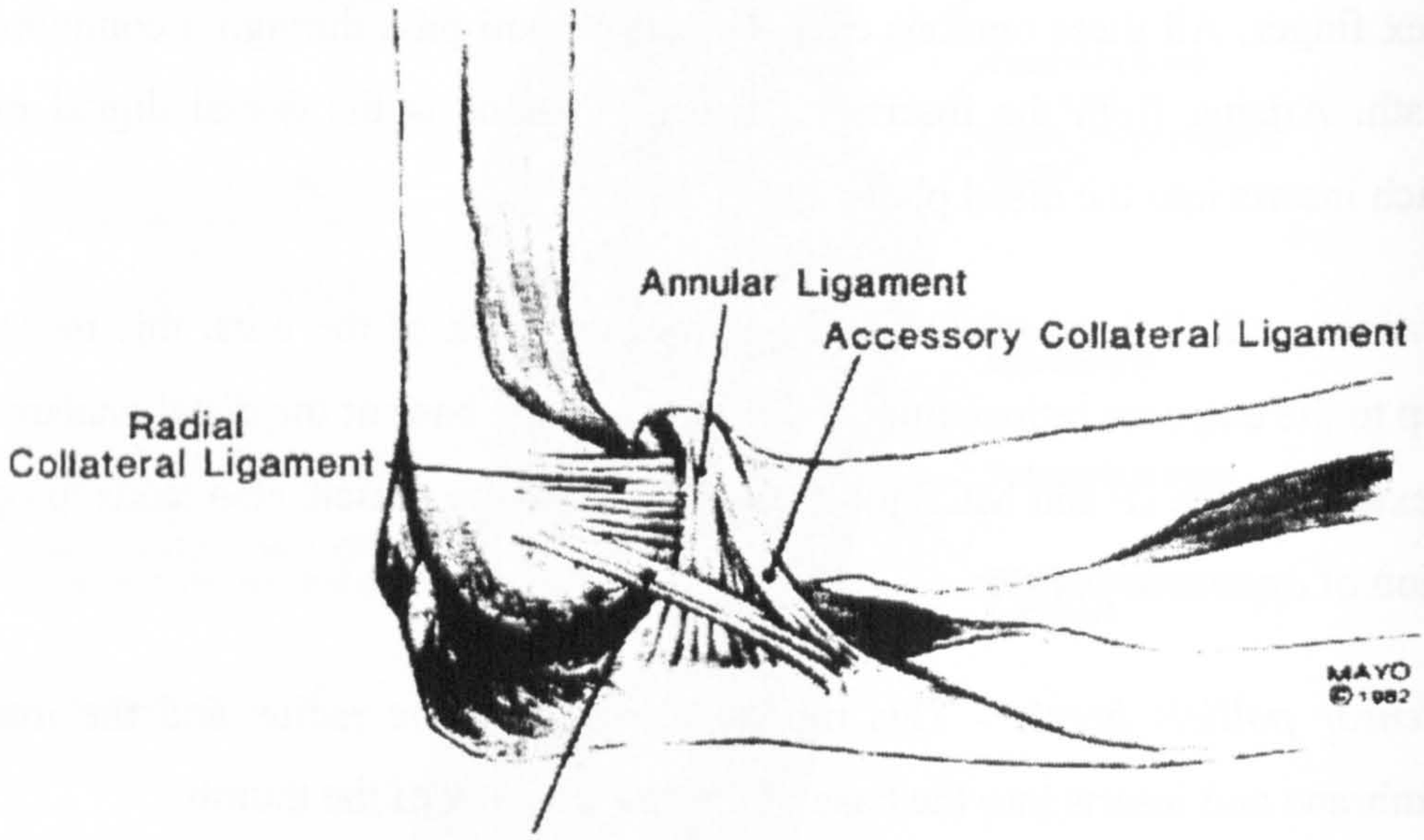

Figure 2.20 Drawing of the lateral elbow ligament complex from Morrey (1993).

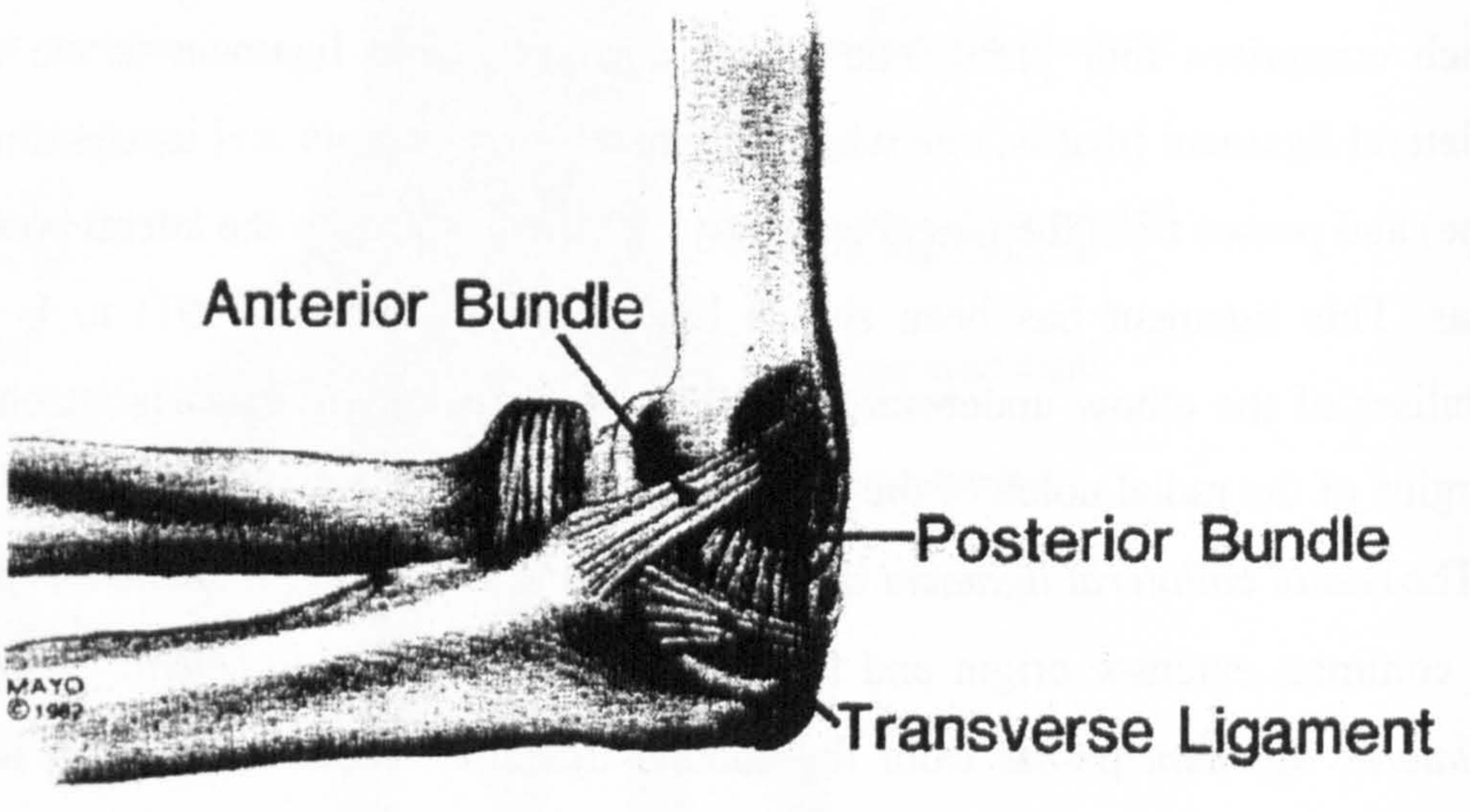

Figure 2.21 Drawing of the medial elbow ligament complex from Morrey (1993).

epicondyle of the humerus to the sublime tubercle on the medial border of the coronoid process. The *posterior* band runs from the coronoid process to the medial border of the olecranon and the transverse band spans the medial olecranon border. The latter band is functionally less important than the other two, and is often barely defined (Morrey (1993)).

2.5.2.5 The Ligaments of the Wrist

A detailed description of the inter-carpal ligaments is outwith the scope of this study, therefore only the proximal extrinsic ligaments will be described here. It is, however, worth expanding a little on the descriptions found in most anatomy texts, and the following information comes from Taleisnik (1976). Figure 2.22 shows the ligamentous anatomy.

Radial collateral ligament - runs from the anterior margin of the radial styloid to the scaphoid, trapezium and first metacarpal.

Palmar radio-carpal ligaments - are divided into superficial and deep. The superficial fibres run from the radius to the capitate and lunate in a V shape. The deep fibres are radio-scapho-capitate, radio-lunate and radio-scapho-lunate.

Ulno-carpal complex - is a group consisting of several components. The ulno-carpal meniscus is a cartilaginous structure separating the ulna and carpus which, in fact, is strongly bound to the ulno-dorsal corner of the radius and inserts into the ulnar border of the triquetrum. The triangular fibro-cartilage (TFC) shares this origin and inserts into the base of the ulnar styloid. The TFC is also joined to the carpus by the ulno-lunate ligament.

Ulnar collateral ligament - although distinguished as a ligament of the dorsum of the wrist, this is simply a thickening of the joint capsule and contributes little to wrist joint stability.

Dorsal radio-carpal ligament - originates from the radius and inserts into the lunate and triquetrum, and is relatively weak.

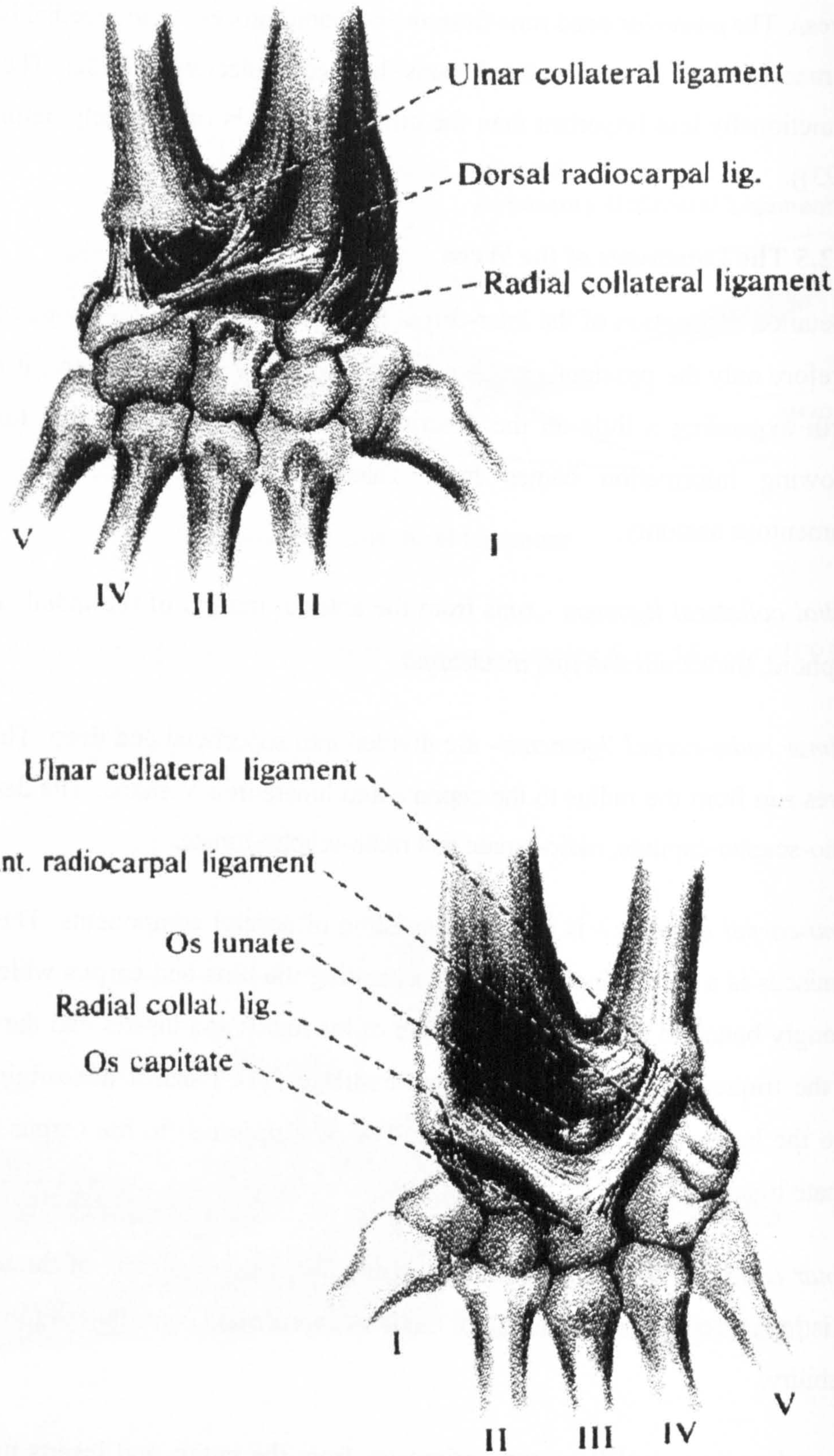

Figure 2.22 The ligamentous anatomy of the carpus (from Hunter et. al. (1995)).

2.5.3 MOMENT ARMS AND LINES OF ACTION

2.5.3.1 Magnetic Resonance Imaging (MRI)

Recent advances in imaging technology have opened the possibility of using *in vivo* data for the origin and insertion points and lines of action of muscles, tendons and ligaments. The fact that the muscles would have tone, and subjects could be imaged in functional positions, for example gripping, would give rise to superior data to that obtained from cadaveric studies.

Few studies involving the calculation of *in vivo* moment arms have been reported. Rugg *et al.* (1990) calculated in vivo moment arms of the tibialis anterior and Achilles tendons from sagittal plane MRI scans. Koolstra *et al.* (1988) presented a method for the calculation of muscle lines of action from MRI or CT scans which avoids the need to align the plane of imaging with the line of action of the muscle. He showed that if a short, thick muscle was imaged oblique to its line of action and this line was determined from the positions of the centroids of each section, then significant errors could be introduced. This is not a problem for muscles that are tendinous as they cross the joints but could be a problem for a muscle such as brachialis which is fleshy as it crosses the elbow joint. An iterative procedure to overcome this was presented by Koolstra *et. al.*

At present, a number of problems are associated with obtaining suitable data from the technique. In order to achieve sufficient resolution and high signal/noise ratio it is necessary to have one or more of the following:

a long acquisition time;

very thick slices;

specialised equipment.

The first of these can lead to the introduction of motion artifacts due to subject discomfort and the second reduces the reliability of any measurements taken from the images. The third point further reduces the availability of suitable scanners, access to which is already difficult due to the high operating costs and heavy clinical demand. It

had been hoped that MRI would be used for the determination of anatomical geometry in this study, however the difficulties outlined above conspired to prevent this, and cadaveric data from the literature had to be used.

2.5.3.2 Moment Arms and Lines of Action for Muscles Crossing the Elbow

Pigeon *et. al.* (1996) compiled the data of several other investigators, including Amis *et. al.* (1979), Horii *et. al.* (1993) and Winters and Kleweno (1993), to obtain the moment arms (MA) of 13 arm and forearm muscles. They described the flexion-extension moment arm versus elbow flexion angle in terms of polynomial equations, of 2nd, 3rd and 5th order. The R^2 value for the correlation was in all cases greater than 0.9904, except for anconeus for which a value of 0.9349 was obtained. The data of Amis *et. al.*, whilst being a comprehensive study of the structures involved in elbow function, relied on the accurate measurement of only one, embalmed cadaver. The data from Pigeon *et. al.* for flexion-extension moment arms were used for this study as they were the most comprehensive, and were available in an accessible form.

Data on the moment arms in the other two planes were harder to find in the literature, but some studies exist. Seireg and Arvikar (1989) published data on the three-dimensional origin and insertion points of muscles of the upper limb, modelling the muscles as straight lines from origin to insertion. The model was comprehensive, including a large number of muscle units, but the measurements were based on the scale drawings of Braus (1954), rather than being directly measured from anatomical specimens. An *et. al.* (1981) adopted a serial cross-sectioning technique, and studied six unembalmed upper extremity specimens, to determine the moment arms of muscles crossing the elbow. Results for a large number of muscles were quoted in the study and moment arm values were given with the arm in six different positions, encompassing three flexion angles and three rotation positions. These data were used for the current study, as they offered data on all the required muscles, and the lack of a sufficient number of elbow joint angles being studied was overcome by interpolation. In addition to moment arm data, it is also essential to know the lines of action of the muscles in order to calculate the force equilibrium. Amis *et. al.* (1980) gave direction cosines of

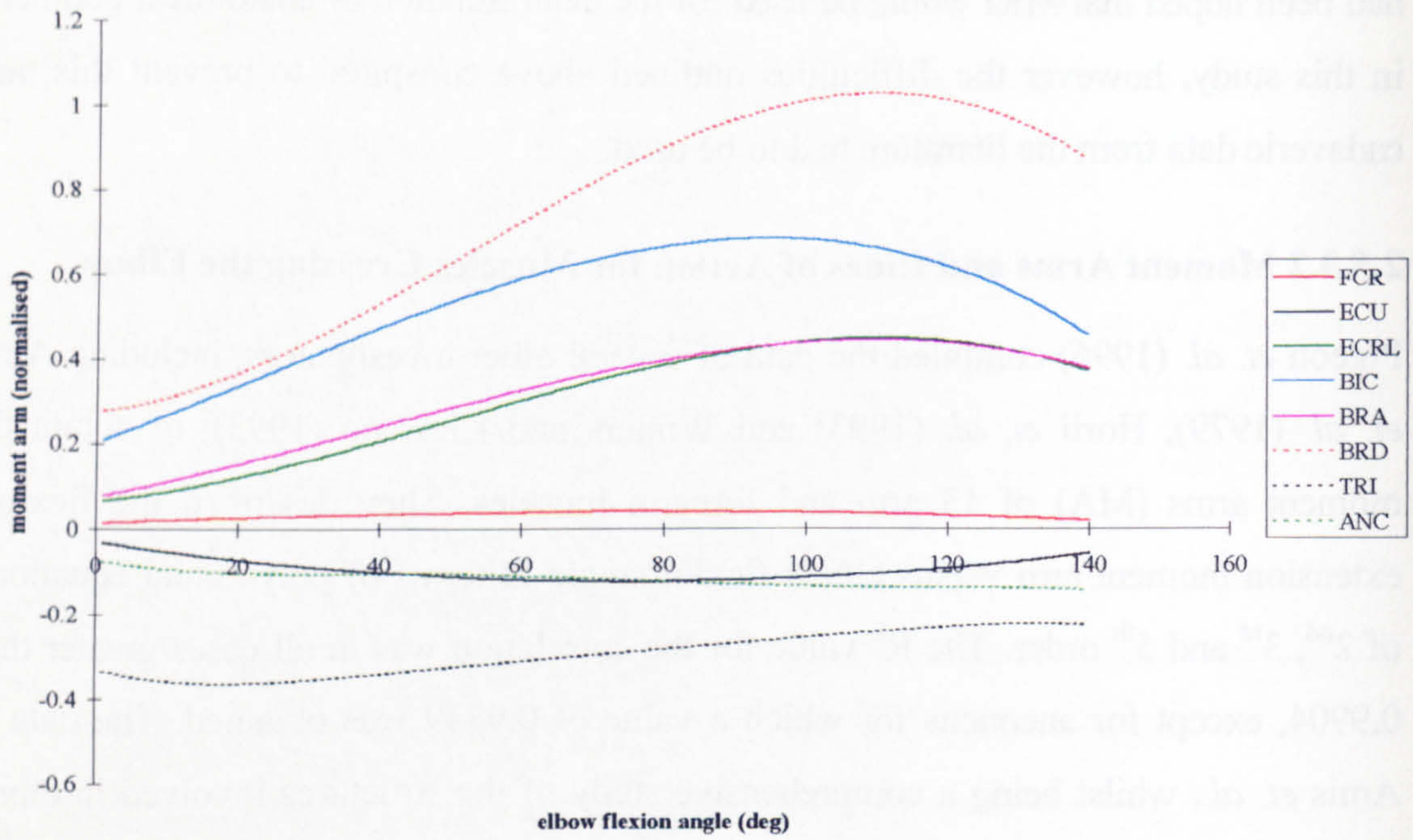

Figure 2.23 Graph of flexion-extension moment arms for elbow muscles, against elbow flexion angle.

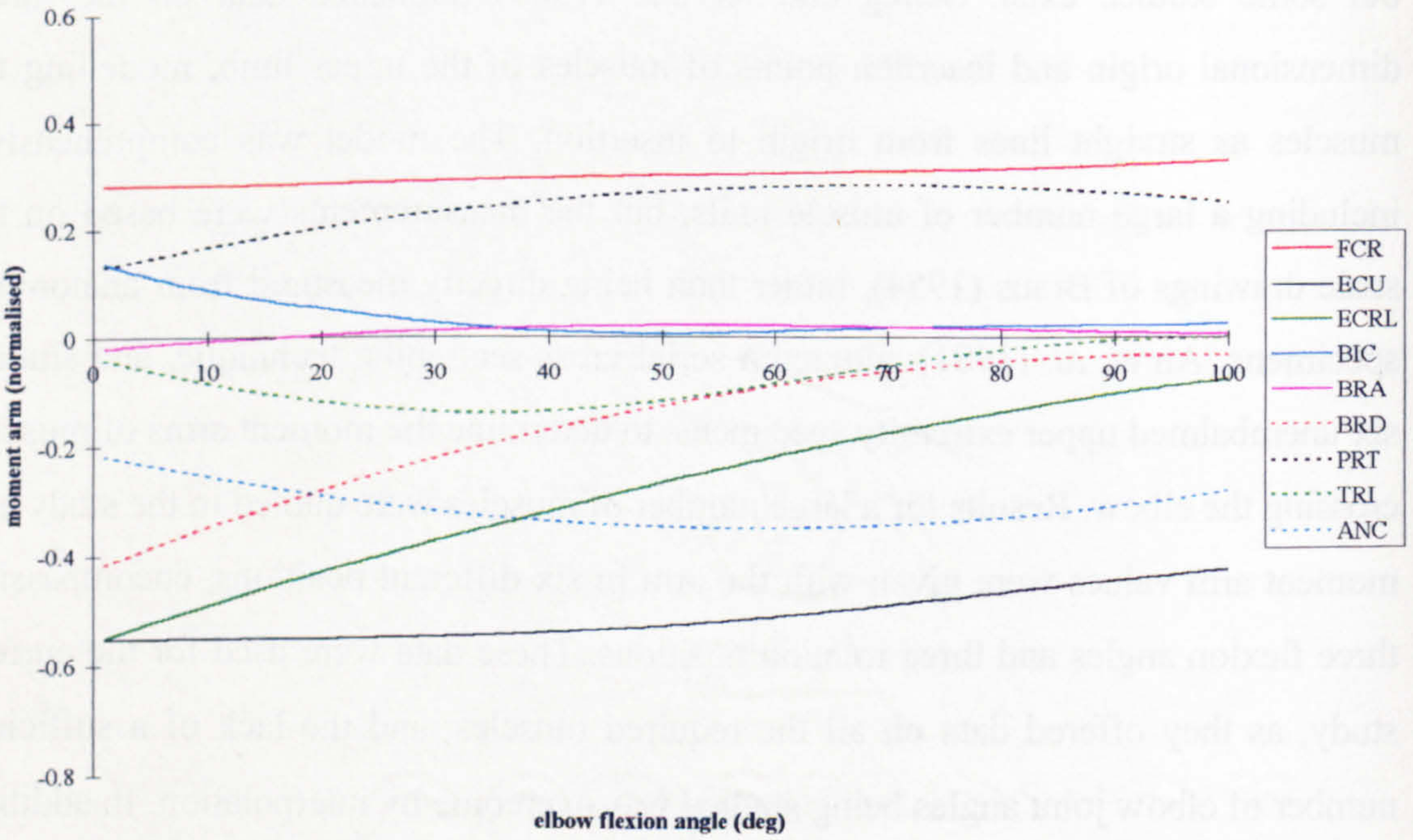

Figure 2.24 Graph of abduction-adduction moment arms for elbow muscles, against elbow flexion angle.

elbow muscles with respect to the bones at various flexion angles, and these were used in the current study.

Other studies on moment arms have been carried out by a number of authors, including Murray *et. al.* (1995), Gonzalez *et. al.* (1996) and Gerbeaux *et. al.* (1996). While each of these is a thorough study of the muscles involved, the muscles included did not extend to cover all the muscles included in the current study, and so the data were not used.

In nearly all studies of anatomical geometry reported in the literature, there is a failure to report normalising factors that can be used to scale the data to a particular subject. In the current study, data from the literature were normalised by taking the largest dimension quoted, for example the distance between tendons arising from the medial and lateral epicondyles, and scaling these to external dimensions, such as measured epicondylar width, using drawings or anatomical images. The data were then scaled to individual subjects by the measurement of external dimensions during the tests.

Three-dimensional moment arms for the muscles crossing the elbow, based on the aforementioned studies, are shown in Figures 2.23 to 2.25.

2.5.3.3 Moment Arms and Lines of Action for Muscles Crossing the Wrist

Extensive data on MA of muscles crossing the wrist were obtained from Buchanan (1996). Buchanan reported MA of 15 forearm muscles with elbow and wrist joint angles, also splitting flexor digitorum profundus and flexor digitorum superficialis into their individual tendons. A comparison of Buchanan's data for the five prime wrist motors with the work of two other investigators (Loren (1995) and Amis (1978) is given in Figure 2.26. Data from Horii (1993) were also studied (but are not shown in the figure) and found to be similar to those of Loren and Buchanan although the values were smaller. Amis' data was recorded only with the joint in the neutral position and the relative magnitudes of the FCR and ECRB tendons do not agree with the other studies. As Buchanan's data were far more comprehensive than others, both in terms of the number of muscles measured and in terms of the range of joint angles over which they were measured, it was decided to use these data in the current wrist joint model.

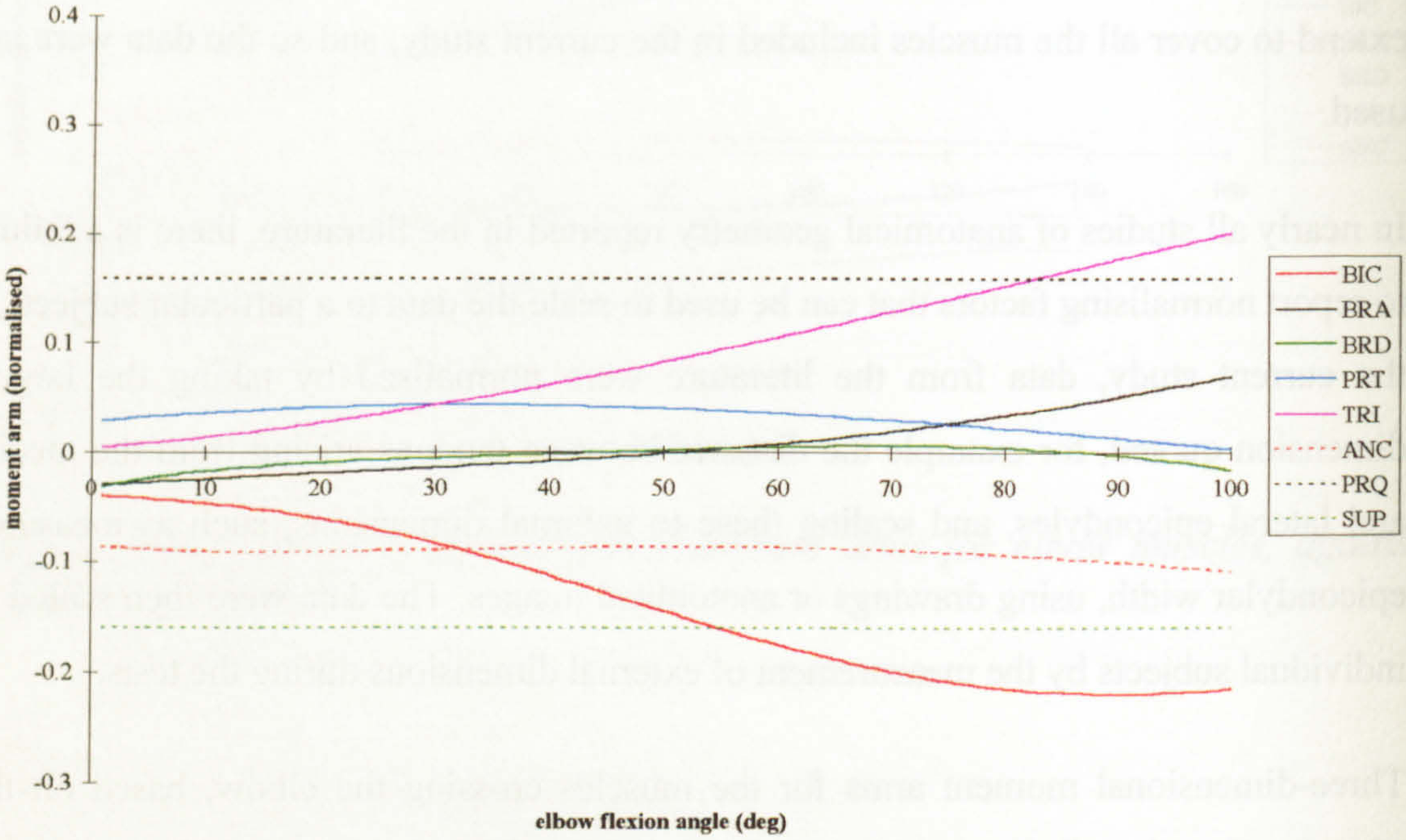

Figure 2.25 Graph of internal-external rotation moment arms for elbow muscles, against elbow flexion angle.

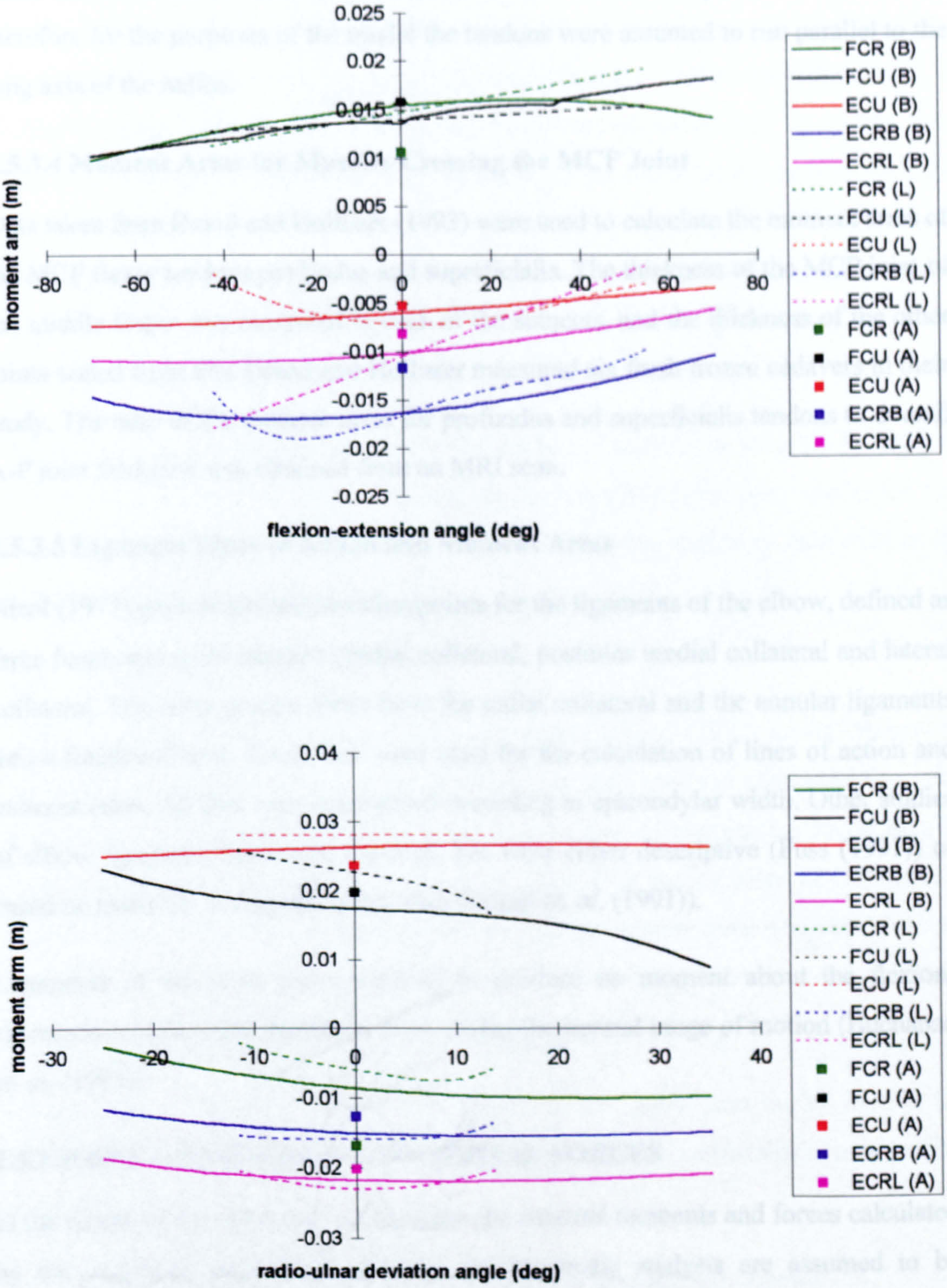

Figure 2.26 Comparison of wrist joint moment arm data from three studies (Buchanan (1996), Loren (1995) and Amis (1978)).

Insufficient data were available on either lines of action, or origin and insertion points from which to derive lines of action, of the tendons crossing the wrist joint and therefore for the purposes of the model the tendons were assumed to run parallel to the long axis of the radius.

2.5.3.4 Moment Arms for Muscles Crossing the MCP Joint

Data taken from Brand and Hollister (1993) were used to calculate the moment arms of the MCP flexor tendons profundus and superficialis. The thickness of the MCP joint of the middle finger was measured in each of the subjects, and the thickness of the other joints scaled from this. Brand and Hollister measured six fresh frozen cadavers in their study. The ratio of the moment arms for profundus and superficialis tendons to overall A-P joint thickness was obtained from an MRI scan.

2.5.3.5 Ligament Lines of Action and Moment Arms

Nicol (1977) gave origin and insertion points for the ligaments of the elbow, defined as three functional units: anterior medial collateral, posterior medial collateral and lateral collateral. The latter groups fibres from the radial collateral and the annular ligaments into a functional unit. These data were used for the calculation of lines of action and moment arms. All data were normalised according to epicondylar width. Other studies of elbow ligaments have been reported, but were either descriptive (Fuss (1991)) or based on materials testing and kinematics (Regan *et. al.* (1991)).

Ligaments of the wrist were assumed to produce no moment about the flexion-extension or radio-ulnar deviation axes, within the normal range of motion (Buchanan *et. al.* (1993)).

2.5.4 JOINT GEOMETRY AND INTERNAL FORCES

In the model of the elbow and wrist joints, the external moments and forces calculated by the combined application of force and kinematic analysis are assumed to be balanced by the moments and forces generated by internal structures such as the muscles, ligaments and joint surfaces.

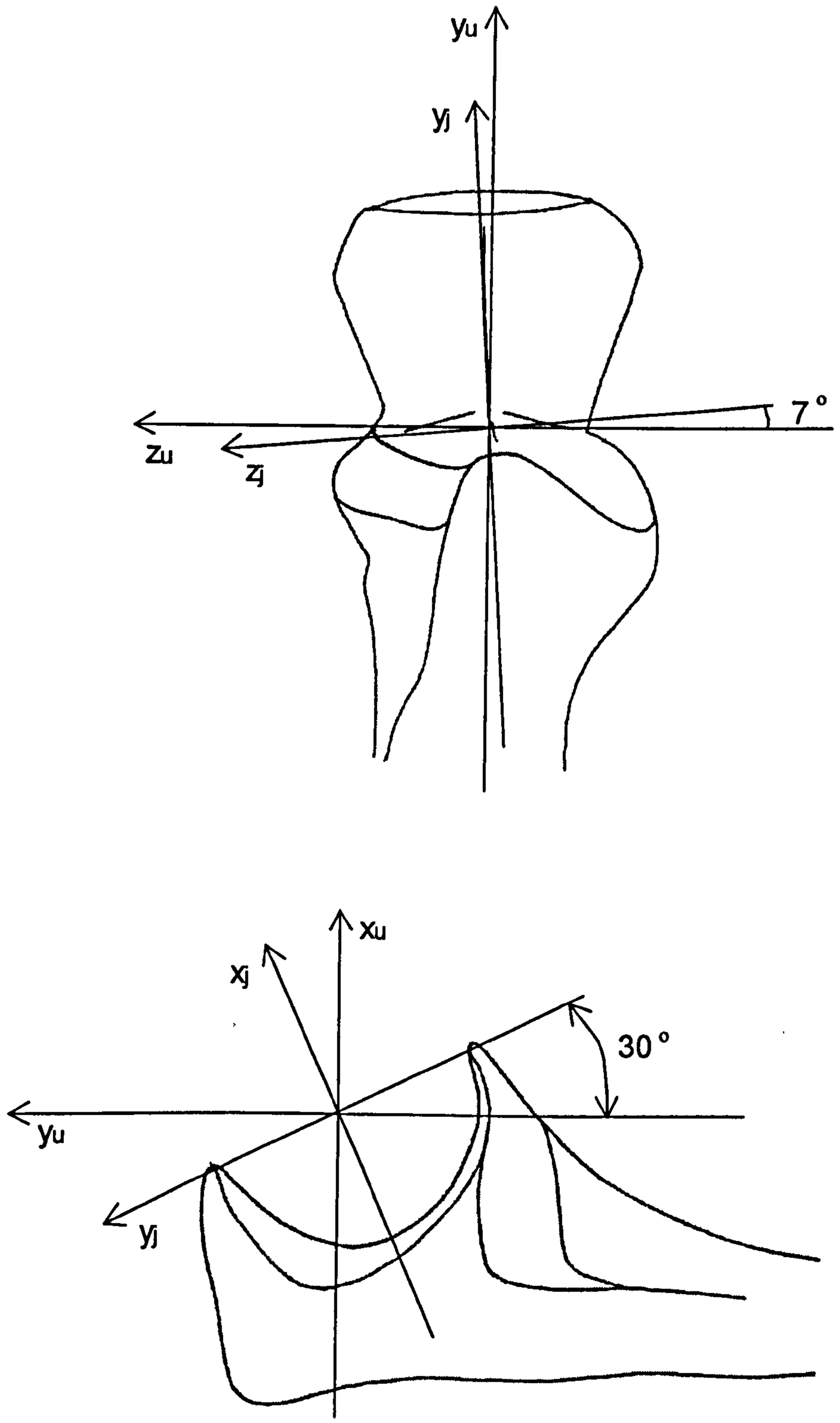

Figure 2.27 Diagram showing the rotation of joint axes in the trochlea, as measured by Nicol (1977).

Knowledge of the geometry of the joints and their structures combined with data on external loading allows the formulation of a set of equations defining the equilibrium of the system. Solution of these equations gives the values of the loads on the internal structures and it is this set of equations that constitutes the 'model' thus far referred to. For each plane, (sagittal, frontal and transverse) three equations may be written. One balancing moments in that plane and two equating the forces along each of the axes. To calculate the moments due to muscle, ligament and joint forces, knowledge of each structure's moment arm about the centre of rotation is needed. To balance the forces in a particular direction, knowledge of the structure's orientation with respect to that direction is needed. These data are obtained from the literature.

Whilst it is recognised that the model should be as realistic as possible in order to provide meaningful data, some simplifying assumptions have been made for two reasons: that the model be mathematically soluble and that sufficient data exist in the literature to allow its completion.

2.5.4.1 Elbow Joint Geometry

A detailed study of elbow joint geometry was made by Nicol (1977) for the design of a prosthesis, in which the force on the trochlea was split into two components, medial and lateral. Nicol measured the geometry of four cadaver elbows and found that the joint axes were rotated relative to the ulnar axes by 30° in the x-y plane and 7° in the y-z plane. Thus, joint forces given in this 'joint' axis system were translated into the ulnar axis system before being equated to external and muscle forces measured in the ulnar system. The relative rotation of joint axes is shown in Figure 2.27.

Figures 2.28 to 2.30 show schematic diagrams of the elbow joint model used in this study and the forces and moments acting on it. The following abbreviations are used in these diagrams:

F_X, F_Y, F_Z are external forces applied to the limb, in the ulnar axis system.

M_X, M_Y, M_Z are external moments applied to the limb, in the ulnar axis system.

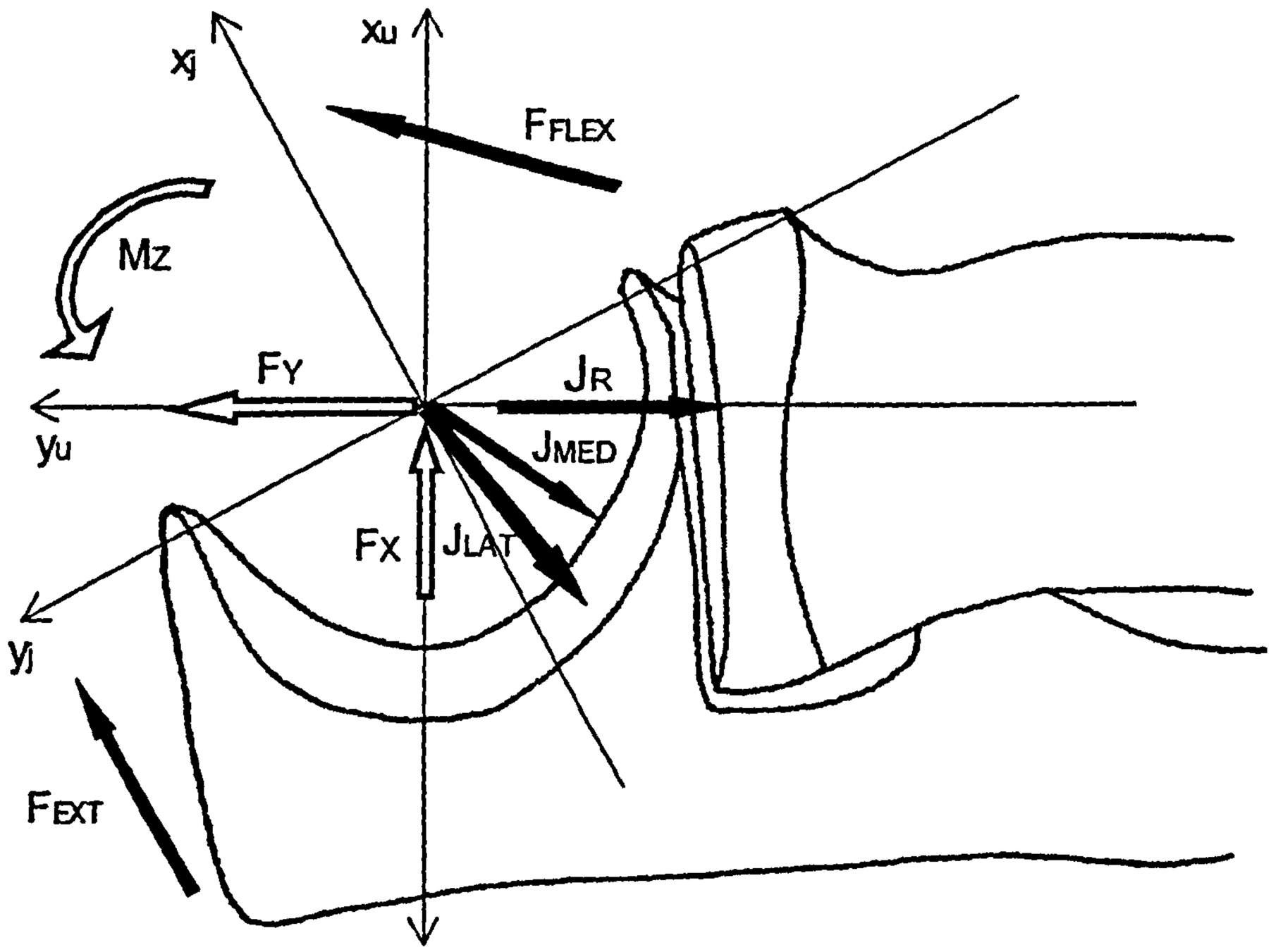

Figure 2.28 System of forces and moments acting on the elbow in the sagittal plane.

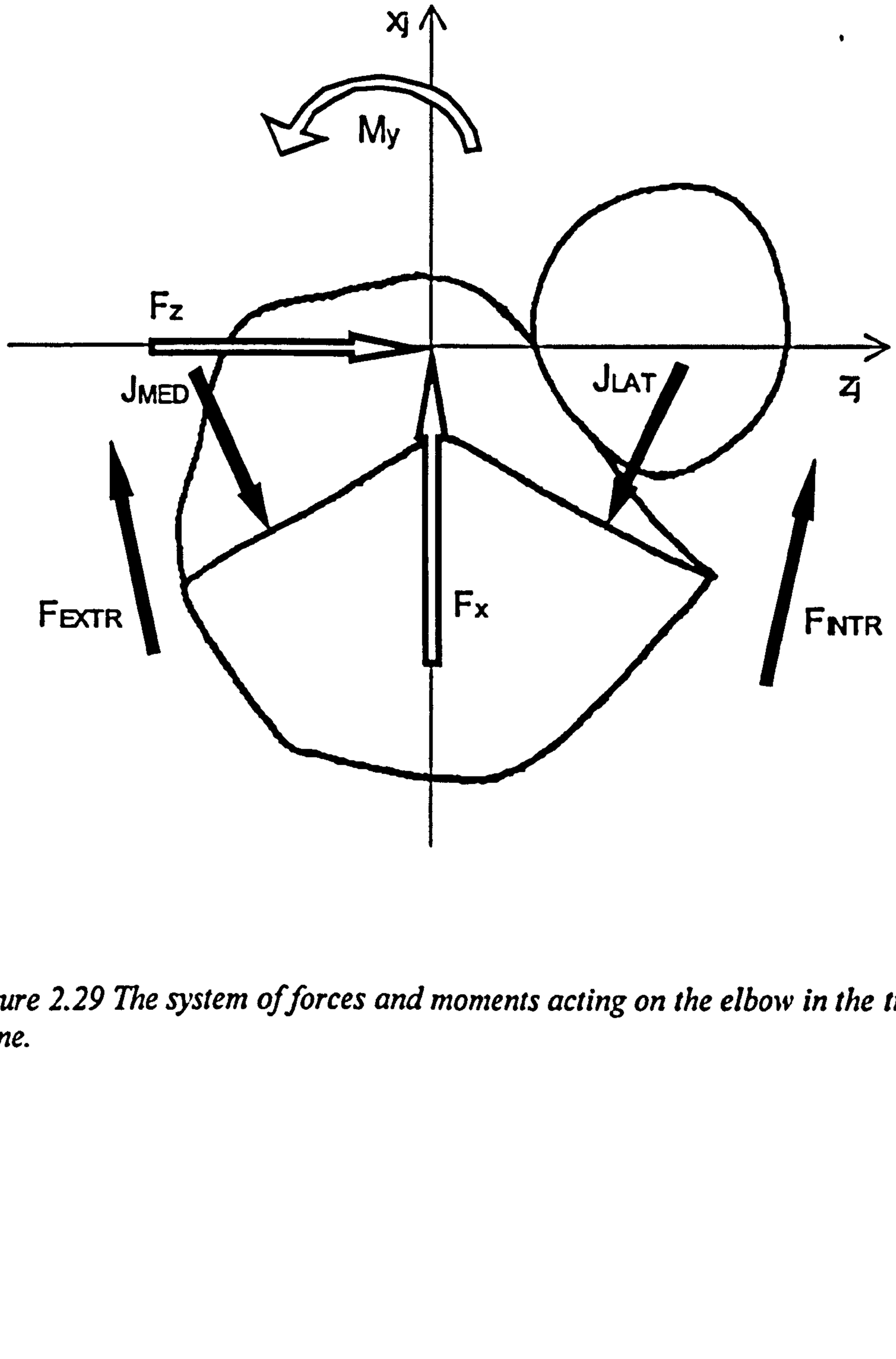

Figure 2.29 The system of forces and moments acting on the elbow in the transverse plane.

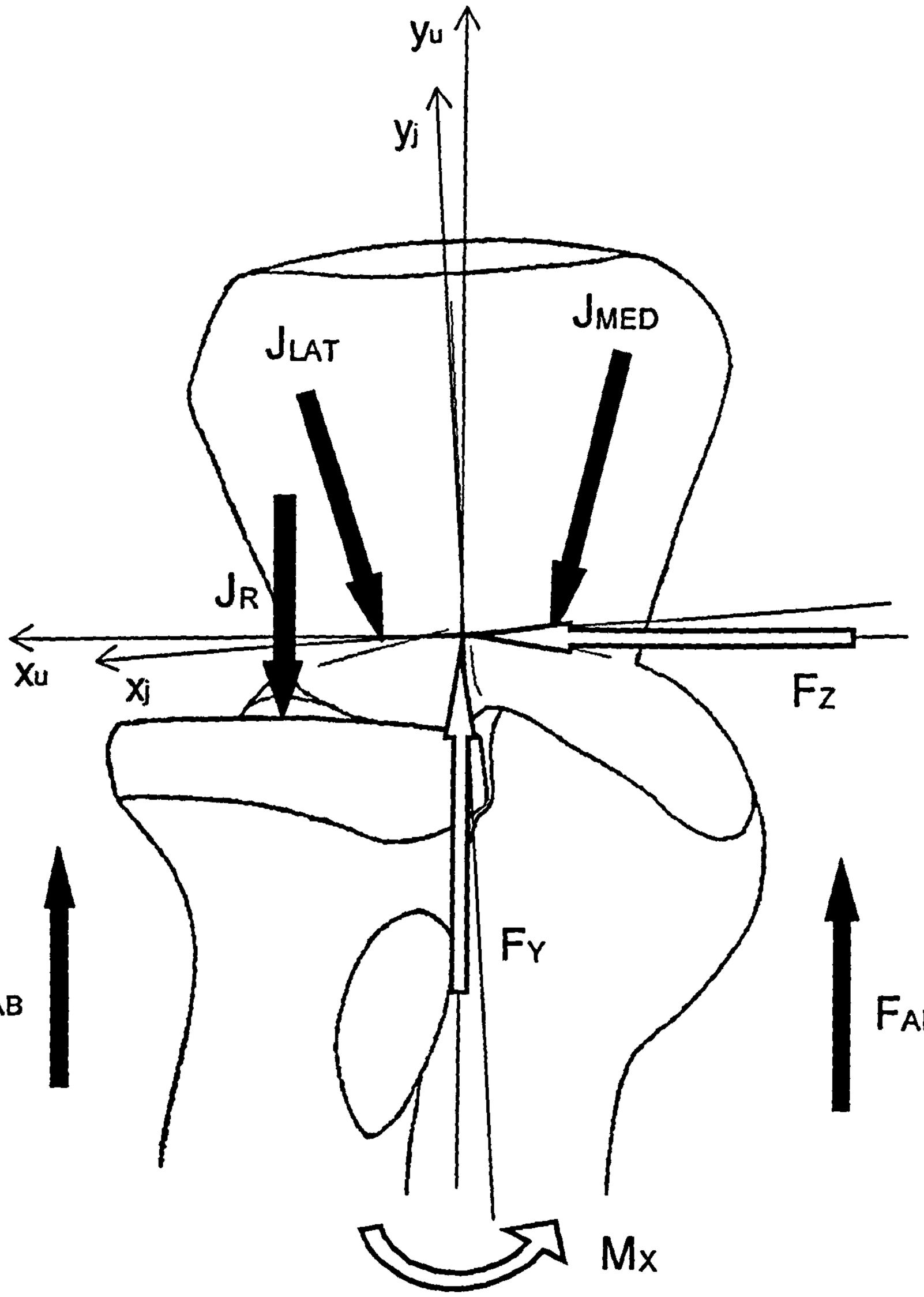

Figure 2.30 The system of forces and moments acting on the elbow in the frontal plane.

J_{LAT} and J_{MED} are forces applied to the trochlea lateral and medial facets respectively, in the joint axis system.

J_R is the force applied to the radial head, assumed to be parallel to the long axis of the ulna.

F_{FLEX} and F_{EXT} are the combined forces of the muscles and ligaments, taking account of their respective lines of action and moment arms, grouped into flexors and extensors respectively. They are too numerous to show individually.

F_{EXTR} and F_{INTR} are external and internal rotator groups, similar to above.

F_{AB} and F_{AD} are abduction and adduction groups as above.

Figure 2.28 shows the model in the sagittal plane. The forces acting on the trochlea and the radial head are assumed to pass through the centre of rotation in the sagittal plane, and thus have no moment effect. It is also assumed that there is no moment effect due to the ligaments, as they originate from a point approximately on the flexion-extension axis.

Figure 2.29 shows the model in the transverse plane. The position of the centre of pressure of the forces along the trochlear surface was calculated by Nicol (1977), and is shown in Figure 2.31 The radial head force has no moment effect in this plane, nor any force contribution.

Figure 2.30 shows the model in the frontal plane. The lever arm for the radial head force about the joint centre is was also obtained from Nicol (1977), and is calculated as 0.3 times the epicondylar width.

For the purposes of reporting, the medial and lateral elbow joint forces are given as single forces acting in a given direction, where the angle quoted is measured anticlockwise from the positive joint x-axis. The resultant joint forces were allowed to take a direction from +80° to -80° to the zero degree direction given (Figure 2.32), ensuring stability in the humero-ulnar joint, and were 25° out of the x-y plane as shown in Figure 2.29. For ease of solution, the forces were split into components along

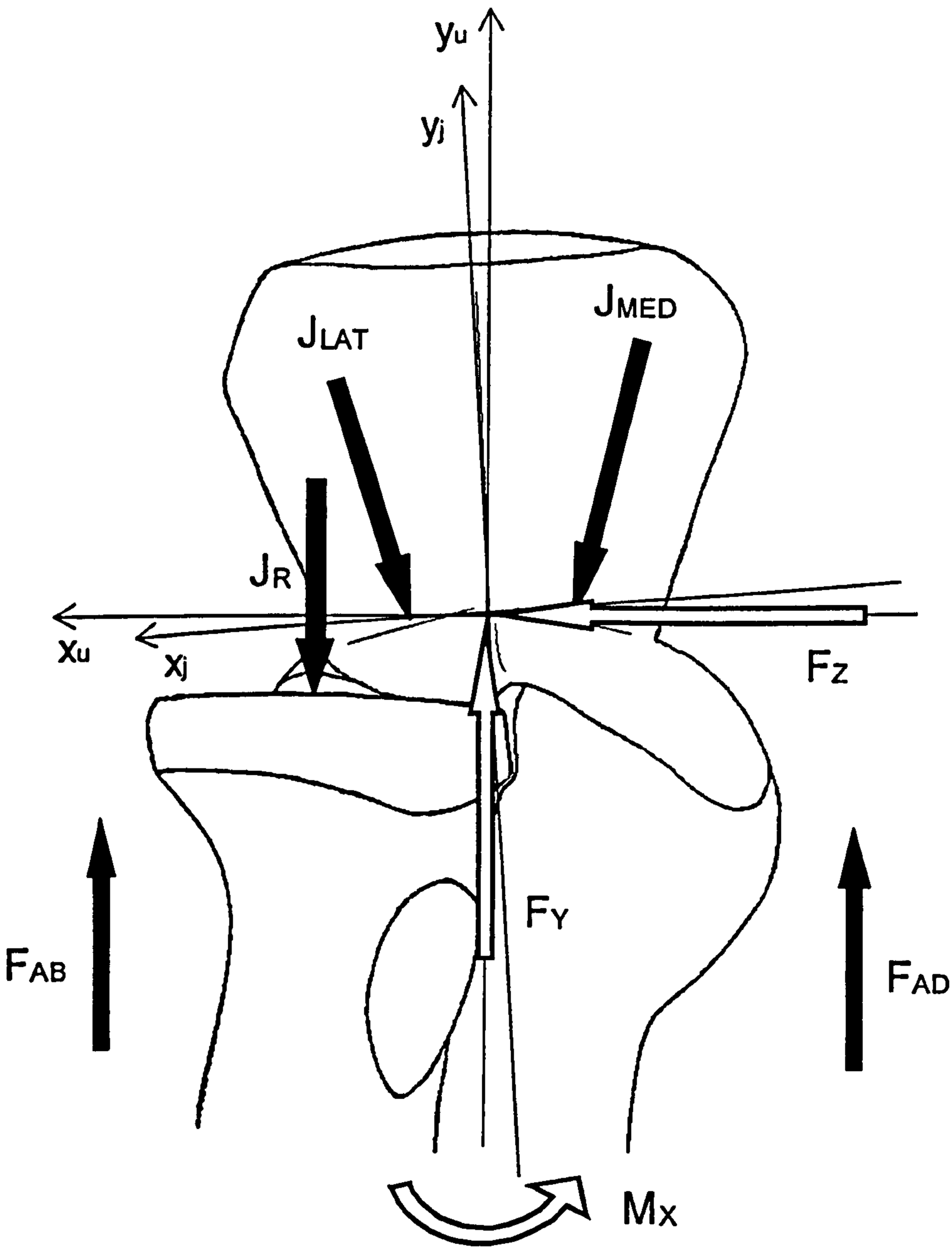

Figure 2.30 The system of forces and moments acting on the elbow in the frontal plane.

J_{LAT} and J_{MED} are forces applied to the trochlea lateral and medial facets respectively, in the joint axis system.

J_R is the force applied to the radial head, assumed to be parallel to the long axis of the ulna.

F_{FLEX} and F_{EXT} are the combined forces of the muscles and ligaments, taking account of their respective lines of action and moment arms, grouped into flexors and extensors respectively. They are too numerous to show individually.

F_{EXTR} and F_{INTR} are external and internal rotator groups, similar to above.

F_{AB} and F_{AD} are abduction and adduction groups as above.

Figure 2.28 shows the model in the sagittal plane. The forces acting on the trochlea and the radial head are assumed to pass through the centre of rotation in the sagittal plane, and thus have no moment effect. It is also assumed that there is no moment effect due to the ligaments, as they originate from a point approximately on the flexion-extension axis.

Figure 2.29 shows the model in the transverse plane. The position of the centre of pressure of the forces along the trochlear surface was calculated by Nicol (1977), and is shown in Figure 2.31 The radial head force has no moment effect in this plane, nor any force contribution.

Figure 2.30 shows the model in the frontal plane. The lever arm for the radial head force about the joint centre is was also obtained from Nicol (1977), and is calculated as 0.3 times the epicondylar width.

For the purposes of reporting, the medial and lateral elbow joint forces are given as single forces acting in a given direction, where the angle quoted is measured anticlockwise from the positive joint x-axis. The resultant joint forces were allowed to take a direction from +80° to -80° to the zero degree direction given (Figure 2.32), ensuring stability in the humero-ulnar joint, and were 25° out of the x-y plane as shown in Figure 2.29. For ease of solution, the forces were split into components along

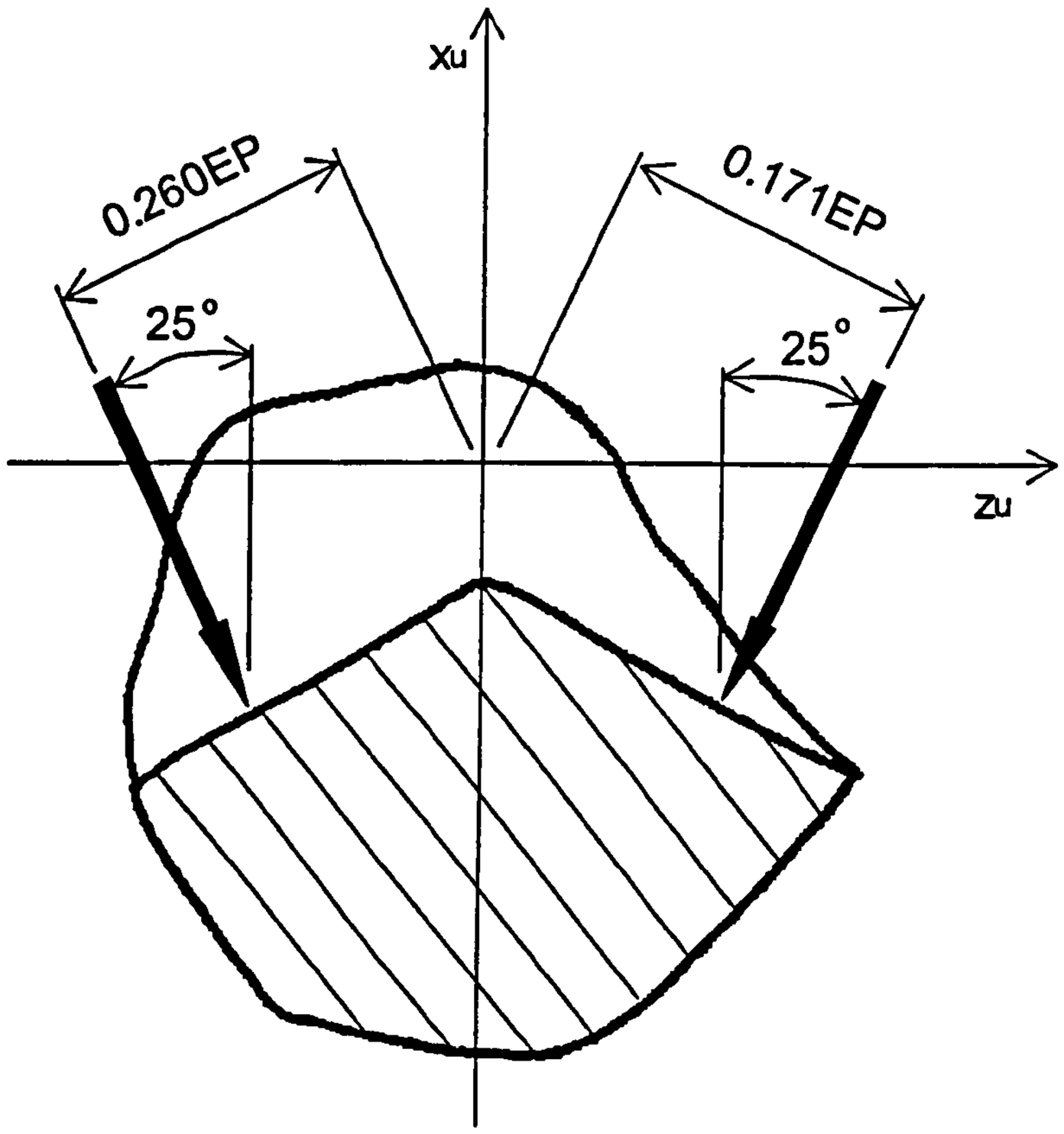

Figure 2.31 Section through trochlea showing position of centre of pressure of trochlear forces in x-z plane, from Nicol (1977).

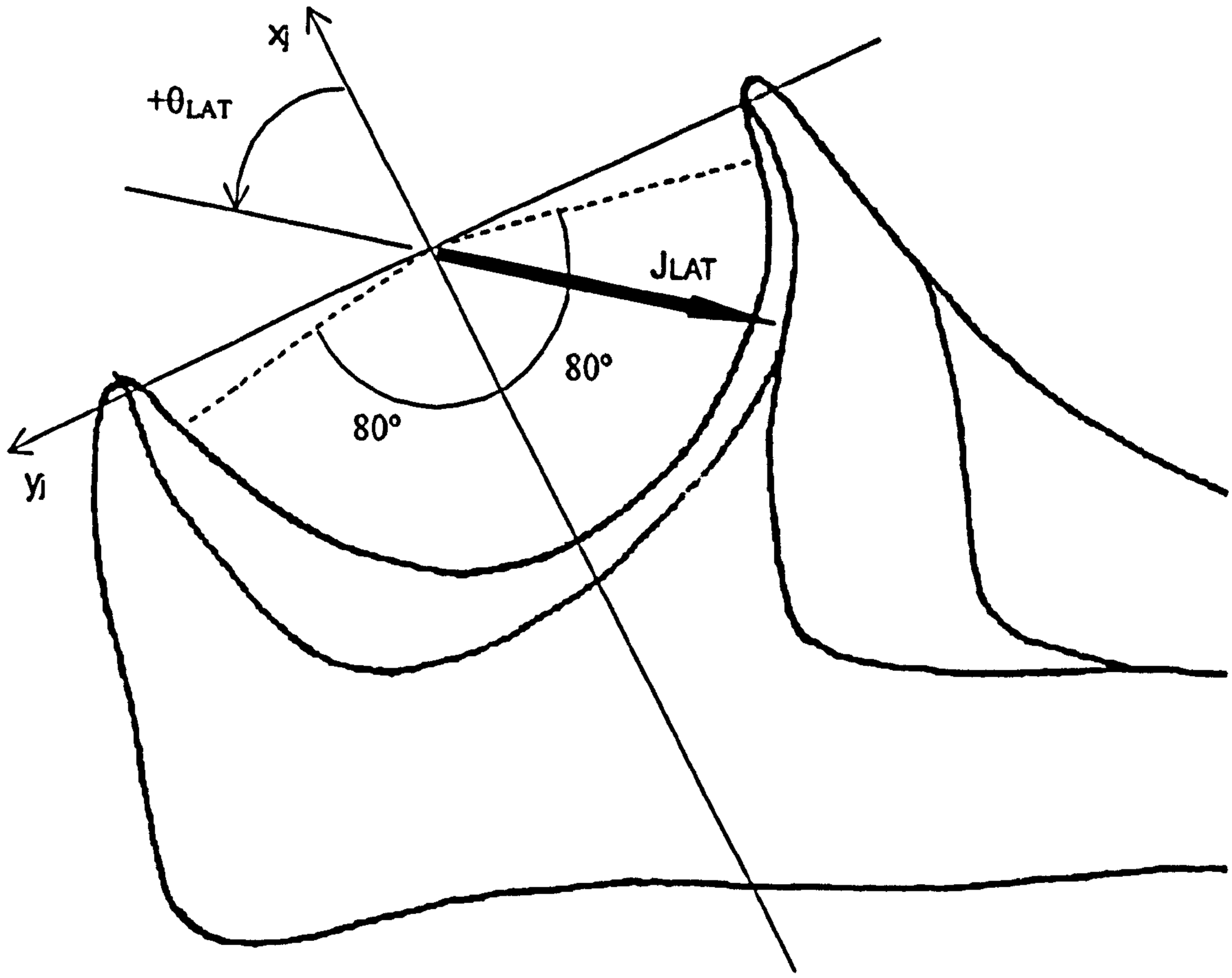

Figure 2.32 Diagram showing the extent of the joint contact area in the trochlea. Lateral force only shown for clarity.

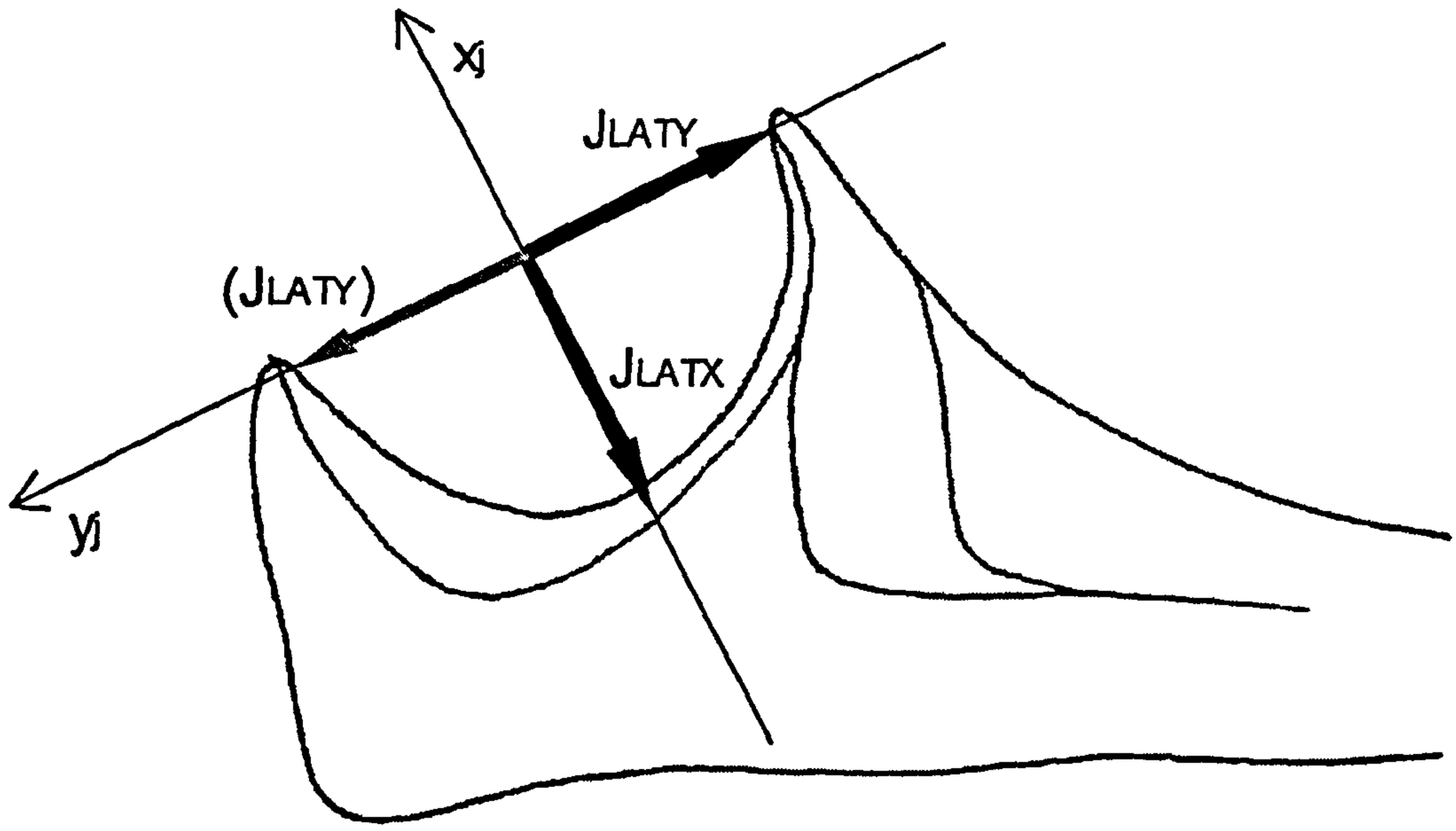

Figure 2.33 The lateral trochlear force resolved into components along the joint axes. Negative direction is shown dashed.

the joint x and y-axes, with the y component able to take positive or negative values. See Figure 2.33. Thus the stability constraints at the elbow were:

$$J_{LATY} - J_{LATX} \tan 80 \leq 0 \tag{2.29}$$

$$J_{MEDY} - J_{MEDX} \tan 80 \leq 0 \tag{2.30}$$

However, as the variables must take non-negative values, according to the primary constraints of the Simplex routine described in Section 2.4, the solution procedure was divided into four stages, with each possible combination of the joint force directions being tested. That is, the y components of the medial and lateral forces were set to anterior-anterior, posterior-posterior, posterior-anterior or anterior-posterior, and the minimum condition according to the objective function was taken as the result.

2.5.4.2 Wrist Joint Geometry

A very simplified model of the wrist joint has been used in this study, as modelling the intercarpal forces was outwith the scope of the study. The wrist joint contact has been modelled as a single force passing through the centre of rotation in the head of the capitate.

Figures 2.34 and 2.35 show the system of forces acting on the wrist joint. Joint stability has been assured by limiting the angle that the resultant joint force can make with the radial long axis, to a maximum of 30° in both planes.

As previously stated, the Simplex algorithm does not tolerate negative values in the variables, and the antero-posterior and medio-lateral forces at the wrist joint were therefore constrained to be positive. In order that they could take the full range of values within the stability constraint noted above, the axes were rotated through 30° in both the sagittal and frontal planes. The stability constraints were then

$$J_x' - J_y' \tan 60 \leq 0 \tag{2.31}$$

$$J_z' - J_y' \tan 60 \leq 0 \tag{2.32}$$

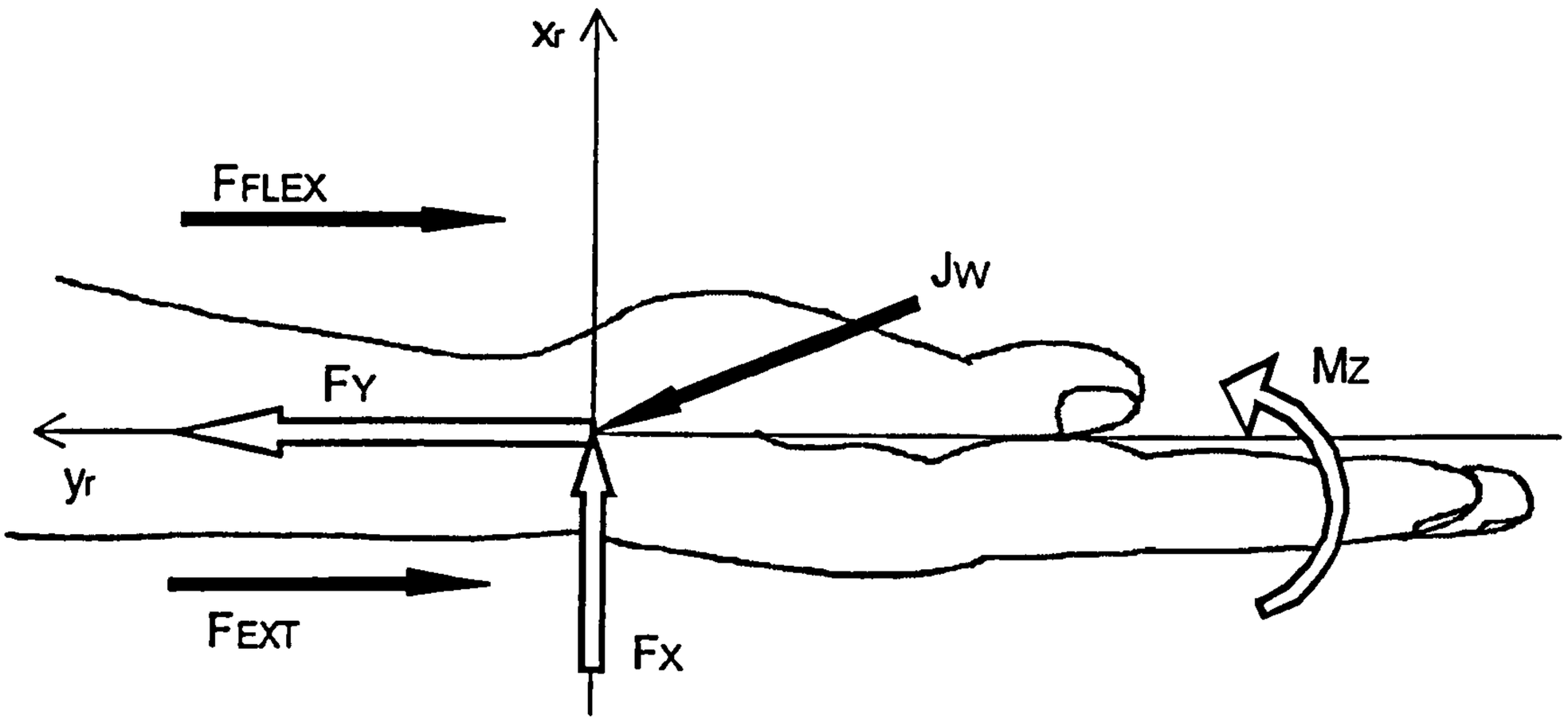

Figure 2.34 System of forces and moments acting on the wrist joint (distal radius) in the sagittal plane.

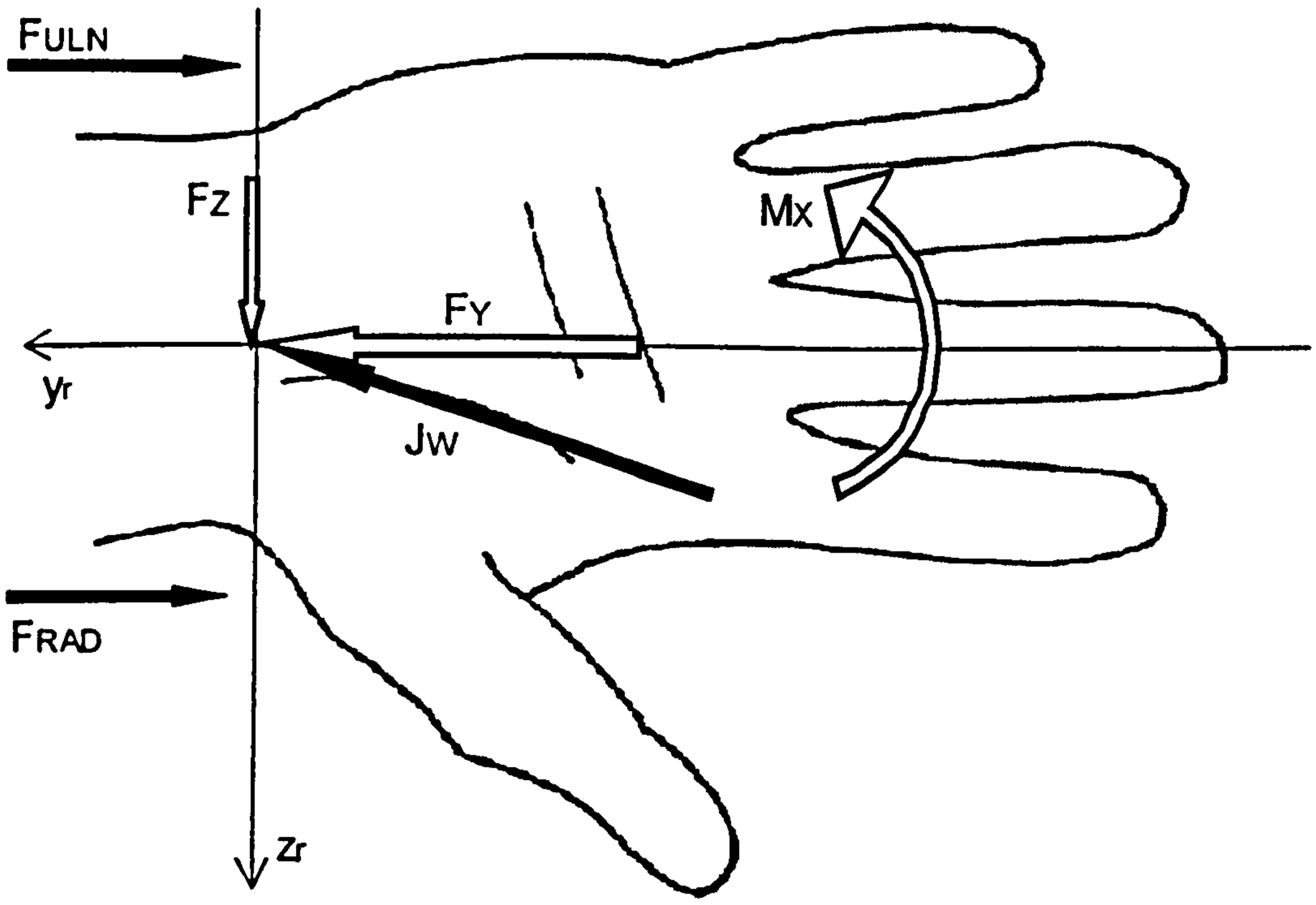

Figure 2.35 System of forces and moments acting on the wrist joint (distal radius) in the frontal plane.

where J_x', J_y' and J_z are joint forces in the rotated axis system.

2.5.4.3 The Simplex Tableau for Optimisation

The Simplex routine requires that the objective function and constraint equations are entered into a tableau, where the coefficients of each equation form a row. In this case, there are 25 variable columns and 31 constraint rows in the first stage, and 24 variables in the second stage as sigma is removed and incorporated as a constraint. The variables are listed in Table 2.1.

Variable type	Variable name	Description
Muscle forces	FCR	Flexor carpi radialis
	FCU	Flexor carpi ulnaris
	ECU	Extensor carpi ulnaris
	ECRB	Extensor carpi radialis brevis
	ECRL	Extensor carpi radialis longus
	BIC	Biceps brachii
	BRA	Brachialis
	BRD	Brachioradialis
	PRT	Pronator teres
	TRI	Triceps
	ANC	Anconeus
	PRQ	Pronator quadratus
	SUP	Supinator
Ligament forces	MCLA	Medial collateral ligament (anterior)
	MCLP	Medial collateral ligament (posterior)
	LCL	Lateral collateral ligament
Joint forces	JLATX	Lateral olecranon (x-component)
	JMEDX	Medial olecranon (x-component)
	JLATY	Lateral olecranon (y-component)
	JMEDY	Medial olecranon (y-component)
	JR	Radial head
	JWX	Wrist joint (x-component)
	JWY	Wrist joint (y-component)
	JWZ	Wrist joint (z-component)
Muscle stress	SIGMA	Maximum overall muscle stress

Table 2.1 Description of variables entered into the Simplex tableau.

CHAPTER 3 SUBJECT TESTING

3.1 RANGE OF SUBJECTS

Ten normal volunteers from within the Unit were recruited to perform the tests, five males and five females. All subjects were right hand dominant. The range of heights and body masses is shown in Table 3.1.

3.2 DESCRIPTION OF ACTIVITIES

The subjects were asked to perform a range of activities chosen to reproduce motions commonly seen in occupational duties. Each activity involved lifting the force transducer from a table, moving it through approximately 500mm to the side and back, and replacing it. This was repeated five times for each grip, using four different types of grip. For two activities, an additional mass of approximately 1.8kg was added to the device in order to move the position of the centre of mass and thus change the moment about the joints. The four activities are described below:

- *Vertical power grip* – the device rests on the table with the handle vertical and is grasped using a power grip. The device has just its own mass of 1.9kg. This is shown in Figure 3.1.
- *Chuck grip* – the device rests on the table with the handle vertical and is grasped with three fingers (index, middle and ring) and the thumb in a form of precision grip. The device has just its own mass of 1.9kg. This is shown in Figure 3.2.
- *Horizontal power grip* – the device rests on the table with the handle horizontal and is grasped using a power grip (as in hammer grip). There is an additional mass attached to the end of the transducer to move the centre of mass away from the hand, bringing the total mass to 3.85kg. This is shown in Figure 3.3.
- *Hook grip* – the device rests on the table with the handle horizontal and is grasped using a hook grip (as in lifting a suitcase). There is an additional mass attached to the device so as to bring the centre of mass under the hand. The total mass is 3.85kg. This is shown in Figure 3.4.

Subject	Height (cm)	Body mass (kg)	Age	Sex
1	168	61.5	35	M
2	166	53.5	28	F
3	180	70.5	26	M
4	166	66.5	26	F
5	166	66.5	24	M
6	182	77.3	29	M
7	166	56.5	25	F
8	167	73.7	27	M
9	162	64.0	34	F
10	164	59.5	27	F

Table 3.1 Details of subjects included in the study

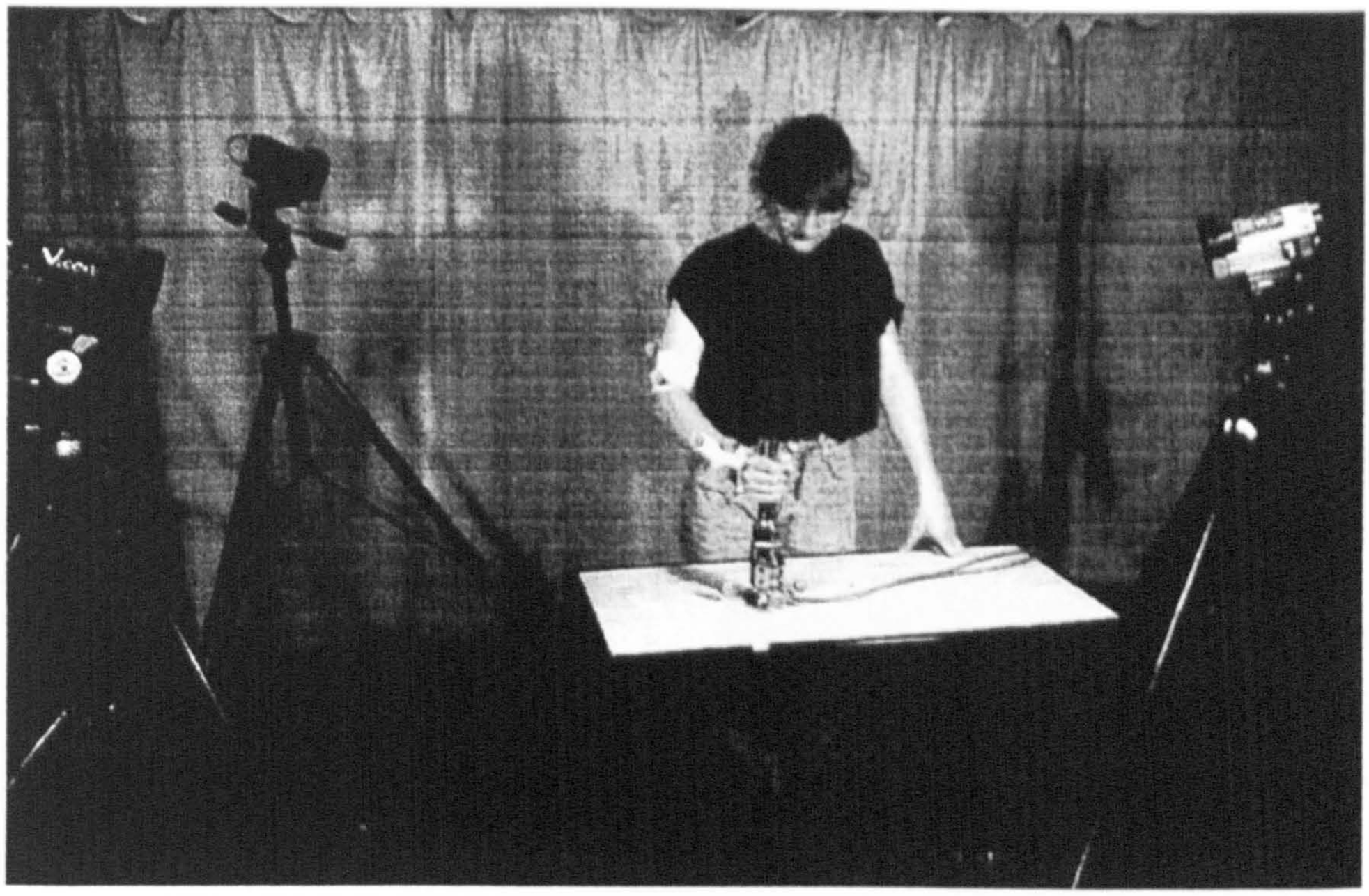

Figure 3.1 Subject performing the power grip with vertical handle.

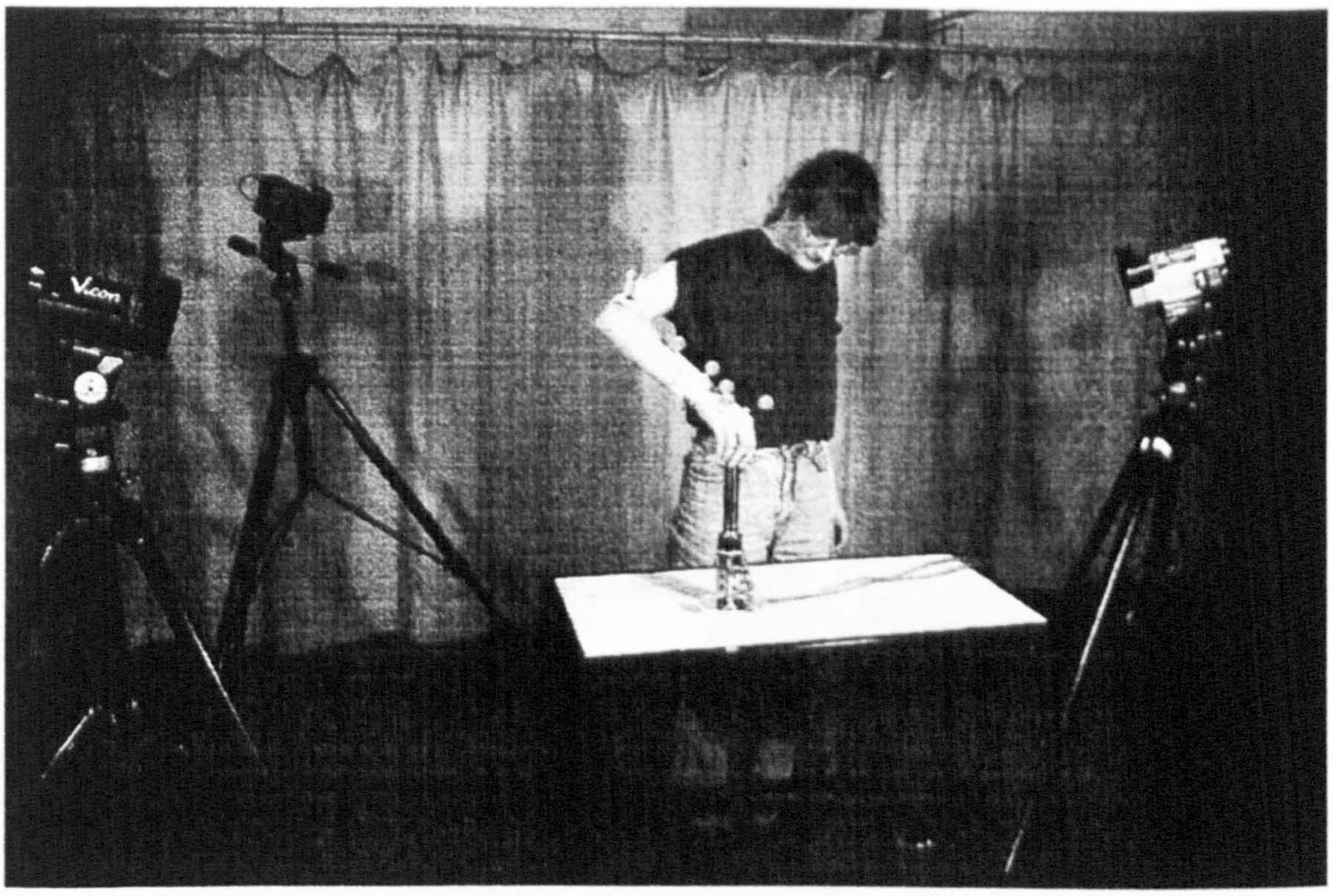

Figure 3.2 Subject performing the chuck grip with three fingers and thumb.

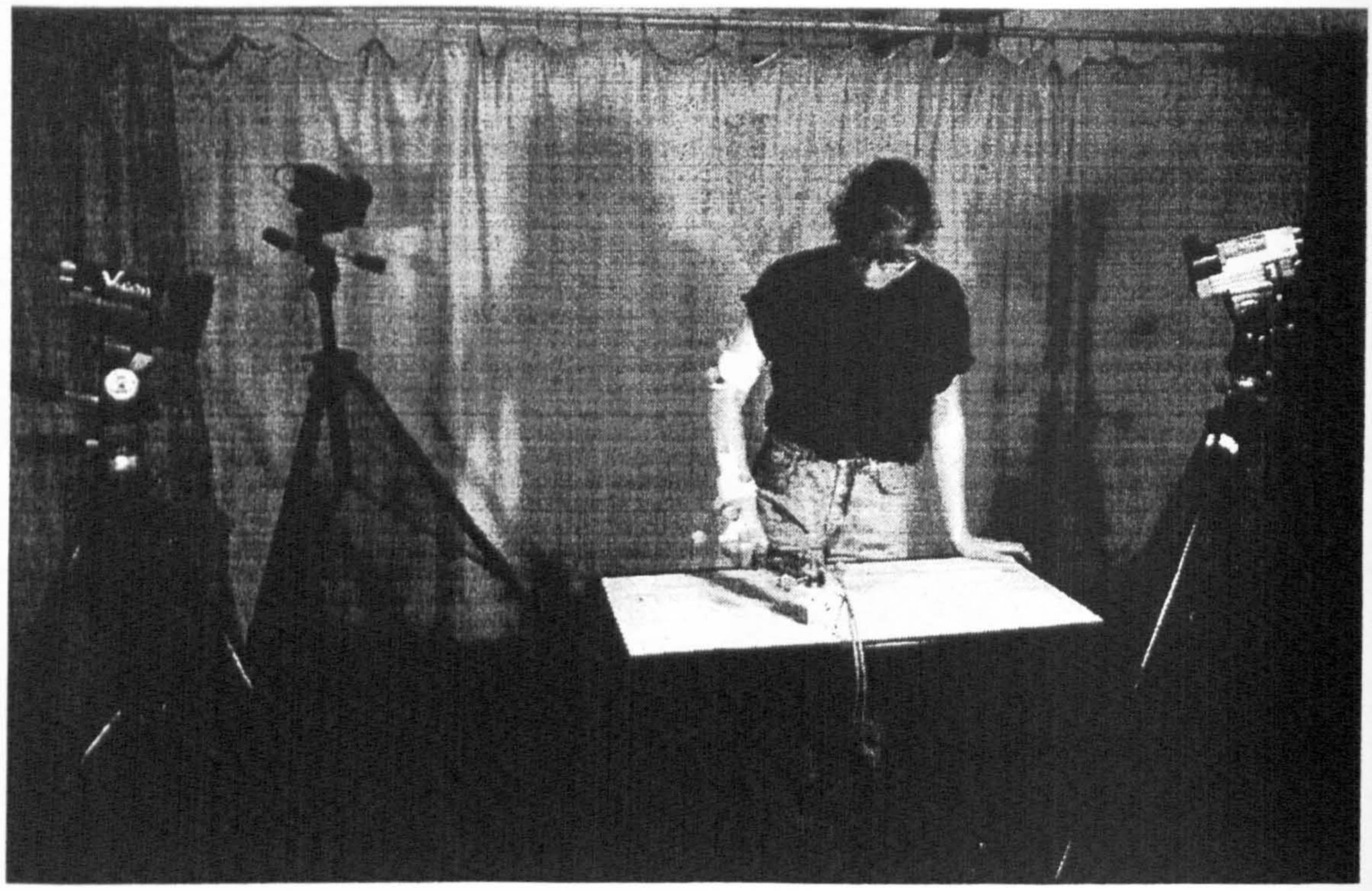

Figure 3.3 Subject performing the power grip with handle horizontal.

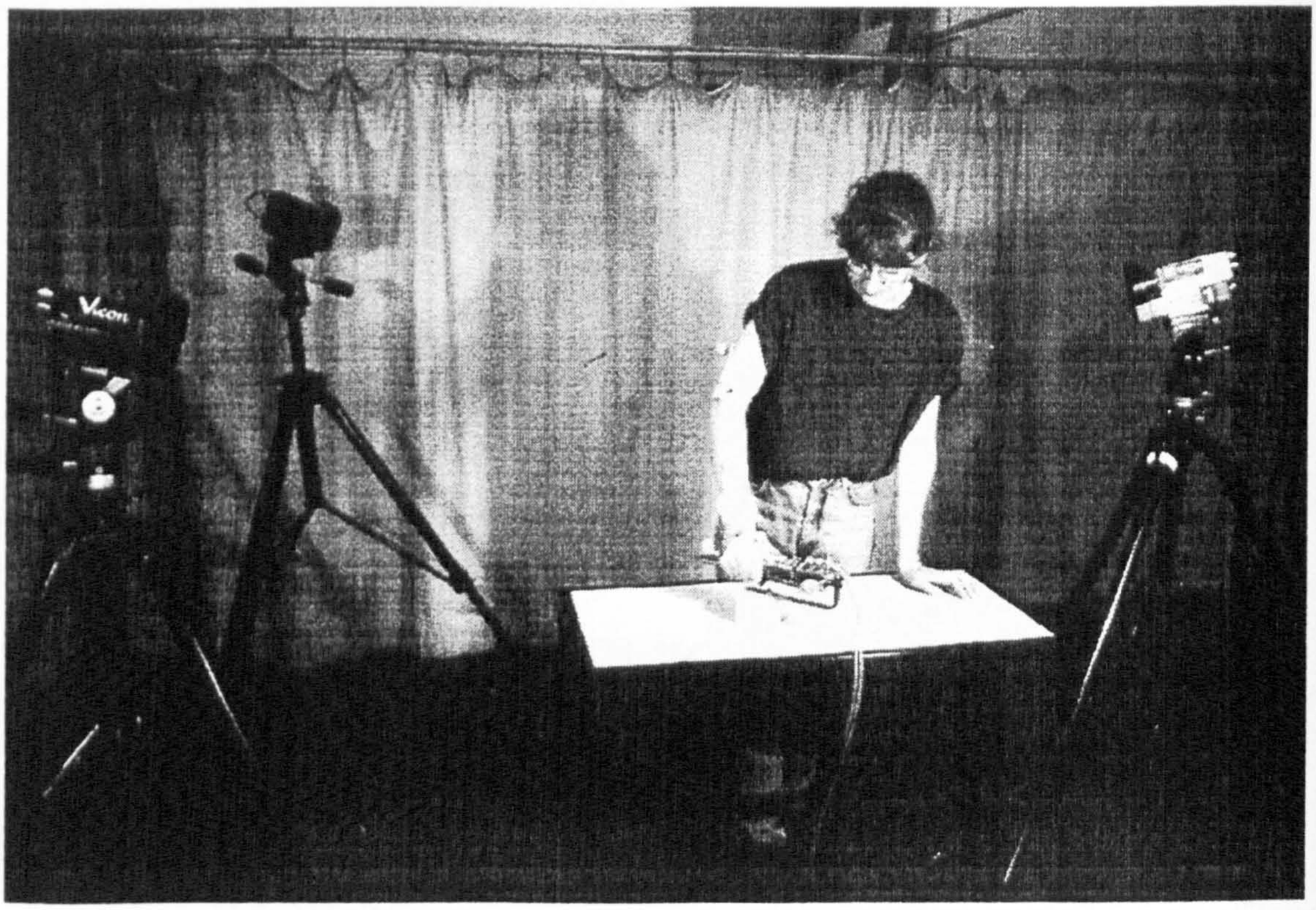

Figure 3.4 Subject performing the hook grip.

CHAPTER 4 DATA PROCESSING

4.1 SOFTWARE

Data processing was carried out in several stages, shown in flowchart form in Figure 4.1. Reconstruction and labelling of the marker trajectories was carried out using the Vicon370® software from Oxford Metrics. From there the data were saved in the c3d file format and converted to text using a program called c3dexporter, also from Oxford Metrics.

All programmes using these data in text format were custom written using LabVIEW G, a graphical programming language with an extensive range of in-built functions, or Borland C++. The simplex algorithm was implemented using a routine adapted from Fowler (1997). Flowcharts outlining the steps involved in the calculation of external forces and moments (Figure 4.2) and the calculation of internal forces (Figure 4.3) are given.

4.2 INTERPOLATION

Due to the inherent difficulties of conducting complex motion analysis, some of the marker trajectories were incomplete. In order to make use of the data, gaps of less than ten frames were interpolated using a 3rd order polynomial interpolator.

4.3 FILTERING

The data were filtered to remove unwanted noise. Effective filtering is essential as small errors are greatly magnified by the double differentiation process used in determining the acceleration values of the markers. The most common sources of noise were systemic (digitisation errors and reconstruction errors) and electrical interference.

Digital filtering was carried out, using LabVIEW routines. The type of filter used was a finite impulse response (FIR) filter with 25 taps, the number of coefficients used in the implementation. After power spectrum analysis, it was decided to use a cut-off frequency of 3 Hz for all trajectories. The force data were also filtered at 3 Hz.

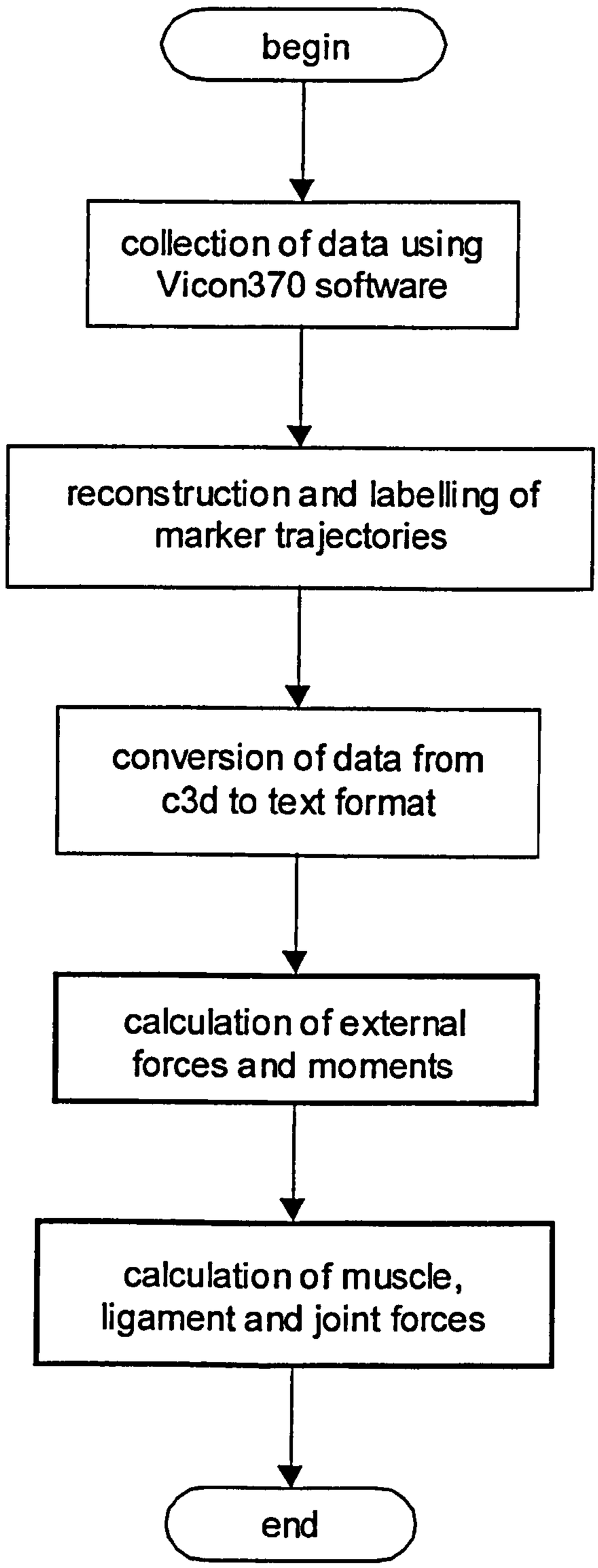

Figure 4.1 Outline flowchart showing the processes between data collection and the calculation of internal forces. Processes shown bold involved custom written software.

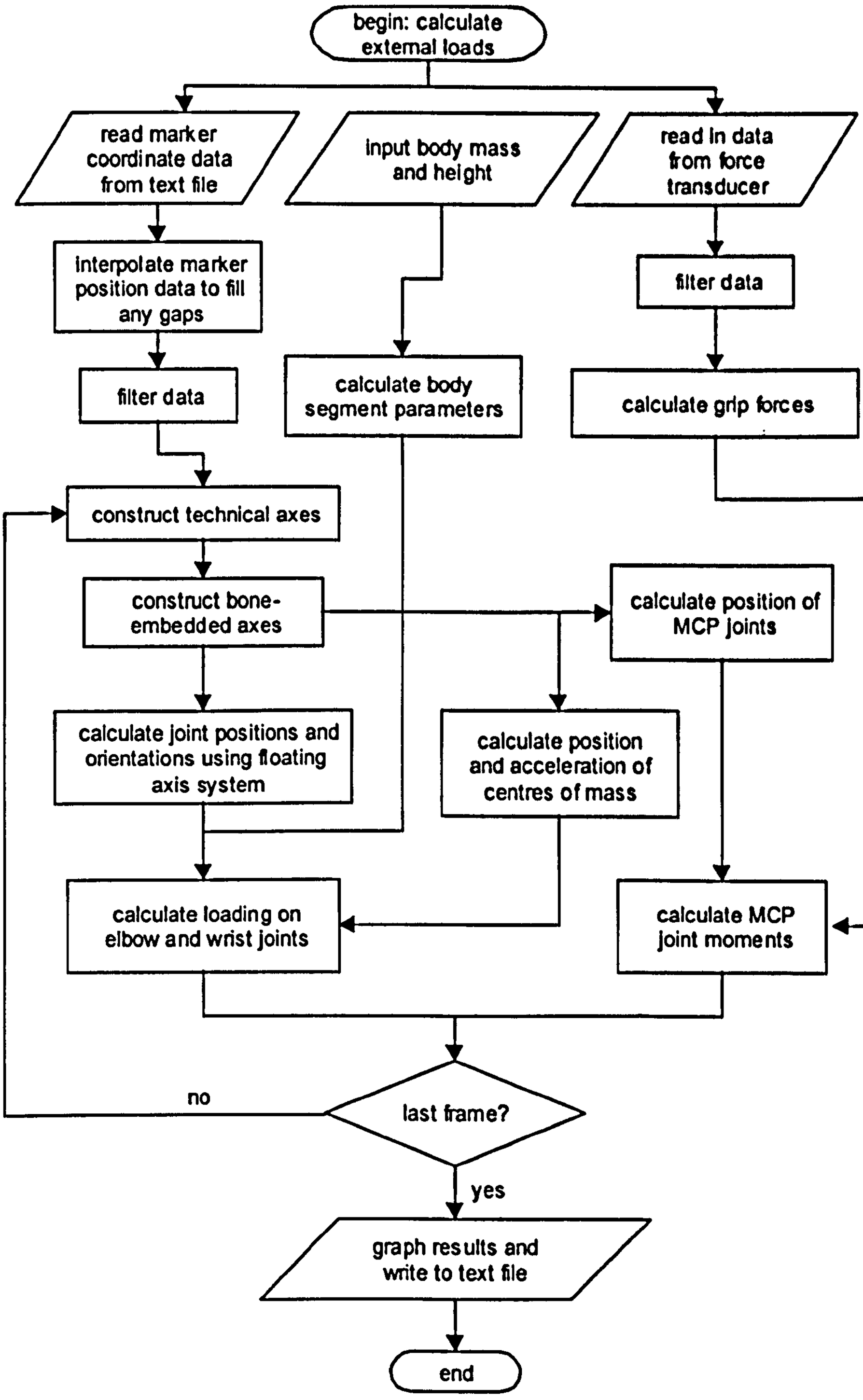

Figure 4.2 Flowchart detailing the stages involved in the calculation of the external forces and moments.

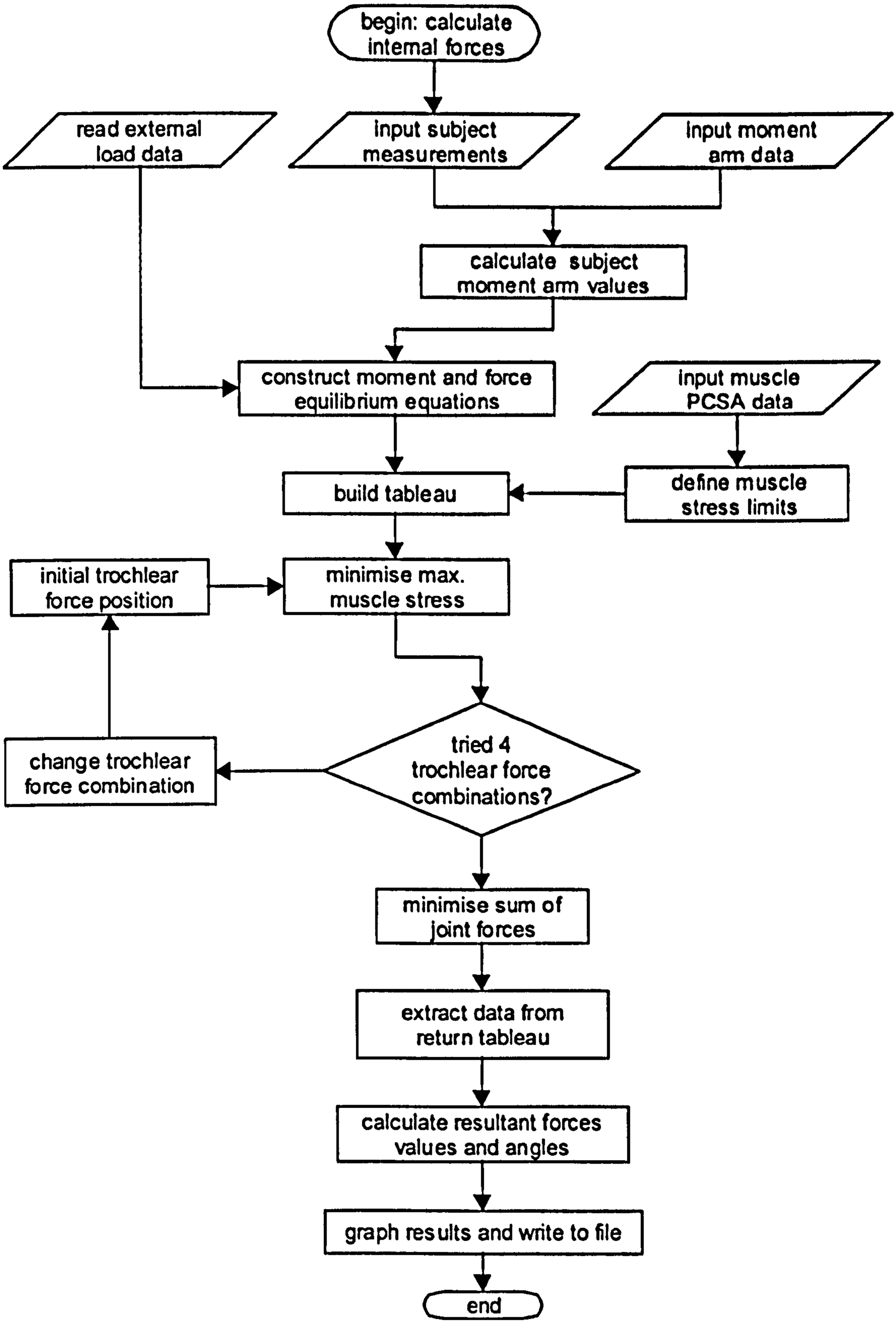

Figure 4.3 Flowchart showing the steps involved in the calculation of internal forces using the optimisation procedure.

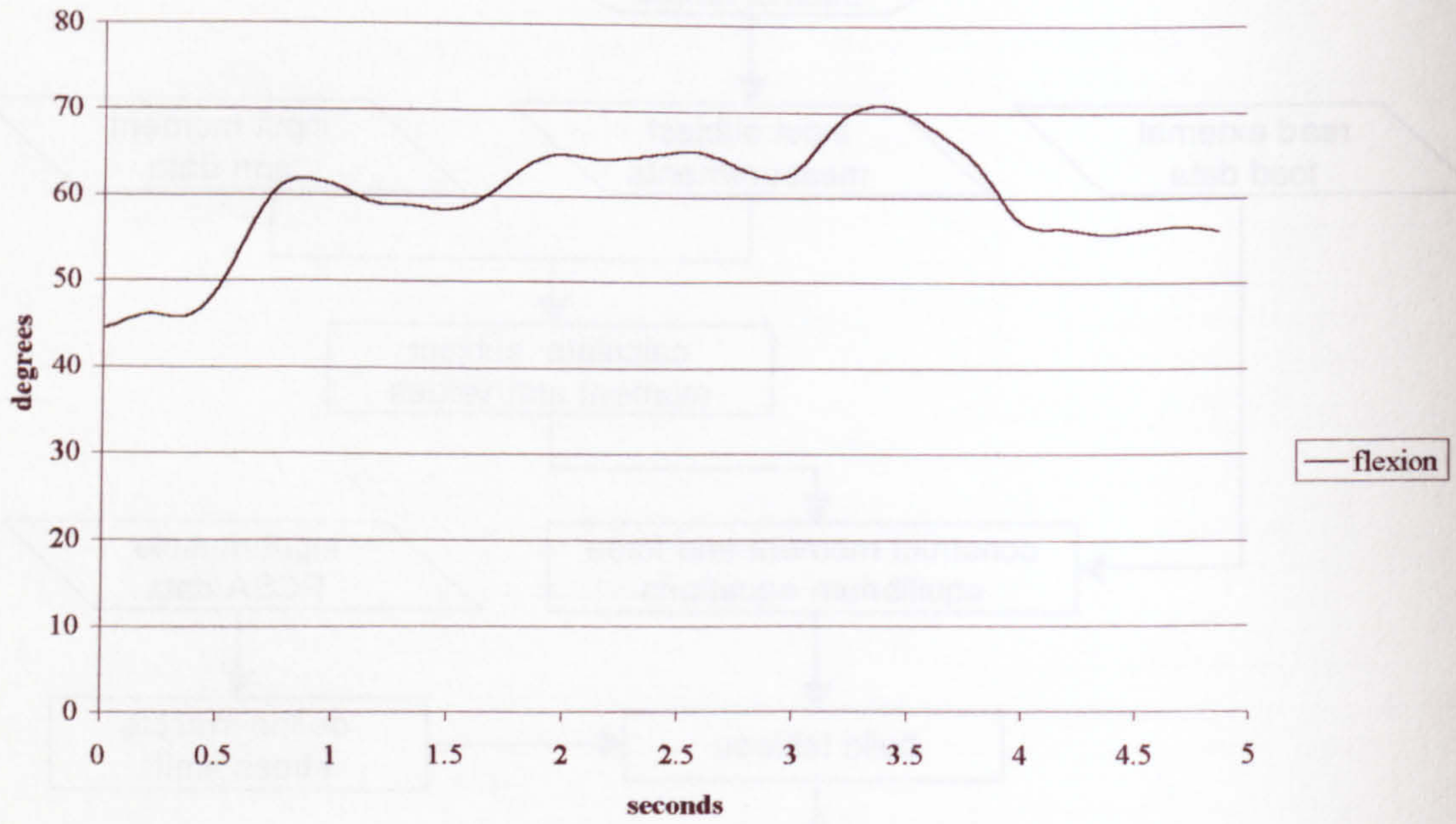

Figure 5.1 Variation of elbow joint flexion angle during the vertical power grip activity.

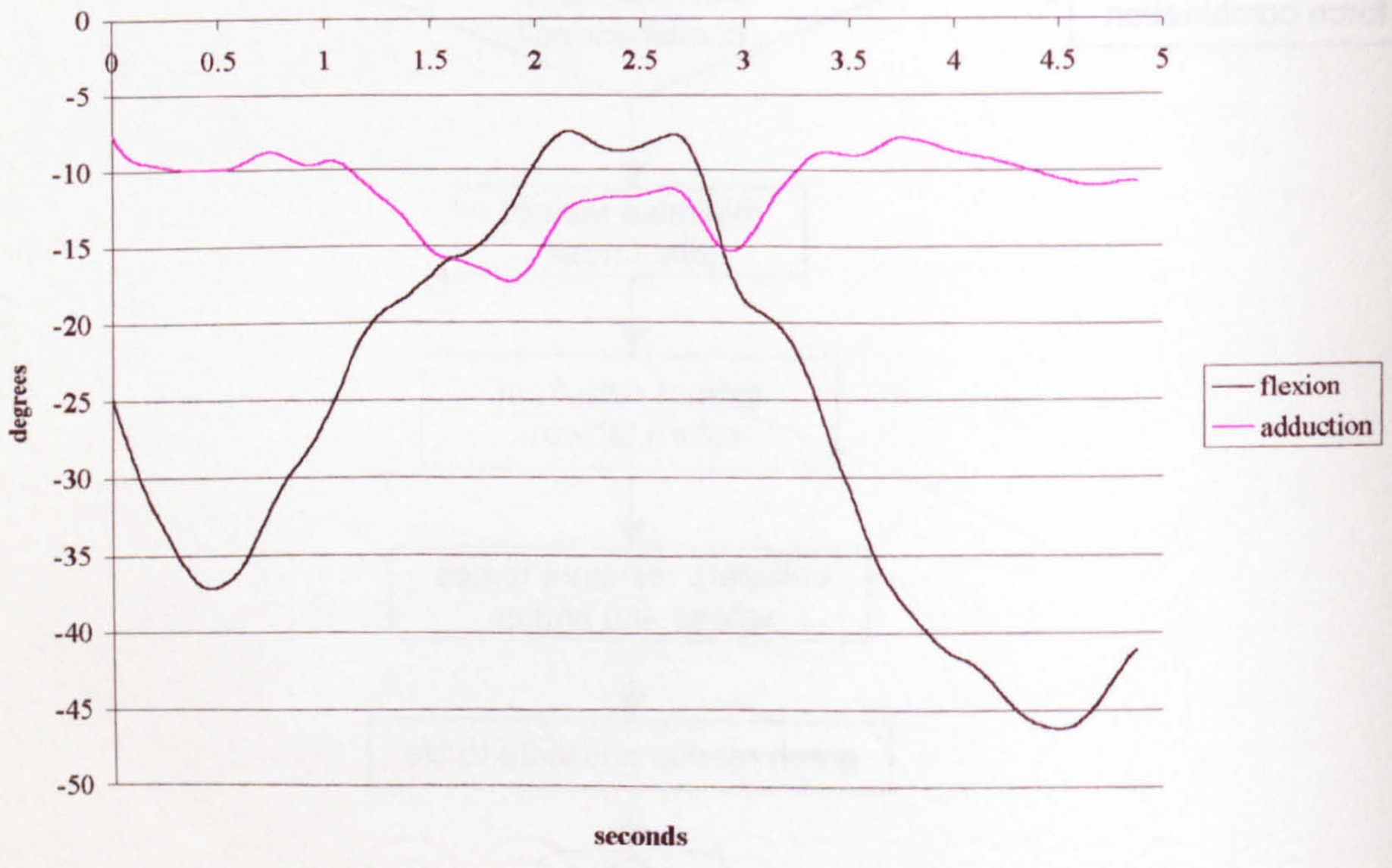

Figure 5.2 Variation of wrist joint angles during the vertical power grip activity.

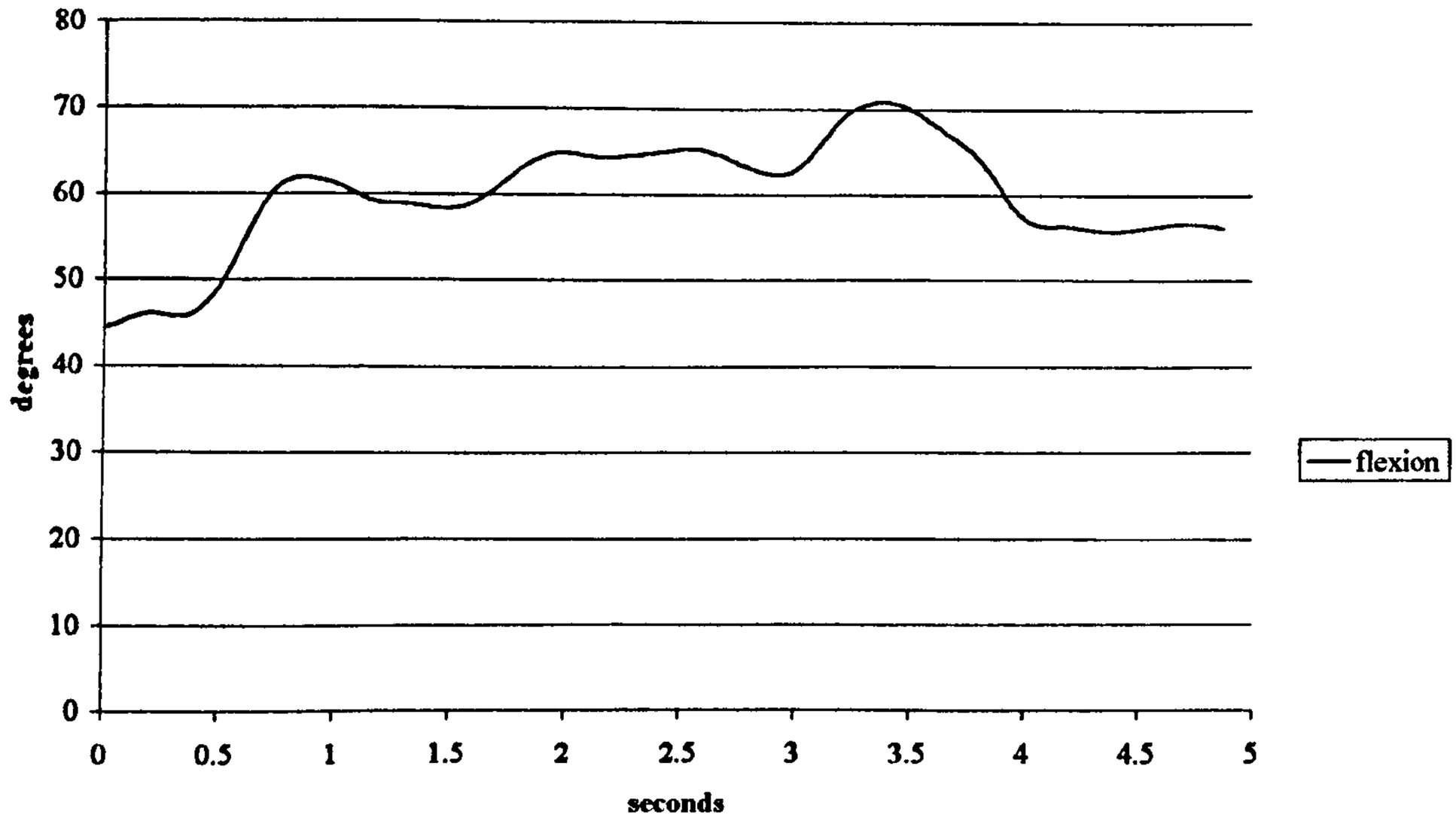

Figure 5.1 Variation of elbow joint flexion angle during the vertical power grip activity.

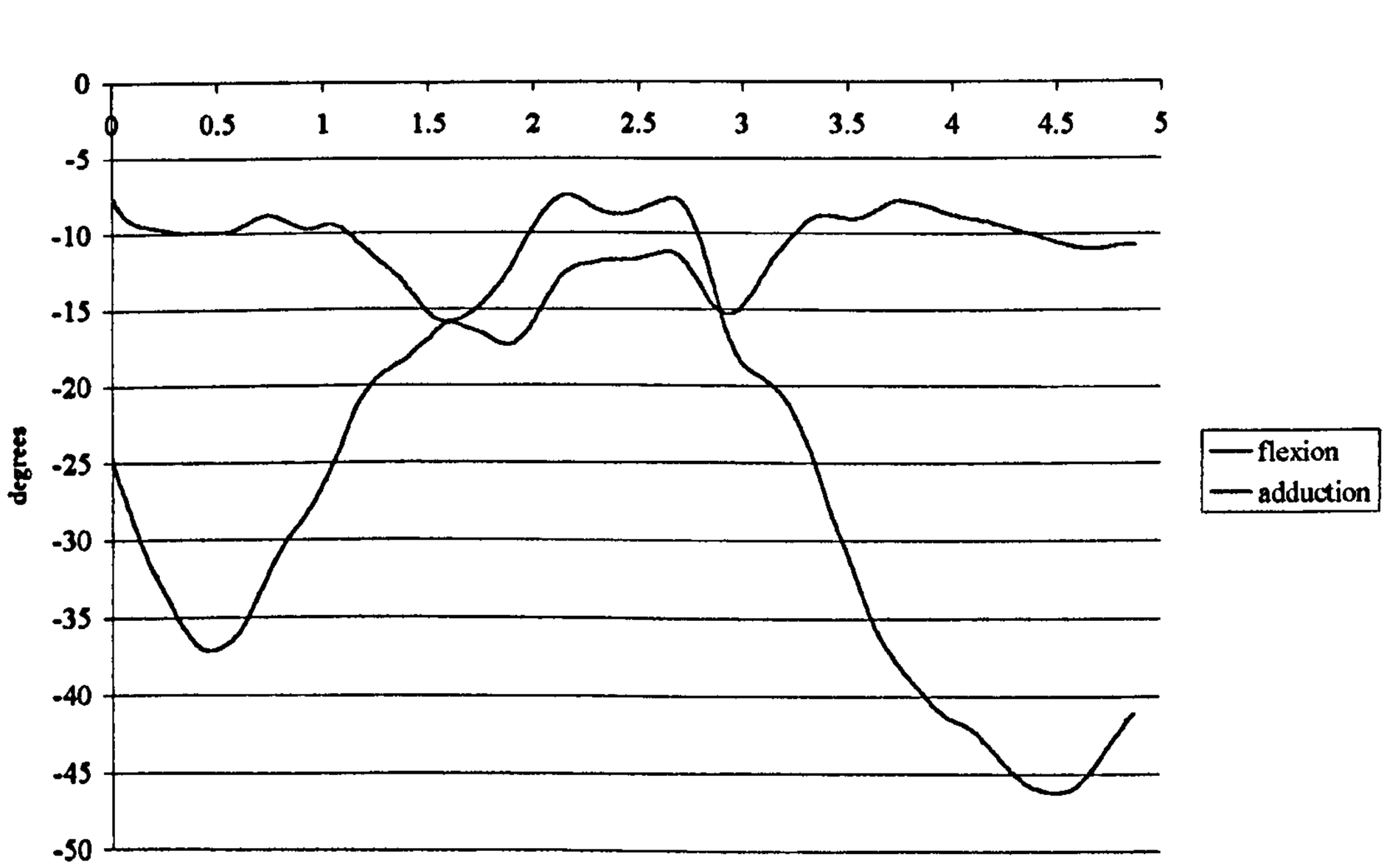

Figure 5.2 Variation of wrist joint angles during the vertical power grip activity.

CHAPTER 5 RESULTS AND DISCUSSION

5.1 ANALYSIS OF ACTIVITY AND MODEL BEHAVIOUR

The graphs presented in this section show a range of parameters against time for each activity. The purpose of these graphs is not to summarise the data, but to present the results in terms of the loading on the structures of the forearm and how that relates to the analysis undertaken here. It is not possible to draw conclusions relating to the whole sample population or to a particular activity from the following results and discussion. Within each activity, data from the same trial are used for direct comparison. One example of each activity is examined.

5.1.1 POWER GRIP (HANDLE VERTICAL)

5.1.1.1 Kinematics and External Loading

Figure 5.1 shows the variation of elbow joint flexion angle during the performance of the vertical power grip activity. The subject moved the device from a near position to a far one and back again, and this is reflected in the increase and then decrease of the joint angle. The range of motion moved through is small, at only approximately 25°. The motion of the wrist joint can be seen in Figure 5.2, where the largest range of motion occurs in flexion-extension. The maximum extension is reached at the end of the motion as the device is returned to its starting position, and is approximately 45°. The motion through radio-ulnar deviation is much smaller, and reaches a maximum of approximately 17° radial deviation.

Figure 5.3 shows the moments applied to the MCP joints during the activity. The labels 2 to 5 represent the index, middle, ring and little fingers respectively. It must be noted here that the distribution between the fingers seen in the graph is calculated based on their relative moment potential, not measured, and the effect of the thumb on the device is accounted for by transferring its load to the fingers, as explained in Section 2.3. The peaks in MCP joint moments occur as the device is picked up, both as it is moved away from and returned to the subject. This is due to two factors: one is that the device is accelerated upwards at this point and the other is that the subject

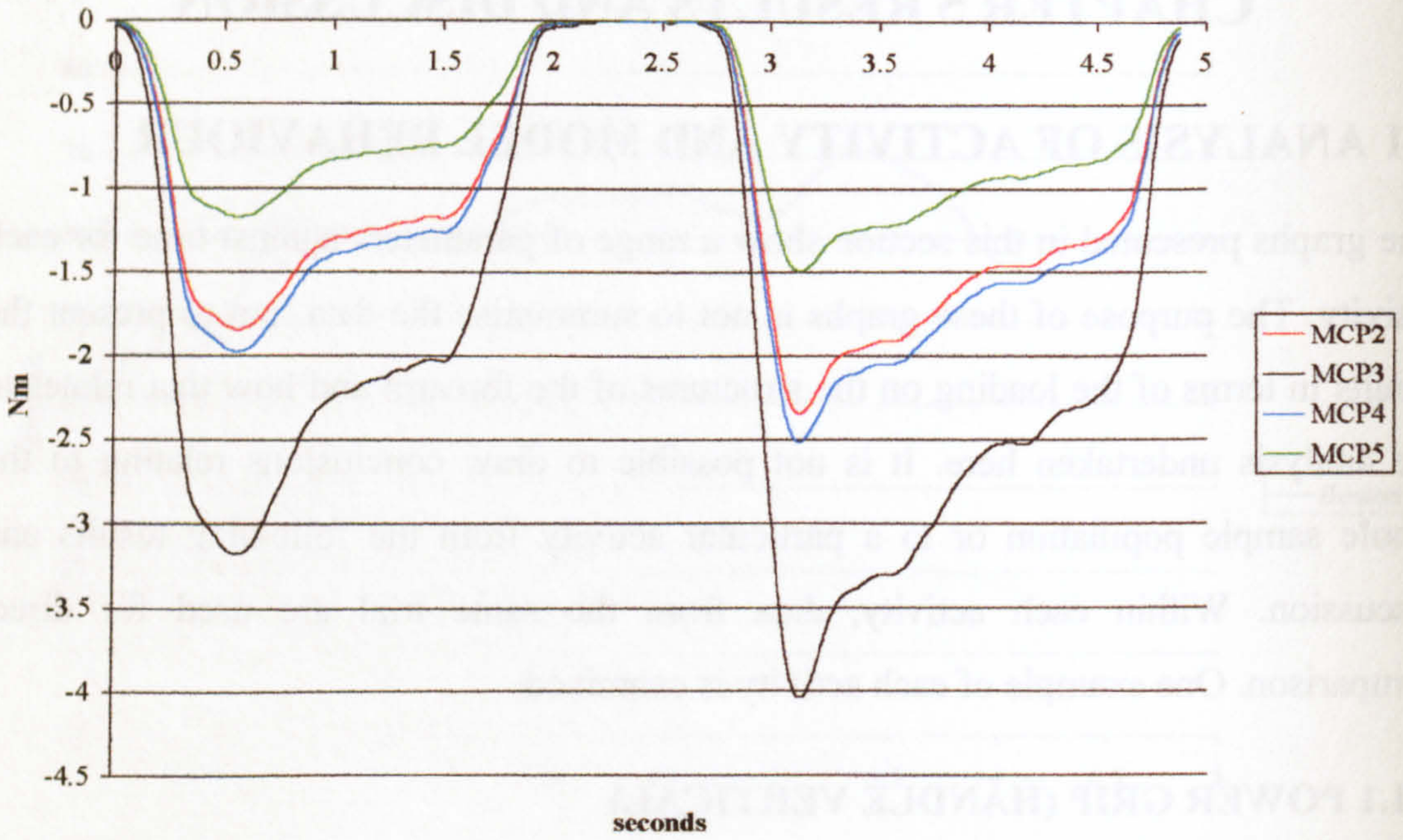

Figure 5.3 Moments applied to the MCP joints during the vertical power grip activity.

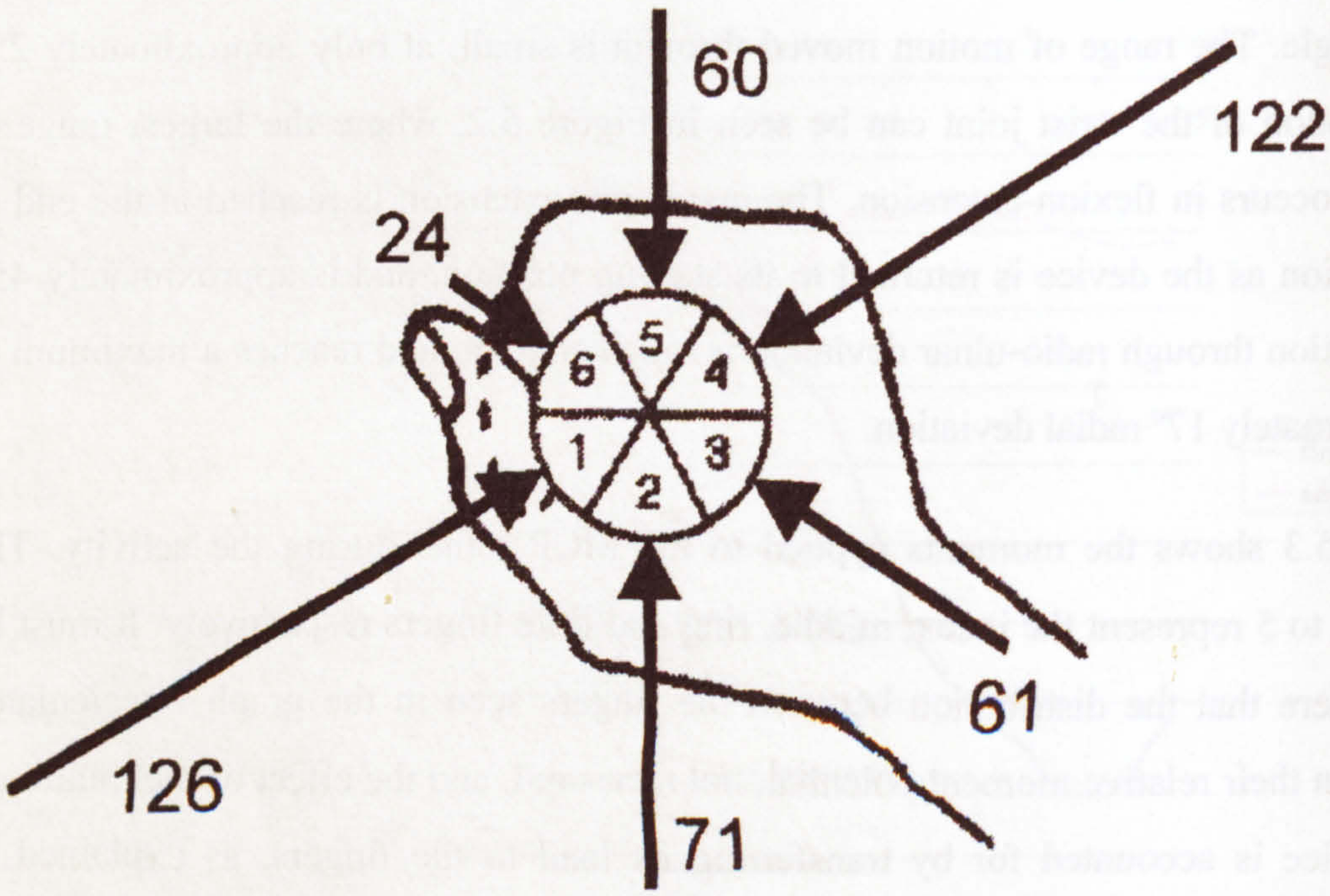

Figure 5.4 Distribution of force around the handle of the transducer during the vertical power grip activity (Newtons).

initially applies more force than necessary to prevent slip, before relaxing the grip a little.

The distribution of forces around the cylinder during the vertical power grip can be seen in Figure 5.4. This is the situation at an instant in time, the time at which the total grip force is a maximum. It can be seen from this that the highest forces occur adjacent to the MCP joints and to where the thumb and finger overlap opposite this. The forces orthogonal to these are significantly lower.

The external moments and forces applied to the elbow and wrist joints can be seen in Figure 5.5 and Figure 5.6. The loads applied to the elbow are defined in the ulnar axis system and the loads applied to the wrist are in the radial axis system. Loads tending to flex, adduct and internally rotate the joints are positive.

It can be seen from these figures that the external loads are relatively constant during the activity. At the point in the middle of the activity where the transducer is placed on the table and the grip force diminishes, the external moments due to the transducer's mass and inertial properties should decrease. However, the threshold for deciding whether the transducer was being held sufficiently tightly to exert a moment at the joints was set too low, and this gave rise to the transducer appearing to continue to affect the joint moments even while it was resting on the table. This leads to the unrealistic loading situation where the elbow and wrist joint moments are high, but the grip force is virtually zero. The data arising from these conditions were excluded from later calculations.

Figure 5.5 shows that the load on the elbow throughout the activity is one tending to extend, pronate and adduct the joint. At the wrist joint, the loading condition is one of flexion and ulnar deviation. The rotation effect at the wrist passes from internal to external and back to internal, but this component of the load was not included in the model.

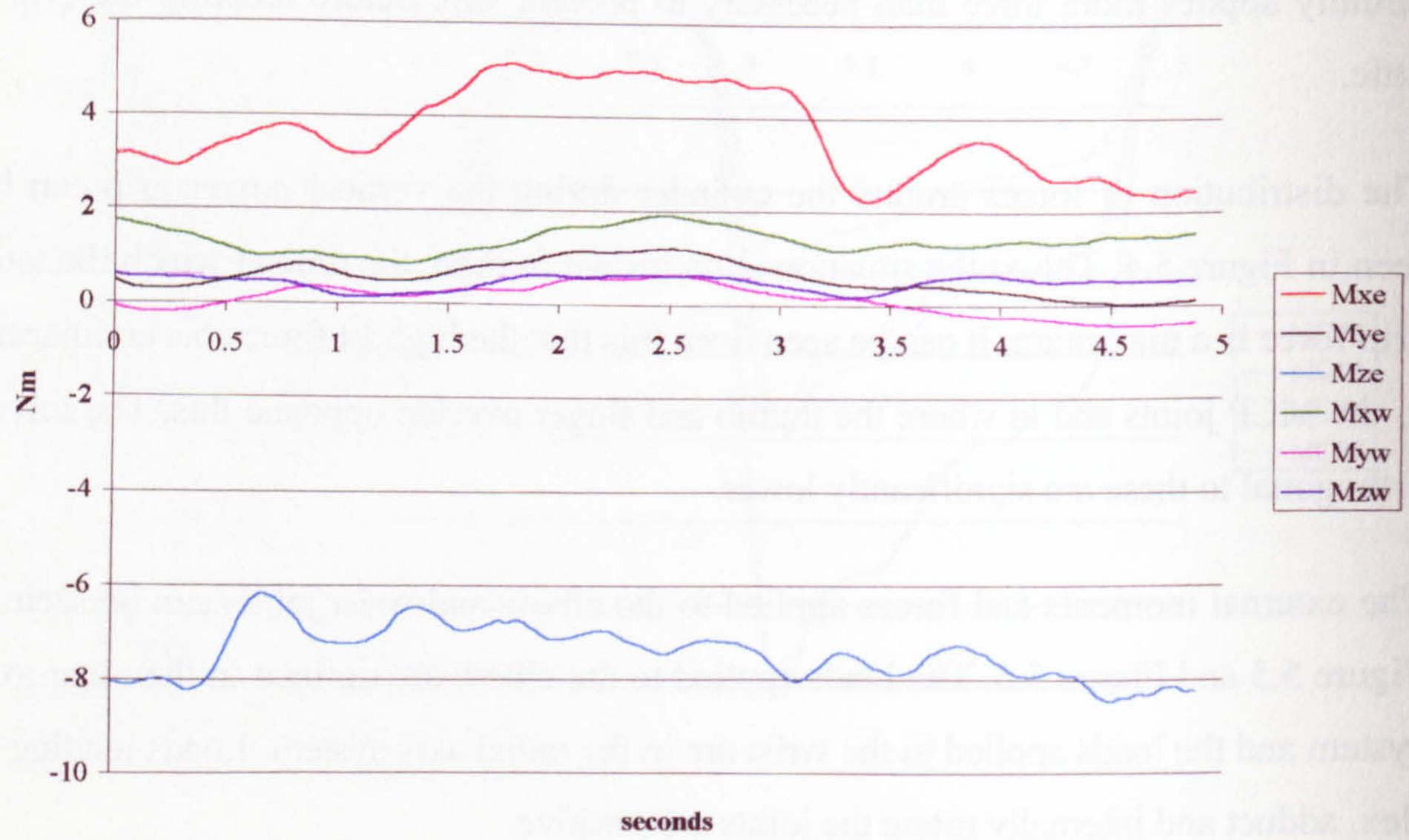

Figure 5.5 Moments applied to the elbow and wrist joints during the vertical power grip activity.

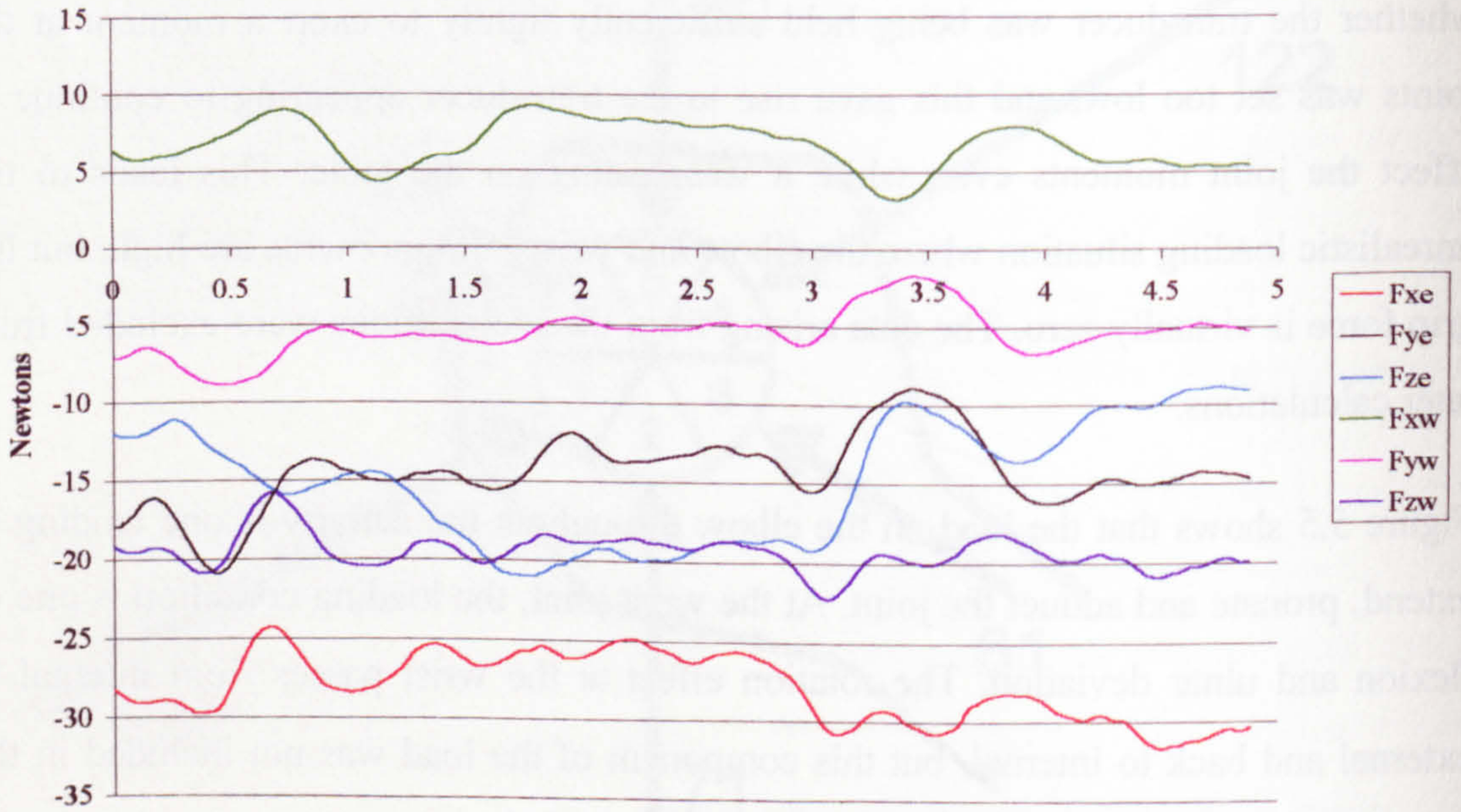

Figure 5.6 Forces applied to the elbow and wrist joints during the vertical power grip activity.

5.1.1.2 Internal forces

Figure 5.7 shows the distribution of forces amongst the structures of the arm during the vertical power grip activity. The values of tension for the flexor digitorum profundus (FDP) and flexor digitorum superficialis (FDS) muscles are calculated directly from the MCP moments, the others are the results of the optimisation routine. The forces in FDS and FDP were found to be very similar after summing the contributions from each digit.

The unrealistic loading conditions described in the previous section led to the model being insoluble, and in these cases the results were artificially set to zero, giving rise to the zero values seen in the curves at the times when the grip force is very low (or zero). This does not affect the maximum values obtained nor the validity of the solution during the rest of the trial.

The maximum forces for each phase of the motion coincide with the maximum grip force, i.e. just after the device has been picked up. The measured loads tend to flex and cause ulnar deviation at the wrist and these moments are opposed by the actions of extensor carpi radialis longus (ECRL), extensor carpi radialis brevis (ECRB) and extensor carpi ulnaris (ECU), which reached peaks of 300N or more in this case. The use of ECU to oppose the load when the load is tending to cause ulnar deviation is brought on by the need to also oppose the flexion moment produced by the tendons of FDS and FDP at the wrist. This is a clear case of co-activation being predicted, in both an antagonistic and a synergistic way, by the use of a highly constrained, linear system.

At the elbow, the loads tend to cause extension, adduction and pronation, and these are resisted by a combination of brachioradialis (BRD) and biceps brachii (BIC) and the medial joint force (Figure 5.7 and Figure 5.8). During most of the trial, BRD is used as the primary flexor as it has the largest moment arm. It is also positioned so as to oppose the adduction moment. Between 3 and 4 seconds through the trial, however, BRD is suddenly switched off and BIC is used in its place. This sudden switch represents non-physiological behaviour of the model, but is explained in terms of the rules and assumptions on which the model is based. This represents a limitation of the model and in particular the linear optimisation technique used to solve it. At this

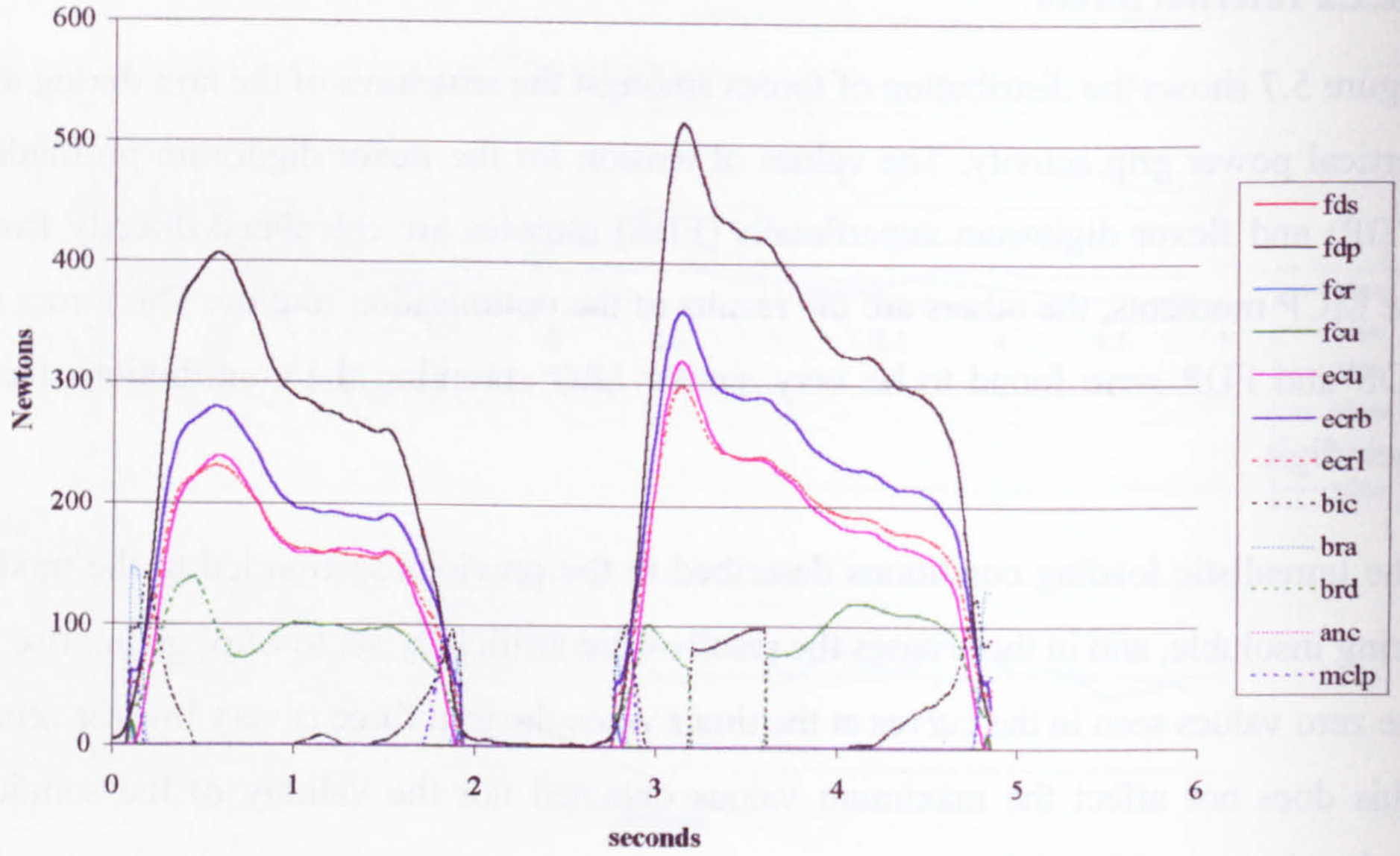

Figure 5.7 Graph of muscle and ligament force levels against time during the vertical power grip activity.

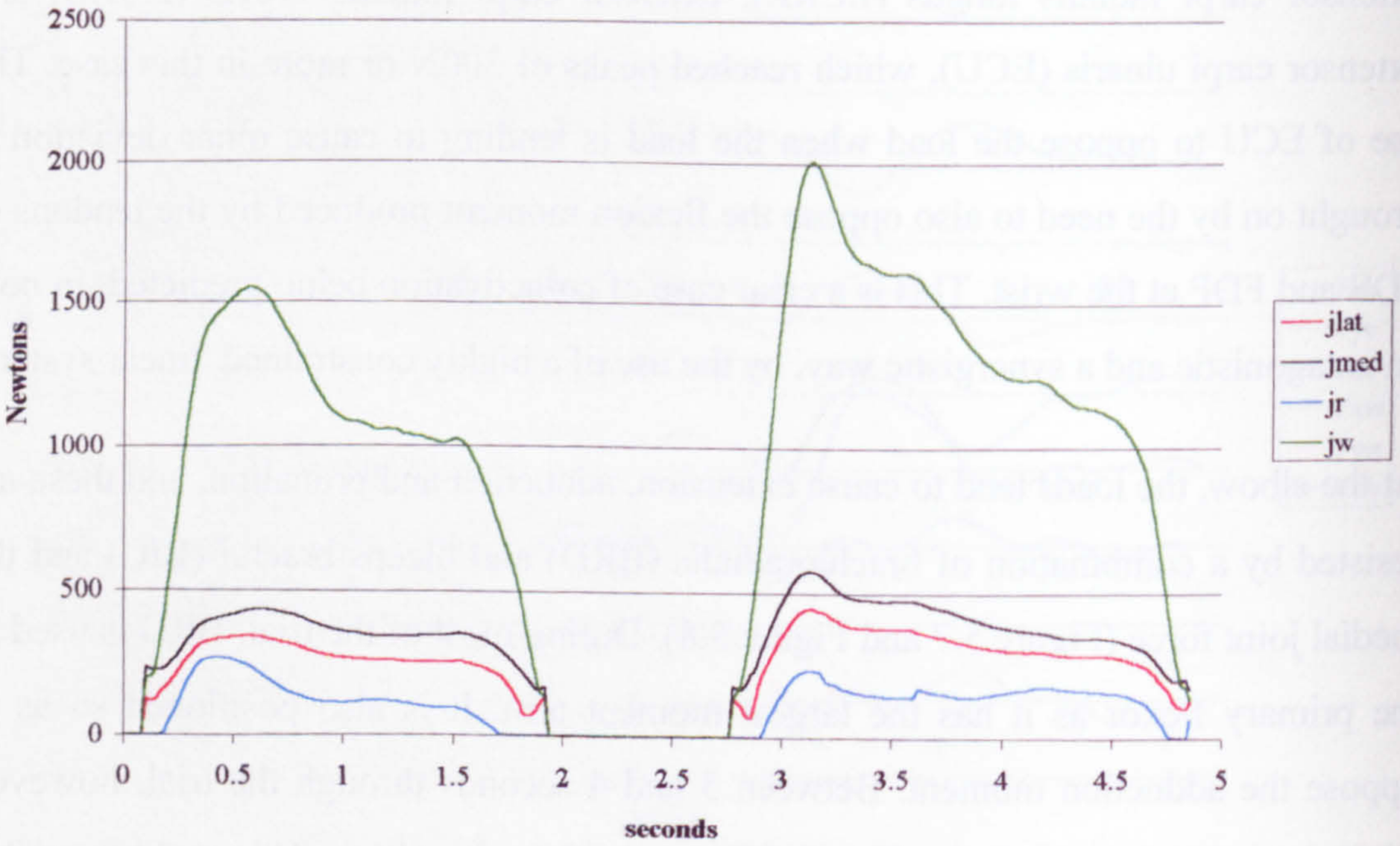

Figure 5.8 Graph of joint contact force levels against time during the vertical power grip activity.

instant during the trial, there is a sudden decrease in the adduction moment at the elbow (Figure 5.5). This reduced need for the abduction action of BRD, combined with the increased flexion moment arm of BIC (Figure 2.23) due to the corresponding increase in elbow joint angle (Figure 5.1), means that it is now possible for the model to select BIC to satisfy the constraints and reduce the overall muscle stress, as BIC is a larger muscle than BRD.

There is also some activity in flexor carpi radialis (FCR), brachialis (BRA) and anconeus (ANC) and some load is taken by the anterior part of the medial collateral ligament (MCLA). Although a large muscle, BRA has a much smaller moment arm in flexion than either the BIC or the BRD, and also tends to increase pronation of the forearm more than BRD at these joint angles (greater than 50° flexion) and this is why it is not used in this case.

Examination of the joint contact forces reveals that the medial trochlear force (JMED) is consistently larger than the lateral trochlear force (JLAT) and the sum of the two trochlear forces exceeds 1000N at its maximum. The radial head force (JR) reaches a value of approximately 250N. It is expected to be lower as the joint loading is that of adduction, although its presence is necessitated by the force in BRD. The force in the wrist joint is very high (up to 2000N) due to the high forces in the large number of muscles that cross it (FDS, FDP, ECU, ECRB, ECRL).

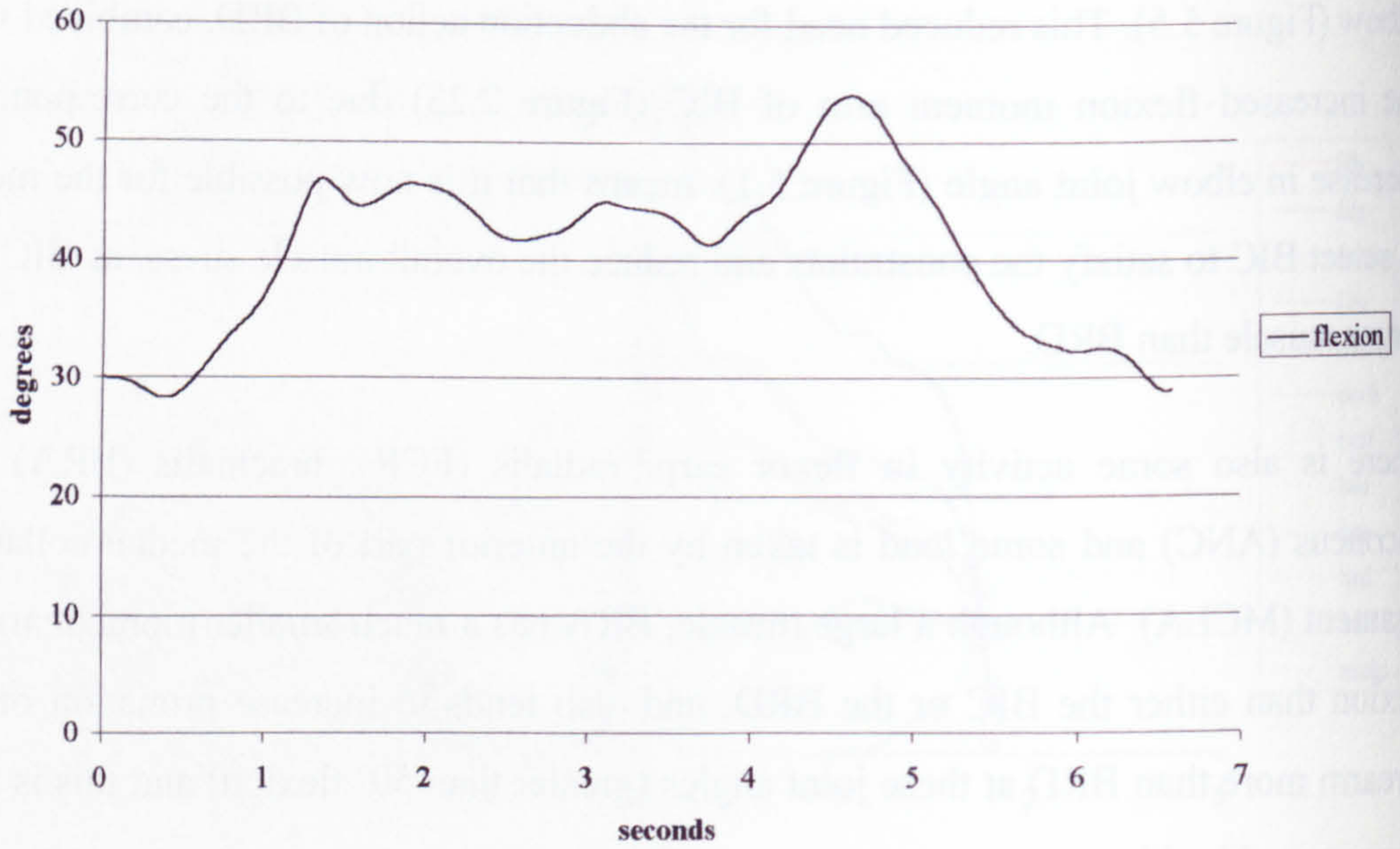

Figure 5.9 Variation of elbow joint flexion angle during the chuck grip activity.

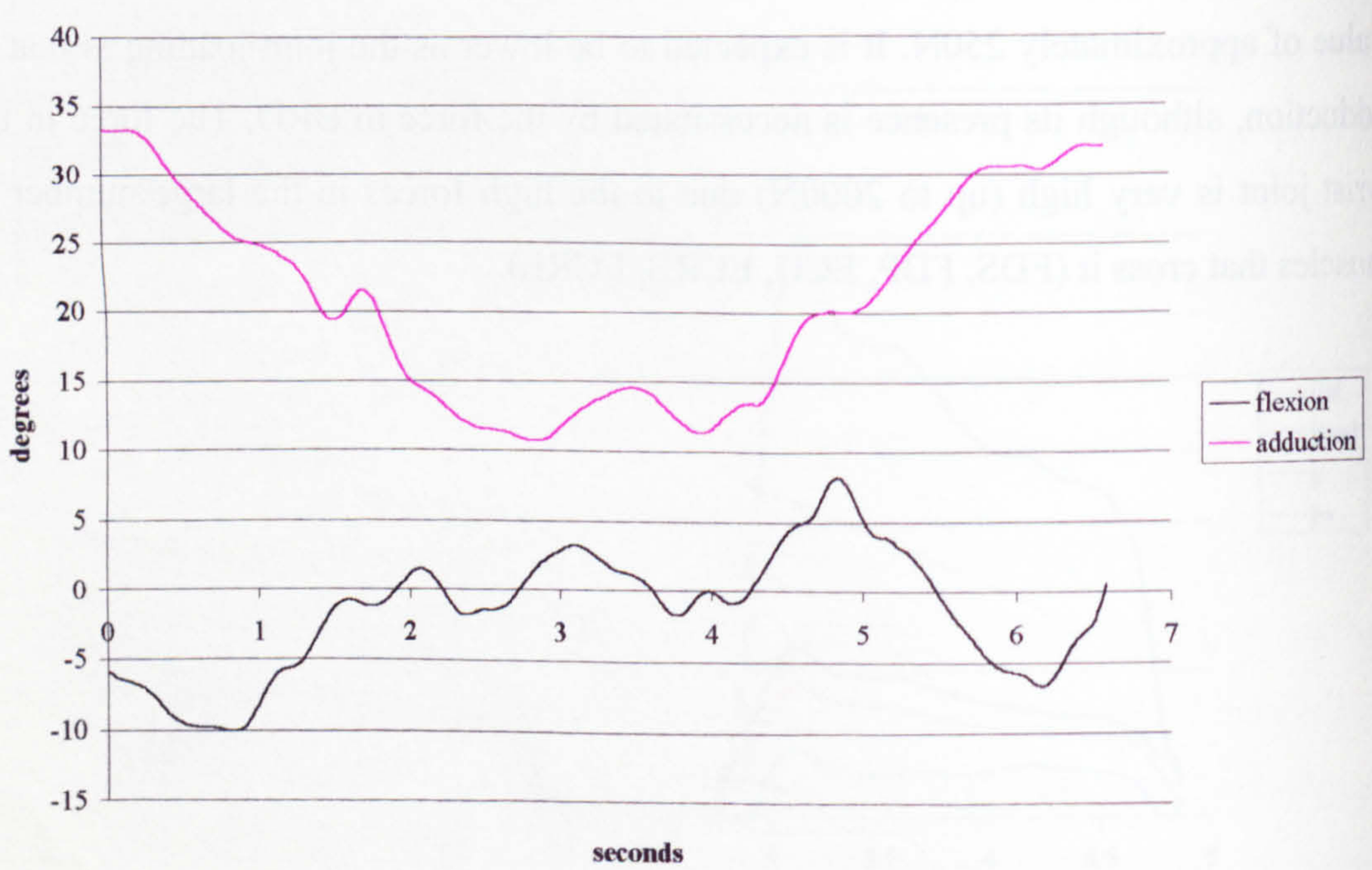

Figure 5.10 Variation of wrist joint angles during the chuck grip activity.

5.1.2 CHUCK GRIP

5.1.2.1 Kinematics and External Loading

Figure 5.9 shows the range of motion of the elbow joint during the chuck grip activity. The flexion angle varies between approximately 28° and 54° during the motion, i.e. slightly more extended than in the previous activity of 'vertical power'.

The wrist joint motion, shown in Figure 5.10, differs from the previous activity in that it is strongly adducted for a large part of the trial, up to 33°, but extended less, up to 10°. The adduction angle decreases to approximately 10° as the transducer is moved away from the body.

Figure 5.11 shows the variation in MCP joint moment, where joints 2, 3 and 4 are those of the index, middle and ring fingers and joint 1 is that of the thumb. In this case, the load sharing between the digits is measured, not assumed. Note that MCP1 and 4 take the highest proportion of the load for most of the trial.

The length of time taken to complete the activity, 6.5s, is longer than the previous activity and the peak seen at the start of each phase is not seen, suggesting the activity is being performed more cautiously.

Figure 5.12 shows the force distribution between the thumb and the three fingers during the chuck grip, at the point where the total grip force is a maximum. In this case, this point occurs 1.76 seconds from the start of the trial. The total grip force is very much lower during this trial than in the previous one, the vertical power grip, but the MCP moment required is similar. This is because the lever arm for the load acting against the distal ends of the fingers is large. It can also be seen that the ratios between the forces do not correspond to the ratios between the grip moments, as the moment arm for the load on each finger is different.

The external moments applied to the elbow and wrist joints during the chuck grip can be seen in Figure 5.13. The values do not change much during the trial, and this is for reasons explained in the previous section. However, it can be seen that towards the middle of the trial there is some decrease in Mz at the elbow and a corresponding

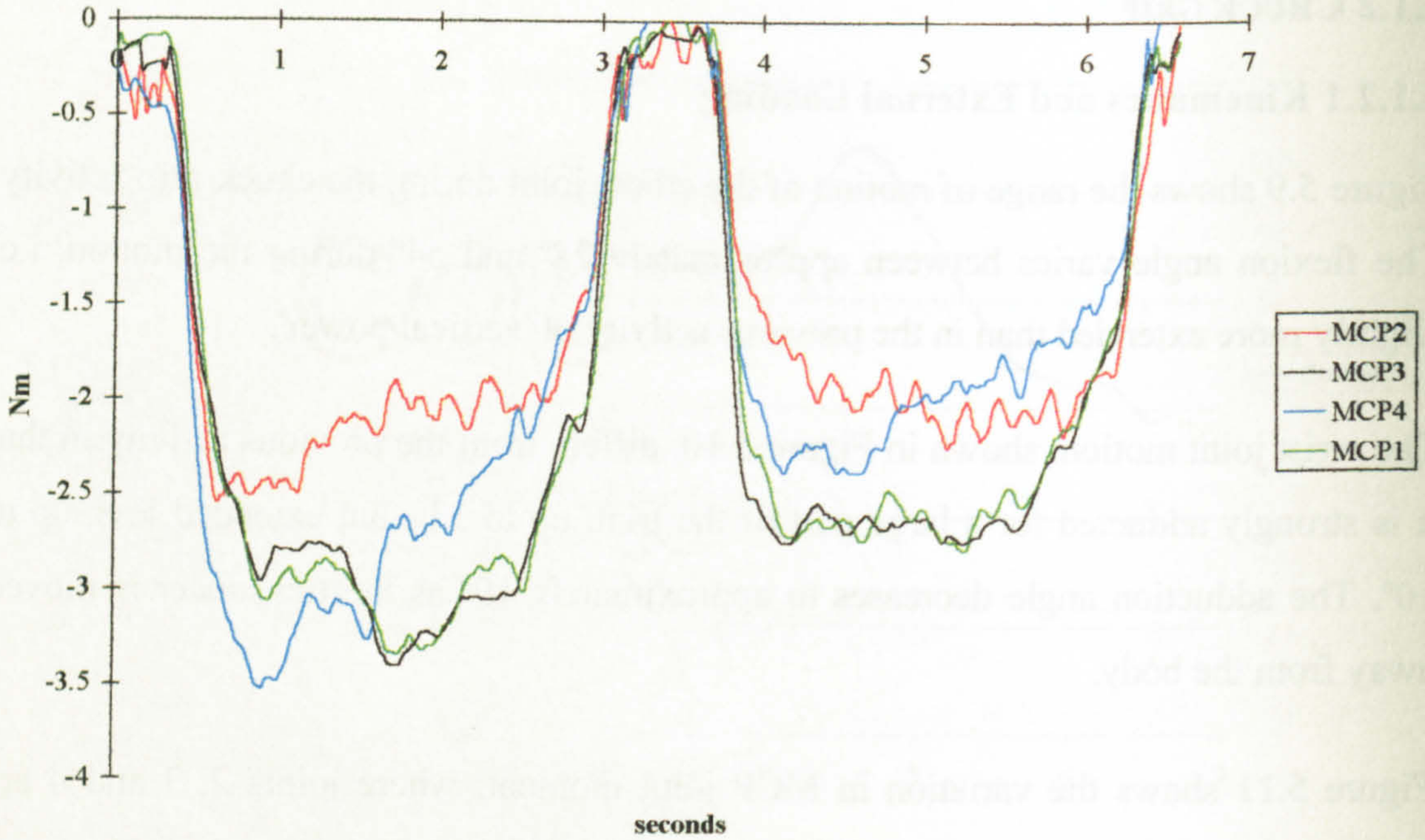

Figure 5.11 Moments applied to the MCP joints during the chuck grip activity.

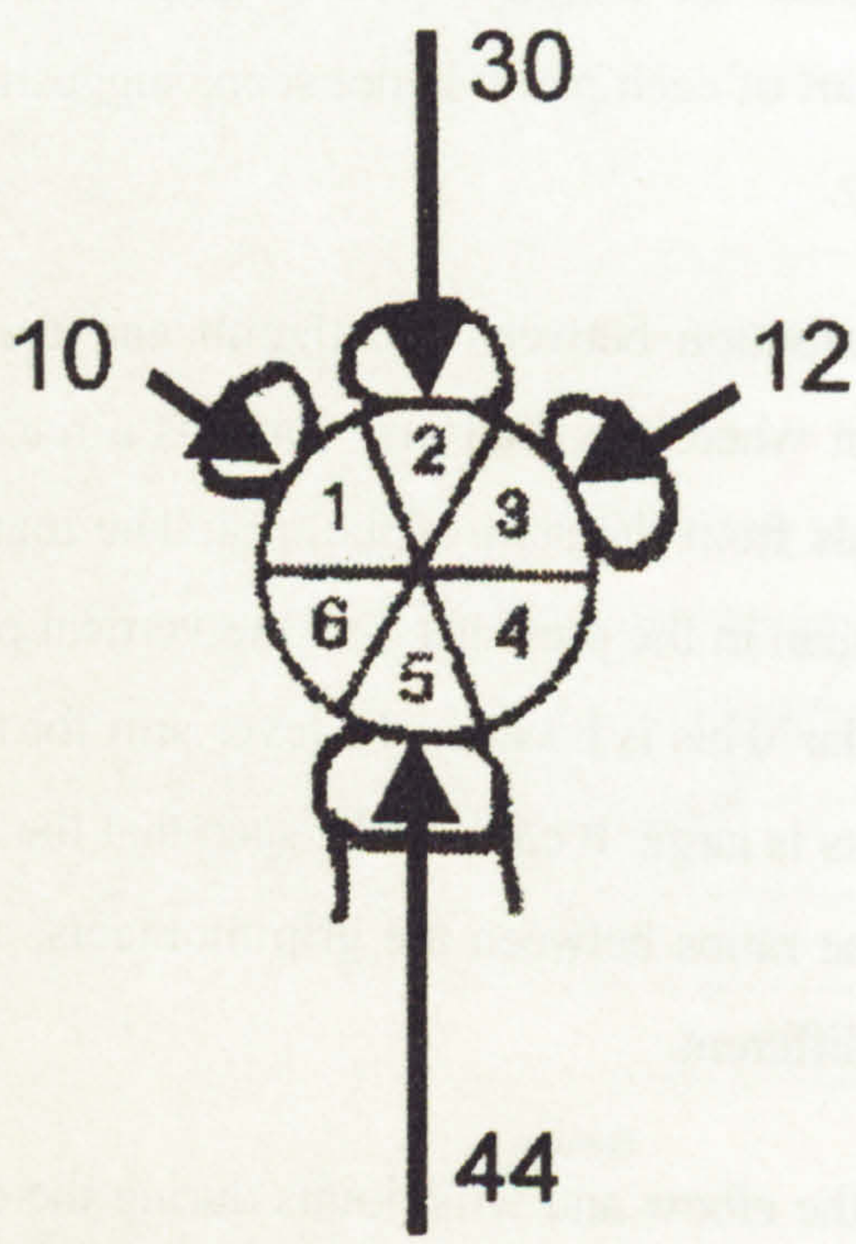

Figure 5.12 Forces on the thumb and three fingers during the chuck grip activity (Newtons).

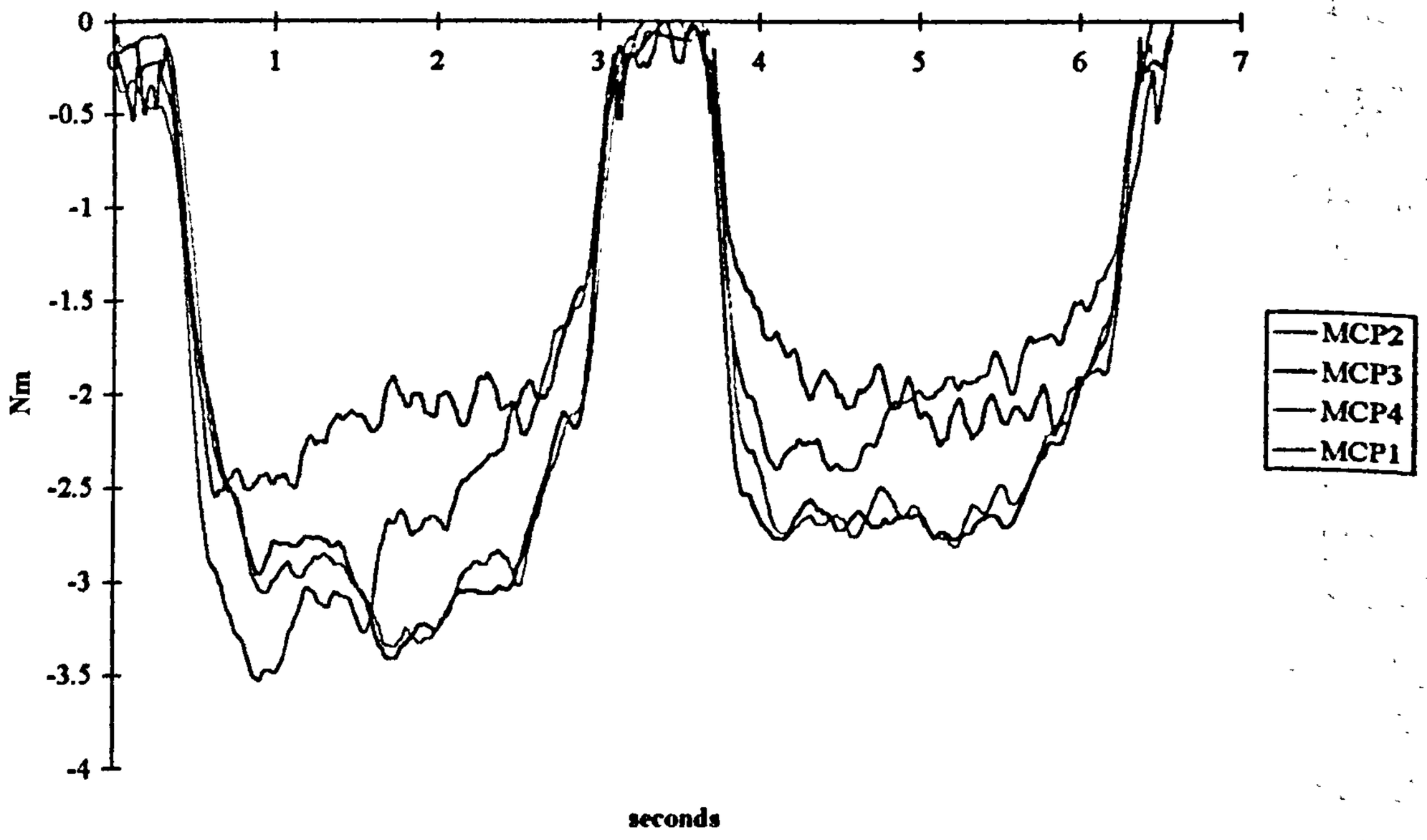

Figure 5.11 Moments applied to the MCP joints during the chuck grip activity.

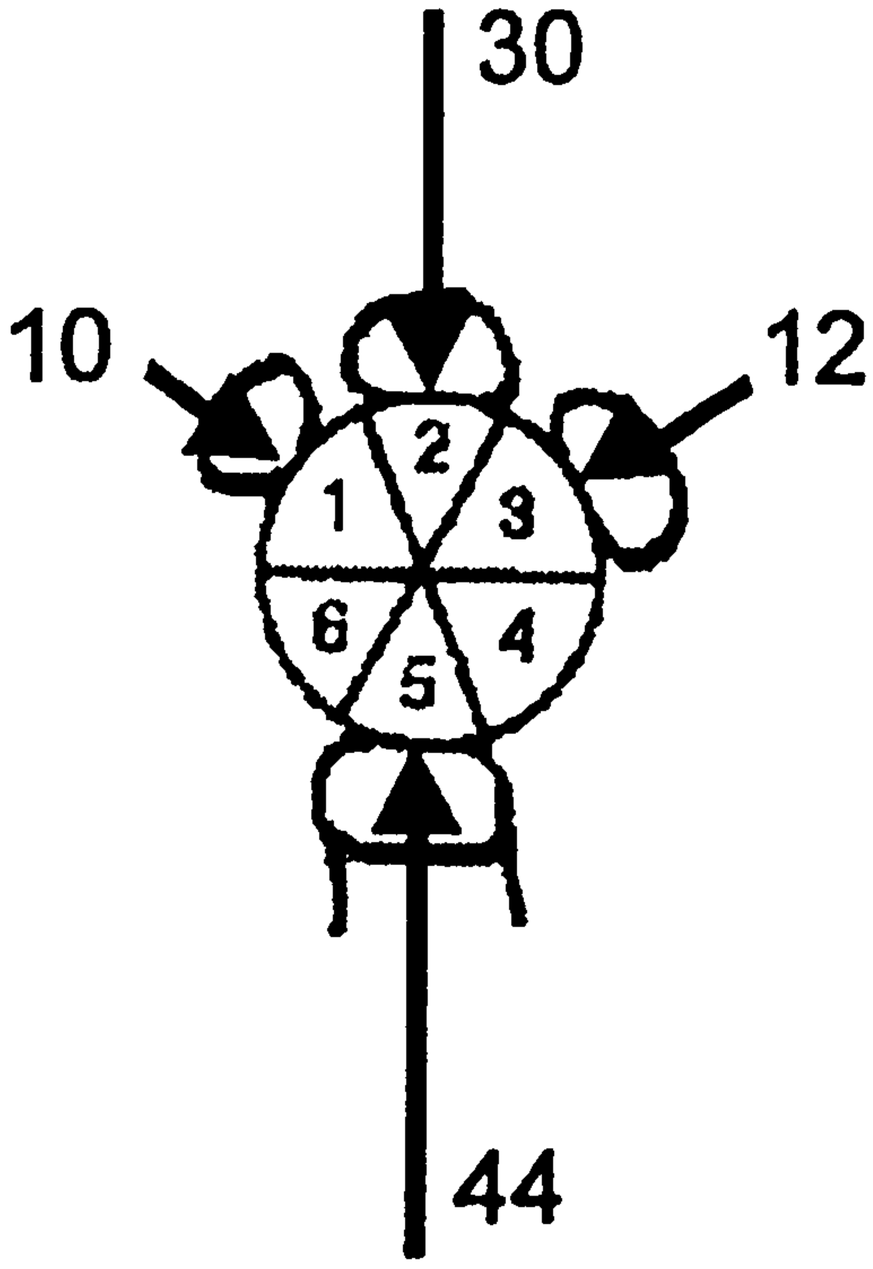

Figure 5.12 Forces on the thumb and three fingers during the chuck grip activity (Newtons).

increase in Mx. This is due to the elbow axes rotating so as to align the flexion axis more closely with the vertical, hence the gravitational forces contribute more to Mx than Mz.

Throughout the trial, the loading on the limb tends to extend, adduct and pronate the elbow. At the wrist joint, the action is that of flexion and ulnar deviation. There is also a small tendency to externally rotate the wrist throughout most of the trial, but as previously stated, this does not affect the model.

5.1.2.2 Internal forces

Load sharing between the muscles and ligaments of the arm during the chuck grip activity is shown in Figure 5.15. The distribution of muscle activity varies only slightly throughout the trial, with the highest forces coinciding with the peak in grip force. In this case, with the thumb acting in isolation on one of the transducer beams, it was possible to calculate the force in flexor pollicis longus (FPL). This reached a peak value of approximately 200N. The peak forces in FDP and FDS were much higher at over 400N and 450N respectively.

The results from the optimisation routine indicate that the required extension and radial deviation moment at the wrist is distributed between the ECRL, ECRB and ECU, as before. ECRB has a higher force than ECRL, and this is because it has a larger moment arm in flexion-extension. However, in this case, compared with the vertical power grip, there is a higher force in ECU, and this may be due to the increased radial deviation moment caused by the introduction of FPL, and the lower external adduction moment.

At the elbow, the flexion moment is provided mainly by the BRD muscle, as this has the largest moment arm, and the ECRL, which is already active to balance moments at the wrist. This has a similar moment arm to that of BRA, but has a lower cost in the optimisation, although it is a much bigger muscle, because the addition of BRA would add to the overall joint compression force. There is a small amount of activity from BRA and BIC towards the ends of the active phase.

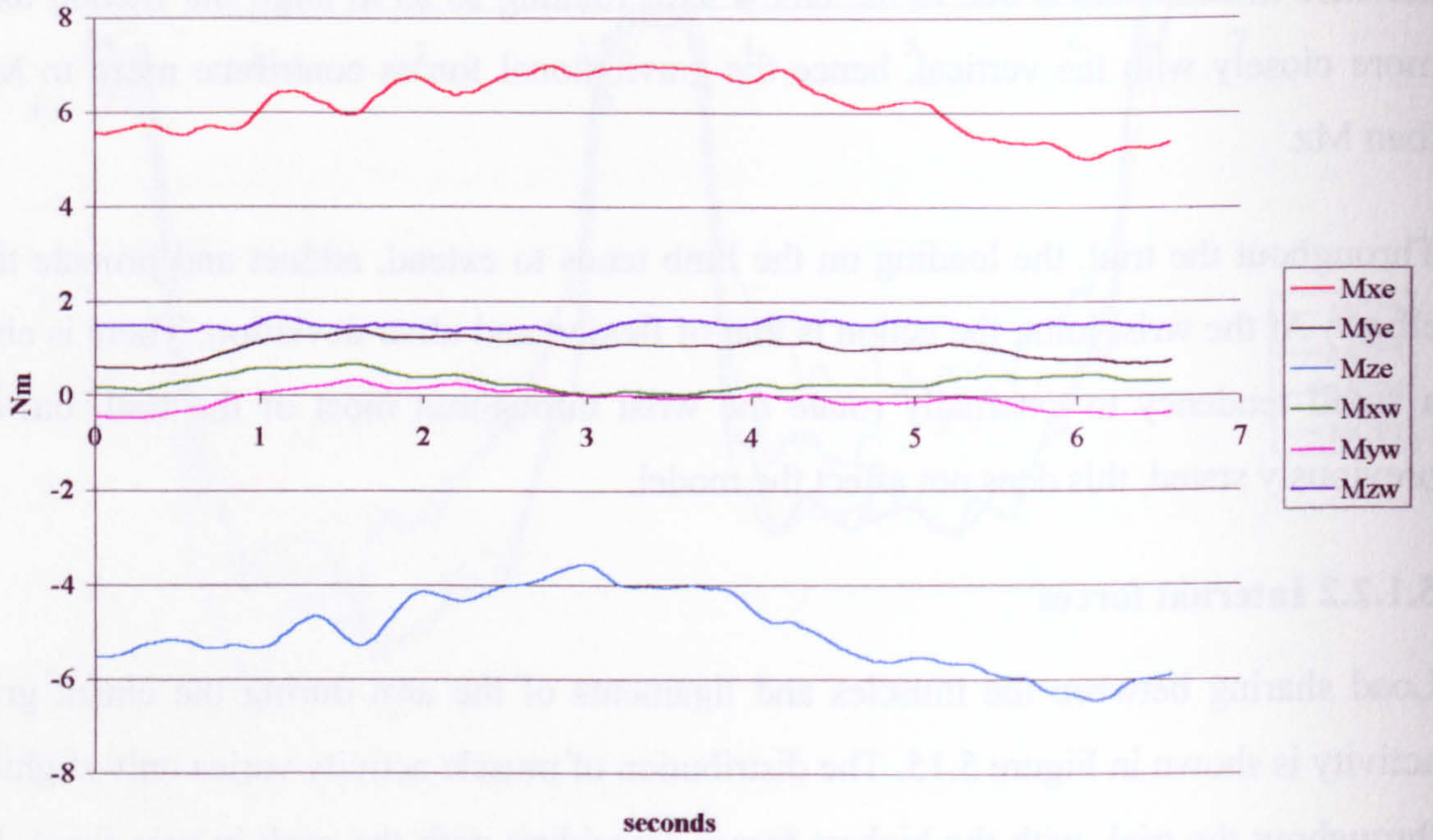

Figure 5.13 Moments applied to the elbow and wrist joints during the chuck grip activity.

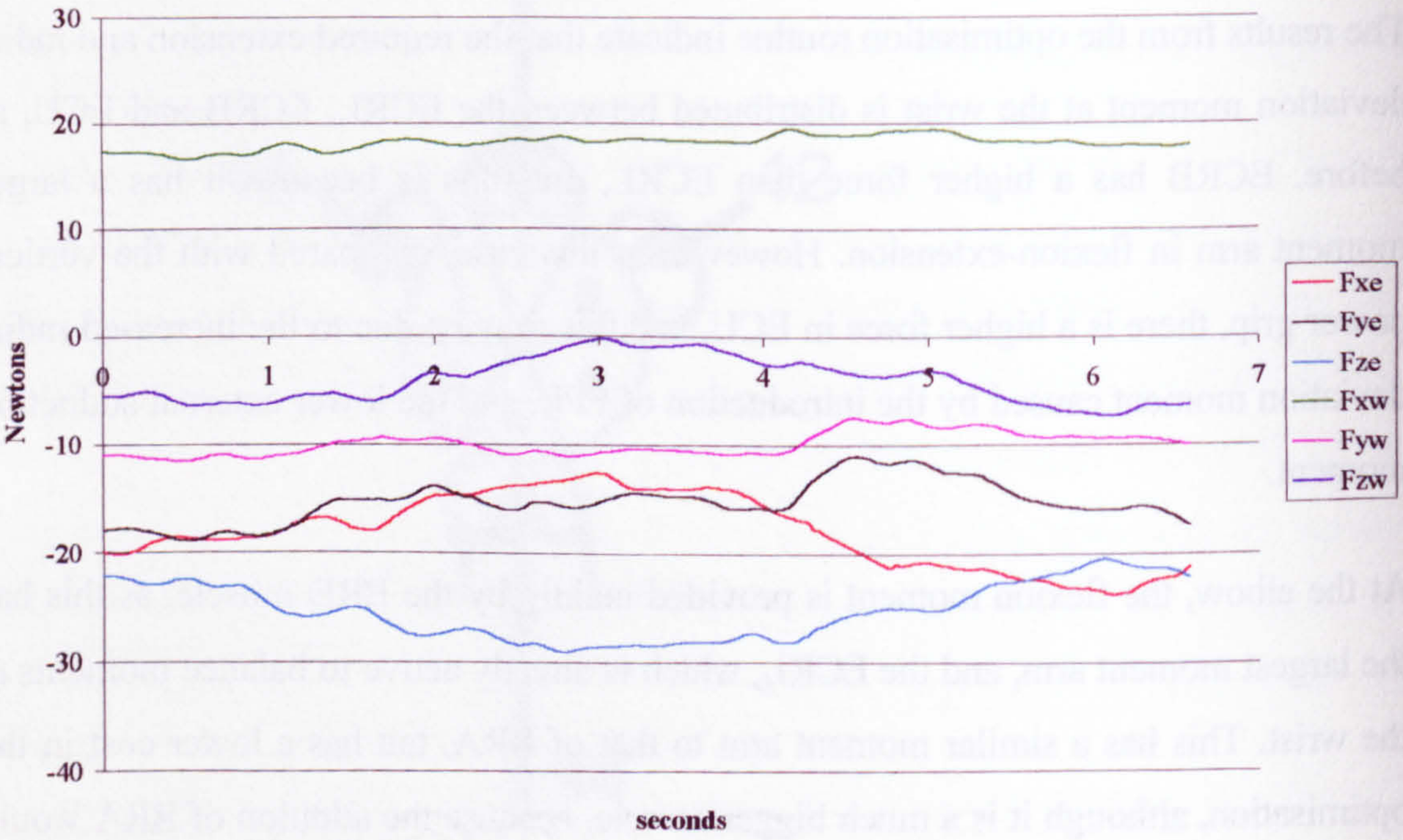

Figure 5.14 Forces applied to the elbow and wrist joints during the chuck grip activity.

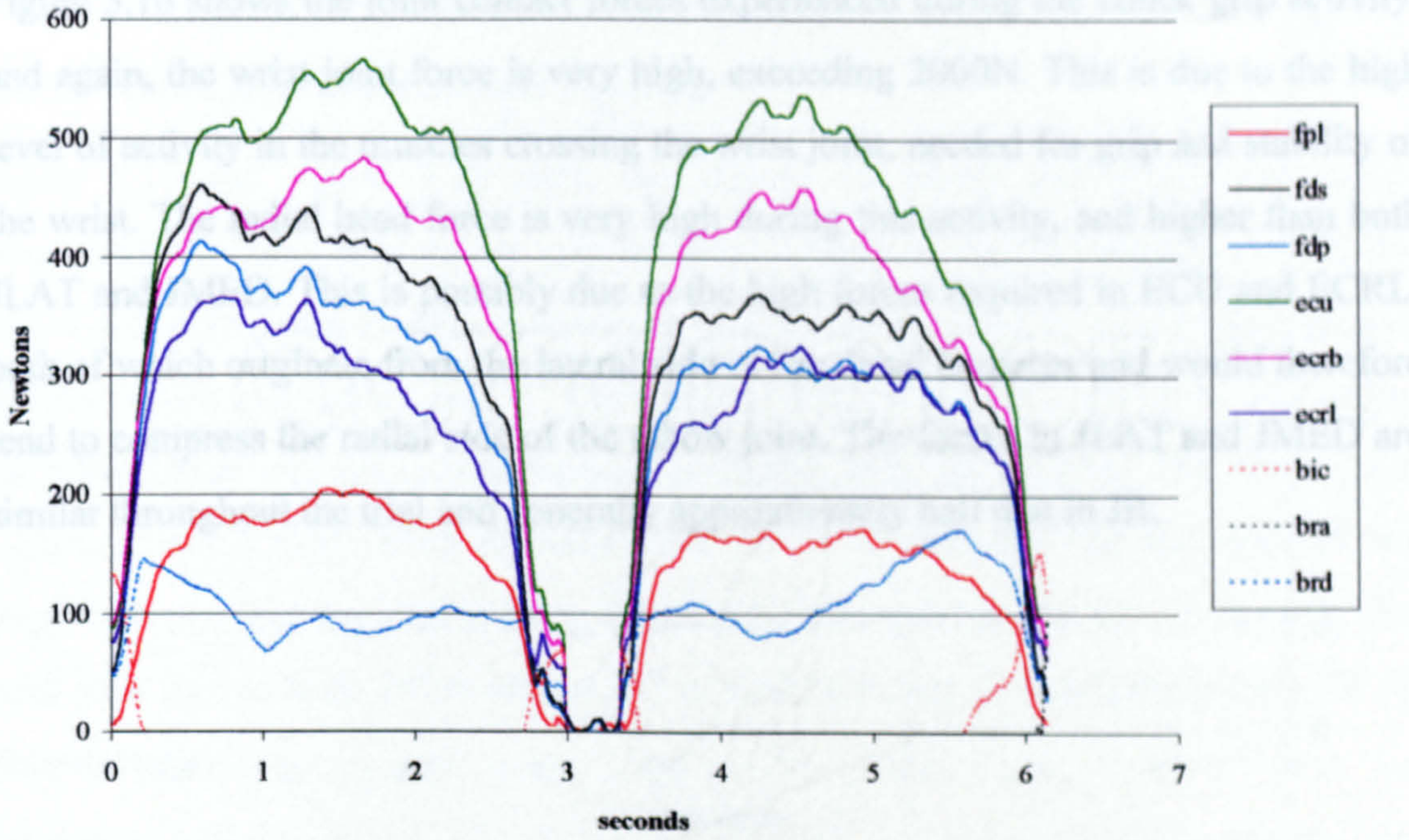

Figure 5.15 Graph of muscle and ligament force levels against time during the chuck grip activity.

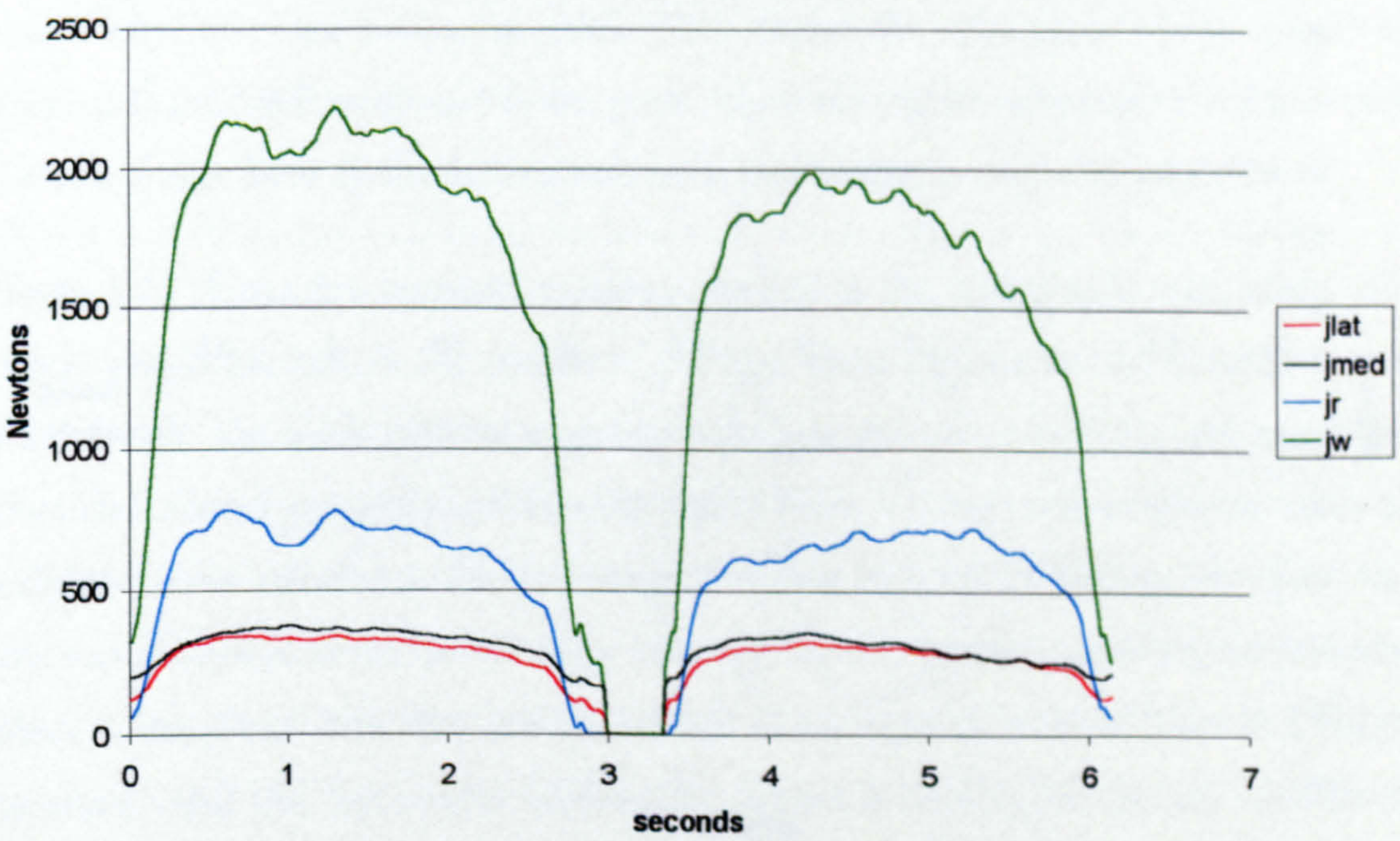

Figure 5.16 Graph of joint contact force levels against time during the chuck grip activity.

Figure 5.16 shows the joint contact forces experienced during the chuck grip activity, and again, the wrist joint force is very high, exceeding 2000N. This is due to the high level of activity in the muscles crossing the wrist joint, needed for grip and stability of the wrist. The radial head force is very high during this activity, and higher than both JLAT and JMED. This is possibly due to the high forces required in ECU and ECRL, both of which originate from the lateral side of the distal humerus and would therefore tend to compress the radial side of the elbow joint. The forces in JLAT and JMED are similar throughout the trial and generally approximately half that in JR.

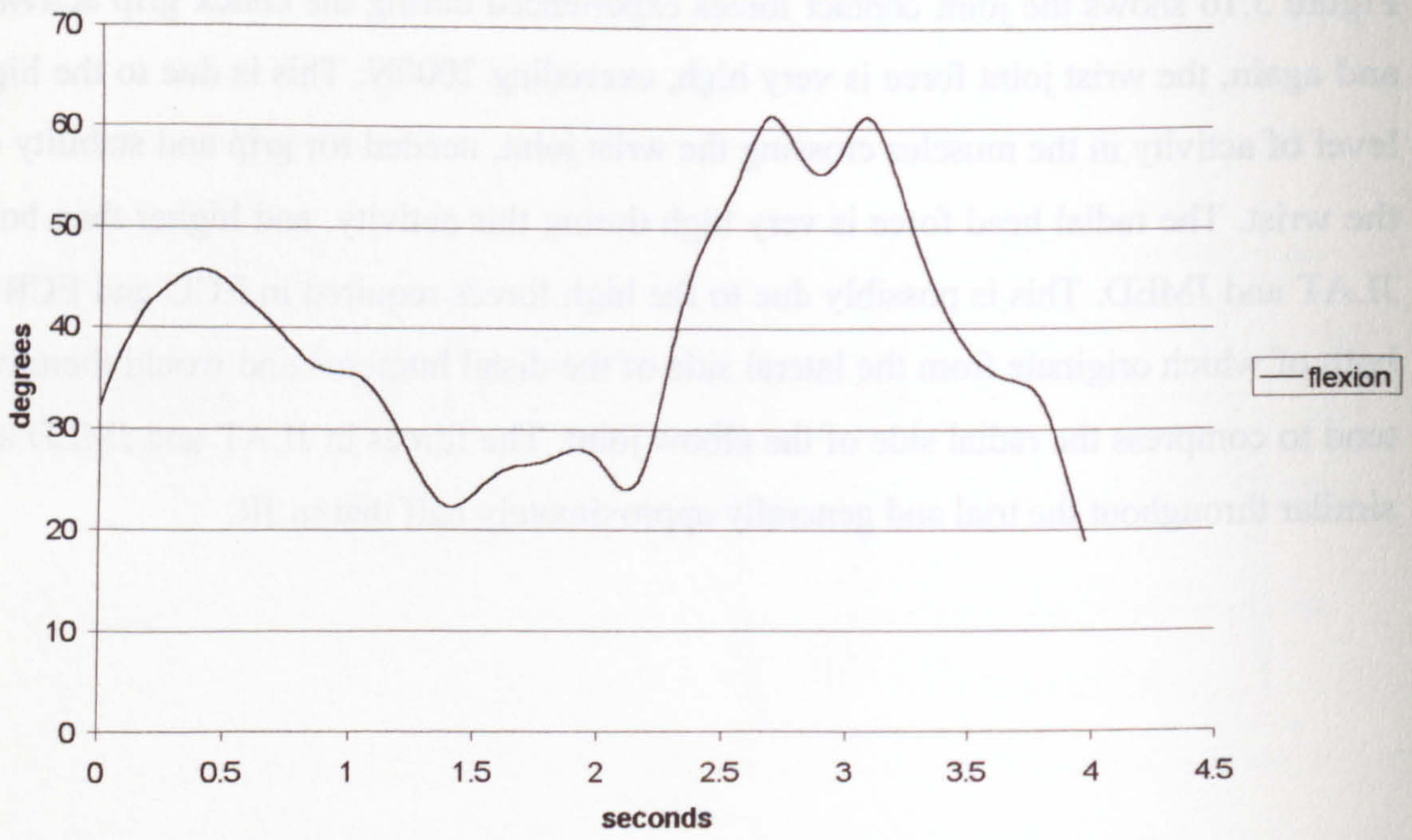

Figure 5.17 Variation of elbow joint flexion angle during the horizontal power grip activity.

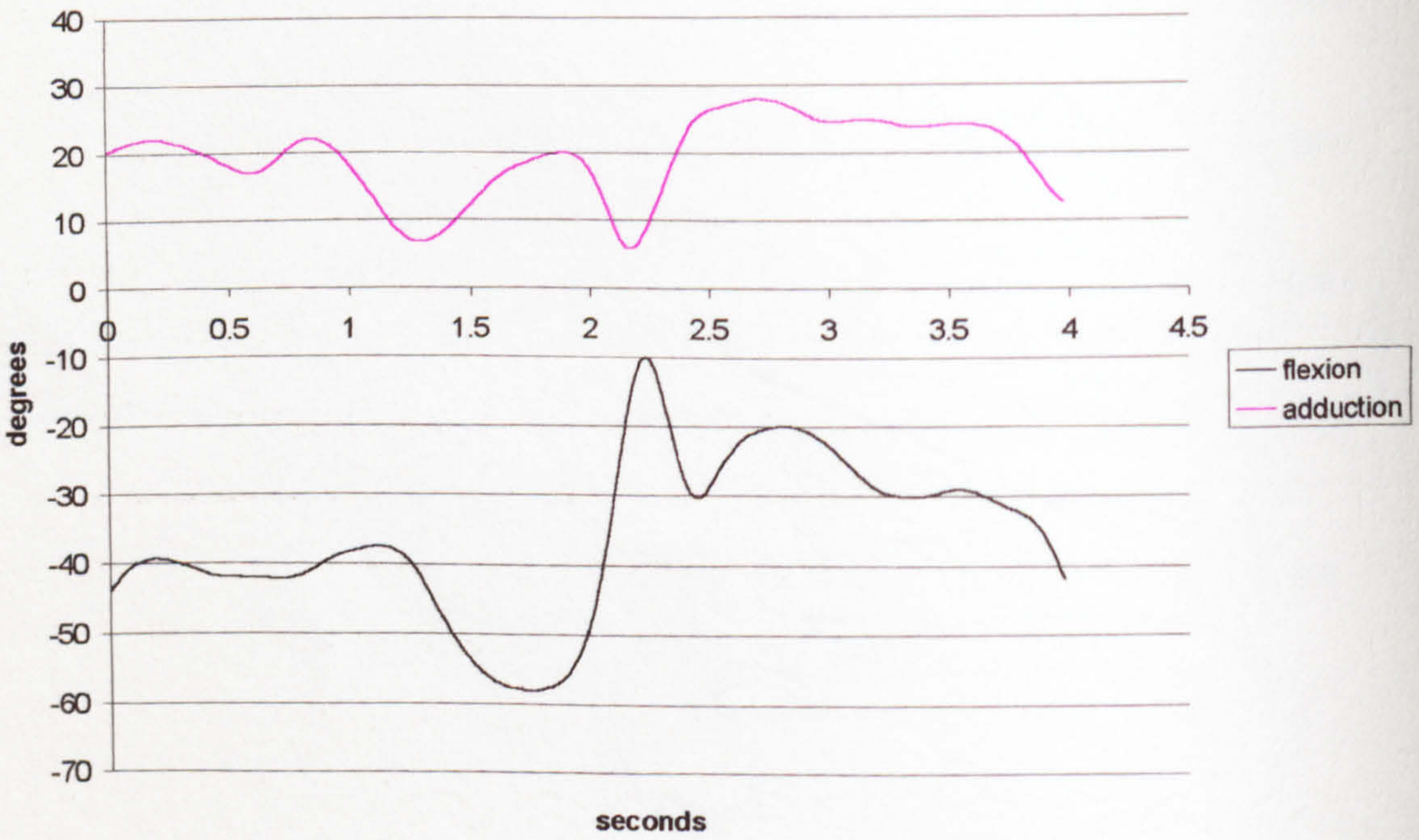

Figure 5.18 Variation of wrist joint angles during the horizontal power grip activity.

5.1.3 POWER GRIP (HANDLE HORIZONTAL)

5.1.3.1 Kinematics and External Loading

Figure 5.17 and Figure 5.18 show the change in elbow and wrist joint angles throughout the horizontal power grip activity. It appears that the motion at both the elbow and wrist joints is more pronounced than in the previous two examples, and the activity occurs in a shorter period. This may be attributed more to the style adopted by the subject than any inherent difference in the nature of the activity. The elbow joint motion covers a range from approximately 20° to 60° flexion, and the slope of the graph indicates that the joint is being flexed relatively quickly (up to 1.75 rad s^{-1}). The wrist joint moves from 10° to almost 60° in extension and up to approximately 28° in ulnar deviation.

The calculated moment on the MCP joints during the horizontal power grip activity can be seen in Figure 5.19. The highest moment in seen in the third MCP joint, that of the middle finger, and peaks at approximately 3.7Nm.

Figure 5.20 shows the distribution of force around the cylinder for the horizontal power activity at an instant in time. This shows the maximum forces occurring adjacent to the MCP joints and to the point where the thumb and finger overlap. There is also a higher force on the bottom surface of the handle, as might be expected.

Figure 5.21 shows that external moments applied to the elbow and wrist joints, and clearly shows the 'rest' in the middle of the trial when the grip on the transducer was relinquished. The small residual moments acting on the arm at this time are due to the mass and inertial properties of the limb itself. This activity was conducted with an additional mass attached to the transducer, bringing the total to 3.85kg. The mass was attached at the end of the device away from the handle, further increasing the moment effect at the joints. The very sudden change in moment is because there is a single threshold value that determines whether the subject is holding the device, whereas in reality the transfer of force would occur with a gradual change. This simplification does not change the maximum values occurring during the trial, which are of primary interest.

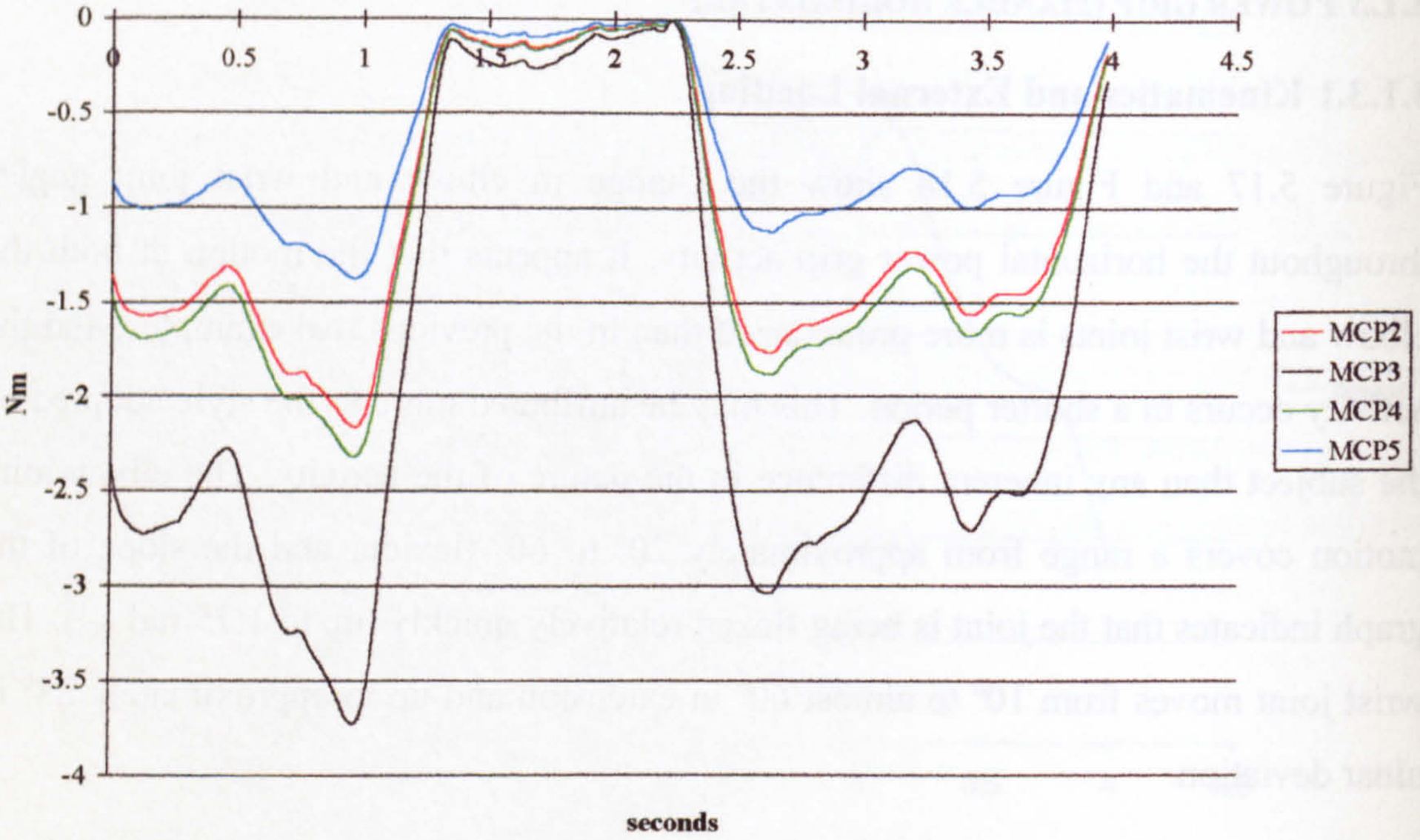

Figure 5.19 Moments applied to the MCP joints during the horizontal power grip activity.

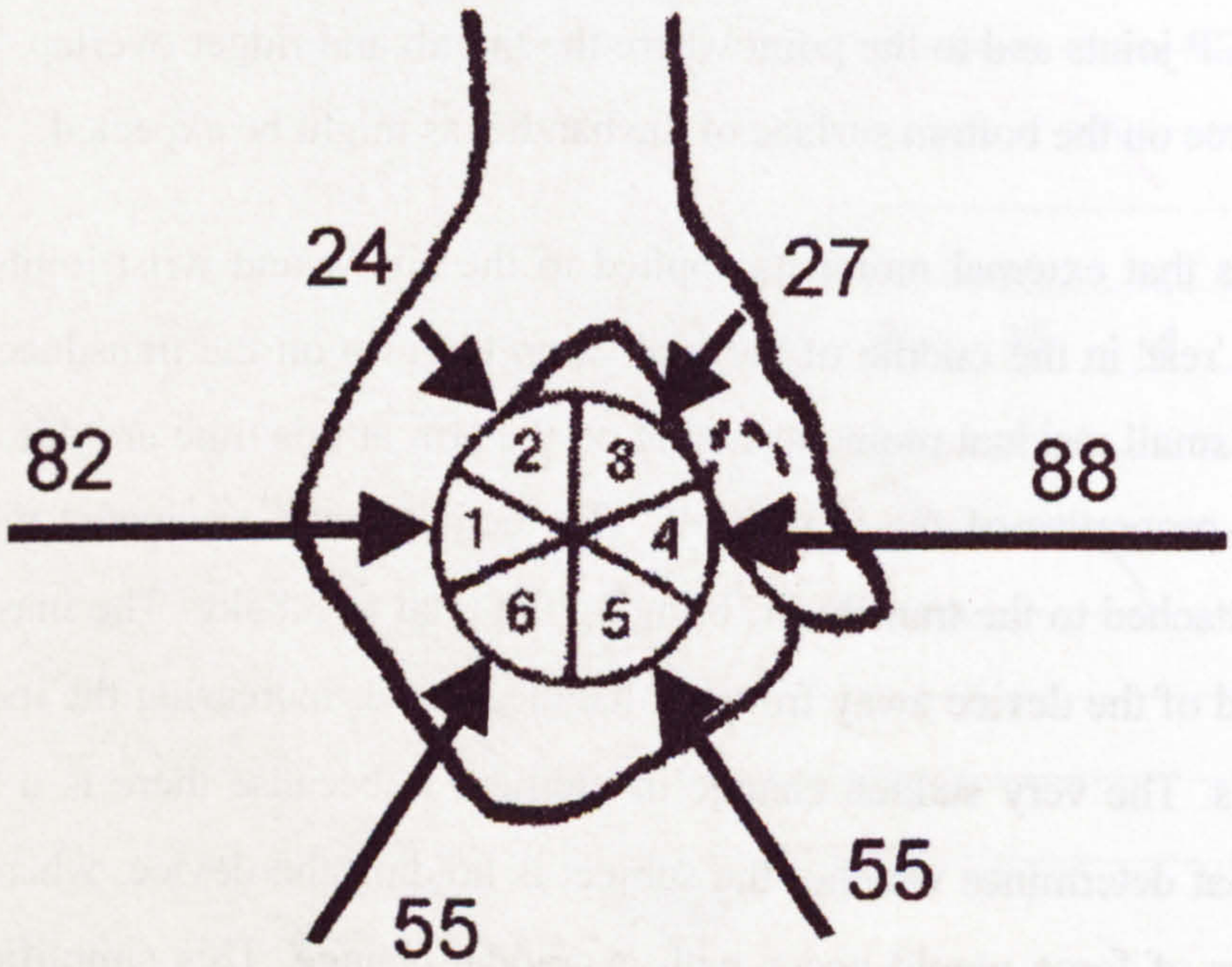

Figure 5.20 Force distribution around the transducer handle during the horizontal power grip activity (Newtons).

Throughout the trial the load tends to extend the elbow joint with the maximum moment being recorded as 20Nm. There is a large variation in the moment value during the trial, and a similar effect is seen in the forces on the joints, shown in Figure 5.22. This pattern can be explained by examining the motion of the joint from Figure 5.17. When the device is being lifted, or accelerated upwards, there is an increase in the inertial force and in the moment produced by the inertial force. As it reaches maximum height and is accelerated downwards, the inertial force acts in the opposing direction and reduces the moment at the joint. There is also a moment tending to adduct the elbow, and to cause pronation during the first half of the trial and supination during the second half.

At the wrist joint, there are much larger moments than seen in the previous two activities due to the increased mass of the transducer. The effect of these moments is to cause flexion and ulnar deviation.

5.1.3.2 Internal forces

Figure 5.23 shows the forces in the muscles and ligaments during the horizontal power grip activity. The forces in the finger flexors, FDP and FDS, are similar to those seen in the previous activities, peaking at approximately 500N. The higher flexion and adduction moment at the wrist is reflected in the higher forces seen in ECRL and ECRB, with the latter reaching a peak of over 700N. ECU is also active, although at a lower level.

At the elbow, the flexion moment is provided by the BRD muscle, and the ECRL muscle, which has a significant flexion moment arm at the elbow. BRD, ECRL and ECU all have significant moment arms in abduction also, and so are able to balance the external adduction moment. BRA is not selected by the model during this activity, despite its bulk, as it has a smaller moment arm in flexion than BRD and tends to adduct the elbow. BIC is used for part of the trial, particularly at the start and end of each phase, as the grip force decreases. At these points the elbow is more extended and the difference in moment arms between BRD and BIC decreases.

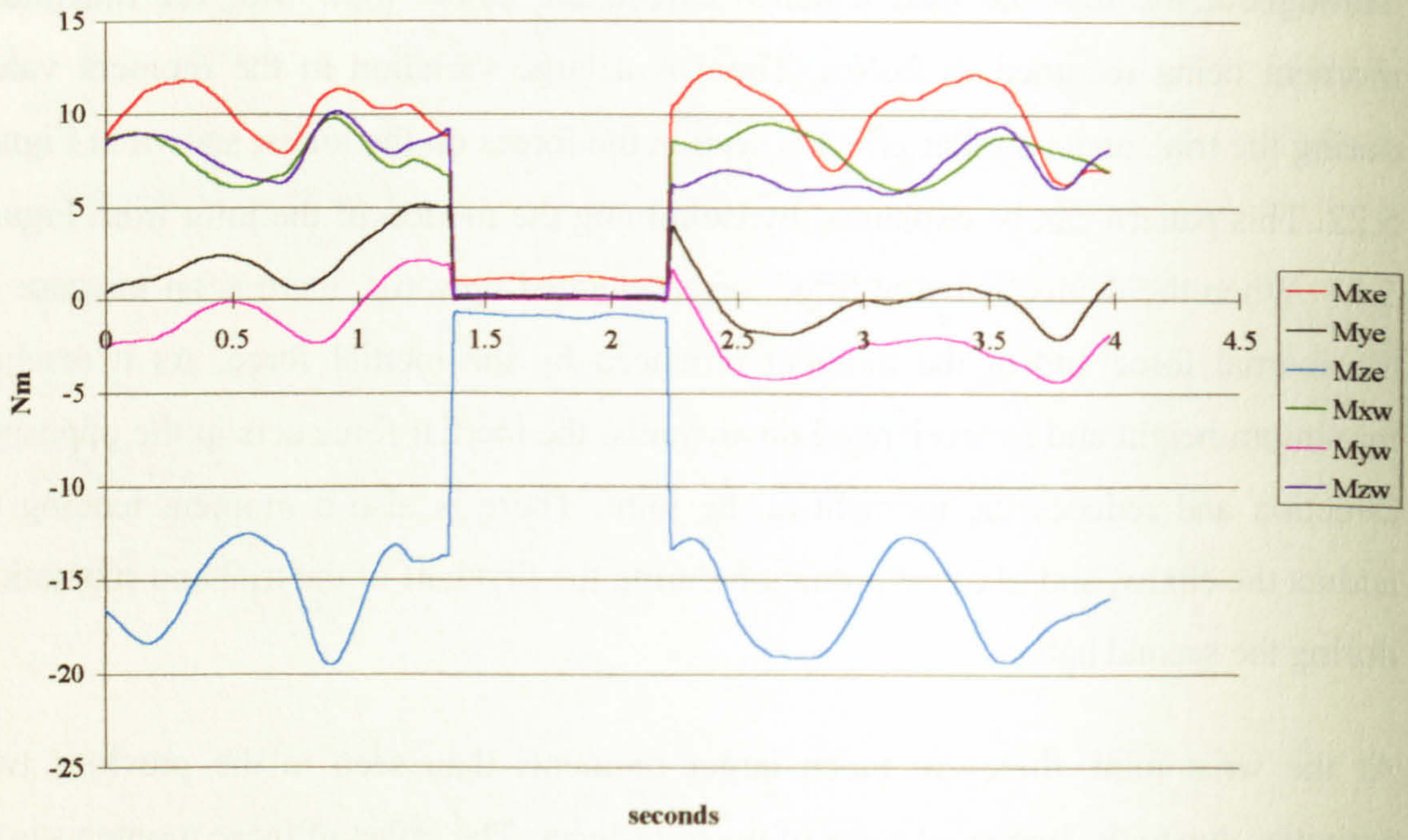

Figure 5.21 Moments applied to the elbow and wrist joints during the horizontal power grip activity.

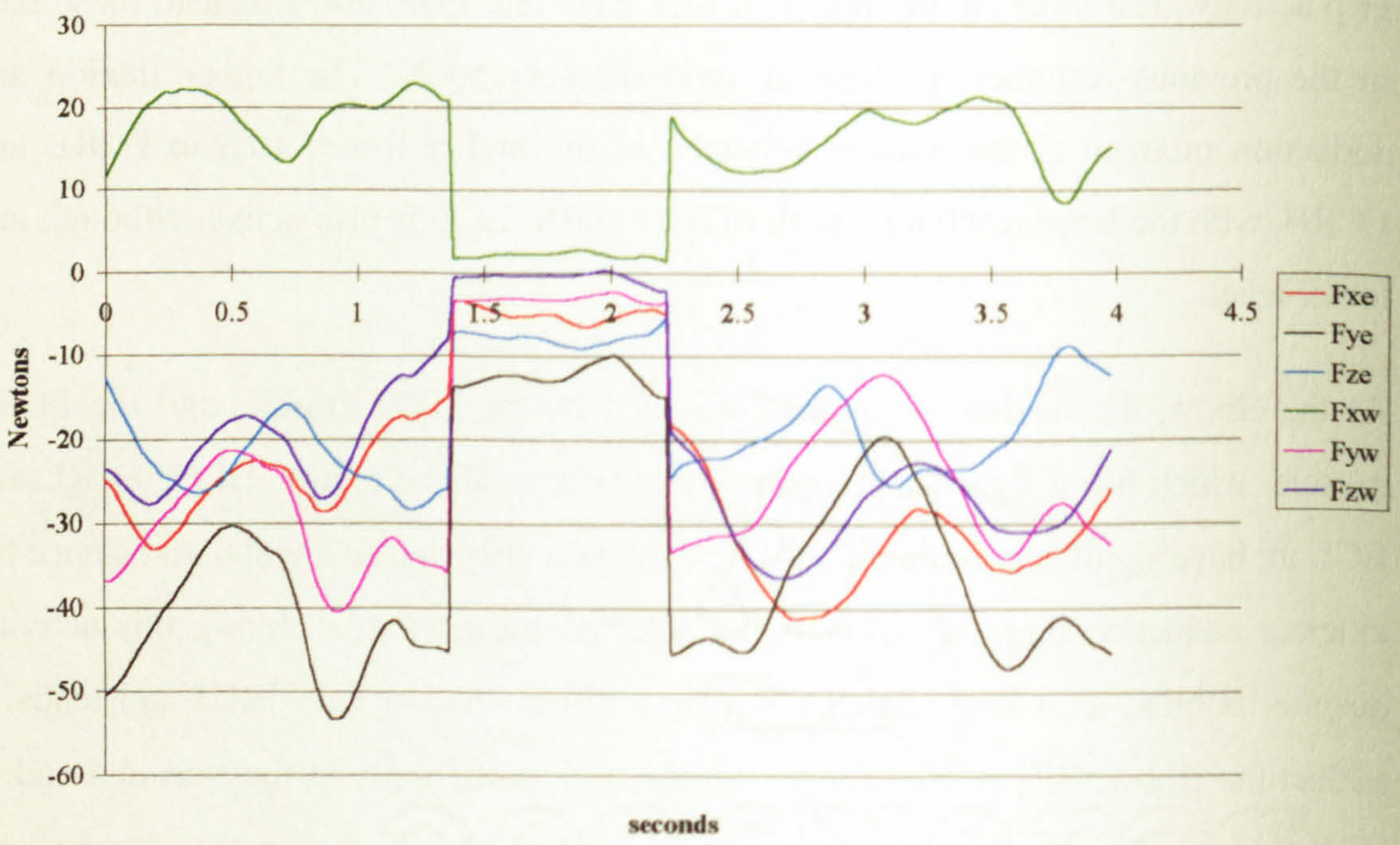

Figure 5.22 Forces applied to the elbow and wrist joints during the horizontal power grip activity.

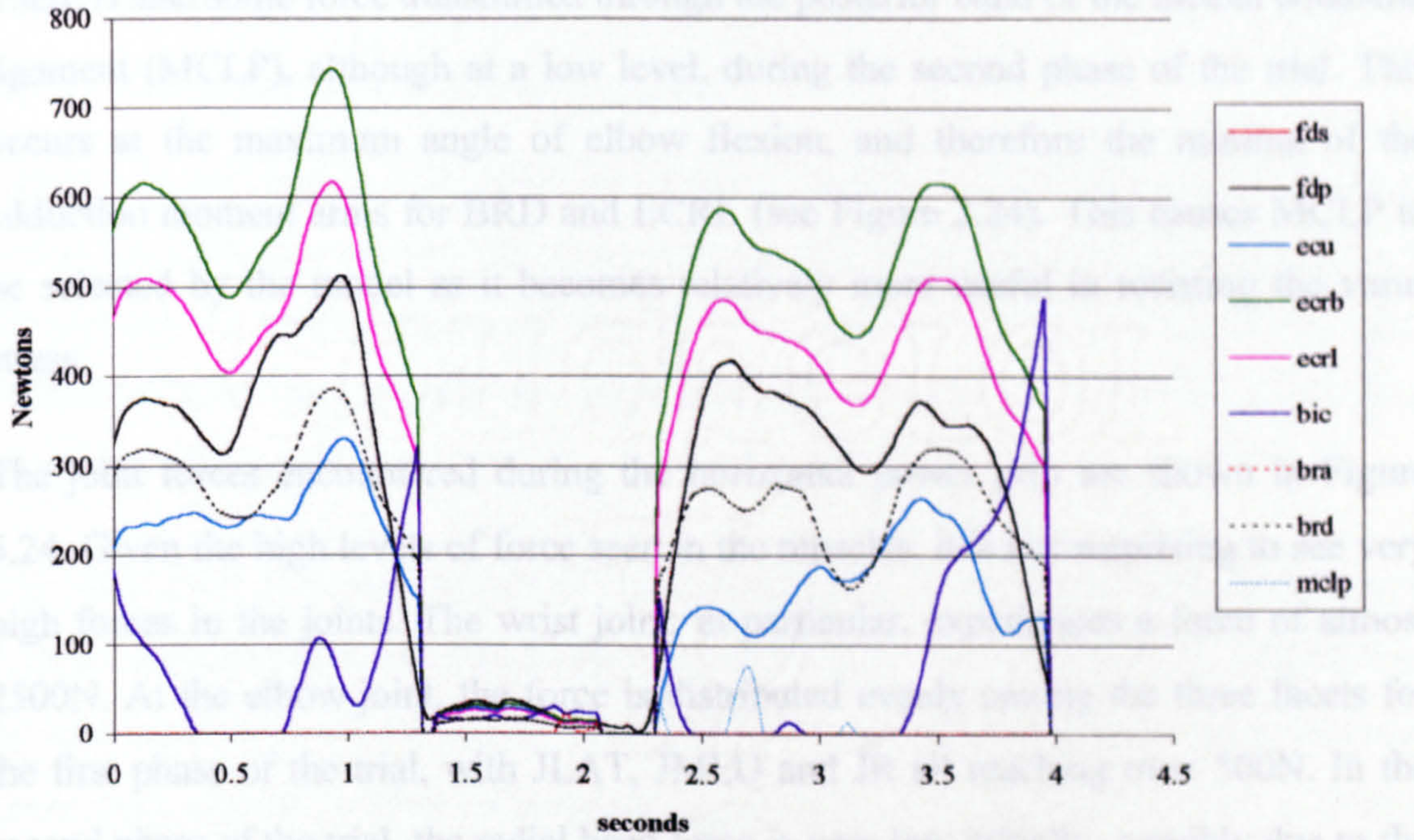

Figure 5.23 Graph of muscle and ligament force levels against time during the horizontal power grip activity.

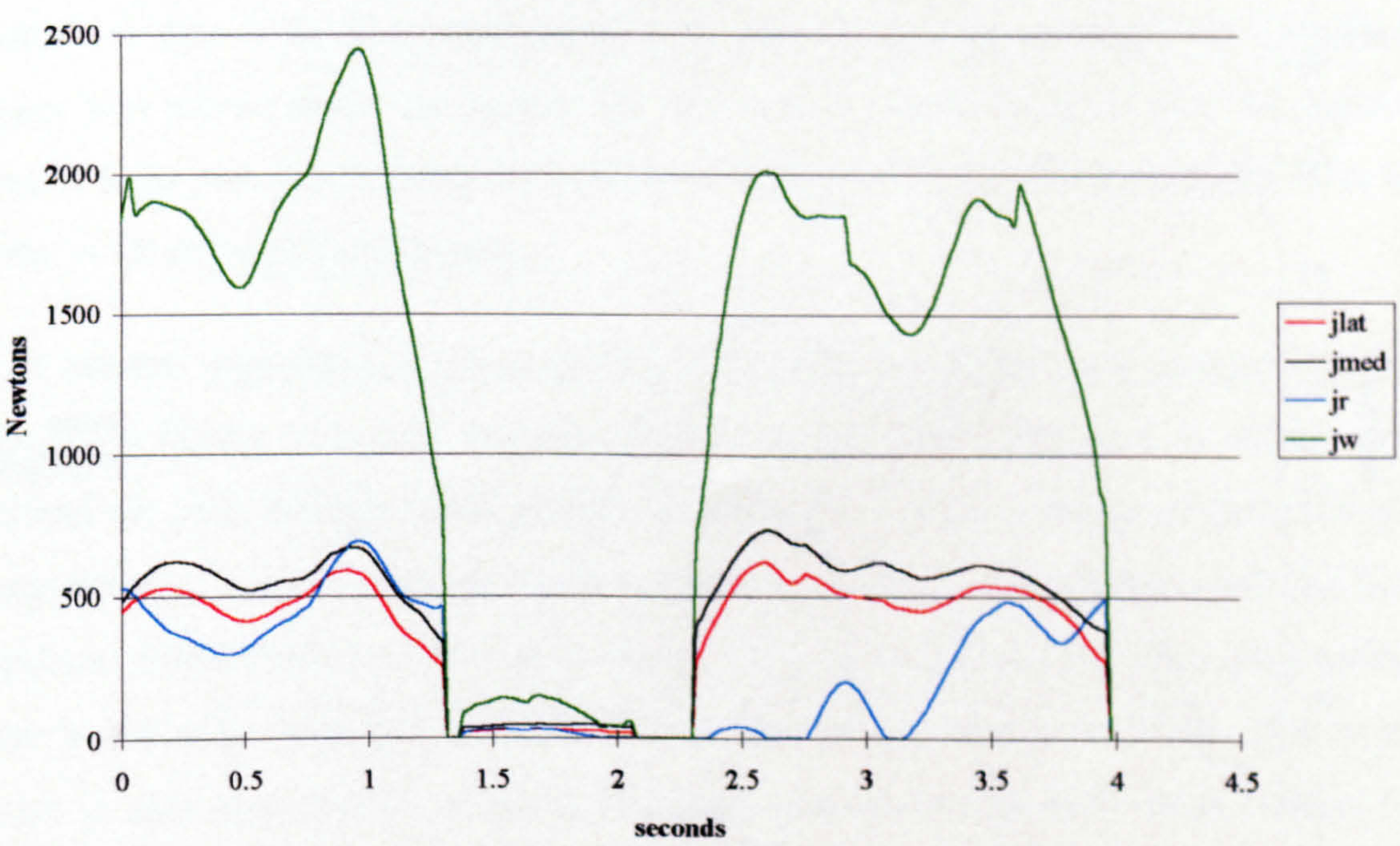

Figure 5.24 Graph of joint contact force levels against time during the horizontal power grip activity.

There is also some force transmitted through the posterior band of the medial collateral ligament (MCLP), although at a low level, during the second phase of the trial. This occurs at the maximum angle of elbow flexion, and therefore the minima of the adduction moment arms for BRD and ECRL (see Figure 2.24). This causes MCLP to be selected by the model as it becomes relatively more useful in resisting the varus stress.

The joint forces encountered during the horizontal power grip are shown in Figure 5.24. Given the high levels of force seen in the muscles, it is not surprising to see very high forces in the joints. The wrist joint, in particular, experiences a force of almost 2500N. At the elbow joint, the force is distributed evenly among the three facets for the first phase of the trial, with JLAT, JMED and JR all reaching over 500N. In the second phase of the trial, the radial head force is very low initially, possibly due to the slightly reduced force in the forearm extensor muscles, but increases towards the end of the trial.

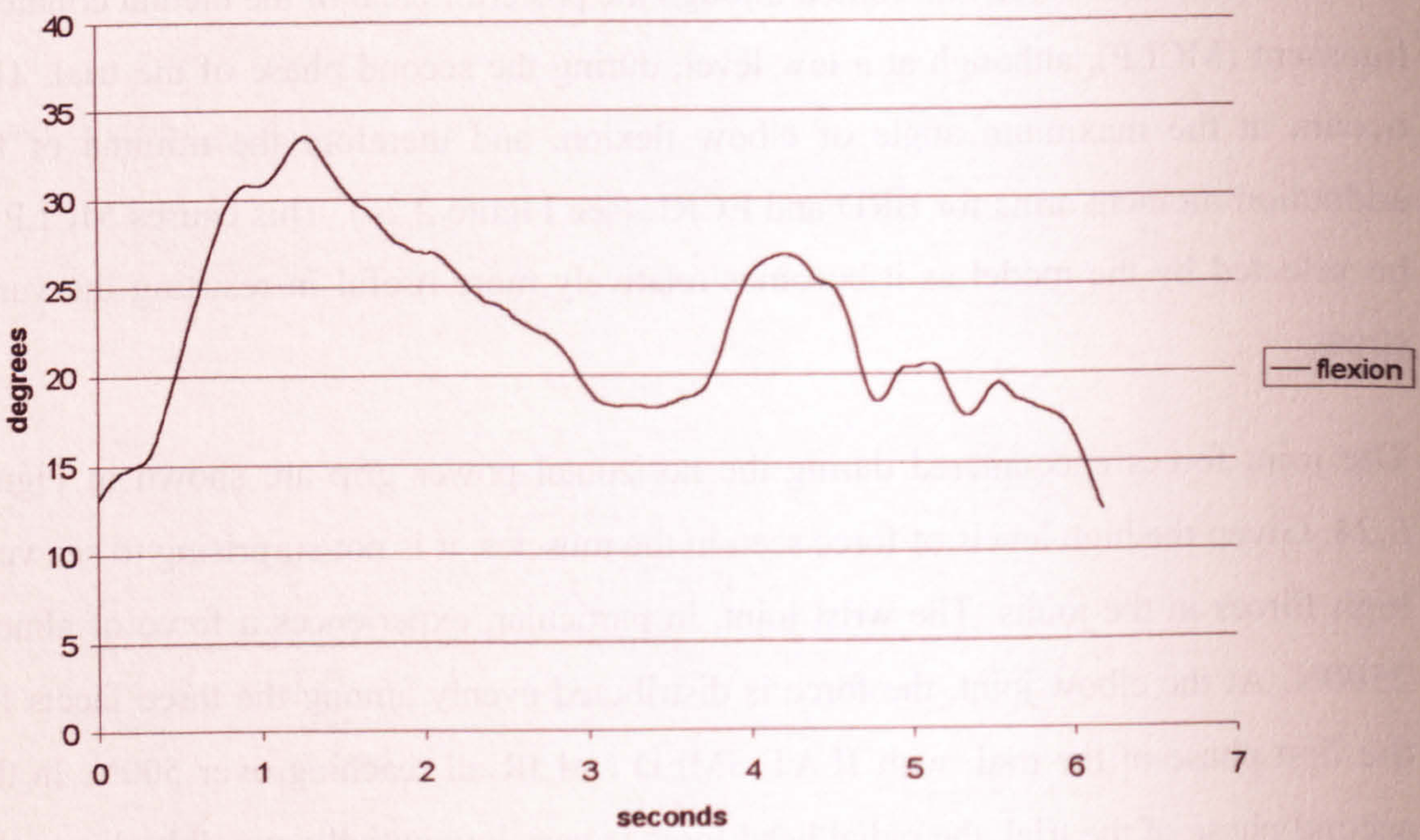

Figure 5.25 Variation of elbow joint flexion angle during the hook grip activity.

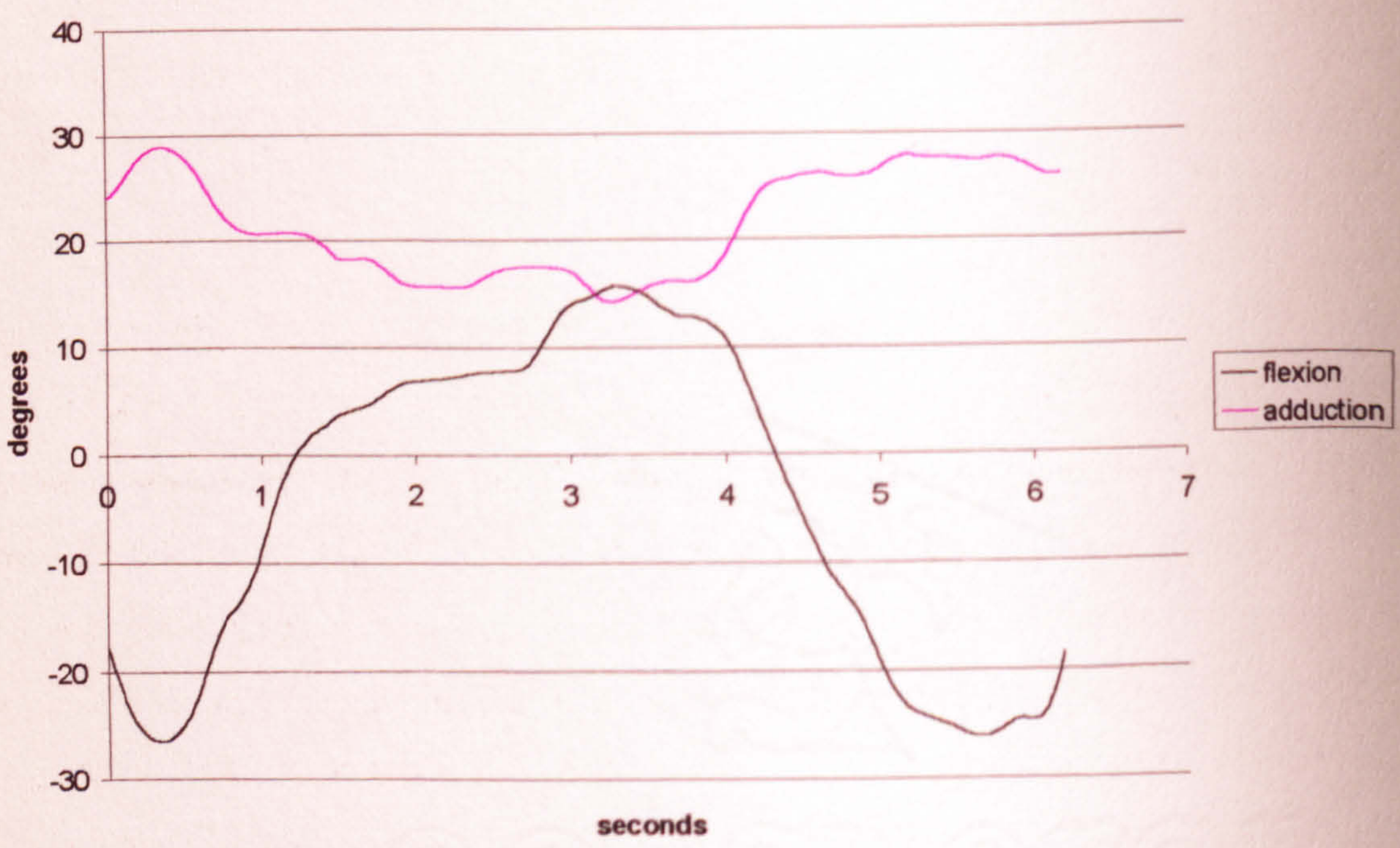

Figure 5.26 Variation of wrist joint angles during the hook grip activity.

5.1.4 HOOK GRIP

5.1.4.1 Kinematics and External Loading

Figure 5.25 and Figure 5.26 show the range of motion of the elbow and wrist joints during the hook grip activity. It can be seen that the maximum elbow flexion angle is 35° and that the wrist joint passes from extension to flexion and back during the trial. The wrist joint also remains in ulnar deviation throughout the trial, reaching a maximum of approximately 30°.

The MCP joint moments, shown in Figure 5.27, reach a maximum of approximately 2.5Nm, significantly lower than in the other three activities. This is to be expected as the additional mass of transducer is placed closer to the hand than in the horizontal power grip, and the problem of having to prevent slip is not seen as it is in the activities where the handle is oriented vertically. The peak moments are seen at the start of each phase of the trial, as the transducer is lifted off the table.

The distribution of force around the grip is shown in Figure 5.28, and shows a similar pattern to that of the horizontal power grip. This is because, although the additional mass was placed under the handle for this activity, some subjects held the handle nearer to its end, thus making the activity similar to the horizontal power grip. This is seen in the external loads graphs.

The external moments and forces applied to the joints during the hook grip activity are shown in Figure 5.29. The moments applied to the elbow joint tend to adduct and extend the joint throughout the motion, and there is a peak in the extension moment seen between 4 and 5 seconds which approaches 20Nm. This coincides with the two peaks in elbow flexion angle seen in Figure 5.25. There is a similar, although smaller, rise in the wrist adduction moment at this time, to approximately 12Nm. The wrist joint is also subjected to a flexion moment throughout the trial. With respect to rotation, both the wrist and elbow joints are subjected to loads tending to externally rotate them at the start and end of the trial, and loads tending to internally rotate them during the rest of the trial.

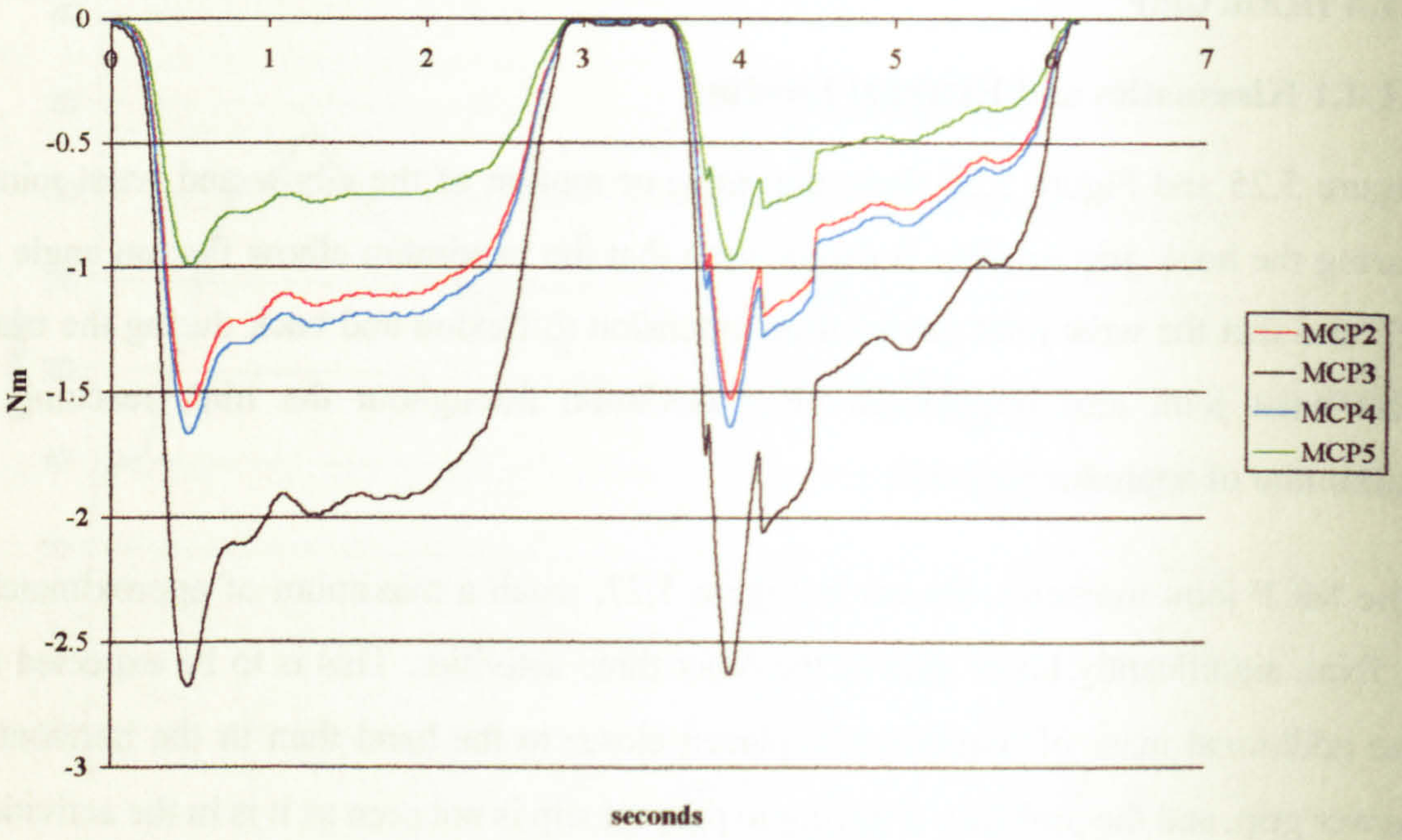

Figure 5.27 Moments applied to the MCP joints during the hook grip activity.

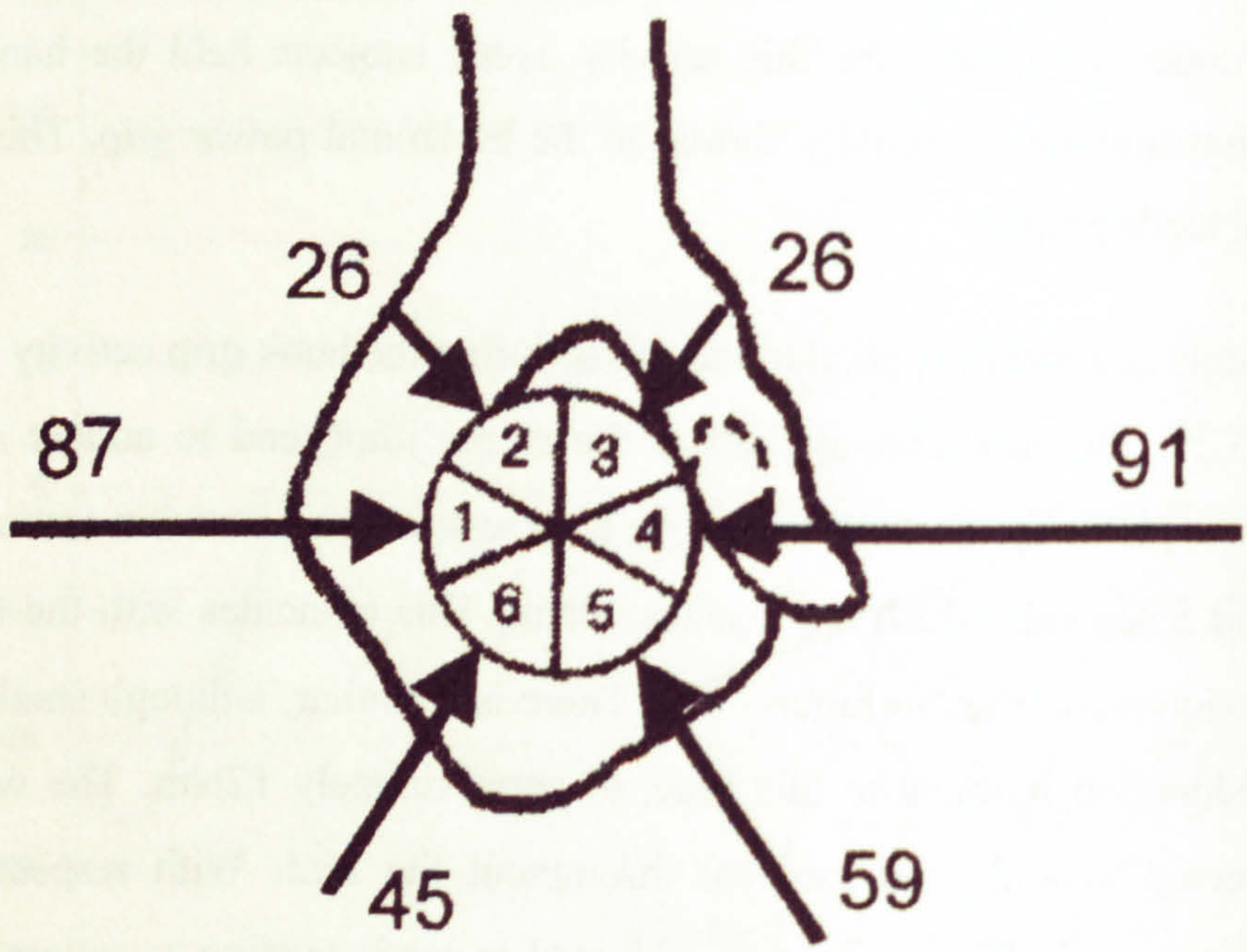

Figure 5.28 Force distribution around the transducer handle during the hook grip activity (Newtons).

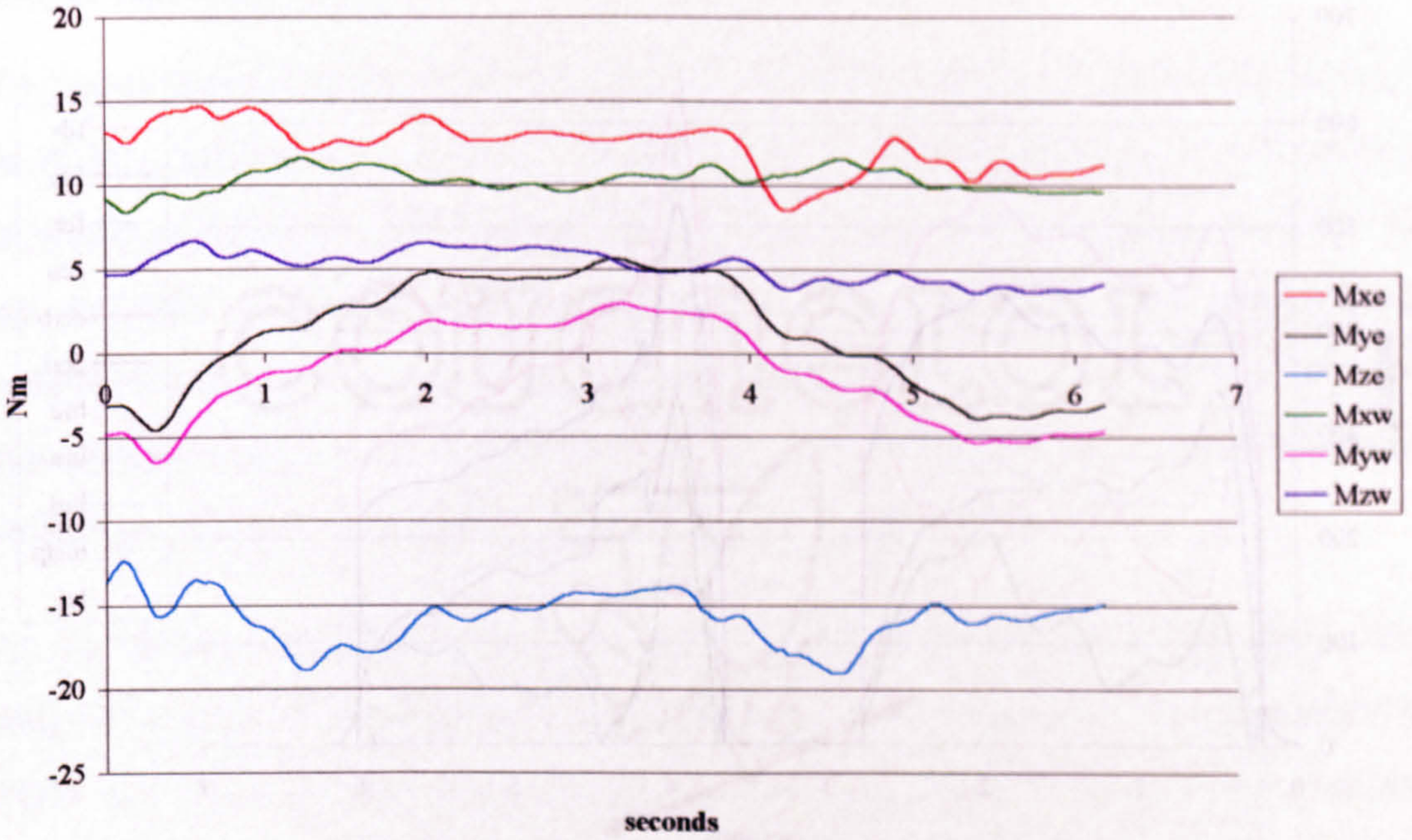

Figure 5.29 Moments applied to the elbow and wrist joints during the hook grip activity.

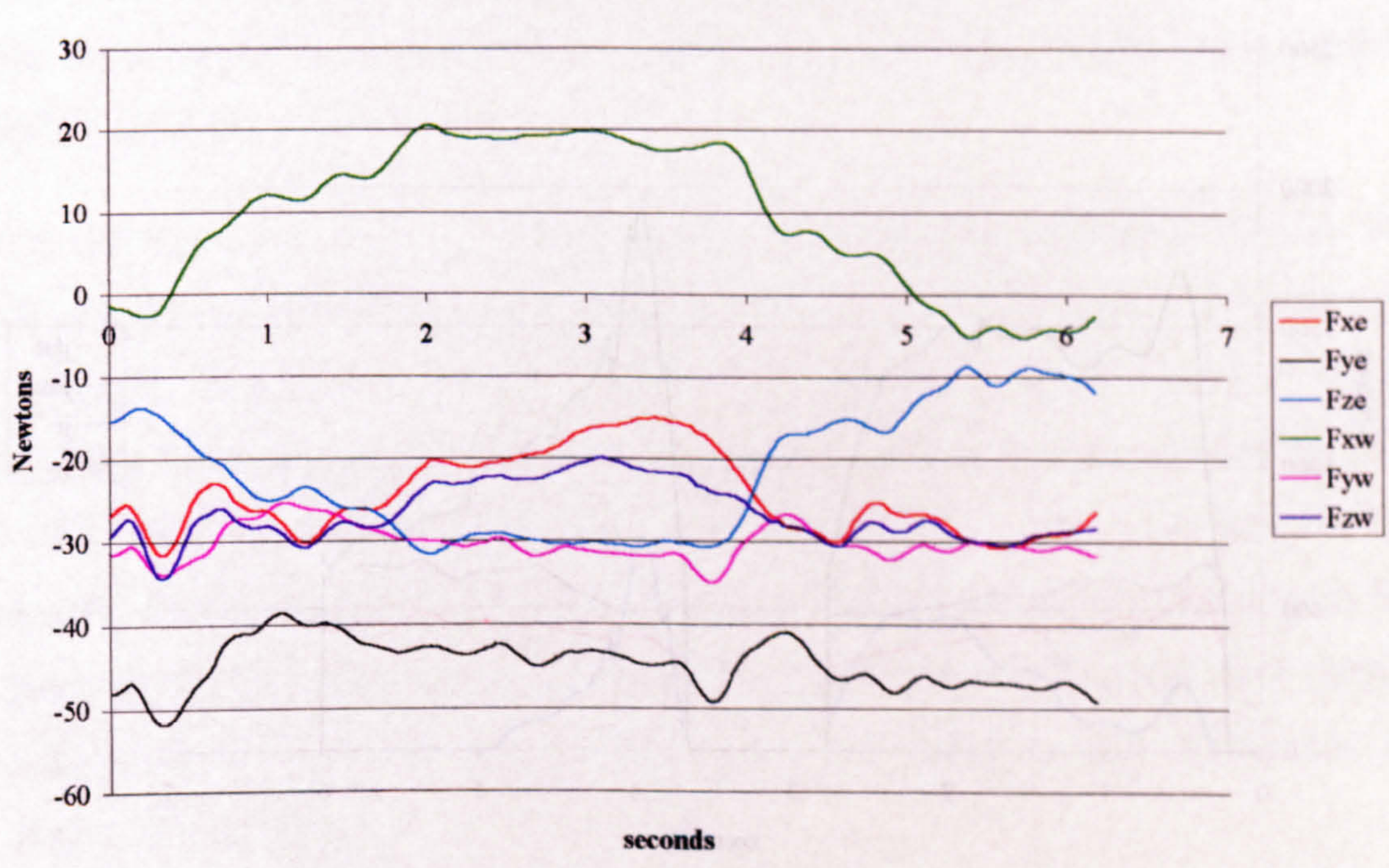

Figure 5.30 Forces applied to the elbow and wrist joints during the hook grip activity.

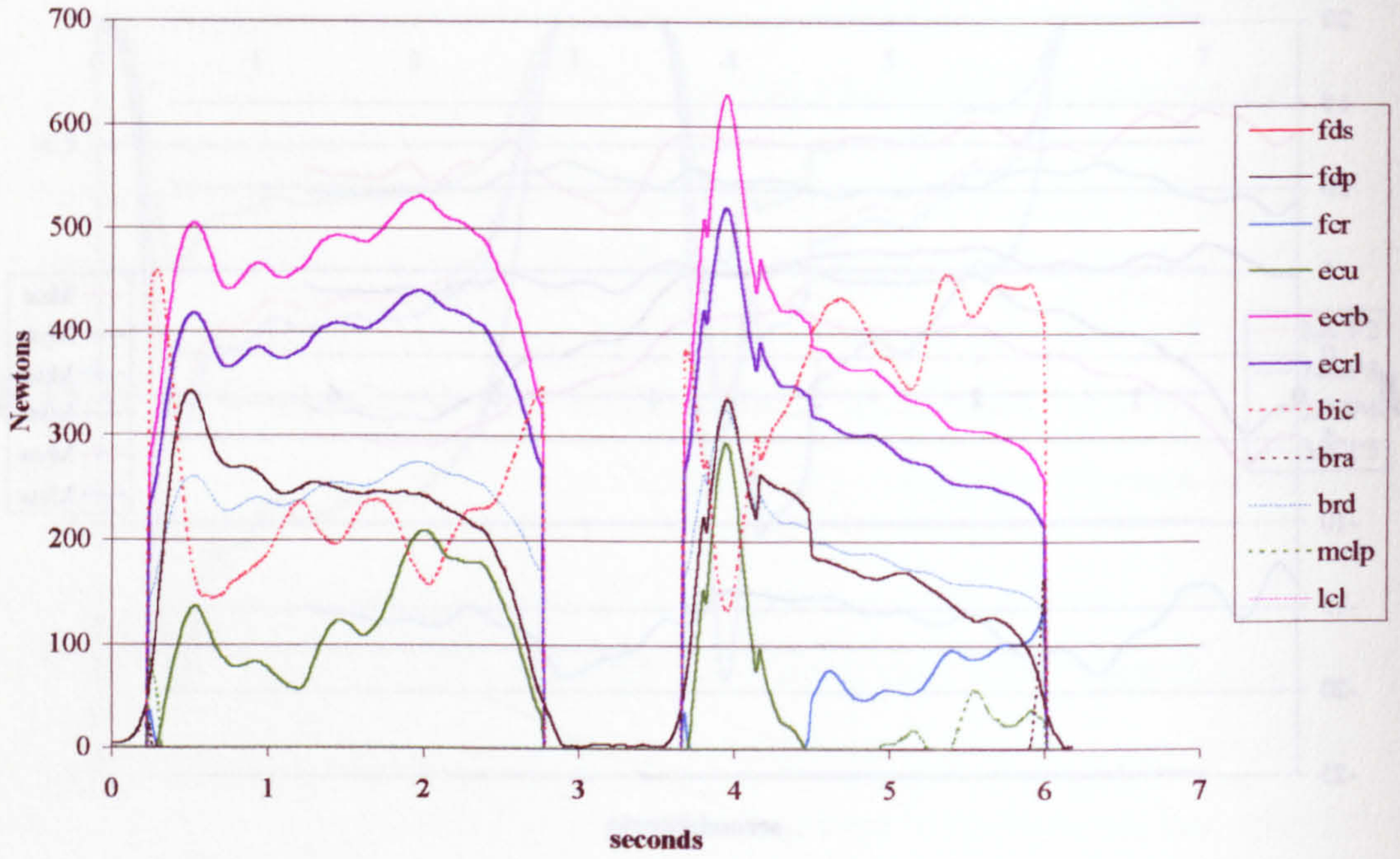

Figure 5.31 Graph of muscle and ligament force levels against time during the hook grip activity.

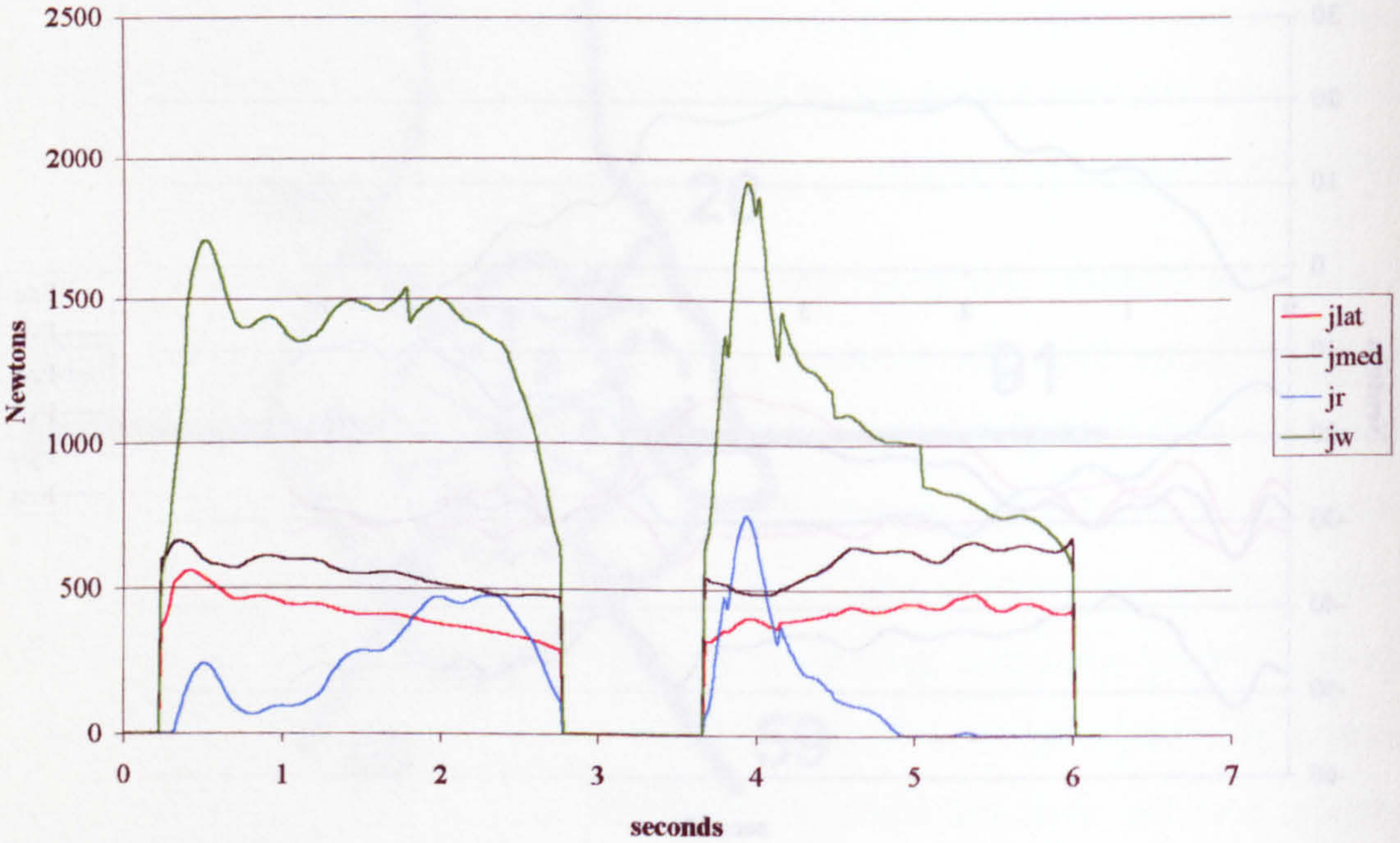

Figure 5.32 Graph of joint contact force levels against time during the hook grip activity.

5.1.4.2 Internal forces

The load sharing experienced between the soft tissue structures of the limb during the hook grip activity can be seen in Figure 5-31. Opposing the flexion and adduction moments at the wrist joint, both ECRB and ECRL are active throughout the trial. They are naturally selected by the model as they directly oppose the external loading condition and the relative contribution from each one is based on their relative sizes and moment arms. Some additional activity is required from ECU, however, in order to balance the flexion caused by the finger flexor tendon forces.

At the elbow, in marked contrast to the previous activities, BIC is the major flexor. BRD is still active throughout the trial, but at a lower level. In the other three activities, BRD has proved to be by far the major contributor to elbow flexion. This is possibly because there is little difference in the flexion moment arms between these two muscles with the elbow in this relatively extended position (see Figure 2.23). This means that the selection of BIC instead of BRD by the model reduces the maximum muscle stress as BIC has the larger cross-section of the two. There is a small amount of force taken through the MCLP towards the end of the trial. This is being used to resist the varus stress on the elbow as the forces in the common extensor tendons (ECRL, ECU) decrease.

The fact that BIC produces its peak forces at the beginning and end of the trial, when the forearm is subjected to a supination moment, is a surprise and is reflected in the values of joint forces seen in Figure 5.32, where the medial trochlear force is significantly higher than the lateral. Also of note is the fact that the time profile of the radial head force follows that of the ECU muscle force. This is because the ECU originates from the lateral epicondyle of the humerus and thus any increase in its force tends to compress the radio-capitellum joint. The force in the wrist joint naturally reflects the forces in the tendons crossing it, and reaches a peak of just less than 2000N, in this case.

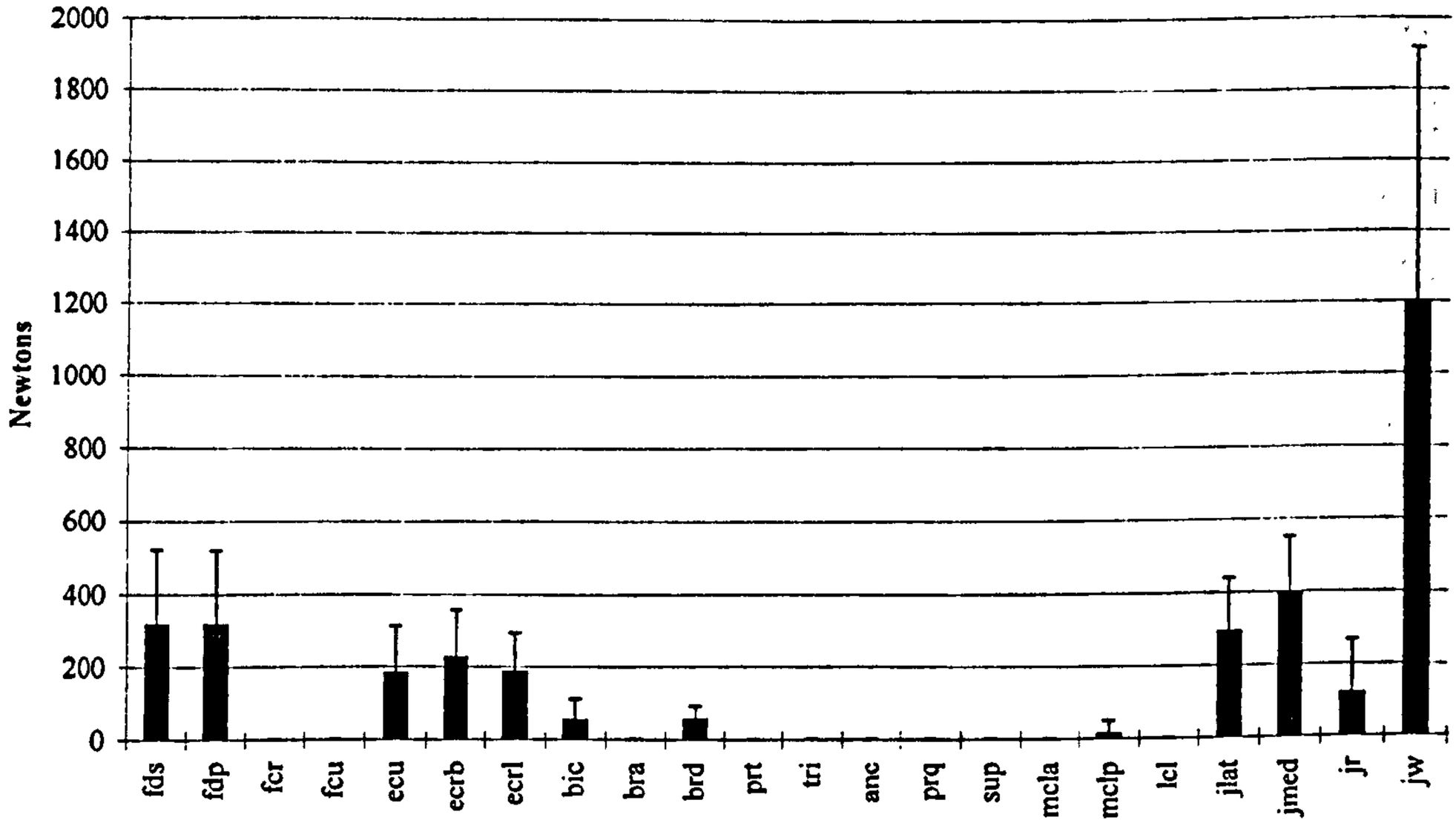

Figure 5.33 Distribution of load between forearm structures for the point at which the total joint force is a maximum, for the vertical power grip activity (mean and SD).

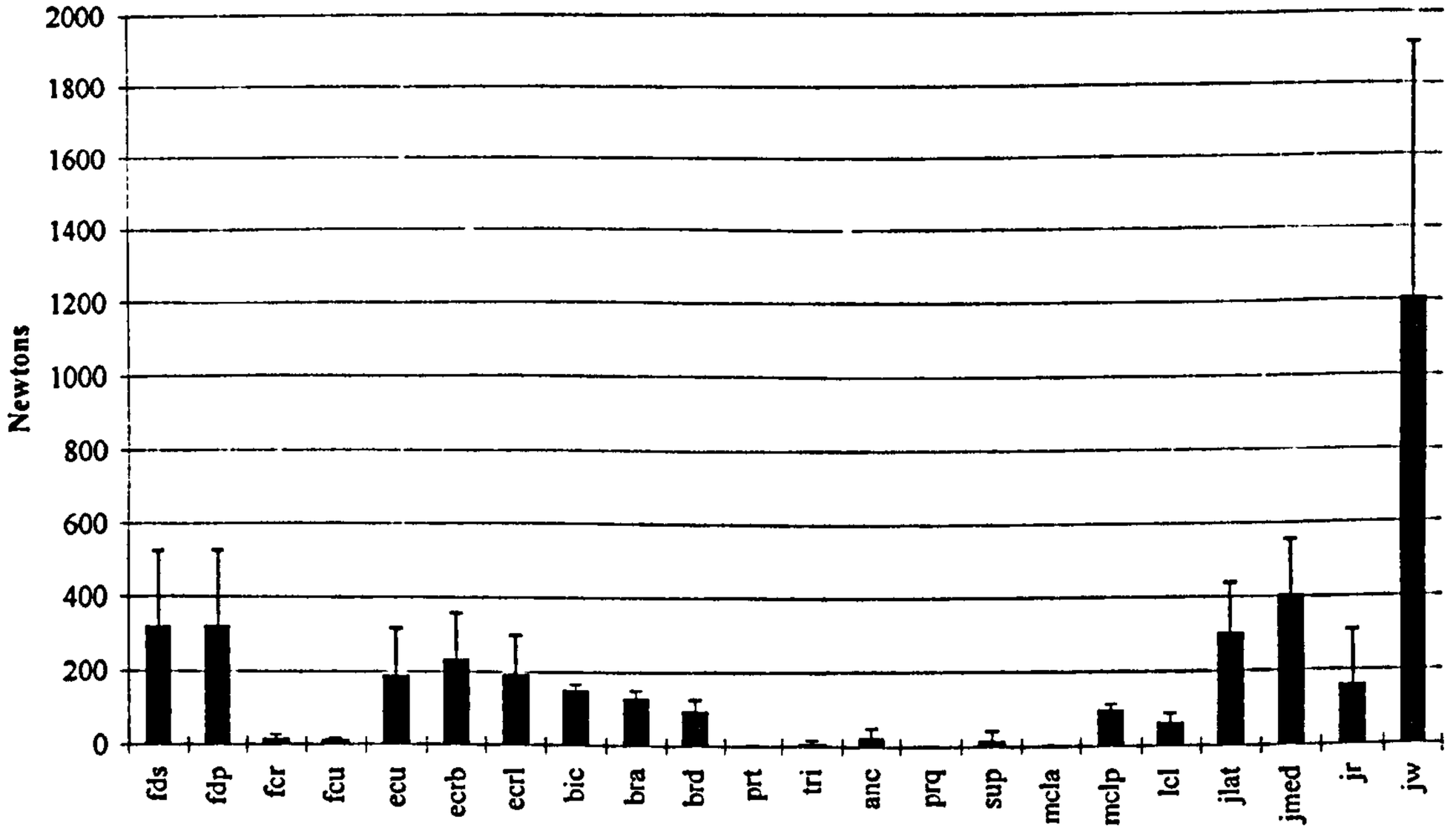

Figure 5.34 Maximum load carried by each structure during the vertical power grip activity (mean and SD).

5.2 Summary of Muscle, Ligament and Joint Forces

Figures 5.33 to 5.40 summarise the data for all subjects and all trials. For each pair of graphs, the first gives the calculated force value in each structure at the point where the total joint force is a maximum. The second graph in the pair gives the maximum value encountered for each structure during the trial. The mean value and the standard deviation are given in each case. It can be seen from these graphs that the differences between the distribution at maximum joint force and the maximum values are small.

The type of loading experienced by the limb during the trials was similar from one activity to the next, although the magnitudes of the loads varied. That is, in each case, the wrist joint was subjected to ulnar deviation and flexion and the elbow joint experienced adduction and extension. This inevitably led to a degree of similarity in the activation patterns of the muscles and the resultant force levels in the ligaments and joint surfaces throughout the trials.

The most commonly active muscles controlling the wrist were those producing extension and radial deviation (ECU, ECRL, ECRB), as might be expected. There was, however, some activity in the wrist flexors (FCR, FCU) for the activities where the transducer had the additional weight attached. This was possibly to ensure stability of the wrist joint against the increased lateral force.

One of the most surprising outcomes of these trials is the lack of activation in the brachialis muscle, elbow flexion being generated by BIC, BRD and ECRL. This occurred because the BIC and BRD both have much larger moment arms than BRA in flexion and thus can satisfy the moment equilibrium with a lower force. Also ECRL has a very similar moment arm to BRA in flexion, but is active to balance moments at the wrist also. Thus it has an extra 'benefit', but incurs no extra 'cost', in terms of the optimisation procedure.

The two activities with the lowest joint contact forces are not surprisingly the ones which were subjectively the 'easiest'. These were the power grip with the handle vertical (with no additional mass attached to the device) and the hook grip (where there was an additional mass but it was located close to the hand). The chuck grip, although

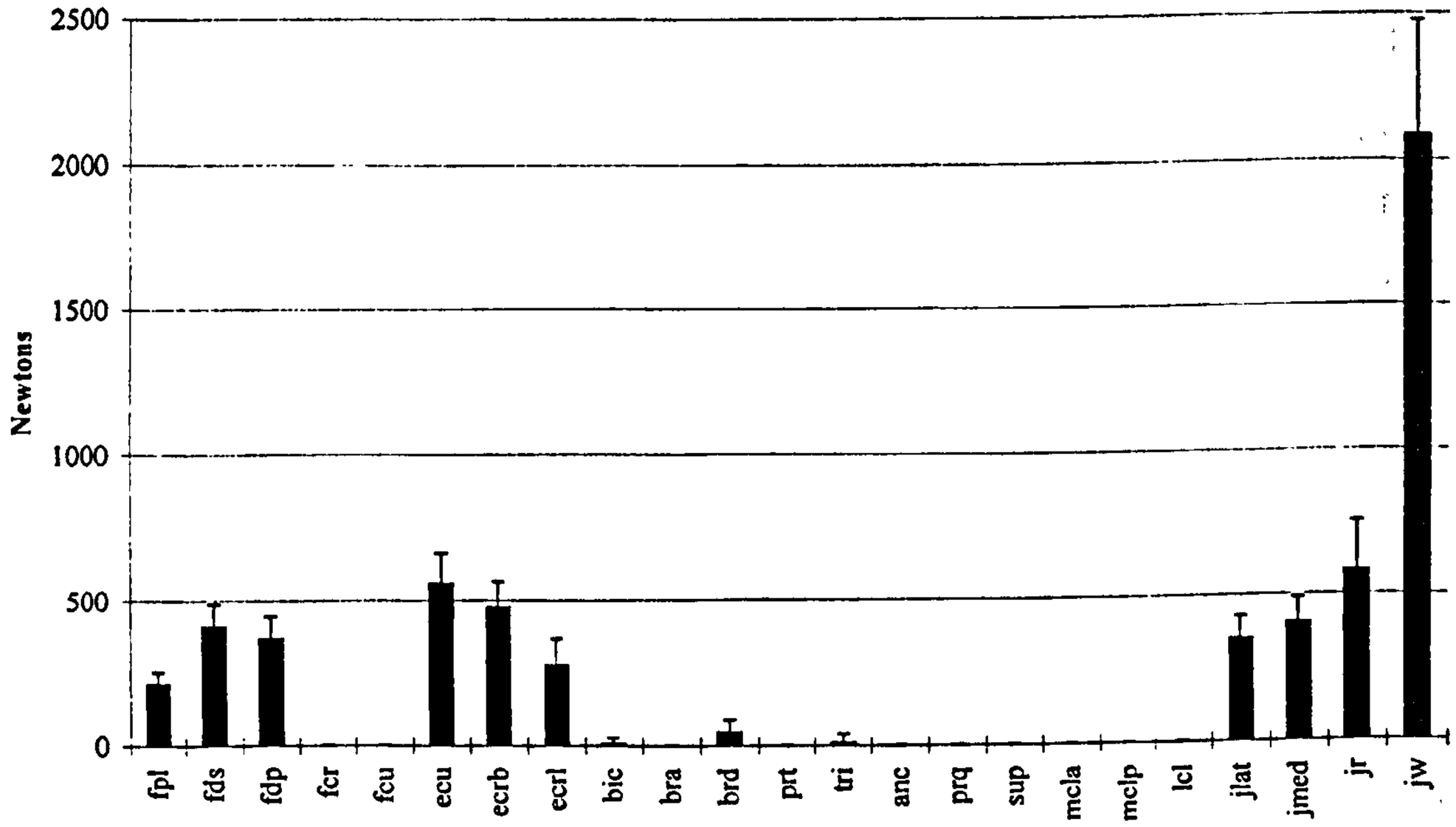

Figure 5.35 Distribution of load between forearm structures for the point at which the total joint force is a maximum, for the chuck grip activity (mean and SD).

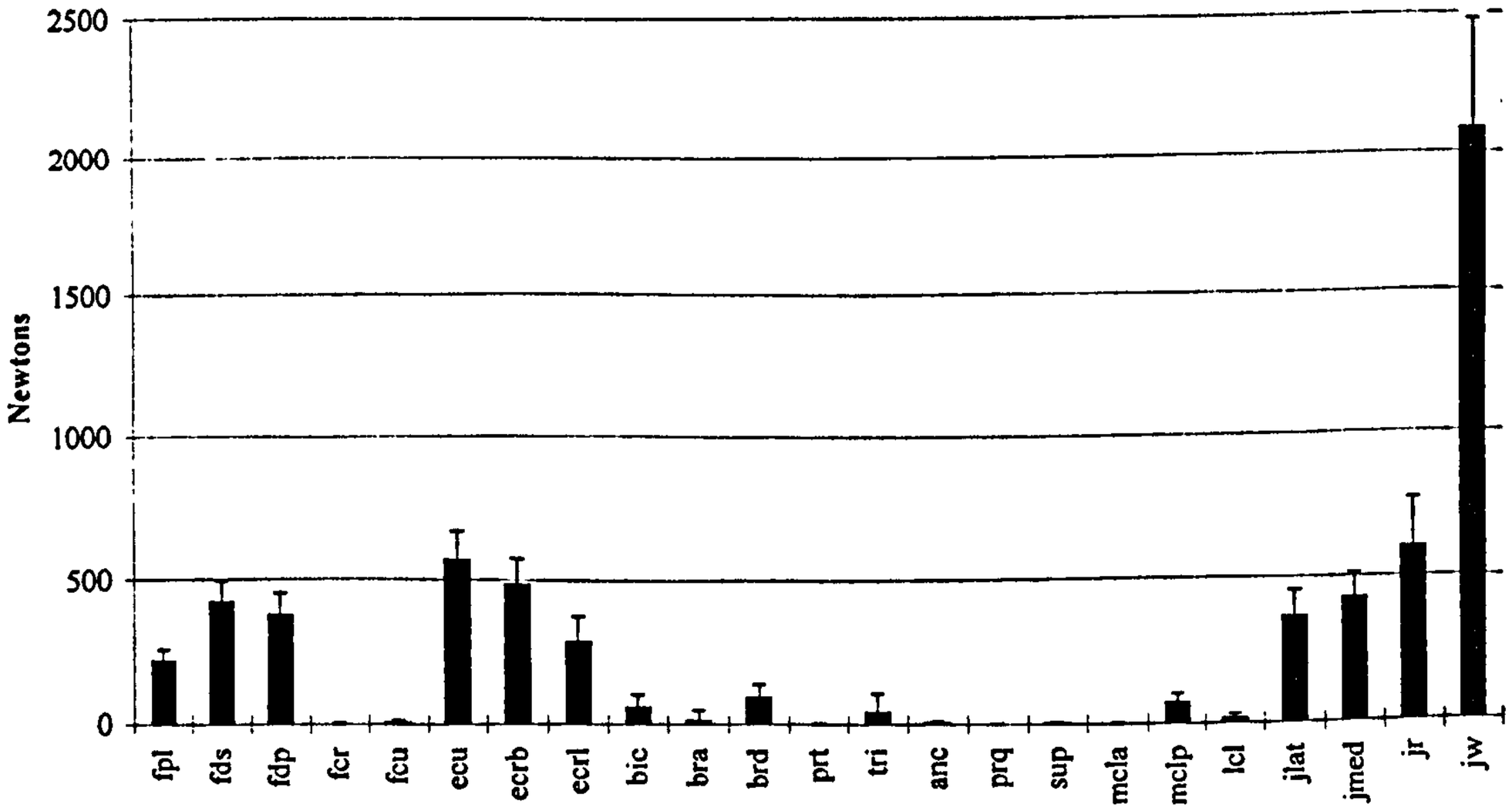

Figure 5.36 Maximum load carried by each structure during the chuck grip activity (mean and SD).

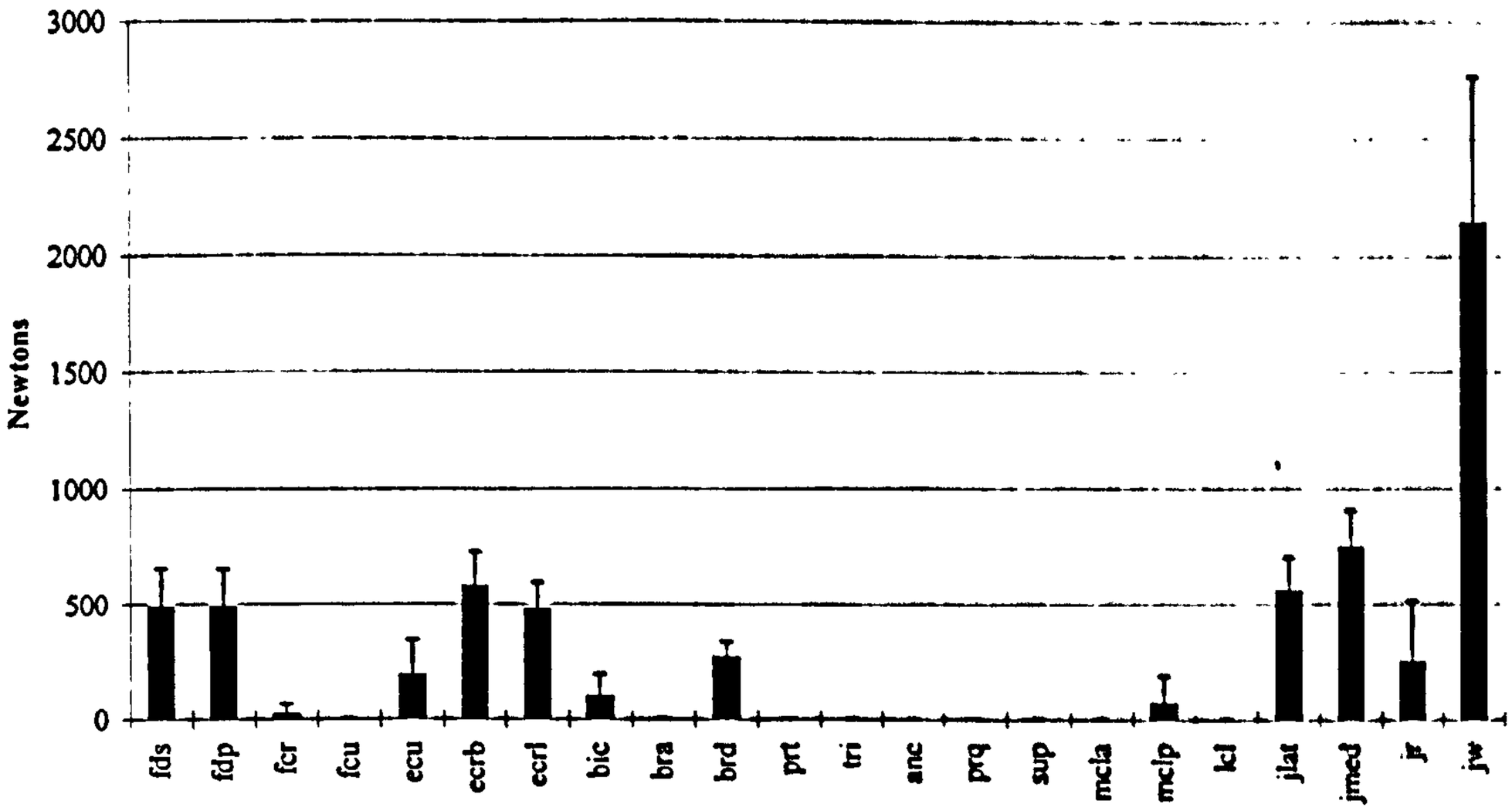

Figure 5.37 Distribution of load between forearm structures for the point at which the total joint force is a maximum, for the horizontal power grip activity (mean and SD).

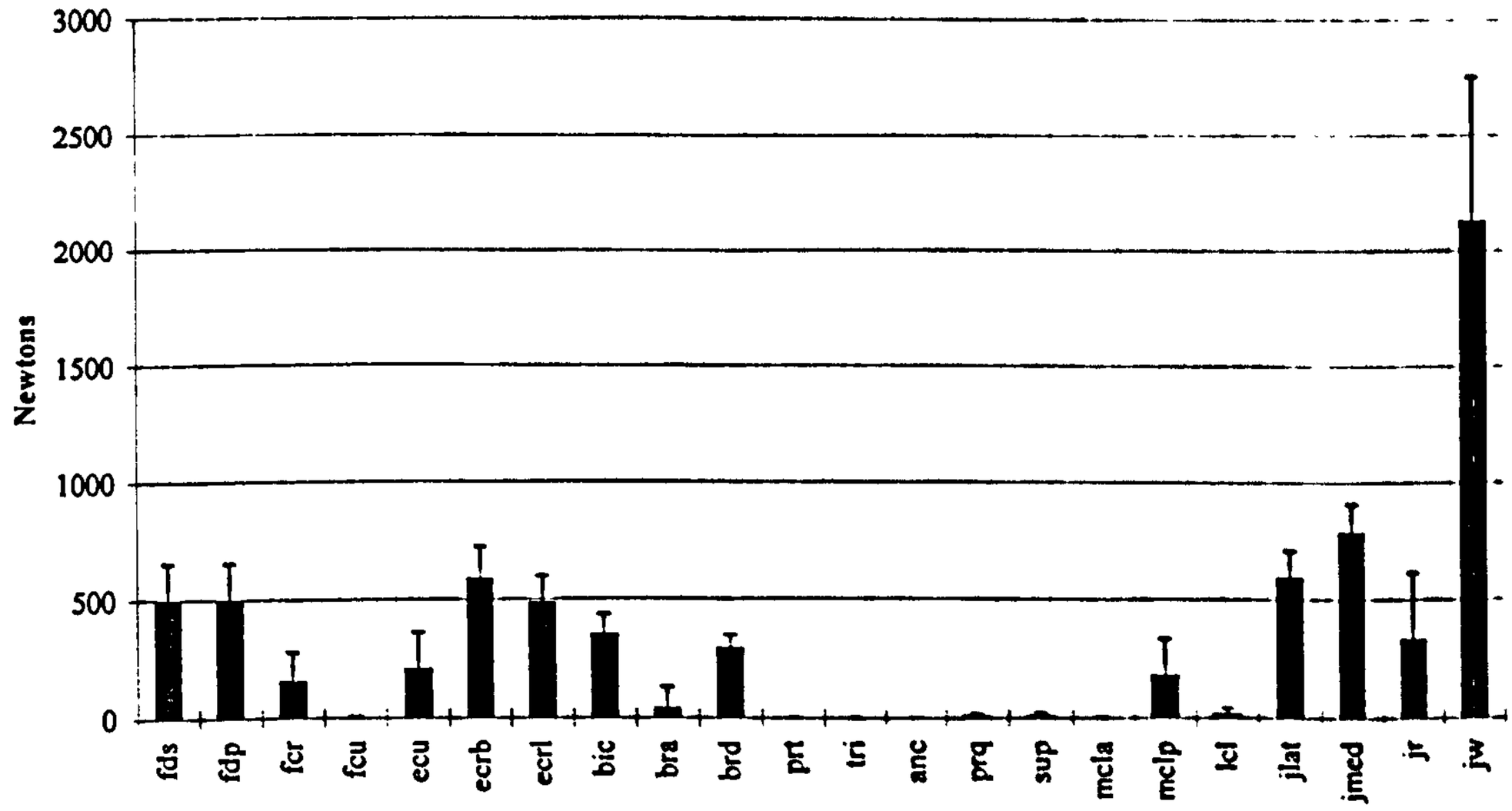

Figure 5.38 Maximum load carried by each structure during the horizontal power grip activity (mean and SD).

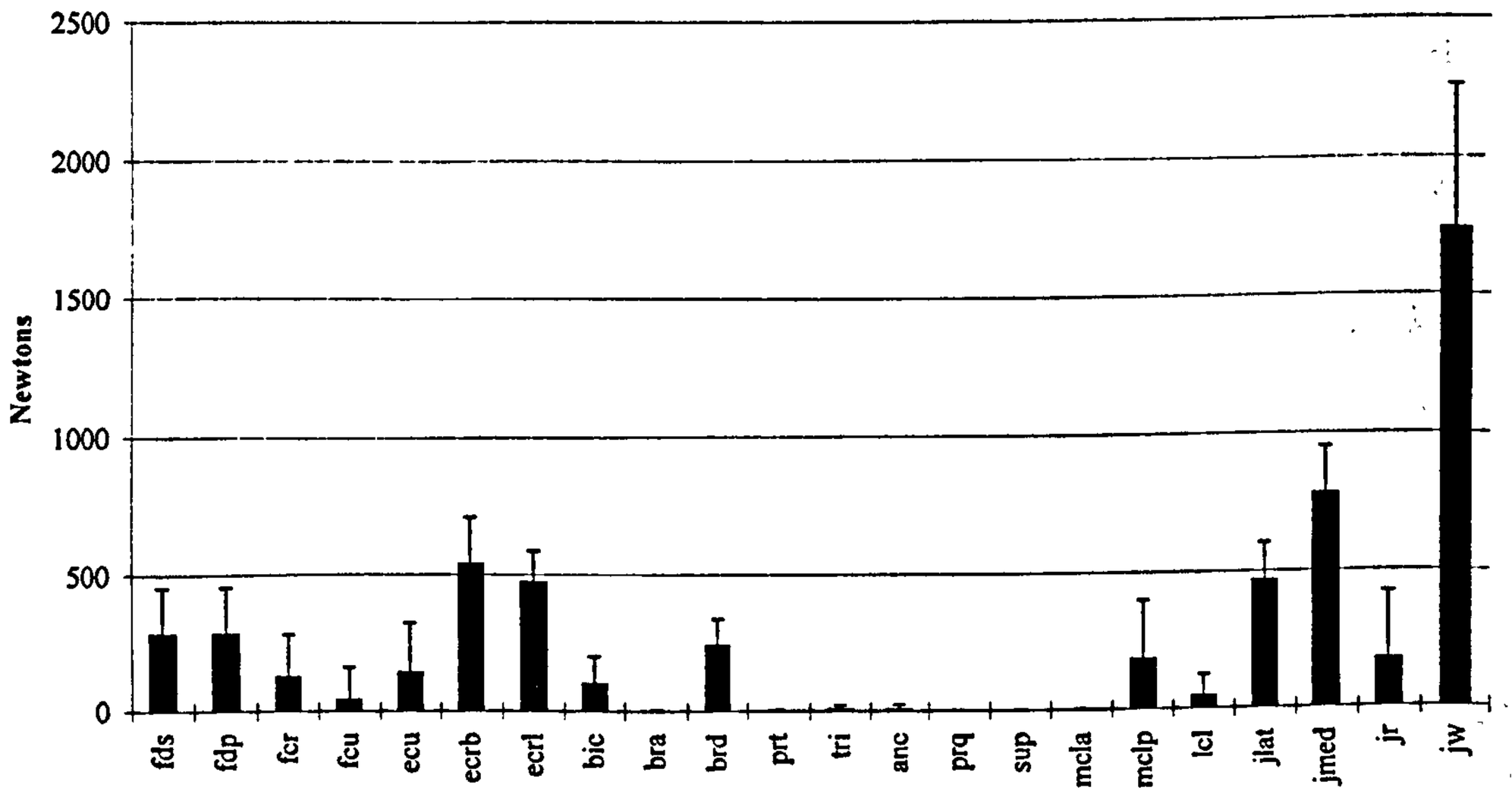

Figure 5.39 Distribution of load between forearm structures for the point at which the total joint force is a maximum, for the hook grip activity (mean and SD).

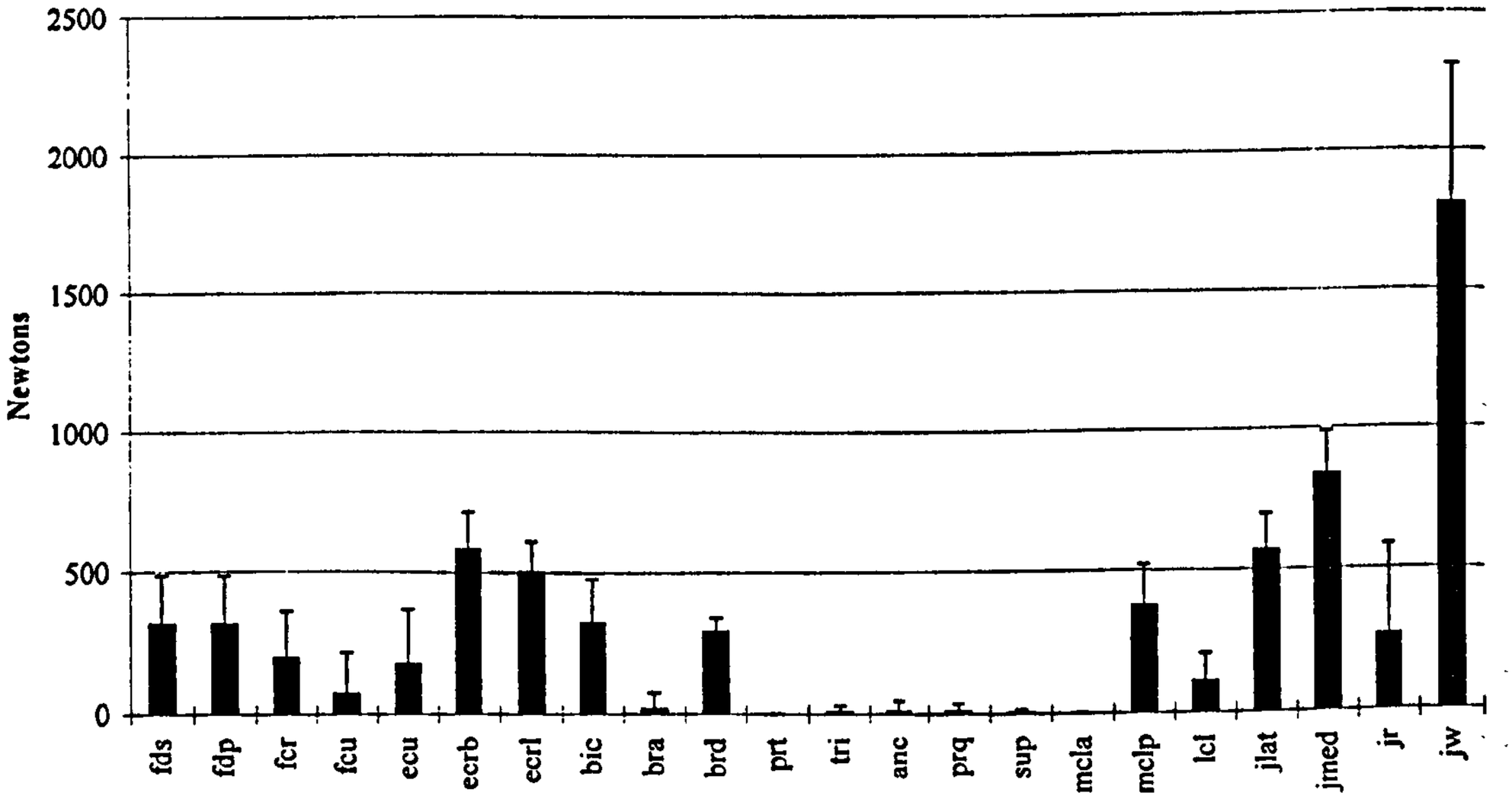

Figure 5.40 Maximum load carried by each structure during the hook grip activity (mean and SD).

performed with the transducer without the additional mass, was difficult as the hand position gave the external load a large lever arm against the MCP joints and the minimal contact area led to the device slipping through the grip.

There is a large standard deviation in all the results, indicating a wide variety of styles employed by the subjects. The resultant joint contact force depends on a number of factors including the individual internal geometry, the limb position during the trial, the speed with which the task is completed and the confidence with which it is completed. The latter point may be interpreted as the force with which the object is gripped, over and above that which is necessary for complete control.

5.3 VALIDATION

There are three ways in which to validate the model used in the current study: direct force measurement, comparison between predicted and recorded muscle activity patterns and comparison with results predicted by other authors. The first of these has very limited potential for obvious practical and ethical reasons, but will be discussed briefly.

5.3.1 DIRECT FORCE MEASUREMENT

Schuind et. al. (1992) carried out intra-operative tendon force measurement on the index fingers of five subjects, using buckle-type force transducers. A maximum force of 118N for the flexor digitorum profundus tendon was measured in the study, with the subject performing a tip pinch activity. Whilst direct comparison with the current study is not possible, the tip pinch activity may be considered similar to the chuck grip activity described here, where FDP forces of approximately 400N were found after summing the index, middle and ring finger tendon forces. This represents a very favourable comparison, with the force levels certainly being of the same order of magnitude. The subjects in the study of Schuind et. al. were being treated for carpal tunnel syndrome and the effect of this on force production is not known.

5.3.2 COMPARISON WITH EMG STUDIES

The ability of individual muscles to perform certain movements or tasks has been assessed with the use of electromyography (EMG) by a number of investigators. Basmajian (1985) is one of the most comprehensive reports of EMG studies available. In studies on the elbow flexors, a number of observations of relevance to the current study were made regarding the function of the brachialis, biceps brachii and brachioradialis muscles. Basmajian's view is that the brachialis muscle may be considered the 'workhorse' of elbow flexion as it was usually active with the arm in pronation, semi-pronation and supination and in unresisted as well as resisted flexion. In one subject, however, it showed no activity at all. The biceps brachii muscle was always active in supination, but showed very little activity with the forearm in the pronated position, whereas the brachioradialis muscle was more likely to be active with the forearm prone or semi-prone.

Of the four activities described in this study, three are performed with the forearm in a semi-prone position and one with the forearm prone (the chuck grip). If the graphs of force sharing at maximum joint force are examined, it is seen that as the limb is used in a more prone position less of the force is provided by the biceps.

The most notable difference between the observations of Basmajian and the results of the current study is the very small amount of activity predicted in the brachialis muscle, thereby precluding its description as a 'workhorse'. This is likely to be due, as previously stated, to its very small lever arm compared to the other two main elbow flexors in the model, and therefore its high 'cost' in the optimisation. This has been noted as a fundamental limitation of linear optimisation techniques in general and of the current model in particular. It must also be remembered, though, that some differences are to be expected as the work of Basmajian was carried out with the volunteers performing simple tasks such as flexion or supination, whereas in the current study the volunteer performed activities leading to complex three-dimensional loading situations involving the wrist and fingers as well as the elbow joint.

The analyses of wrist and finger muscles indicate that load sharing between the extensors carpi radialis longus and brevis is expected, particularly in abduction of the wrist. Also commonly seen, as in the current study, is antagonistic activity of the wrist motors as stabilisers of the wrist joint and opponents of the grip flexors.

5.3.3 JOINT FORCE VALUES FROM THE LITERATURE

5.3.3.1 Elbow joint forces

Amis et al. (1980a) found elbow joint forces of up to 3200N (humero-ulnar) at 120° flexion for isometric force actions. His studies were based on strenuous activities such as pulling up to 600N, and triceps antagonism was included. For high speed actions, forces were found not to exceed those of isometric efforts (Amis et al. (1980b)). Amis et al. (1981) found higher forces in the humero-ulnar than in the humero-radial articulation during elbow extension and vice versa during elbow flexion.

Nicol (1977) developed a simplified model of the elbow joint and predicted joint contact forces of up to 2450N at the humero-ulnar articulation and up to 1500N at the

humero-radial articulation, for a range of activities of daily living. The activities studied included eating, reaching to a shelf, pulling a table across the floor and rising from a chair without assistance from the legs. The highest forces were found for the table pulling exercise.

An et al. (1984) calculated resultant humero-ulnar contact forces of 0.3 - 0.5 times body weight for activities of daily living using a simple two-dimensional model. Gonzalez et al. (1996) described a model of the elbow joint complex in which they predicted values of muscle force of up to 1750N (for triceps). Their model was based on data from Seireg and Arvikar (1989). Morrey et. al. (1988) measured force transmission through the radial head in three cadaver elbows. They loaded the elbow by applying forces to the muscles biceps brachii and brachialis, but failed to simulate the action of brachioradialis.

Halls and Travill (1964) found that the forces transmitted across the elbow joint were split between the humero-ulnar and humero-radial joints in the ratio 43:57, for a static load applied to the fully extended cadaver elbow. It must be noted that their results were obtained from implanted transducers, which could lead to alteration of the contact areas and therefore alteration of the load transmission.

In the current study, values of up to approximately 1600N humero-ulnar force (mean plus standard deviation) were predicted, and the radial head forces reached approximately 800N. The ratio between the humero-ulnar force and the humero-radial force varied from approximately 88:12 to 54:46.

5.3.3.2 Wrist joint forces

There is a lack of information on wrist joint contact forces in the literature, although a number of studies on contact pressure and pressure distribution have been published. Ketchum et al. (1978) measured wrist extension moments and derived forces in the extensor carpi ulnaris (ECU), extensor carpi radialis brevis (ECRB) and extensor carpi radialis longus (ECRL) of 140, 200 and 246 N respectively. In the absence of activity in other muscles such as finger extensors, which they claim is the case, this would give rise to a joint contact force of approximately 600N. This is considerably lower than the

forces encountered in the present study for two reasons. The first is that the extension moments at the wrist measured in this study were considerably higher than those reported by Ketchum et. al. Also, in the current study, the hand was being used to grip an object and thus the finger flexor forces were high; these forces obviously add to the wrist joint force.

Amis (1978) reported forces in the prime movers of the wrist and finger flexors, as part of a study of the elbow, and deduced wrist compression forces from 2.23Nto 17.7N per unit of force applied to the hand. He then quoted a maximum force of 249N on the hand, giving wrist compression forces from 555N to 4407N. The results of the current study are well within these limits.

5.3.3.3 Ligament forces

In the present study, only the posterior portion of the medial collateral ligament and the lateral collateral ligament were found to be significantly loaded, with the highest mean occurring during the hook grip activity. For this activity, the MCLP reached approximately 400N. Nicol (1977) calculated maximum values of up to 2290N in the medial ligaments and 800N in the lateral ligament for more strenuous activities. Amis (1978) calculated a value of over 1300N in the medial ligament.

The value calculated in this study is well within the range reported by the other authors but may still be an over-estimate as work reported by Regan et. al. (1989) indicates that the ligaments may not be as strong as this. They tested the medial ligaments and the lateral ligament in a materials testing machine and found that the strongest one, the anterior medial ligament, failed at an average of 260N (standard deviation 71N). The MCLP failed at an average load of 159N (standard deviation 40N). For the tests, bone-ligament-bone preparations were made from eight fresh frozen upper extremities, six of which were from women. The age of the subjects from whom the specimens were taken was not given.

CHAPTER 6 CONCLUSIONS AND RECOMMENDATIONS

6.1 CONCLUSIONS

A three dimensional mathematical model of the elbow, forearm and wrist has been developed. A biomechanical analysis of occupational lifting activities has been performed and the muscle, ligament and joint forces resulting from this have been calculated.

Validation of the model has shown that it produces results within the expected range of values and compares favourably to other studies in most aspects. Elbow joint forces were predicted to reach approximately 1600N in the trochlea and half this value in the radial head. These values are consistent with the level of activity studied but may be underestimated by a limitation of the model. This is seen in the distribution of force between the muscles, with activity in brachialis being severely underestimated. The reasons for this have been discussed. Forces in the ligaments were lower than those calculated by other investigators, but were justified by comparison with empirical results. The wrist joint contact forces predicted were higher than expected, given the level of activity. In previous studies, the effect of grip force on the wrist and elbow joints has been neglected or underestimated. As a result of this, it is felt that wrist joint contact forces may have been seriously underestimated in the past.

In the context of cumulative trauma disorder (CTD), these results indicate that lifting activities where grip force is significant may lead to unexpectedly high contact forces at the elbow and particularly the wrist. The small surface area of the wrist combined with the high contact forces predicted will inevitably lead to high contact pressures, which can lead to joint degeneration. This should be borne in mind when assessing work duties as some correlation between force on the limb and CTD has been shown.

This work provides a valuable database of external and internal loading encountered during occupational activities which may also be used by biomechanists and clinicians to assess the suitability of potential replacement structures and surgical procedures.

6.2 RECOMMENDATIONS FOR FURTHER WORK

There are several areas where advances may be usefully made with respect to the current study; the first is the model itself. Anatomical data in the literature is incomplete and significant improvement may be made by the completion of this, and by the measurement of in vivo geometry through magnetic resonance imaging. Also, the interaction of the radius and ulna has not been examined here, and the forces in the distal and proximal radio-ulnar joints as well as the force in the interosseous membrane would prove to be valuable information.

Secondly, the optimisation procedure used to overcome indeterminacy has been shown to be limited and implementation of a more sophisticated technique could produce more physiologically realistic results.

Lastly, in order to provide a more comprehensive data set for the analysis of occupational activities, a wider range of activities needs to be studied, encompassing a greater range of joint motion.

PART B

INVESTIGATION OF KNIFE STAB CHARACTERISTICS

CHAPTER 7 INTRODUCTION

7.1 BACKGROUND

In a recent study of assault victims presenting at an Accident and Emergency unit in the West of Scotland, it was found that penetrating weapons had been used in 23% of the 235 cases reported in a two month period (Wright and Kariya (1997)). In another study, in London, knives had been used in 15% of assaults, and accounted for 90% of the serious injuries (Hocking (1989)). Another recent report notes that after a concerted effort by Strathclyde Police to reduce the number of incidents involving knives, the number of serious stabbings attending one hospital fell for a period of ten months, only to rise again after this time (Bleetman *et. al.* (1997)).

The need for police officers attending incidents of serious assault to be afforded protection is obvious, yet few suitable garments are on offer. Body armour designed for anti-ballistic use can, in some situations, allow penetration of a blade and armour designed to withstand blade penetration is prohibitively bulky and heavy. The development of stab resistant body armour has been a low priority for manufacturers until now as they are largely based in the USA, where police officers are more likely to face the threat of shooting than stabbing (Cross (1996)).

In order to design suitable new garments that will offer the desired level of protection without being prohibitively bulky, accurate knowledge of the level of threat posed by a knife attack is needed. Information in the literature about the mechanics of knife stab attacks is scarce. Knight (1975) examined the force necessary to penetrate the human skin for use in medico-legal cases, and found that a force of as little as 5N was sufficient with the sharpest of knives. A similar study, using porcine tissue, was carried out by Jones *et. al.* (1994), who published the shape of the force time profiles on the knife blade but sadly failed to quote the magnitudes of the forces involved. Finally, a study into the most important factors affecting penetration of soft armour was conducted by Calvano (1993), concluding that blade geometry was of prime importance and that backing material had little or no effect.

7.2 AIMS

This study aims to provide scientifically verified data on the characteristics of knife stab attacks, allowing the development of more realistic test procedures for stab-resistant materials compared to the current, subjectively derived standard of 42J energy input. The objective of the research is to measure a range of parameters relevant to knife stab attacks, including: velocity of knife, energy and momentum of the attacker and knife before impact and the three-dimensional forces, torque, work done and impulse on the target after impact.

The ability of the current drop-tower tests to replicate human knife stab attacks is also assessed, using a telemetry force-measuring knife.

CHAPTER 8 METHODOLOGY

8.1 MOTION ANALYSIS

8.1.1 TECHNIQUES FOR KINEMATIC DESCRIPTION

In contrast to the previous part of this thesis, the primary aim of the analysis of stab forces was their effect not on the body, but on the target, resulting in simpler kinematic descriptions than previously. The body holding the knife was modelled as a series of rigid segments: trunk, upper arm, forearm and hand, and knife. Local, technical axis systems were set up in each segment, as described in Part A Section 2.2.2, and used to define anatomical points allowing location of joint centres. Bone embedded axis systems were not used, however, as only the motion of mass centres was of interest, and these were calculated as being along lines joining joint centres.

The midpoints of the following pairs of points gave the location of the joint centres:

Joint centre	First point	Second point
Shoulder	Anterior shoulder	Posterior shoulder
Elbow	Medial epicondyle	Lateral epicondyle
Wrist	Ulnar styloid	Radial styloid

Table 8.1 Definition of joint centres.

For the shoulder, the first point was approximately over the lesser tuberosity of the humerus and the second point was directly posterior to this. The positions of the anatomical points were determined by a physiotherapist during data capture.

The calculation of the velocities of the segments by differentiation of the position data, and knowledge of the mass distribution from published tables (Contini and Drillis (1966) and Zatsiorsky *et al.* (1983)), allowed the calculation of segment linear energies and momenta in three dimensions. From this, the total, resultant energy and momentum of the system just before impact was calculated. It was assumed that any energy or momentum that the head, non-involved arm or legs may have had would not be transferred to the target.

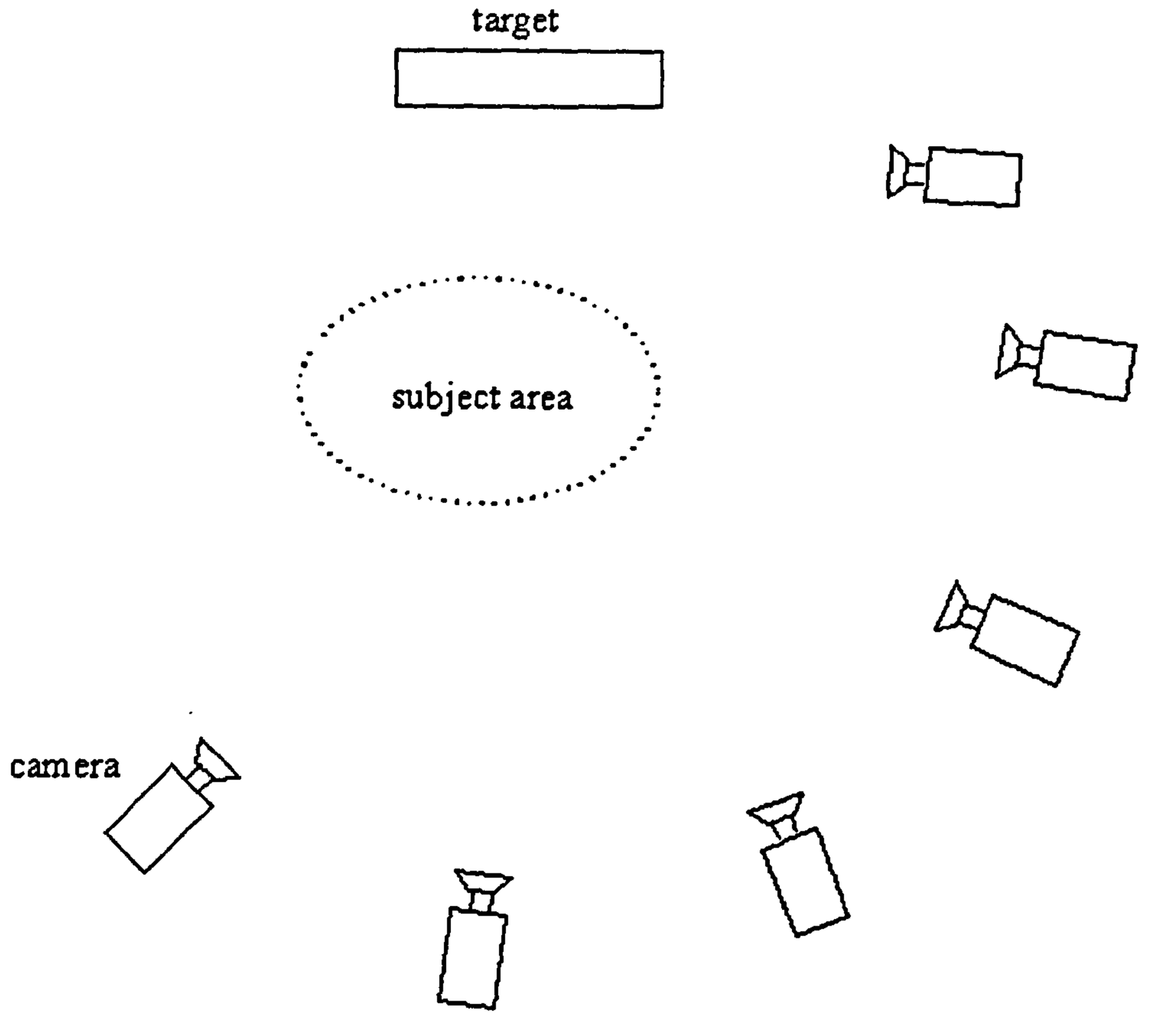

Figure 8.1 Plan view of Vicon camera configuration.

$$Total\ Energy = \mathbf{E} = \sum \frac{1}{2} m_i \mathbf{v}_i^2$$

$$Total\ Momentum = \mathbf{P} = \sum m_i \mathbf{v}_i$$

where m_i is the mass of the i^{th} segment and $\mathbf{v}_i$ is the velocity of the centre of mass of the i^{th} segment. The magnitudes of the resultant values are then given by

$$E = \sqrt{E_x^2 + E_y^2 + E_z^2}$$

$$P = \sqrt{P_x^2 + P_y^2 + P_z^2}$$

8.1.2 TECHNIQUES FOR MEASUREMENT

Methods similar to those described in Part A of this thesis were used for the measurement of the kinematics of the limb and force transducer, with various modifications. As in the previous section, three markers per segment, mounted on rigid plastic cuffs, were used for the measurement of the upper arm, the forearm and hand and the transducer. In addition to this, the torso was marked using three markers mounted directly on to the subject's skin. The marker set-up can be seen in Figure 8.8.

Some problems were encountered with data collection which were unique to the study of this activity, and arose from its high speed. It was found that the knife was impacting the target with speeds of up to 10m/s, making the distance travelled by markers between subsequent Vicon samples up to 200mm.

In order to track the markers throughout the motion, the camera set-up shown in Figure 8.1 proved necessary, with the cameras concentrated on the subject's dominant side. The camera positions shown are approximate and were decided upon after a great deal of experimentation.

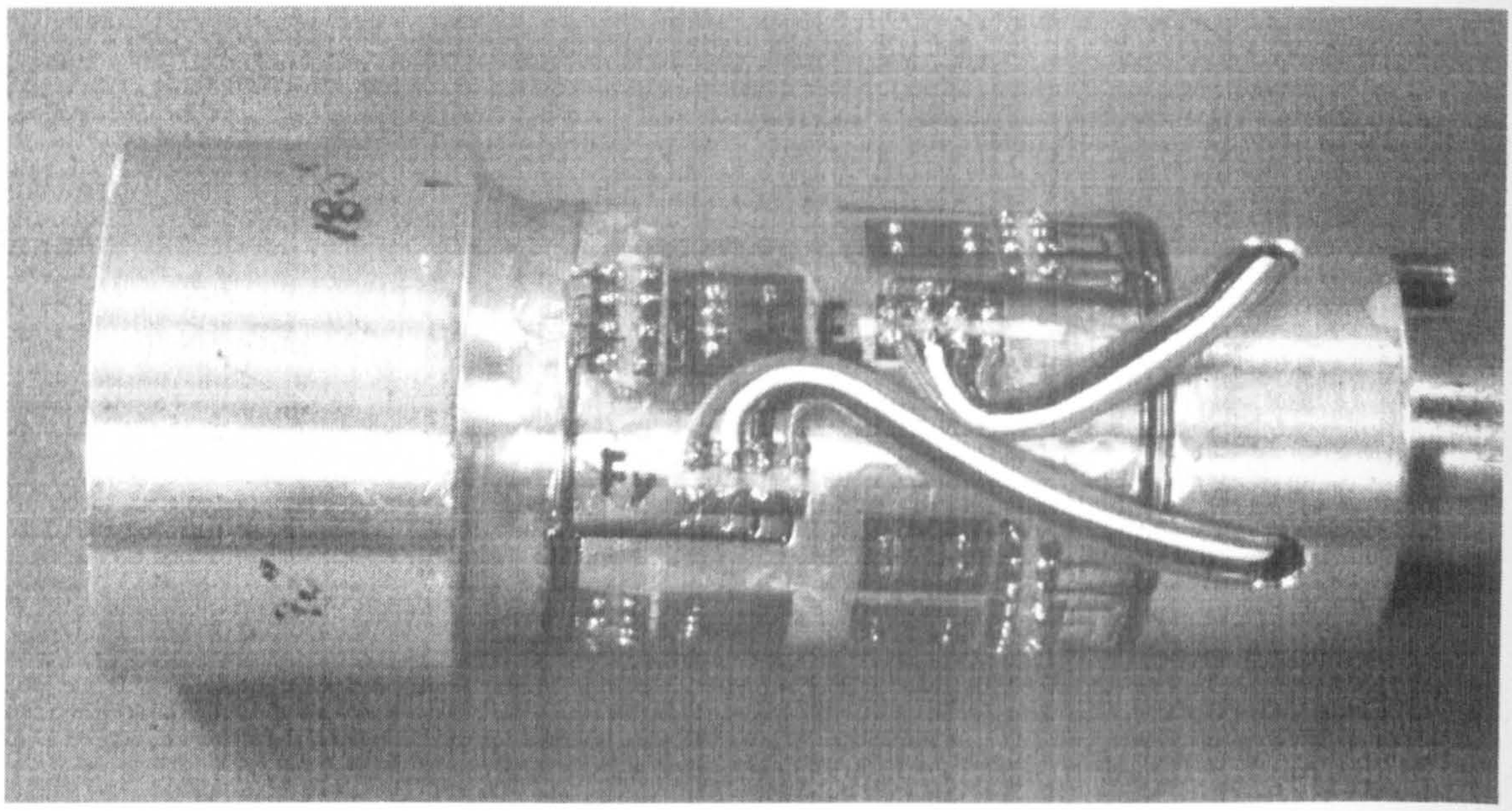

Figure 8.2 Detail of active component of force-measuring knife.

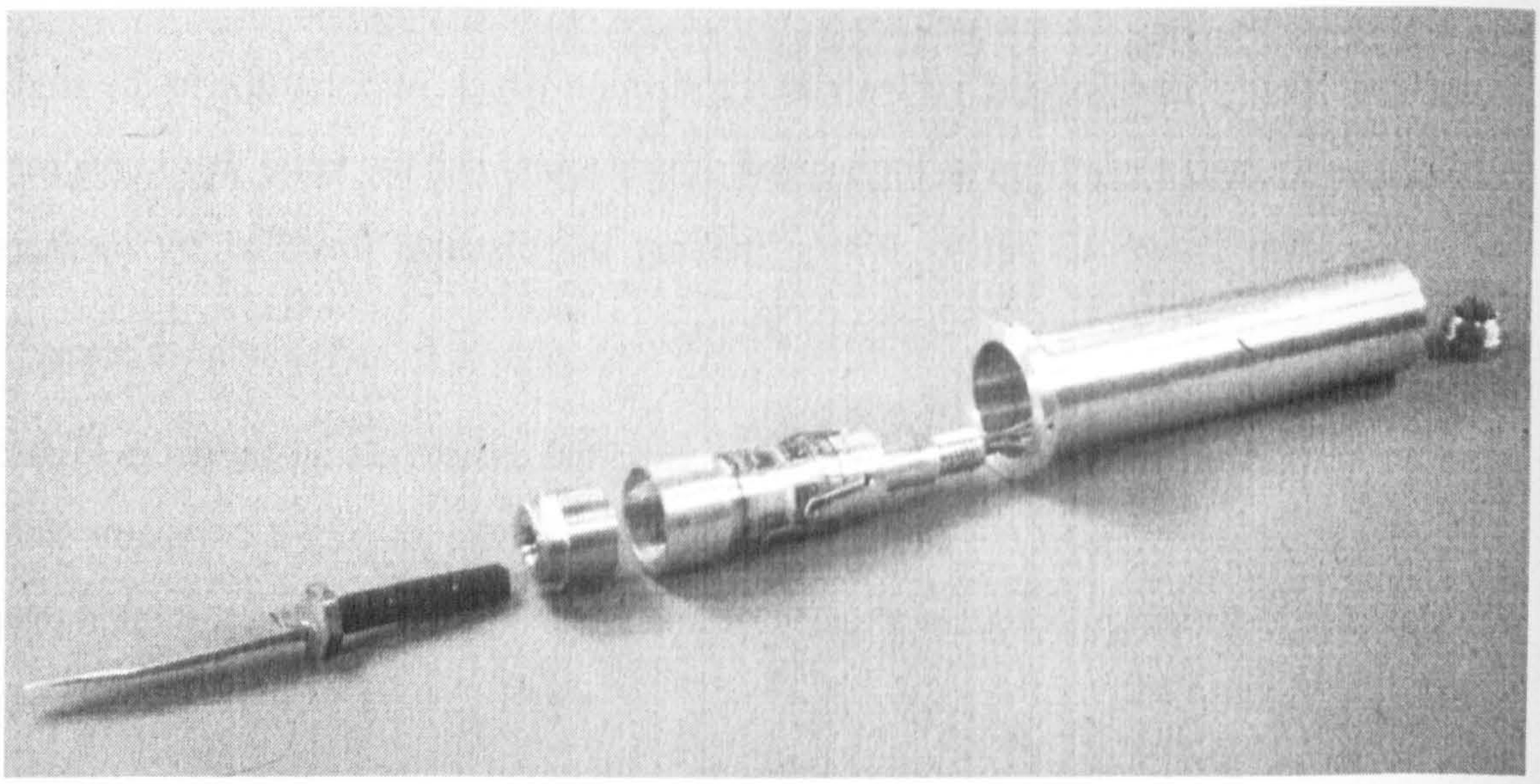

Figure 8.3 Components of force-measuring knife prior to assembly.

8.2 FORCE ANALYSIS

8.2.1 PROTOTYPE KNIFE

A strain gauge force transducer, initially designed for the measurement of loads in a prosthetic limb, was used in preliminary tests to determine the approximate values of forces encountered during knife stab attacks. A cylindrical handle of diameter 35mm was mounted at one end while a standard test blade, of length 75mm, was mounted at the other. Two volunteers from within the Bioengineering Unit were then asked to stab a target using the knife. Based on results from these tests, a new force-measuring device was designed to fit into the handle of a knife.

8.2.2 DESIGN OF A NEW FORCE-MEASURING KNIFE

The device was designed to measure four components of load: axial force (F_y, along the length of the blade), cutting force (F_x), lateral force (F_z) and torque (M_y). The active part of the transducer consists of an aluminium alloy cylinder of inner diameter 21mm and outer diameter 24mm on which the gauges are mounted (Figure 8.2). A brass boss, threaded M10, is pressed into the end of this to allow fixture of the knife blade. This assembly then fits into the outer handle (Figure 8.3). For safety reasons a padded hilt of diameter 90mm is located at the base of the handle. The mechanical specification of the knife is given in Table 8.1 and the physical dimensions are given in Table 8.2. Detail drawings are given in Appendix E.

Axial force	2000N
Cutting force	200N
Lateral force	200N
Torque	3Nm
Gauge strain at rated load	270με
∴ Factor of safety*	6

Table 8.1 Mechanical specification of force-measuring knife.

*Based on an Ultimate Tensile Strength of 115MPa.

Length of handle	140mm
Diameter of handle	35mm
Total mass of knife	360g

Table 8.2 Physical specification of force-measuring knife

Data from the instrumented knife were sampled at 2500Hz, the maximum possible with the Vicon software. Minor processing to take account of any calibration cross-effects produced the magnitudes of the four components of load. An estimate of the impulse transferred to the target was then obtained from the integral of the axial force with respect to time:

$$Impulse = \int \mathbf{F}.dt$$

8.2.2.1 Calibration of the knife

The device was calibrated using an Instron Materials Testing Machine and using calibrated, dead weights. The calibration allows for the presence of cross-talk and results in a matrix which is used to calculate load from an array of signals. For a detailed description and results of the calibration, see Lane (1996).

8.2.3 THE ADDITION OF AN ACCELEROMETER

8.2.3.1 Work done

To allow calculation of the work done on the target during impact, an accelerometer was mounted in the handle of the knife, on the back of the blade mounting boss. Trial tests with existing equipment indicated that acceleration values of up to 2000ms^{-2} were likely to be encountered. To allow for a large factor of safety and to ensure the device was sufficiently robust, an accelerometer with a range of ±5000g was installed.

Acceleration data were used to calculate the displacement of the knife while under load, and thus the work done in bringing the knife to rest, where work is the integral of force with respect to distance. Thus:

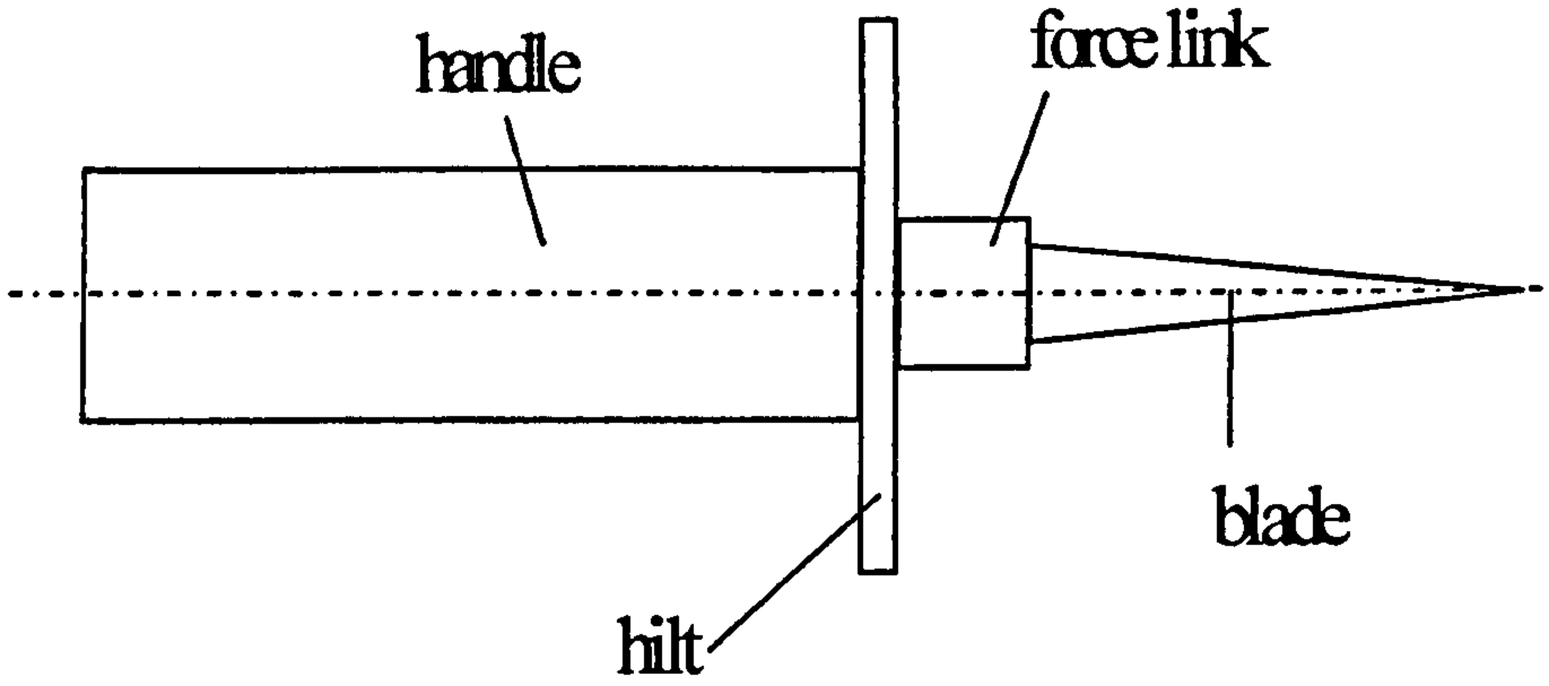

Figure 8.4 Schematic view of the force-measuring knife showing the placement of the piezo-electric force link.

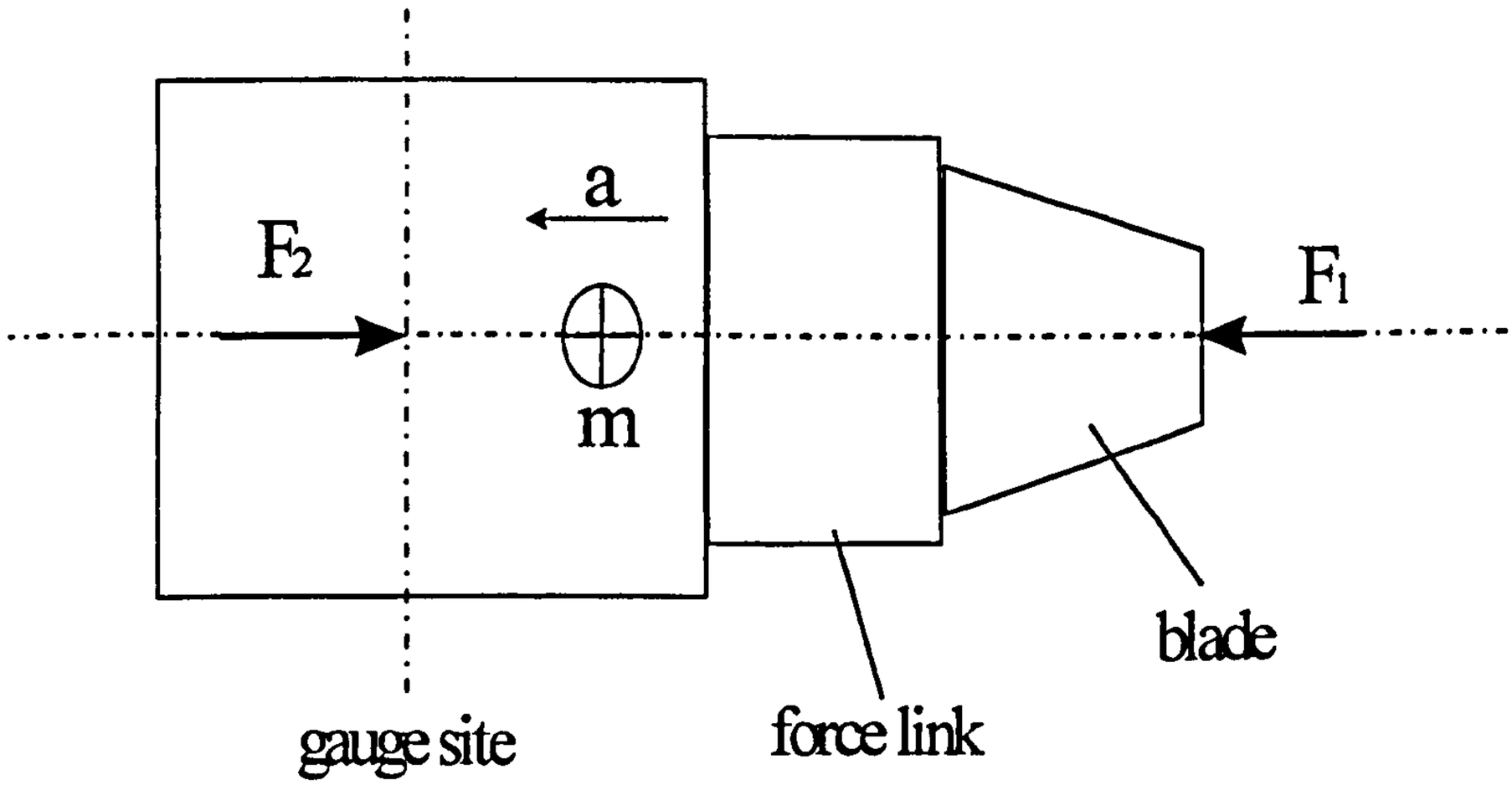

Figure 8.5 Detail of the force measuring knife showing the position of the strain gauge mounting site.

$$Work done = \int \mathbf{F}.ds.$$

where distance s is the double integral of acceleration a. Thus:

$$s = \int \mathbf{v}.dt = \int\int \mathbf{a}.dt$$

hence $$Work\ done = \int \mathbf{F}\mathbf{v}.dt$$

8.2.3.2 Inertial Force

Figure 8.4 and Figure 8.5 show a schematic representation of the knife blade assembly and the position of the strain gauges relative to it. It was found during comparison tests with a piezo-electric force-measuring device (referred to in the figures as a force link) that the force measured by the strain gauges was less than that recorded by the piezo-electric device. There were two contributions to this error:

- the inertia of the mass of metal in front of the gauge site prevented all the force being transmitted in the very short time-interval;
- the connection of the gauge foil to the metalwork was not completely rigid due to the visco-elastic properties of the gauge backing material and adhesive.

The first of these was corrected by determining the mass of metal in front of the gauge site and calculating the 'lost force' based on the acceleration measured. Hence

$$\mathbf{F}_1 - \mathbf{F}_2 = m\mathbf{a}$$

$$\mathbf{F}_1 = m\mathbf{a} + \mathbf{F}_2$$

where m represents the mass of the blade, piezo-electric force link, brass boss in which the link is mounted and the portion of the aluminium cylinder on which the gauges are mounted as far as the centre-line of the gauges, and **a** is the acceleration of that mass. The second factor proved to be small after correction for the first. Typical results of these tests are shown in Figure 9.24.

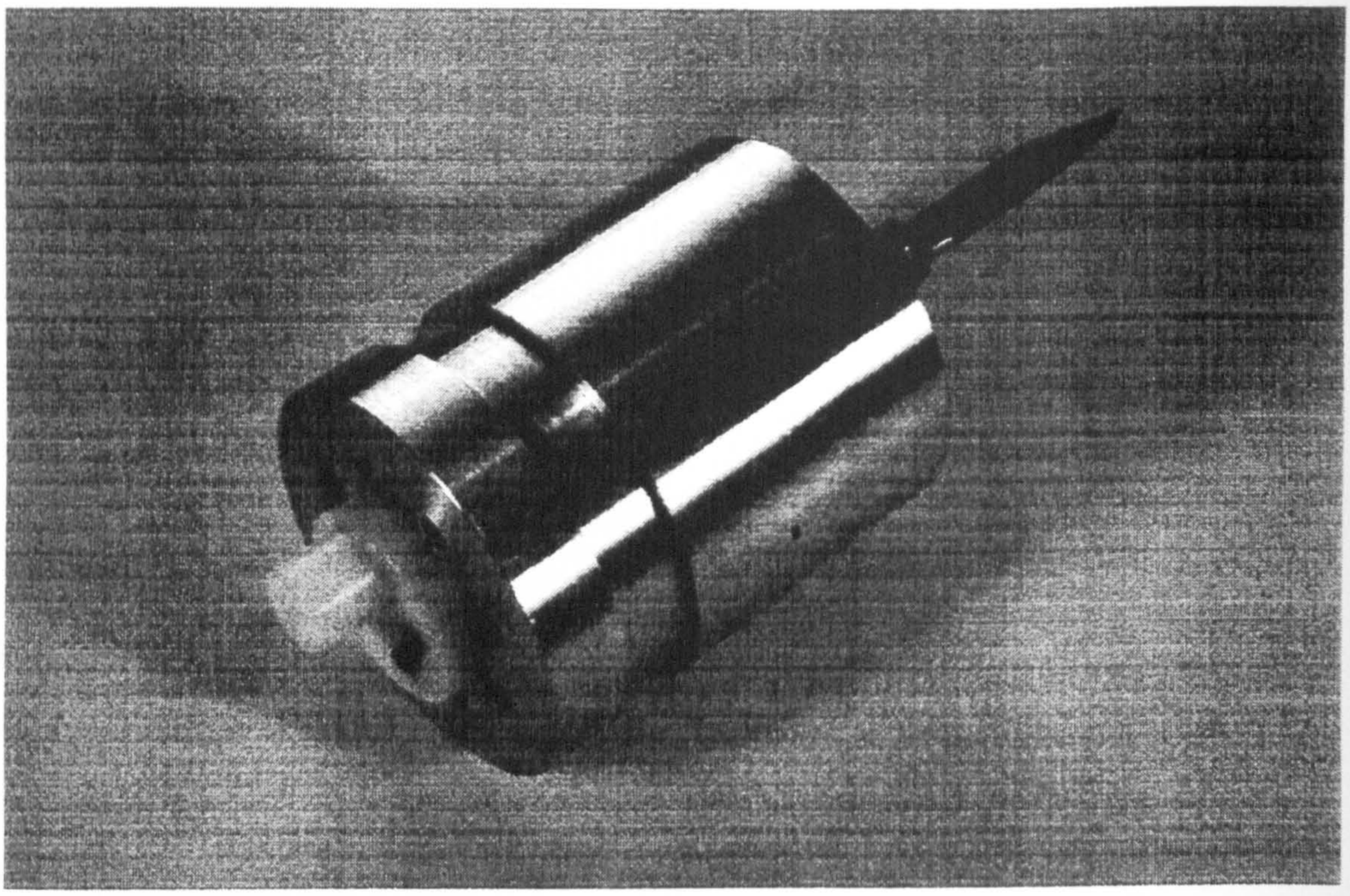

Figure 8.6 Fully assembled telemetry-based force-measuring knife.

Figure 8.7 Detail of strain gauge amplifier and transmitter circuitry, with aerial, of telemetry-based force-measuring knife.

8.2.4 TELEMETRY

To assess the ability of the current drop-tower test to replicate the forces found in human stab attacks, a telemetry force-measuring knife was built. This is a single channel strain gauge device, housing a strain gauge amplifier and radio transmitter, allowing the axial force on the knife blade at impact to be recorded. The overall diameter and length of the casing are 100mm and 125mm respectively. The receiver and data collection equipment can then be operated at a safe distance from the tower. The device is shown in Figure 8.6 and the circuit board contained within it is shown in Figure 8.7.

The momentum and energy of the knife were varied by varying its mass and the height from which it is dropped. Tests were carried out with three different masses and three starting heights. Three trials at each combination of velocity and mass were taken. All trials were completed without the foam backing used in volunteer tests in keeping with current testing practice.

Subject number	Body mass (kg)	Height (cm)	Sex
1	93	178	M
2	68	179	M
3	80	173	M
4	83	182	M
5	92	184	M
6	86	173	M
7	91.5	179	M
8	89	184	M
9	79	184	M
10	69	166	F
11	80	190	M
12	87	179	M
13	74.5	179	M
14	83	179	M
15	54	163	F
16	70	182	M
17	64	163	F
18	98	198	M
19	85	177	M
20	66.5	185	M

Table 8.3 Profile of volunteers used in the study.

8.3 SUBJECT TESTING

On arrival in the biomechanics laboratory, the procedures were explained to the volunteer and an information sheet provided. The subject was then given the opportunity to ask questions and asked to sign a consent form. Prior to the test starting, the subject was given the chance to practise stabbing the target with a dummy knife to become familiar with the response of the target.

The subjects removed clothing from their upper bodies and markers were attached to the upper arm, the wrist and the trunk. As the subject performed the stab, these markers were tracked by the six infra-red cameras of the Vicon motion analysis system. Tests were performed on the target with and without the foam backing.

The subjects performed five stabs for each style with and without foam totalling thirty stabs per subject. The target was positioned vertically for the thrust and sweep and inclined to 30° for the overhand stab.

All equipment and procedures had been approved by the Departmental Safety Committee and the University Ethics Committee. All subjects were asked to don safety glasses for the test.

After the test, the height and body mass of the subject were recorded.

8.3.1 VOLUNTEER PROFILE

Volunteers were recruited from within the Bioengineering Unit and from Strathclyde Police and consisted of 17 males and 3 females. The subjects' body masses ranged from 54kg to 98kg and their heights varied from 163cm to 198cm (Table 8.3).

Examination of an audit of stab attacks committed in Strathclyde in 1995 showed that 91% of attackers were male.

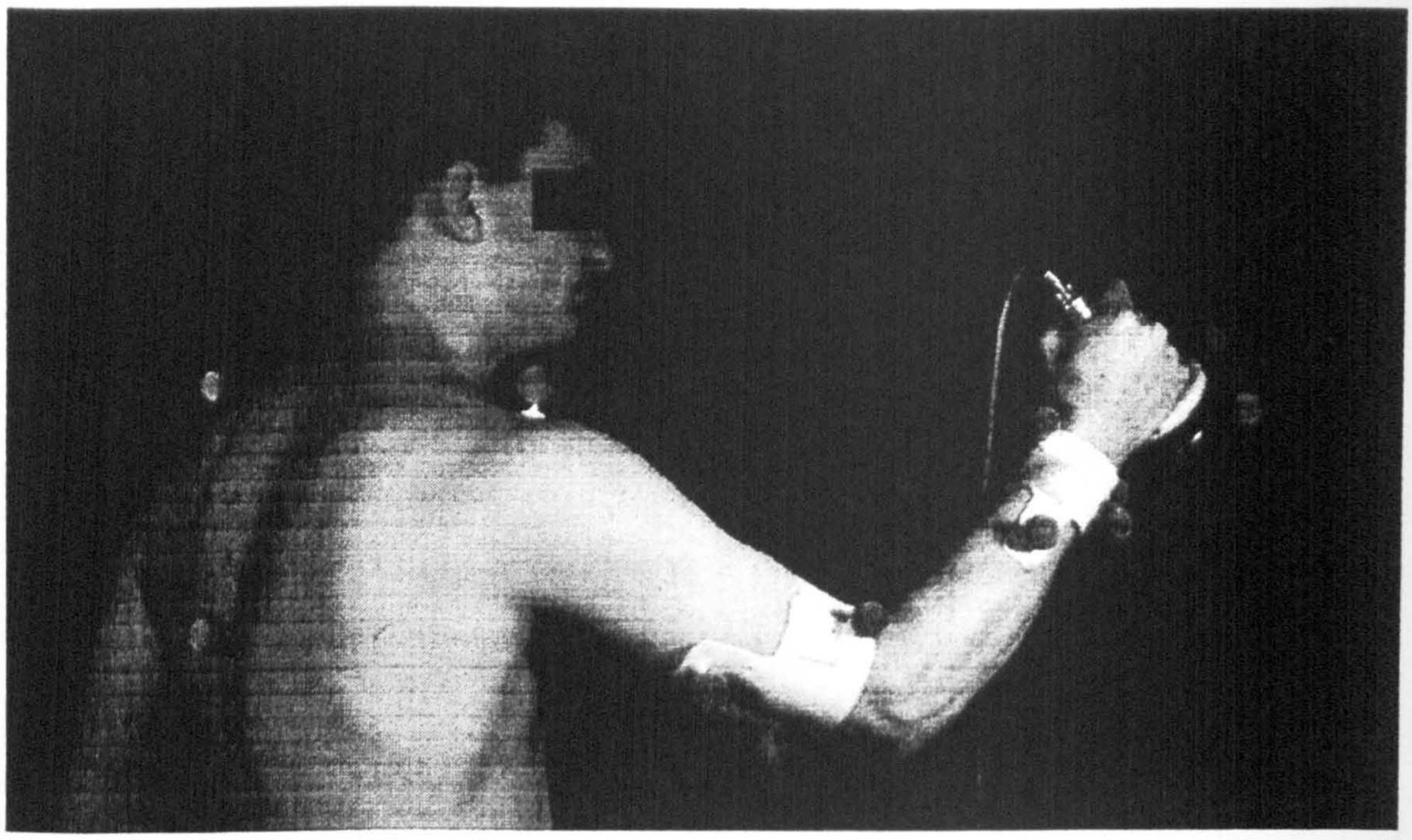

Figure 8.8 Volunteer performing 'overhand' stab.

Figure 8.9 Volunteer performing 'sweep' stab.

8.3.2 STYLES OF STAB ATTACK

Three styles of stab were decided upon following consultation with Strathclyde Police: a short thrust forward, a horizontal style sweep around the body and an overhand stab. (See Figures 8.8 and 8.9)

8.3.3 THE TARGET

The target consisted of a box of plasticine, previously used in stab simulation tests and intended to simulate the compliance of human flesh, covered with a sample of stab-resistant material. Following preliminary trials, it was thought that the plasticine did not sufficiently mimic the flesh and thus a piece of foam of density 33kg/m^3 and thickness 30mm was placed between the box and the material. Calvano, N. J. (1993) used foam of density 35 kg/m^3 to simulate resistance of the human body.

The stab-resistant material was made up of 28 layers of kevlar 0.3mm thick, in a 1.4mm pitch weave, arranged in 2 groups of 14, backed by 2 sheets of polypropylene of thickness 1.0mm covered with tightly woven nylon. Overall thickness was 10mm.

CHAPTER 9 RESULTS AND DISCUSSION

9.1 VOLUNTEER TESTS

Following data collection, the data were processed using the software provided with the Vicon motion analysis system, and software written for the project using the Labview graphical programming language.

Of the five trials taken for each style of stab, the three with the most complete data were analysed and the trial giving the maximum value is reported. For three subjects the accelerometer data appeared corrupt and therefore has not been used. It was also found, after analysis, that the motion data were incomplete for some styles for some subjects. Table 9.1 displays the number of subjects for whom motion data were of sufficient quality to be included.

Stab Style, Target	Subjects	Abbreviation
Thrust, foam	1-11, 14-19	*TF*
Thrust, no foam	1-12, 15-20	*TNF*
Sweep, foam	1-6, 10-12, 14-18, 20	*SF*
Sweep, no foam	1-6, 9-12, 15-20	*SNF*
Overhand, foam	1, 2, 4, 6, 9-11, 13, 14, 16-20	*OF*
Overhand, no foam	1, 2, ,4 , 6, 10, 11, 13-20	*ONF*

Table 9.1 Number of subjects analysed for each style.

STYLE	FOAM				NO FOAM			
	Max	Min	Mean	95%ile	Max	Min	Mean	95%ile
Thrust	61	14	39	60	85	9	40	68
Sweep	90	17	45	74	103	15	46	73
Overhand	78	12	38	72	72	7	35	66

Table 9.2 Energy of system before impact (Joules).

STYLE	FOAM				NO FOAM			
	Max	Min	Mean	95%ile	Max	Min	Mean	95%ile
Thrust	66	16	43	59	68	15	42	61
Sweep	85	22	45	69	104	21	45	67
Overhand	75	17	43	70	64	12	42	63

Table 9.3 Momentum of system before impact (kg.m/s).

STYLE	FOAM				NO FOAM			
	Max	Min	Mean	95%ile	Max	Min	Mean	95%ile
Thrust	7.6	3.4	5.2	7.2	8.1	3.2	5.2	7.7
Sweep	8.8	4.2	6.5	8.5	9.2	3.8	6.6	9.0
Overhand	8.3	3.6	6.0	8.1	8.6	2.6	5.9	8.3

Table 9.4 Knife velocity prior to impact (m/s).

9.1.1 ENERGY, MOMENTUM, WORK DONE AND IMPULSE

The data from the motion analysis are summarised in Tables 9.2 to 9.4. The amount of energy the volunteers were able to generate in a stab attack took a wide range of values, and often far exceeded the previously used index level of 42J, as seen in Figure 9.1. The values appear to be influenced by the style of approach, with the sweep producing the highest values, followed by the overhand and finally the thrust. Figure 9.2 shows that the values of momentum encountered were also high, with 60kgm/s being exceeded in some cases with every style. The effect of style on the values for momentum follows the same pattern as that for energy.

The work done quoted here is defined as the work done in bringing the knife to rest, and was considerably lower than the energy contained in the system before impact, often less than half (Figure 9.5). Due to the sudden nature of the impact, it was impossible to measure the amount of energy remaining in the body segments, due to their continued motion following the impact, and it is possible that this was significant. Another factor is that the tip of the knife blade does not lie exactly along the axis of the knife, causing the knife to rotate on impact and transferring some of the linear kinetic energy into rotational energy. The calculation of work done was subject to an exceptionally large uncertainty, due to difficulty in determining the precise instant when the knife came to rest, which could have been as much as ±50%. The introduction of the foam backing tended to increase the amount of work done in bringing the knife to rest; that is, the amount of energy 'absorbed' by the target was larger (Figure 9.5). The same is true of the impulse values measured, which were very much less than the momentum values (Figure 9.6).

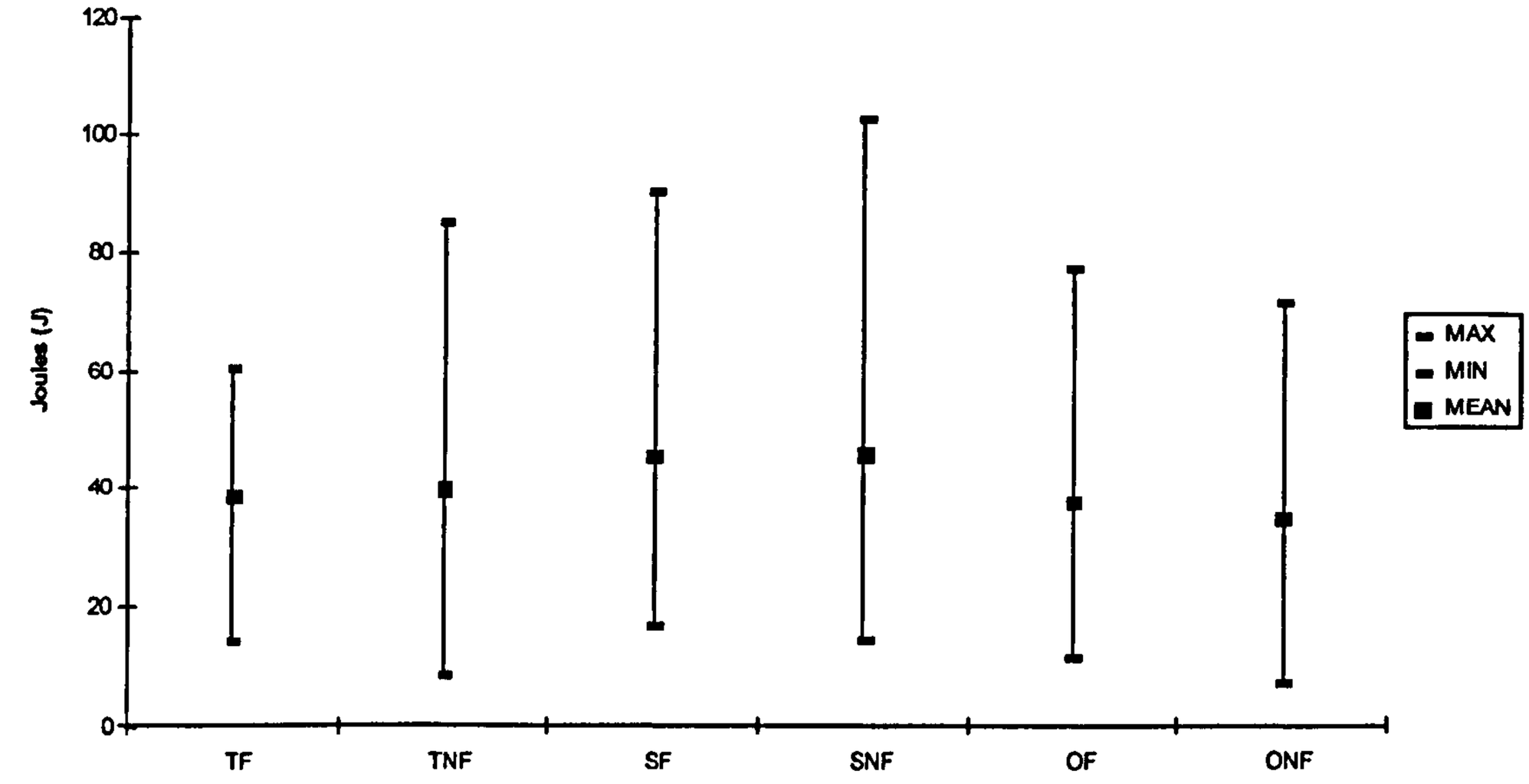

Figure 9.1 Energy of system before impact - mean values with maximum and minimum points for the three styles of attack.

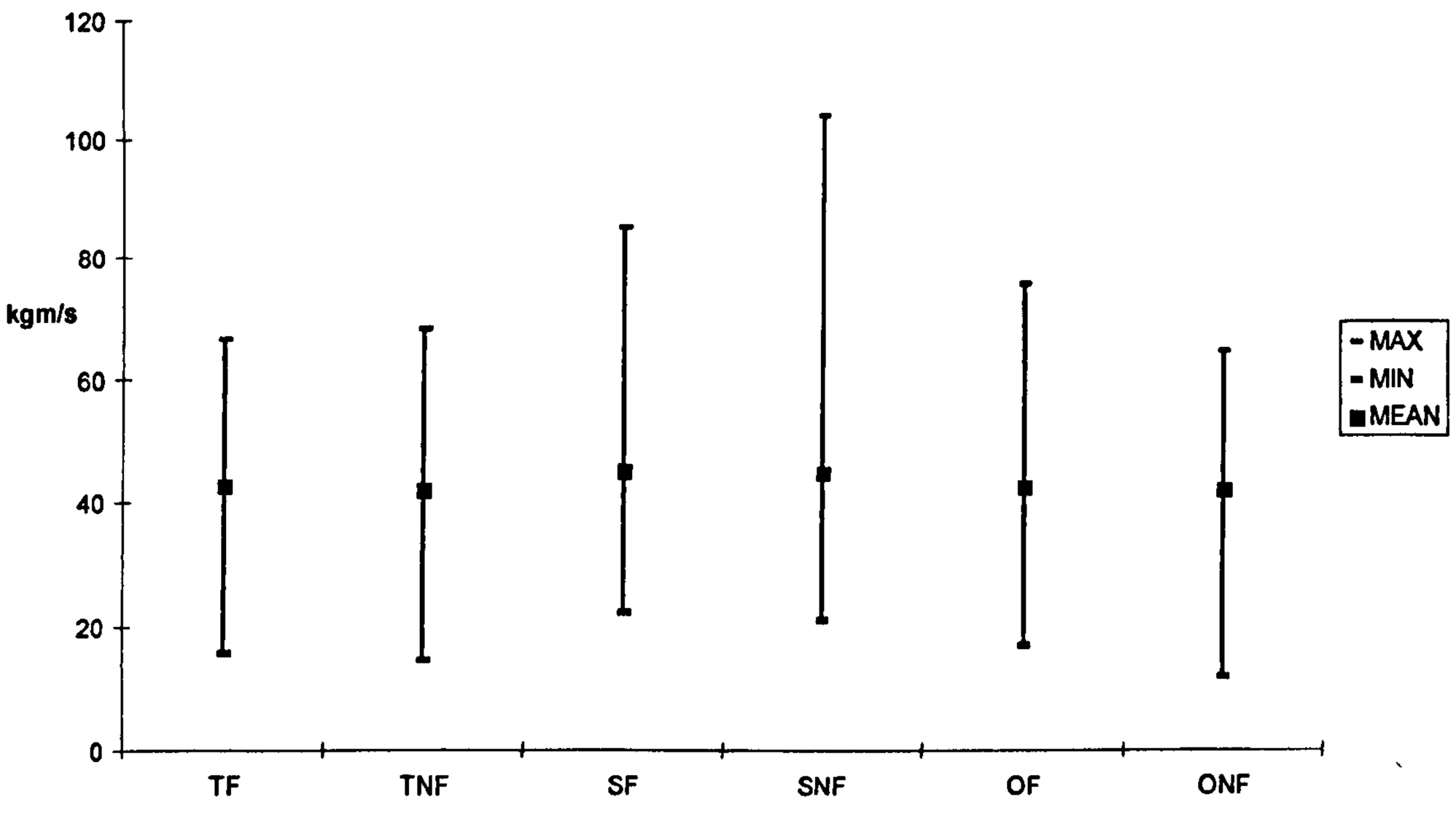

Figure 9.2 Momentum of system before impact.

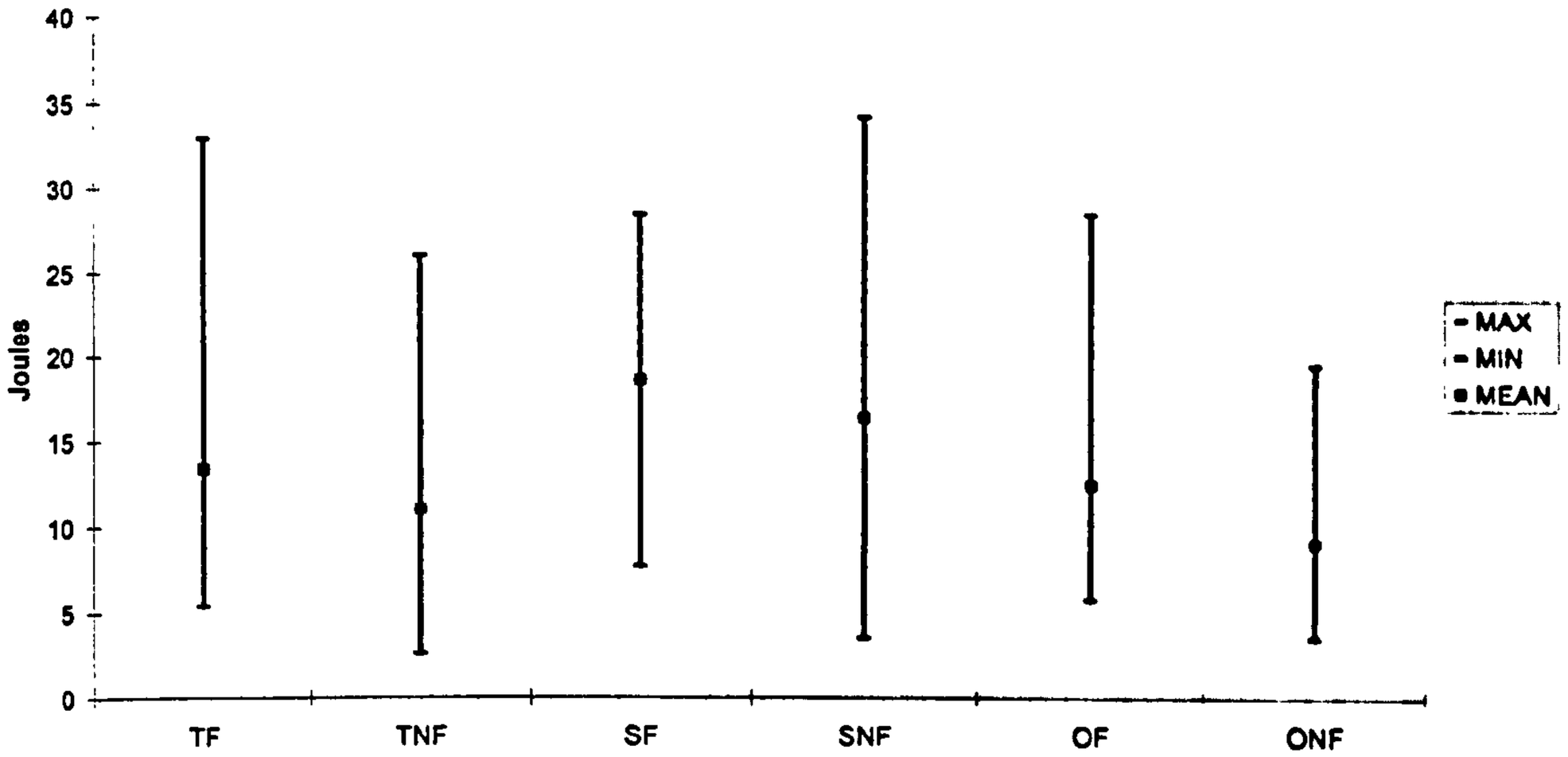

Figure 9.3 Work done on the target for each style.

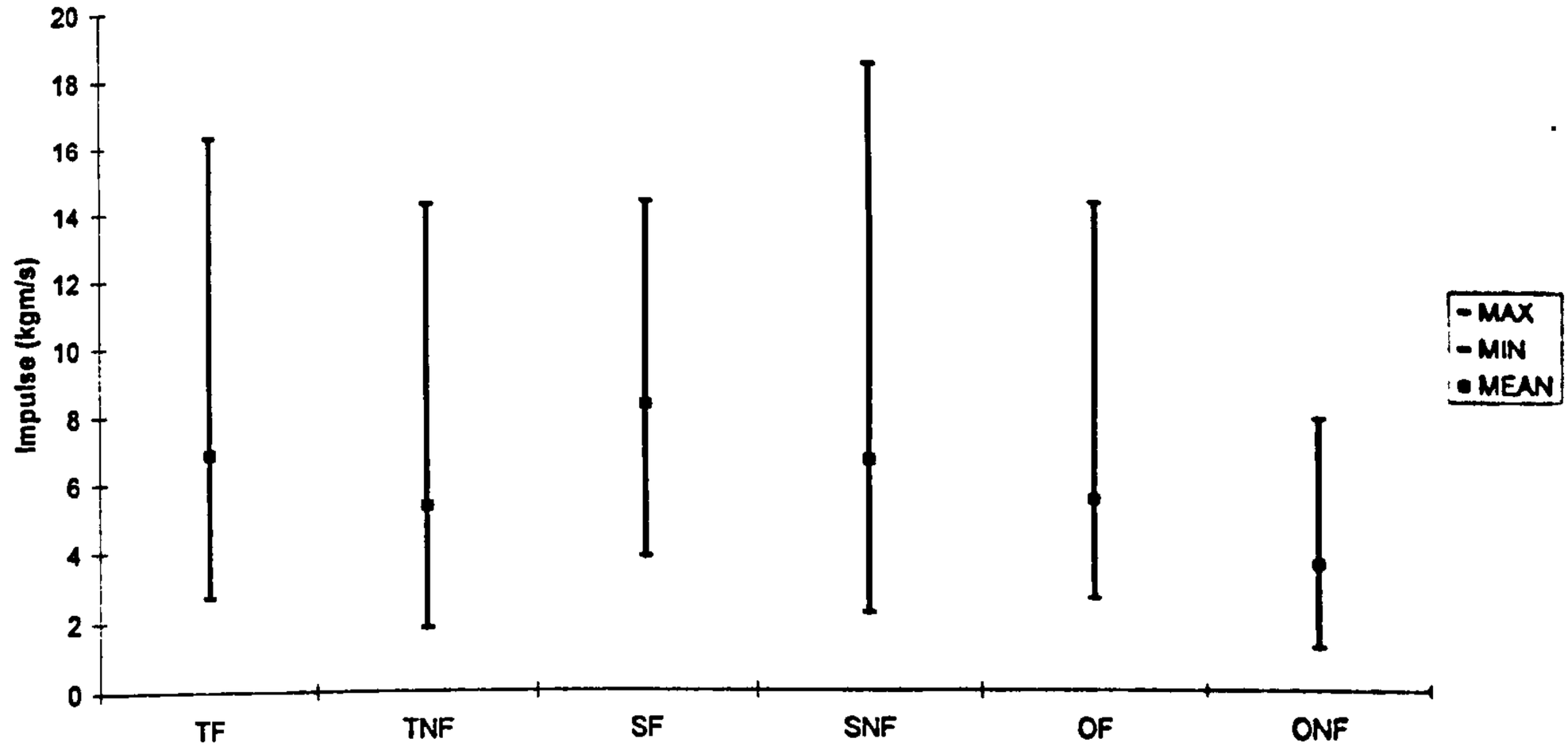

Figure 9.4 Impulses transmitted to the target for each style

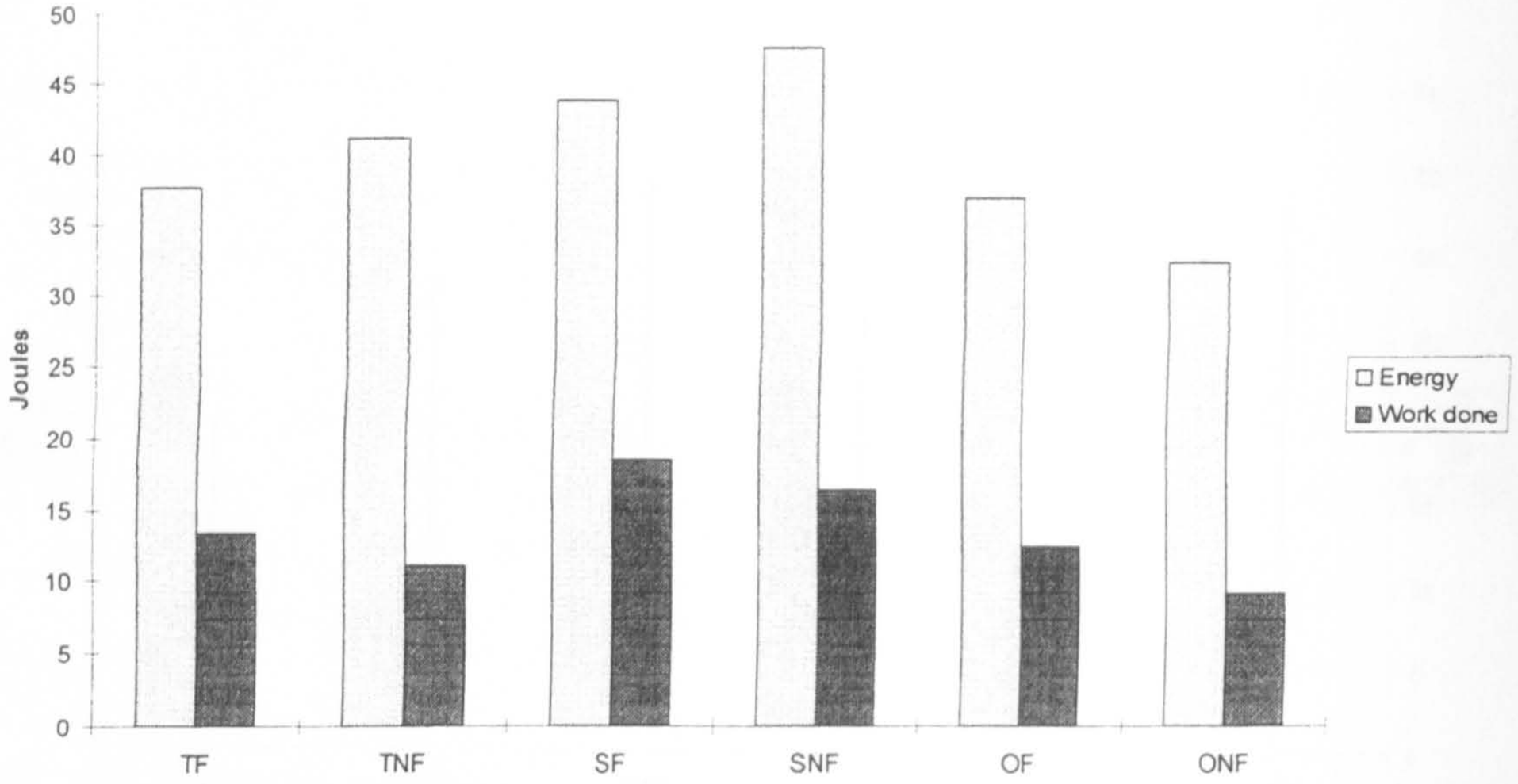

Figure 9.5 A comparison of the average energy immediately before impact and the average work done after impact for each style.

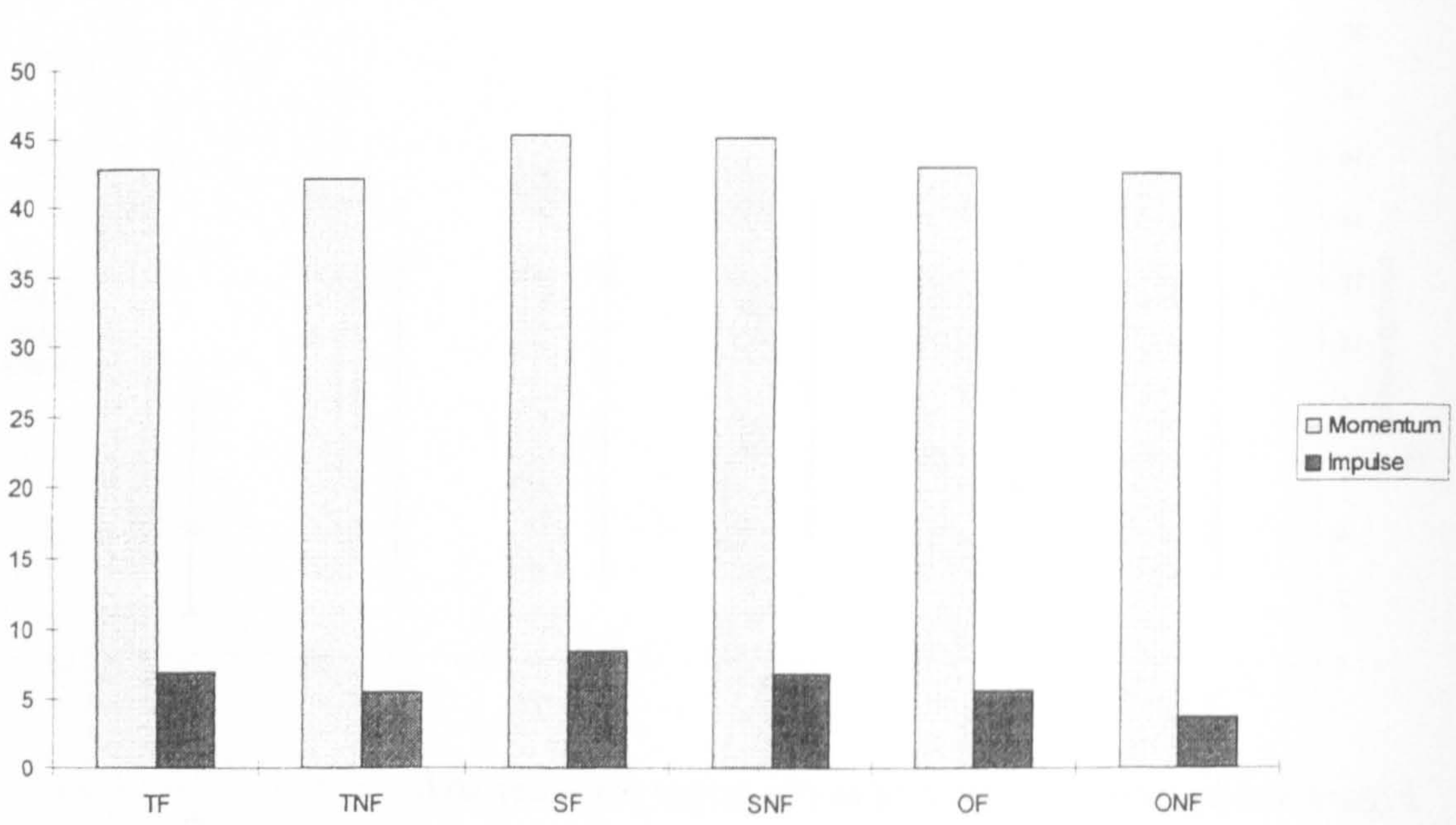

Figure 9.6 A comparison of the average momentum before impact and the average impulse required to stop the knife after impact for each style.

9.1.2 FORCES AND MOMENTS

The force along the blade (axial force) often reached values in excess of 2000N, as shown in Figure 9.7. The average value shown in the graphs of forces and torque are median values because the distribution of results was skew, and this would have led to mean values, a more commonly quoted measure of average, being misleading. Again, some influence of style was seen on the forces generated, with the overhand stab tending to produce the largest forces and the thrust producing the smallest values.

The cutting force and lateral force values were also found to be large in some cases, and were noticeably style dependent. The highest cutting forces were found with the overhand style, where the action tends to drag the knife down, and had a median value of approximately 300N (Figure 9.8). Lateral force values tended to be highest during the sweep style of stab, but were generally lower than the cutting forces (Figure 9.9). The measured torques, or twisting effects, were also highest during the sweep (Figure 9.10).

Figures 9.11 to 9.13 show the combined load effects acting on the knife for each type of stab, indicating that the maxima for each component of load do not necessarily occur simultaneously. Figure 9.14 shows the effect of placing a layer of foam between the stab-resistant material and the plasticine box. With the foam in place the forces tended to be lower than without, and the duration of the impact was longer.

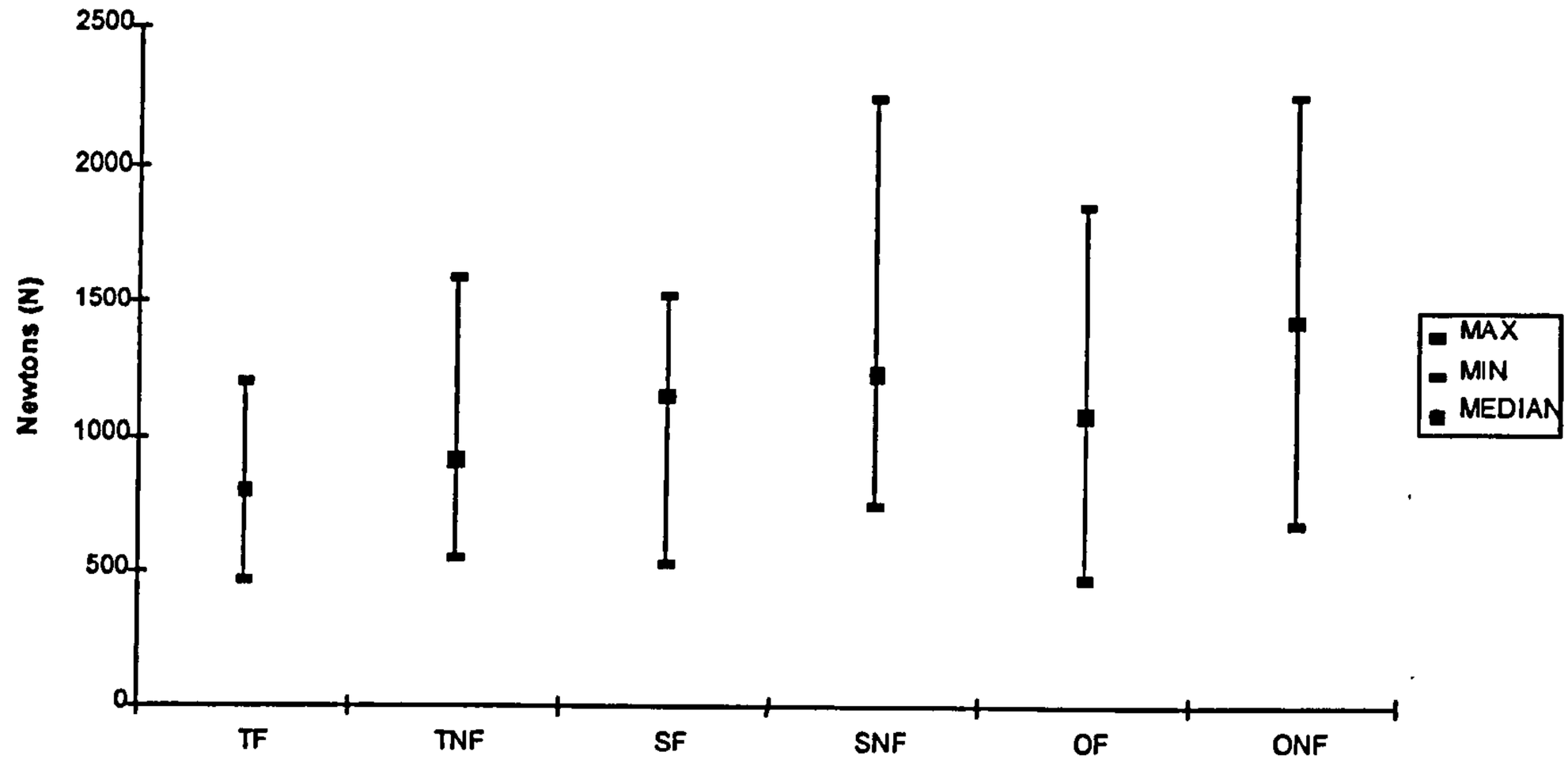

Figure 9.7 Axial forces for each style.

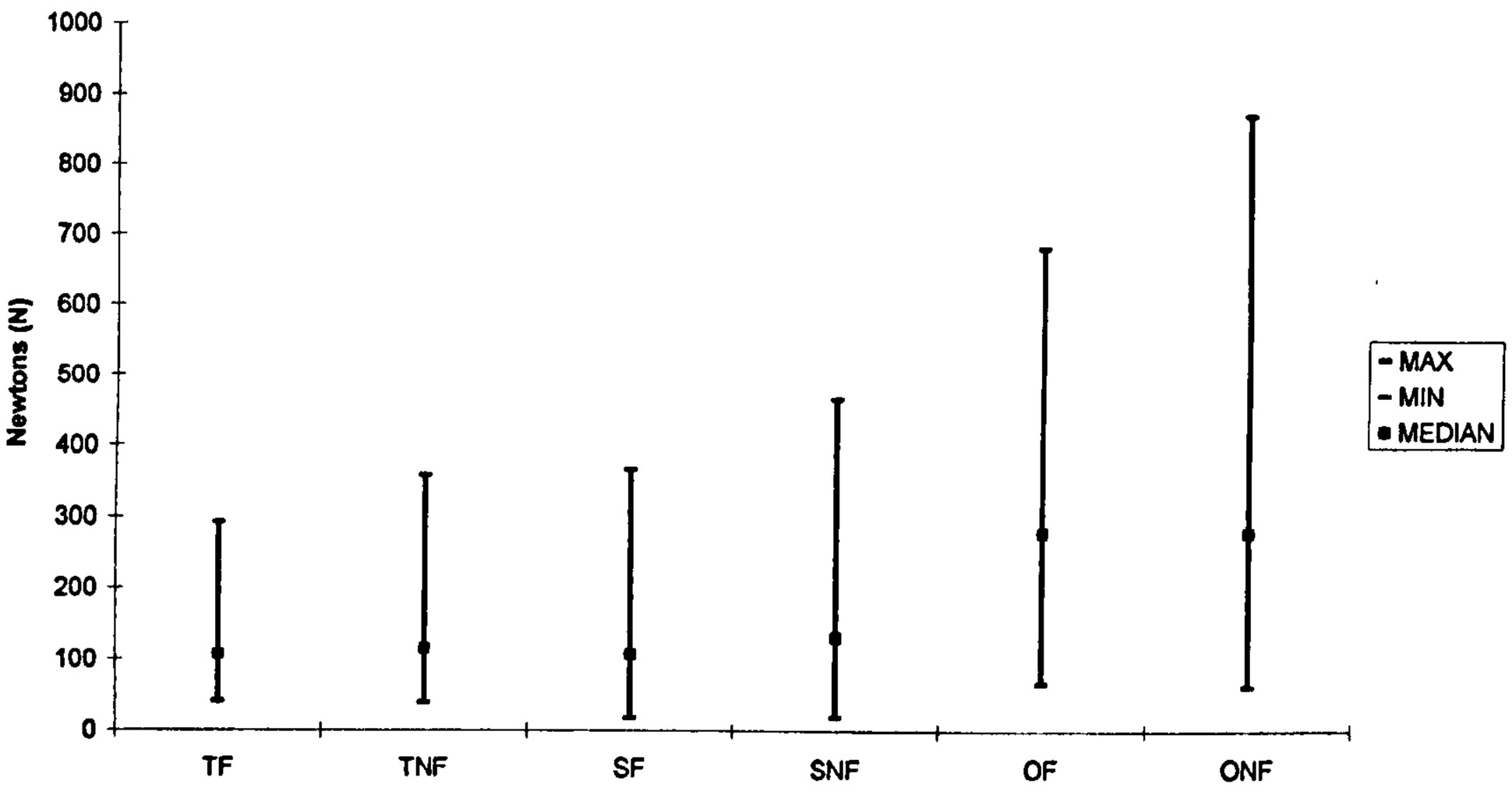

Figure 9.8 Cutting forces for each style.

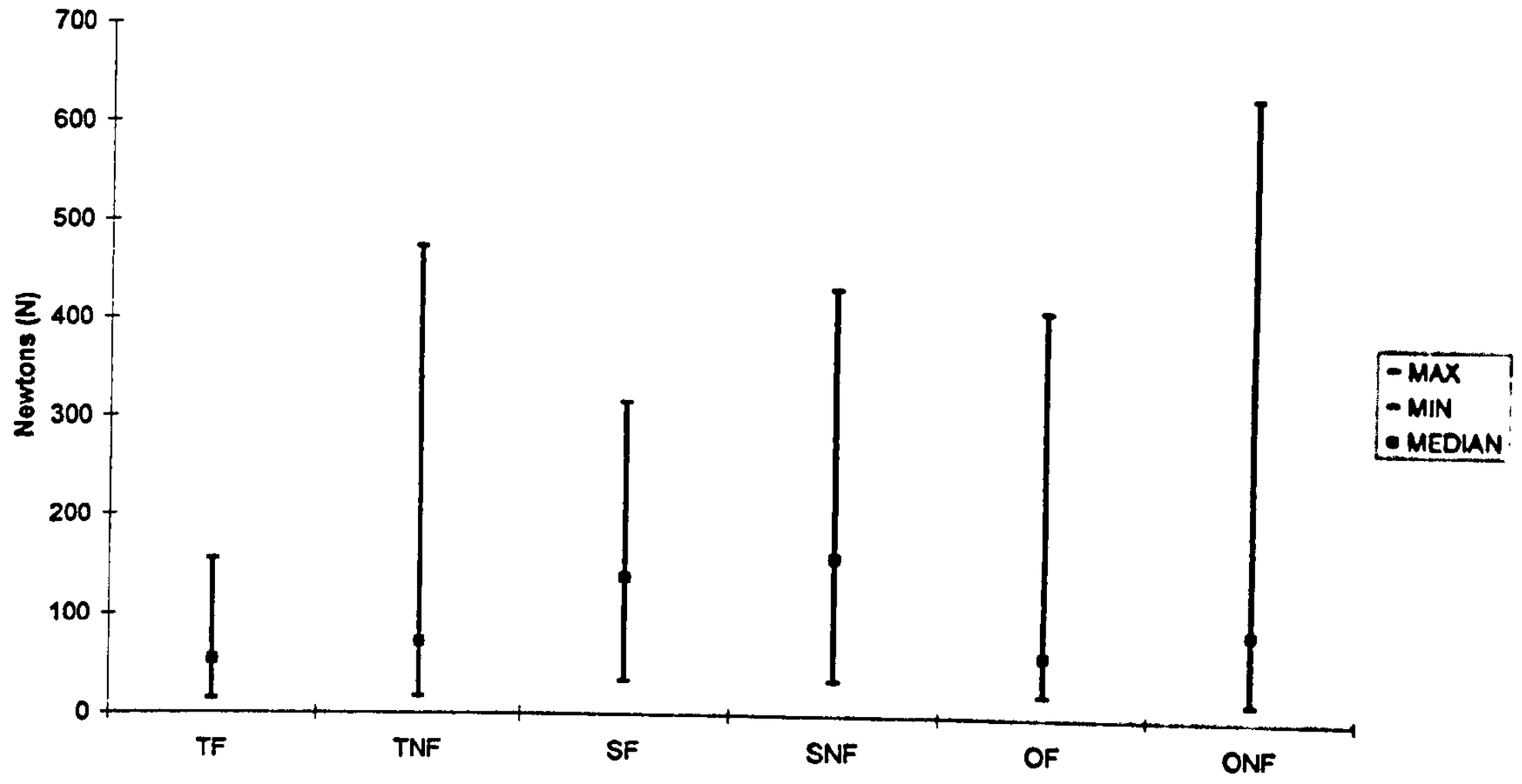

Figure 9.9 Lateral forces for each style.

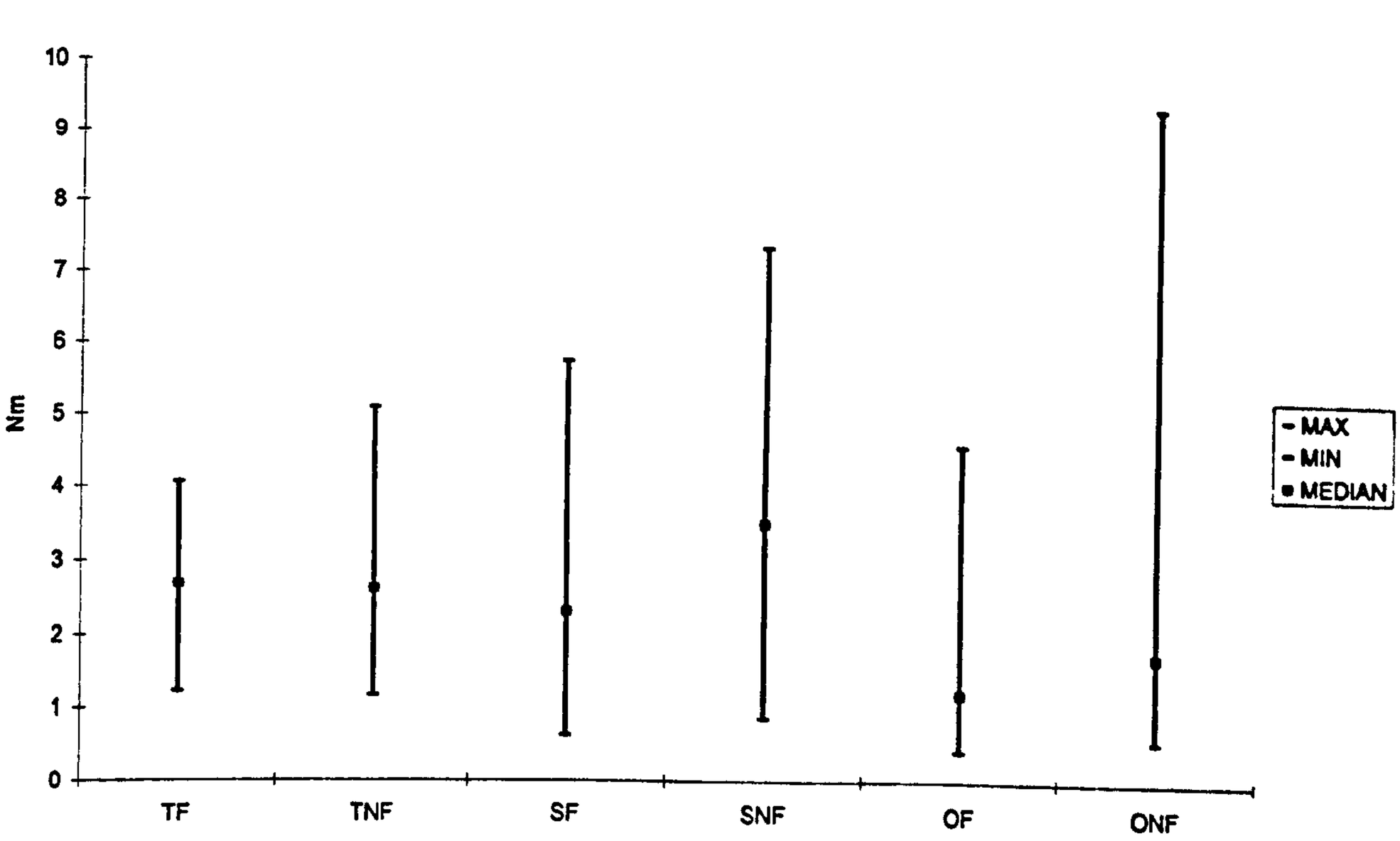

Figure 9.10 Torque values for each style.

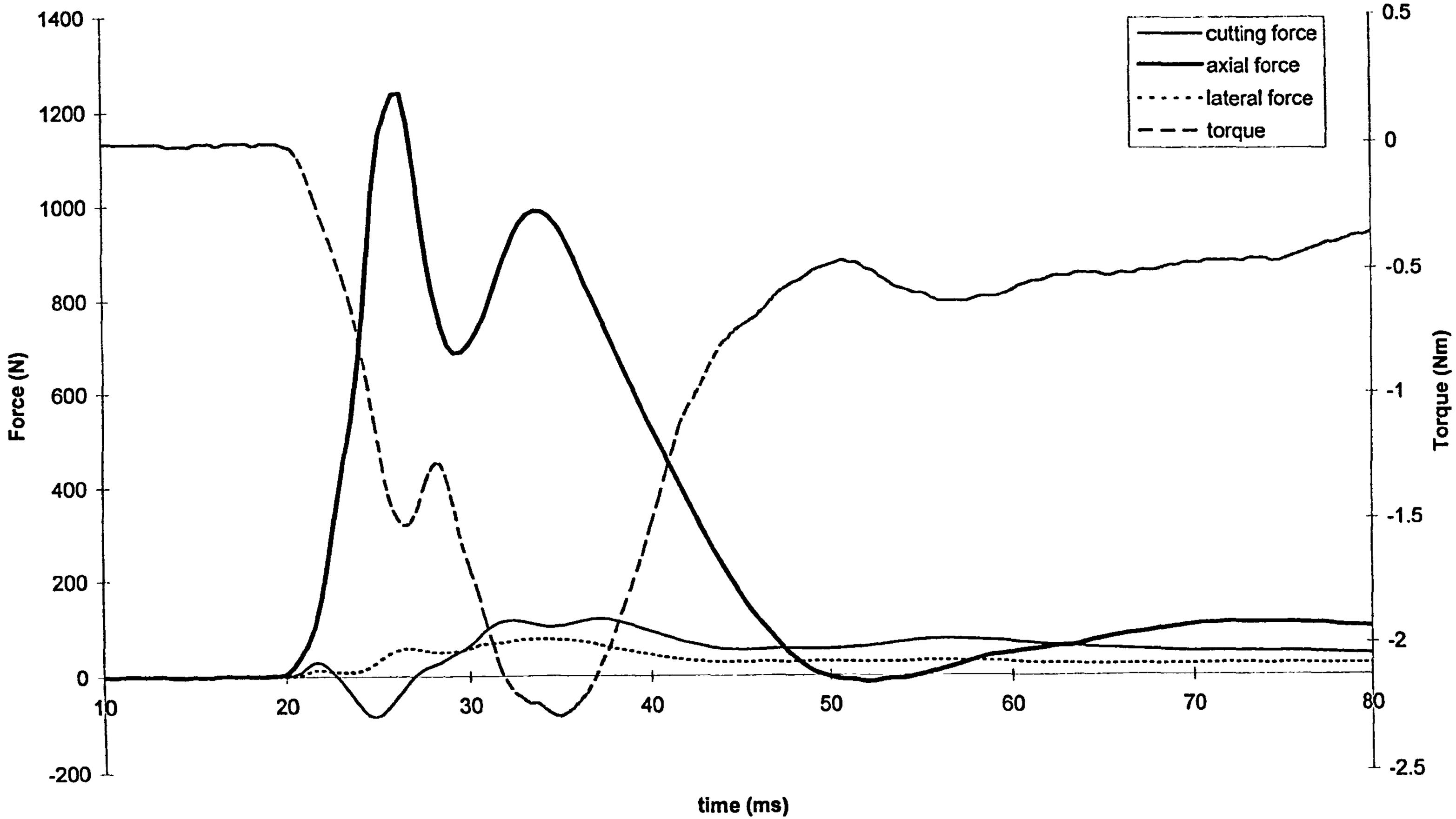

Figure 9.11 The four components of load measured during a thrust style stab (no foam).

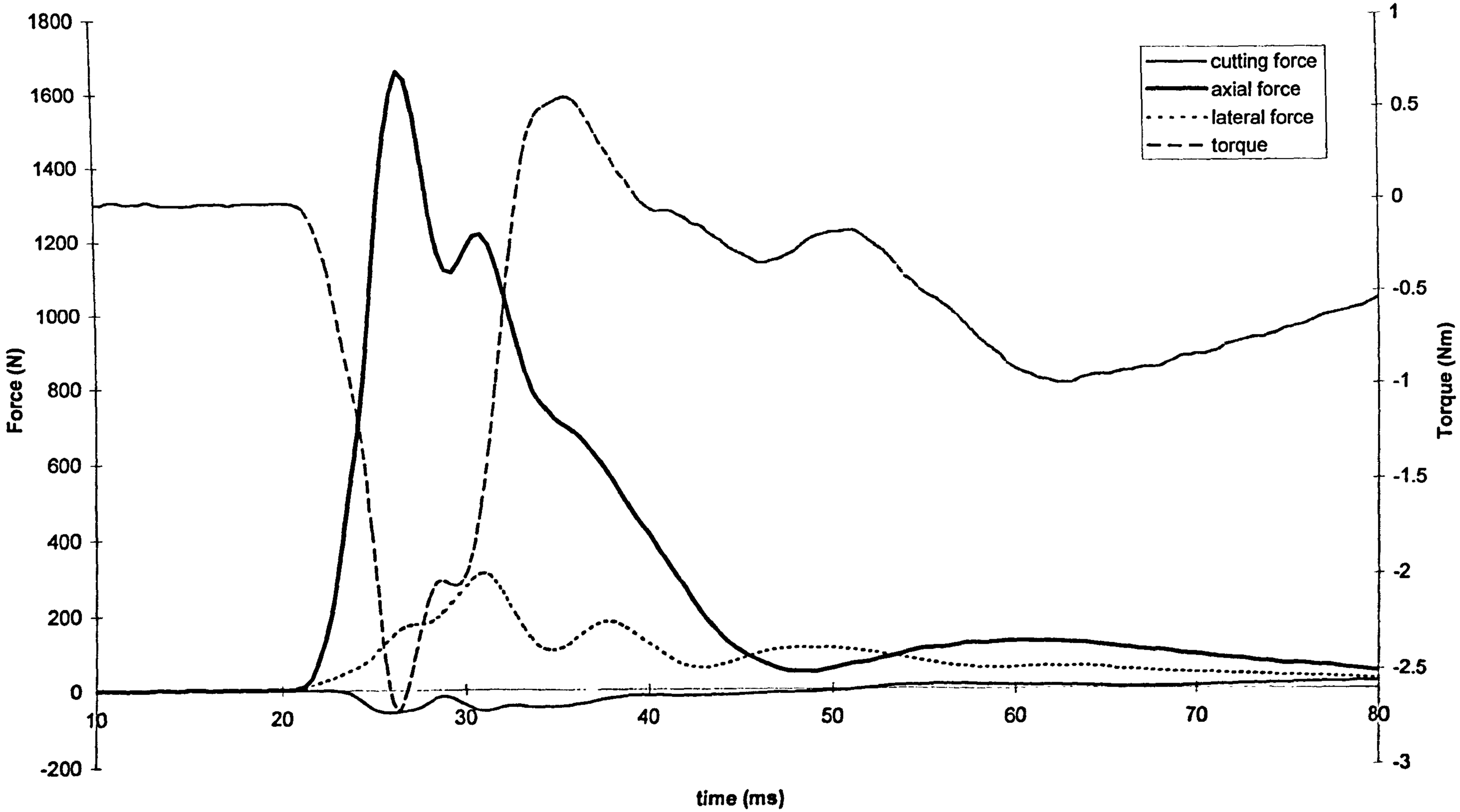

Figure 9.12 The four components of load measured during a sweep style stab (no foam)

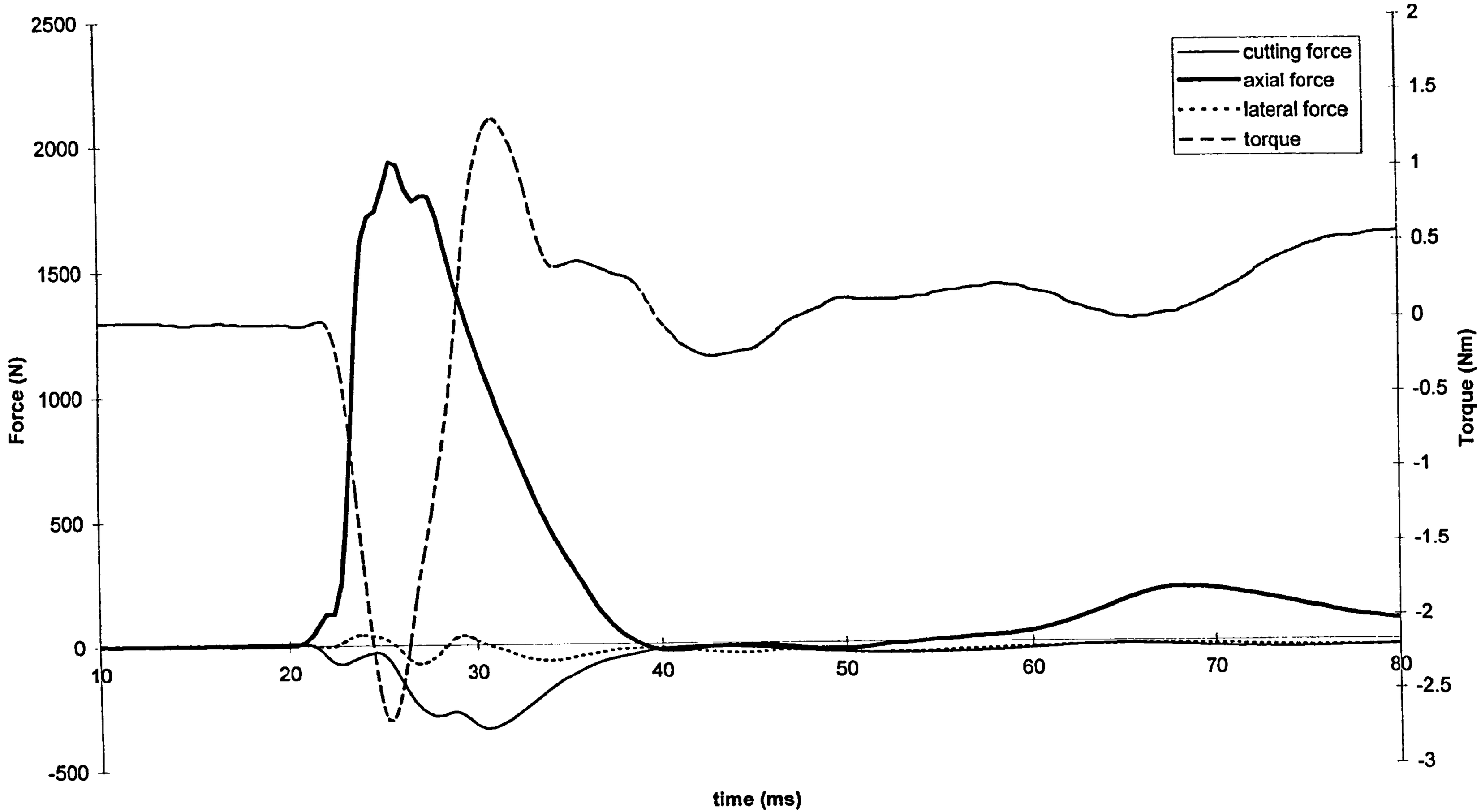

Figure 9.13 The four components of load measured during an overhand style stab (no foam).

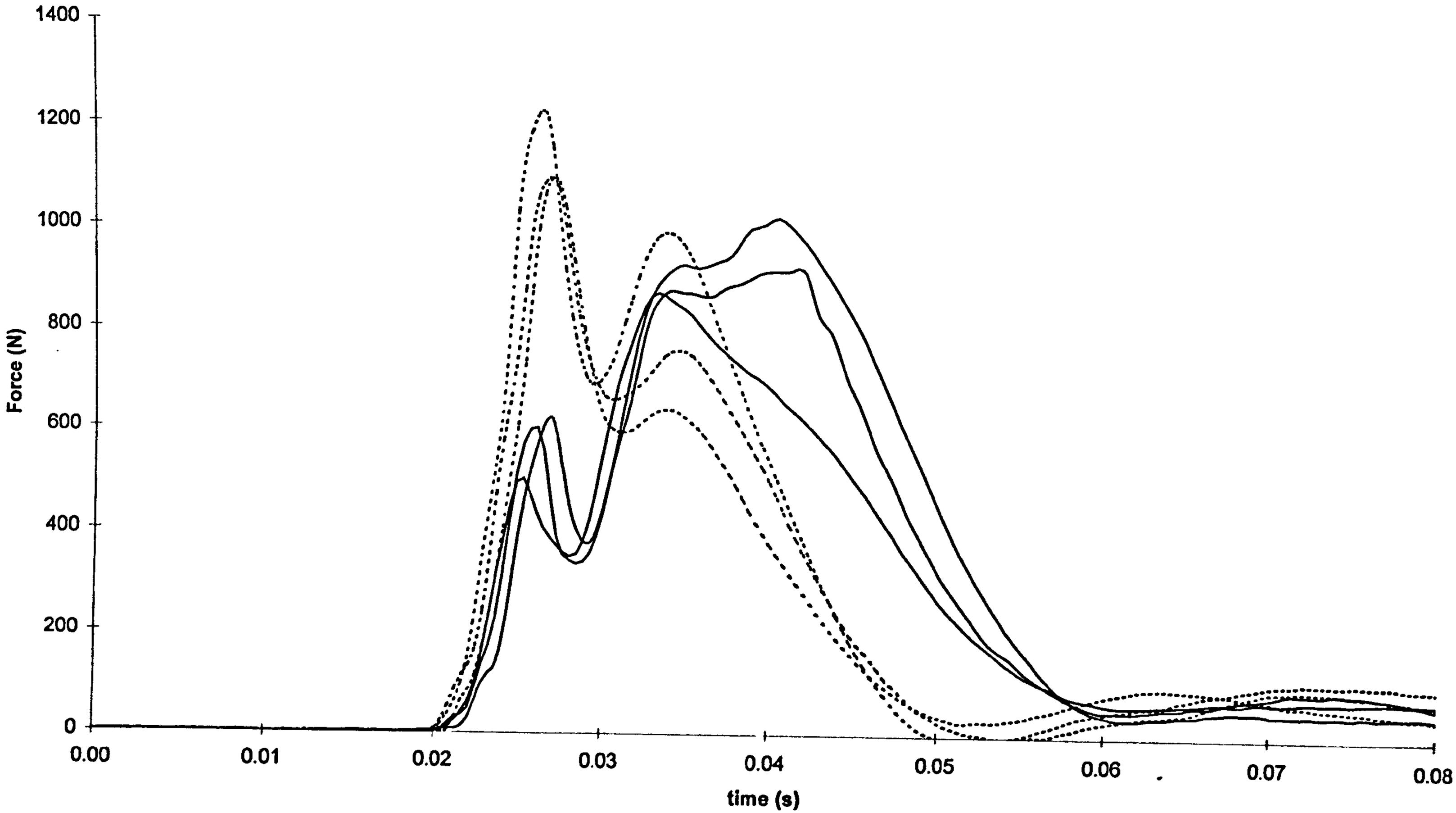

Figure 9.14 Effect of backing foam on axial force profile - typical plot from one subject, thrust style, three trials per target. (Solid line with foam, dashed line without foam.)

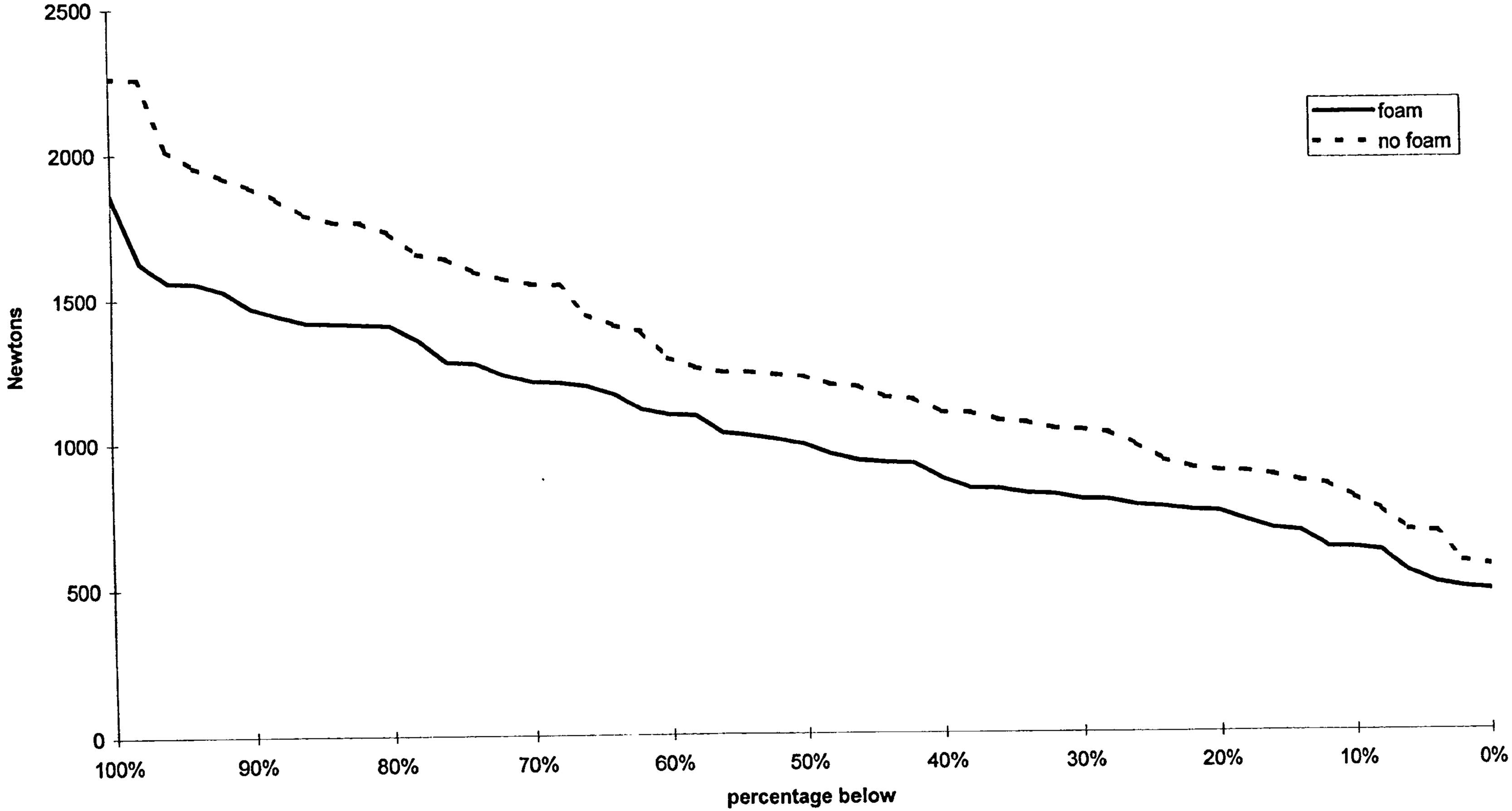

Figure 9.15 Distribution of axial force values among volunteer group (total of 51 stabs with foam and 51 without).

9.1.3 CLUSTERING OF RESULTS

Some of the most important parameters have been quoted as percentiles, that is the percentage of stabs falling on or below a given value, in Figure 9.15 to Figure 9.22. The results of this study suggest that it may be impractical to design a garment that will protect against every possible threat, since in such a case the garment would be unwearable. It is also the case that different levels of protection would be required in different scenarios, and that in some situations the garment would need to be worn covertly. There is thus a decision to be made about the level of protection to provide, and clustering the results in this way allows this to be done. For example, although the energy exceeded 100J in one case, 95% of values were below 70J but only 50% were below 40J.

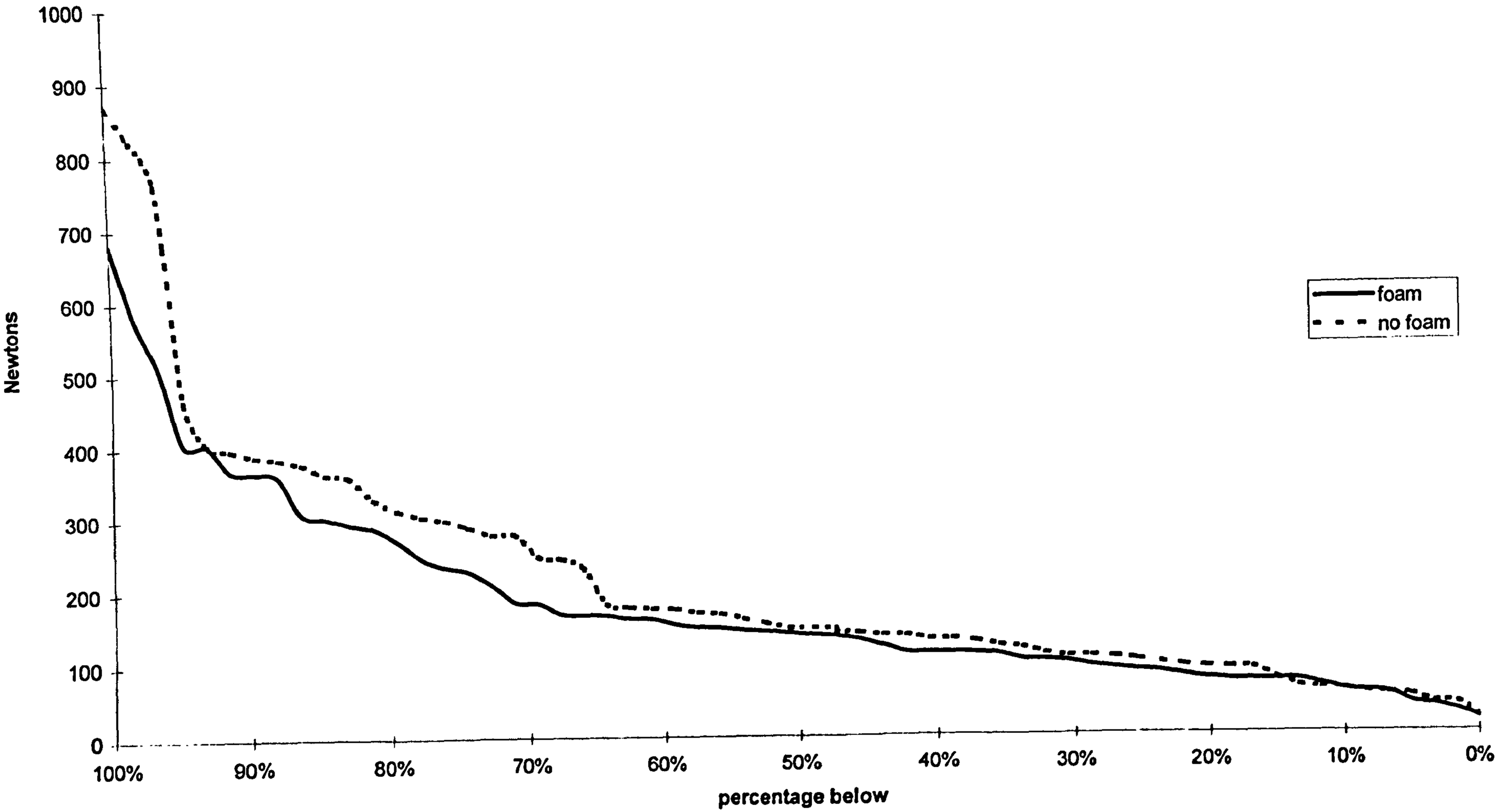

Figure 9.16 Distribution of cutting force values among volunteer group (total of 60 stabs with foam and 60 without).

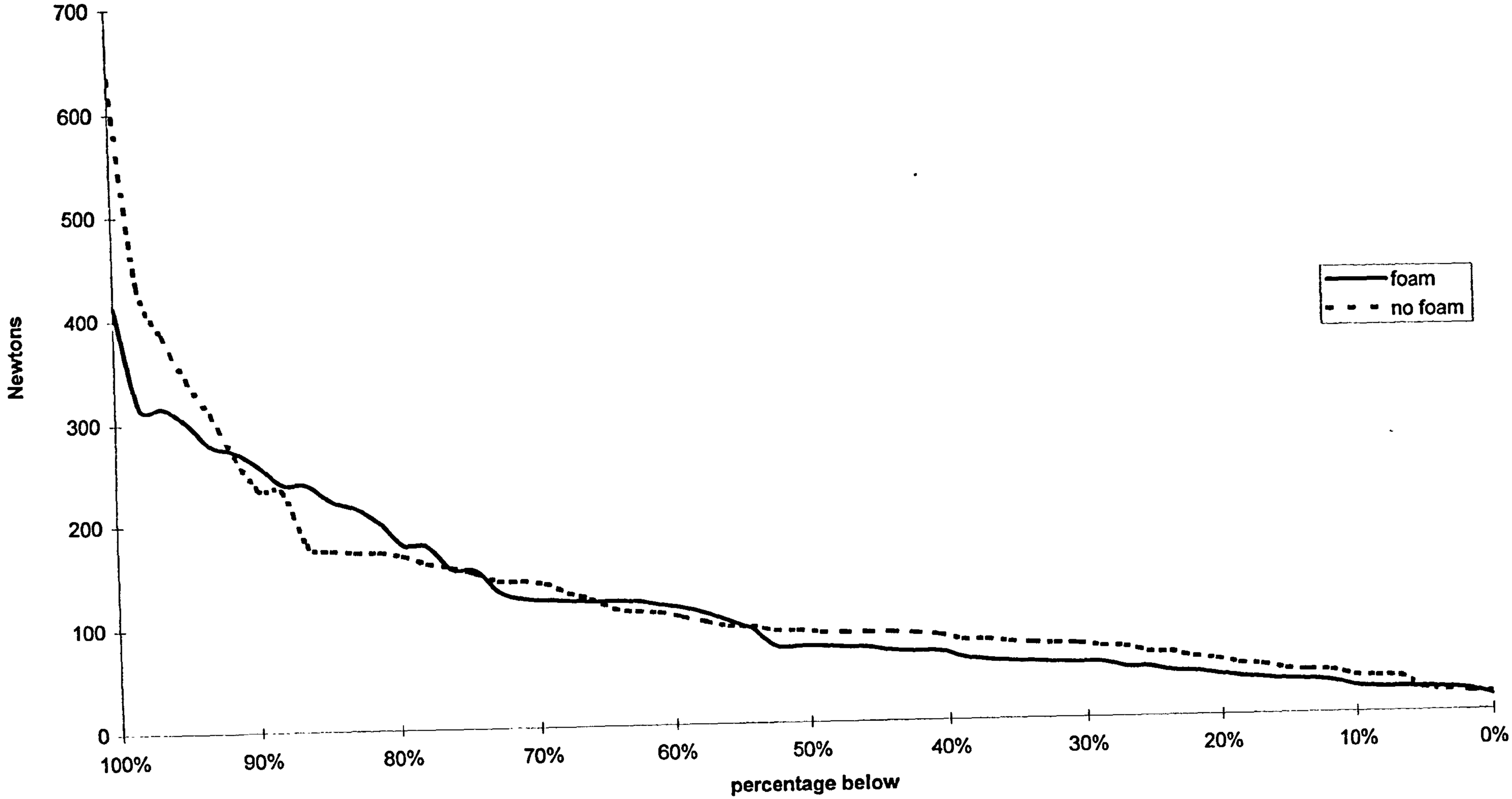

Figure 9.17 Distribution of lateral force values among volunteer group (total of 60 stabs with foam and 60 without).

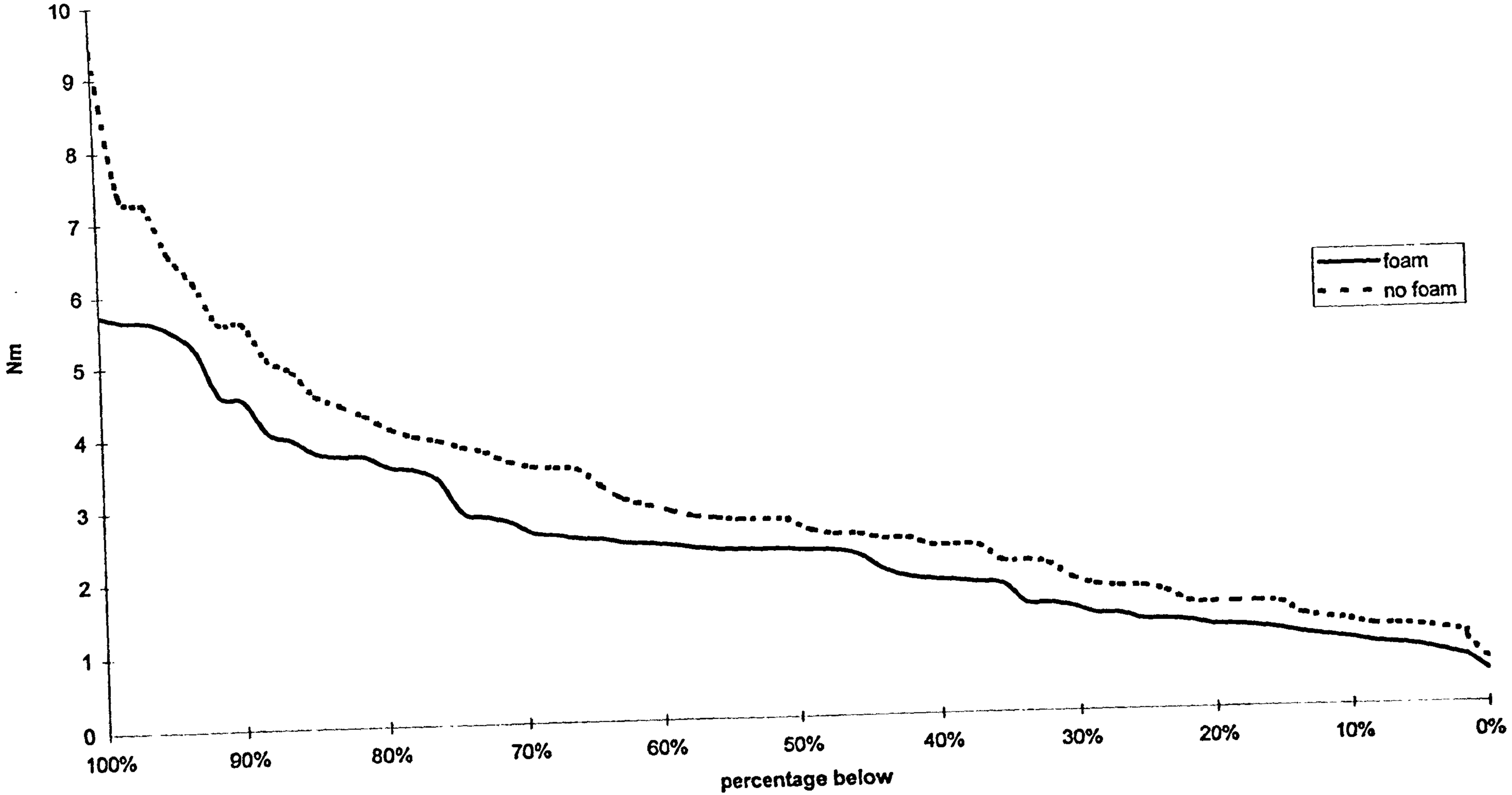

Figure 9.18 Distribution of torque values among volunteer group (total of 60 stabs with foam and 60 without).

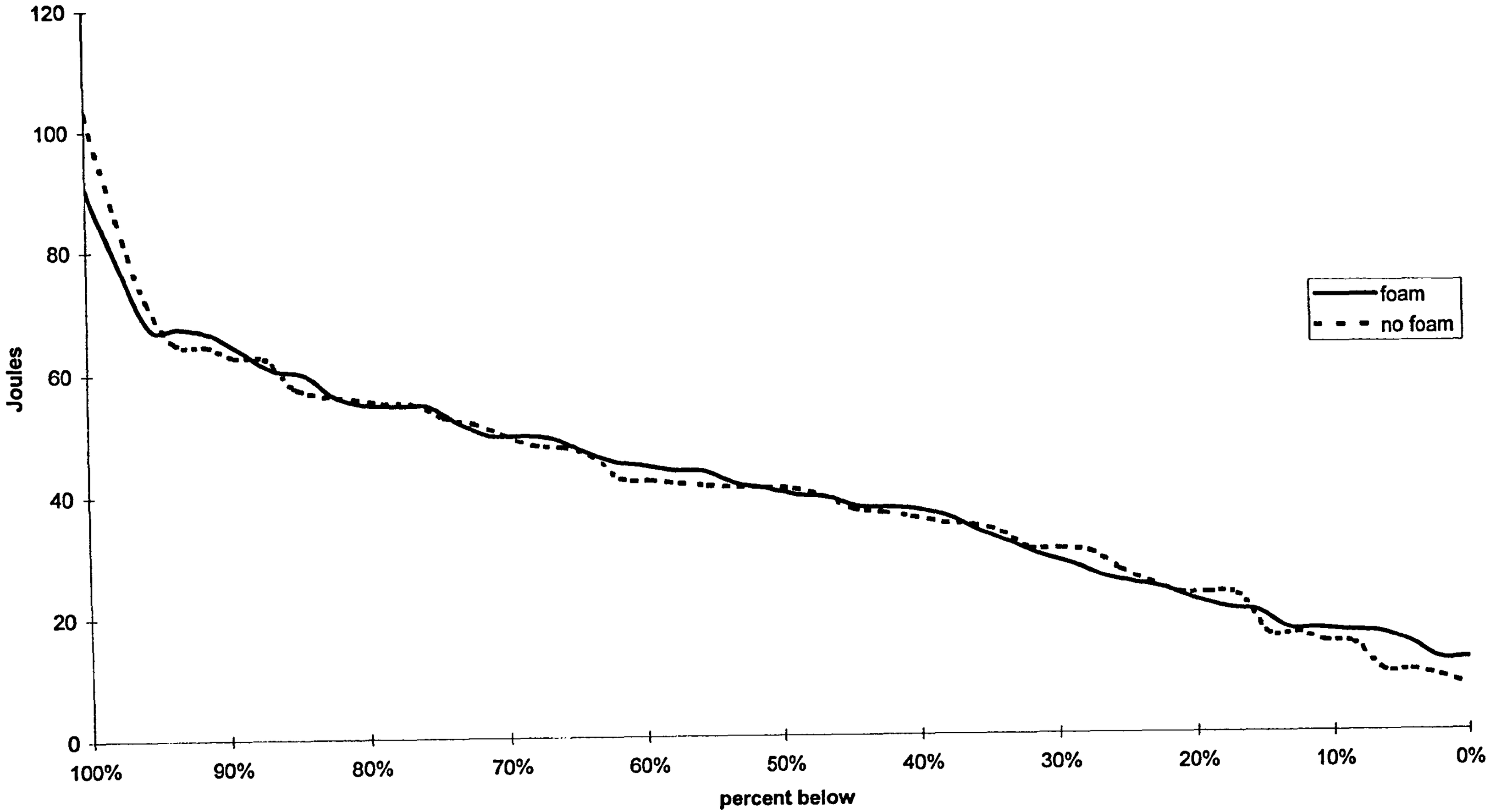

Figure 9.19 Distribution of energy values among volunteer group (total of 46 stabs with foam and 48 without).

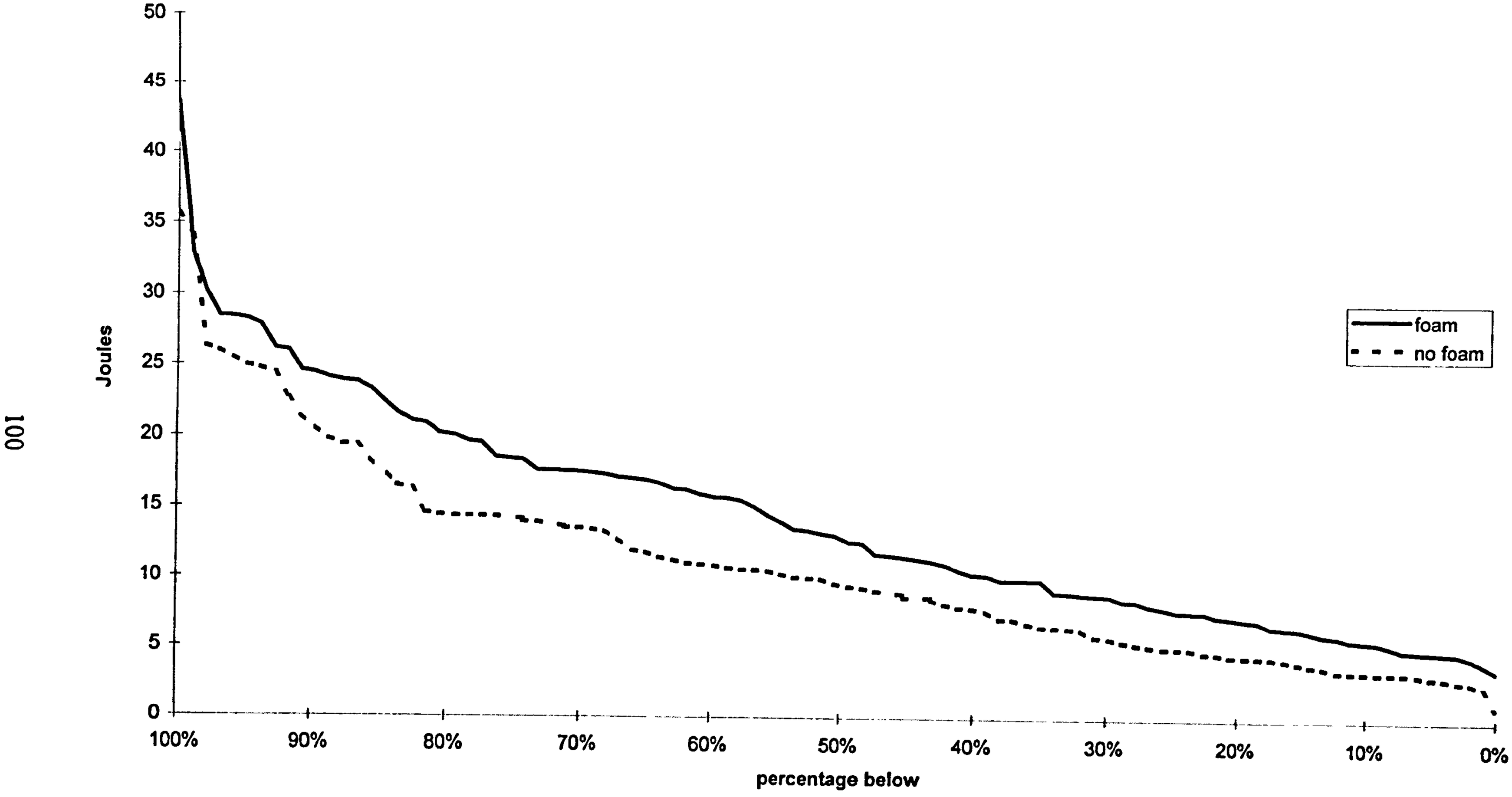

Figure 9.20 Distribution of work done on target values among volunteer group (total of 34 stabs with foam and 37 without).

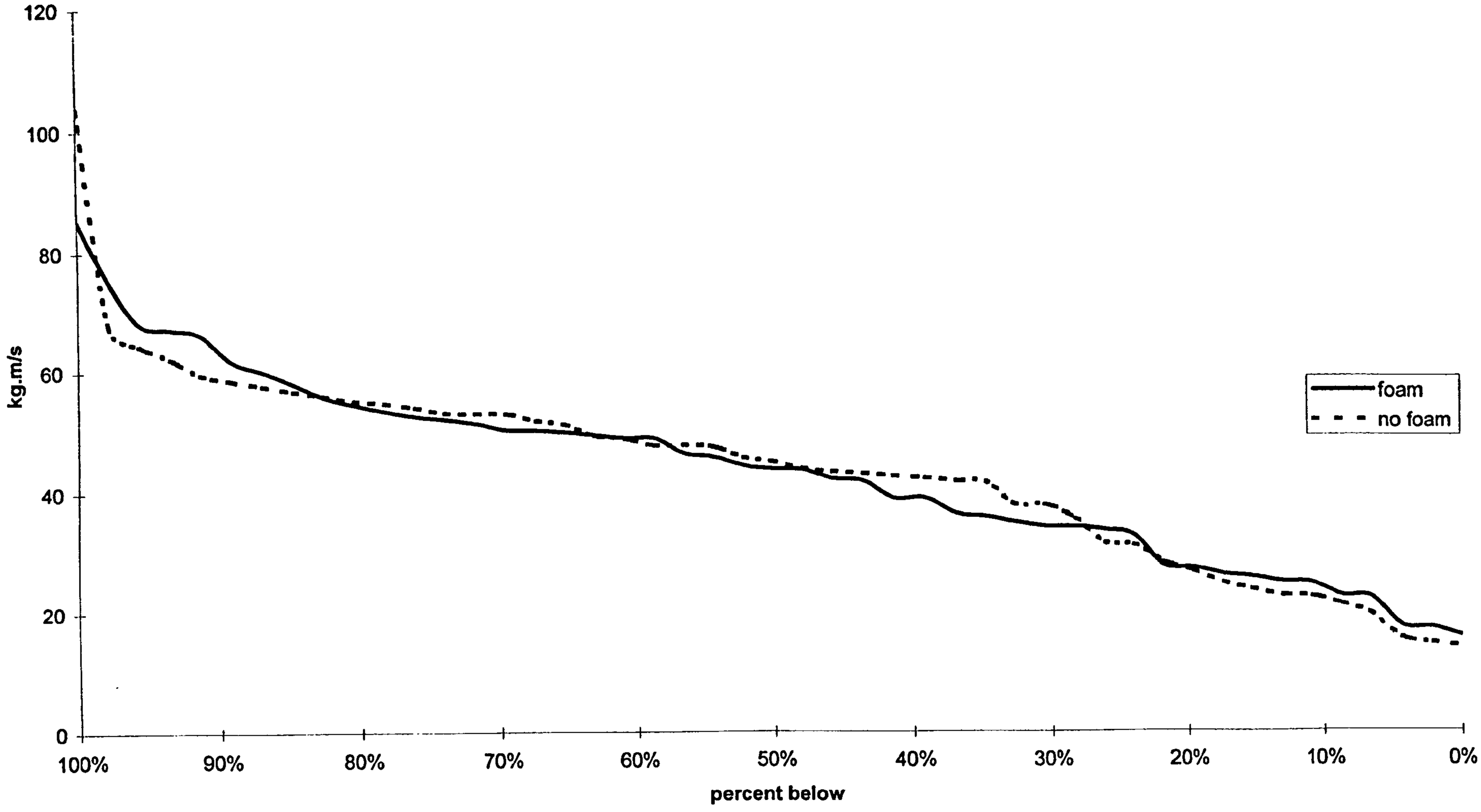

Figure 9.21 Distribution of approach momentum values among volunteer group (total of 47 stabs with foam and 48 without).

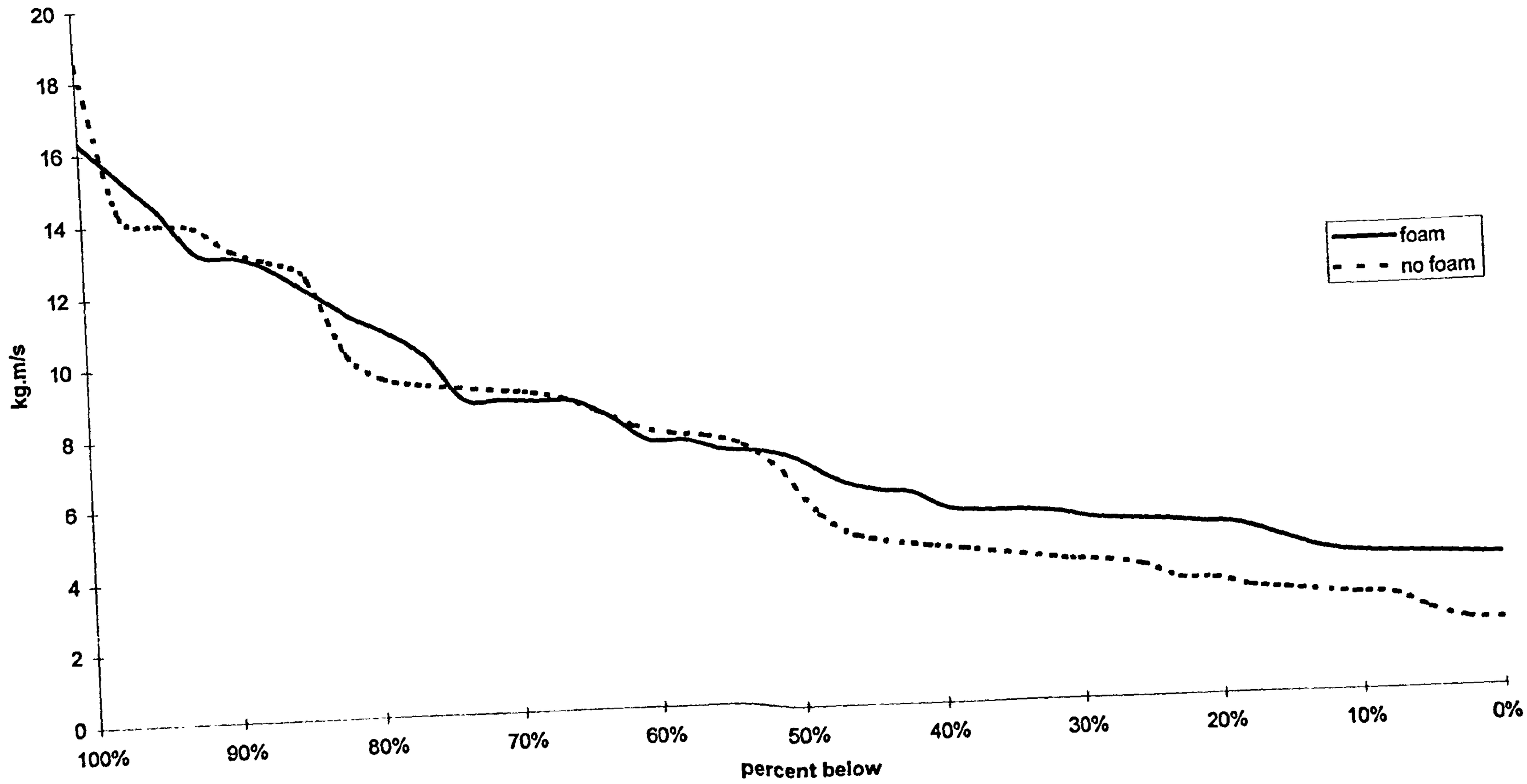

Figure 9.22 Distribution of impulse values among volunteer group (total of 39 stabs with foam and 40 without).

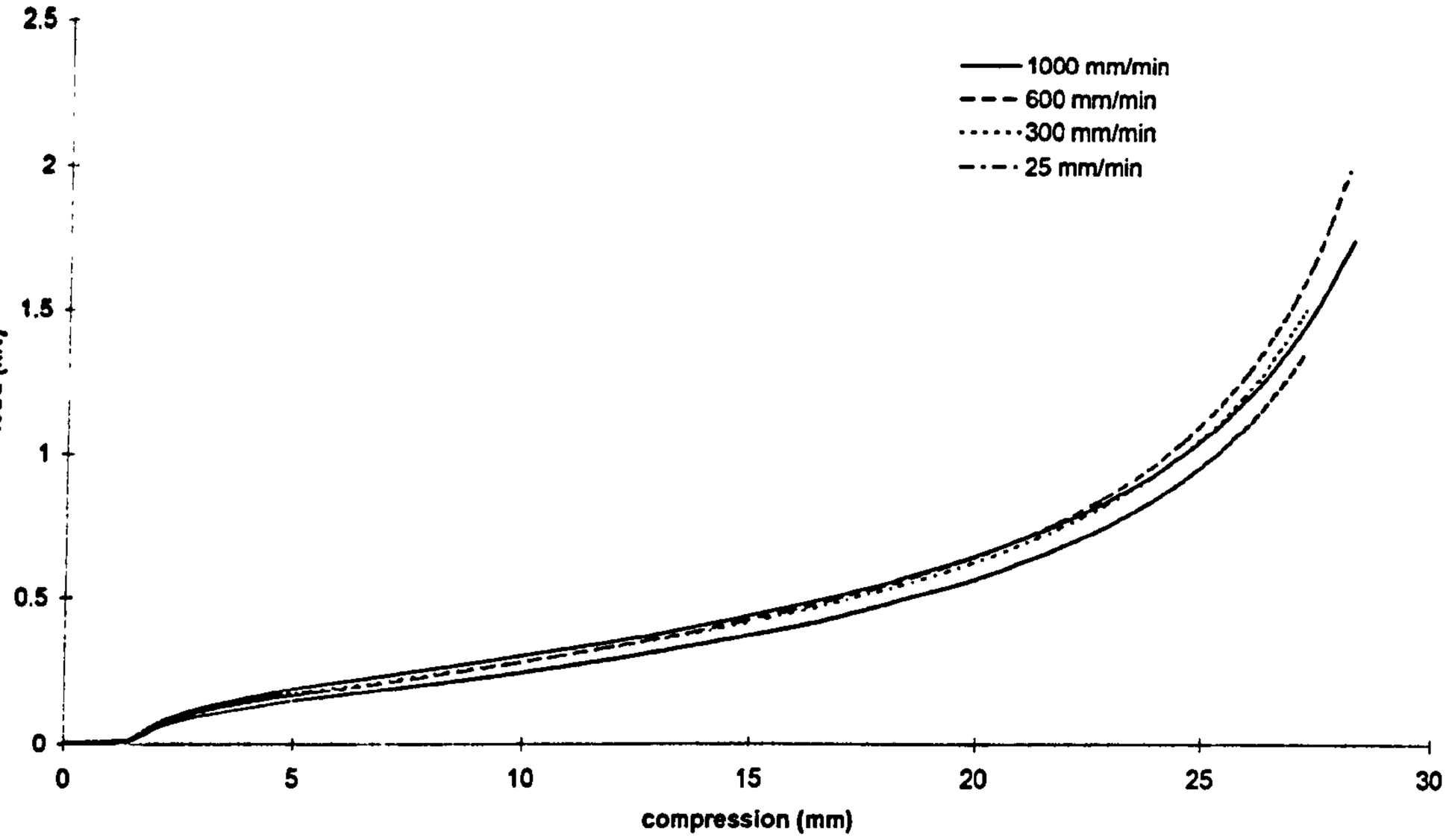

Figure 9.23 Load-displacement curves for the backing foam at different loading rates.

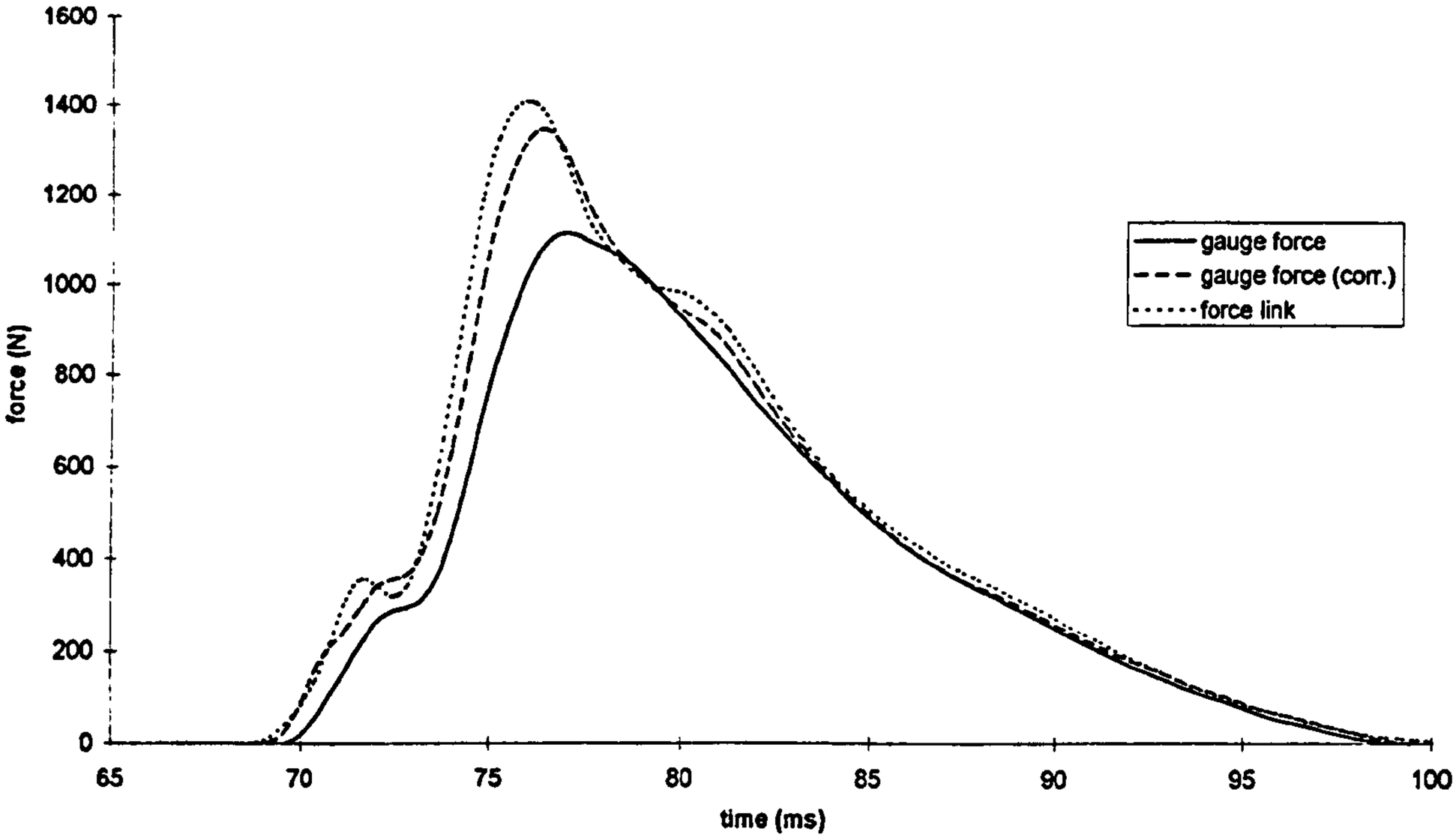

Figure 9.24 Typical force-time profiles found during calibration tests with piezo-electric force link

9.1.4 FOAM CHARACTERISATION

In order to define the mechanical characteristics of the foam used in this study, graphs of load against compression for the foam at different loading rates have been plotted. The tests were carried out using an Instron Materials Testing machine with a plunger of diameter 50mm. An example is shown in Figure 9.23.

The loading rate produced here is approximately 1kN/s (1000 Newtons per second), whereas the maximum loading rate encountered during stab tests was approximately 200kN/s. It is accepted that the loading rates encountered during the stab tests are orders of magnitude higher than those achievable on the Instron machine, but the tests provide reproducible, comparable numbers which can be used by other researchers to compare the properties of the foam.

9.1.5 DYNAMIC CALIBRATION OF KNIFE

Figure 9.24 shows the effect of the addition of the calculated inertial force to that measured at the gauge site. It is evident that this corrected figure gives good agreement with that measured by the separate piezo-electric force link.

9.1.6 LIMITATIONS OF THE METHODOLOGY

Although these values appear to be very high, it must be realised that these values represent the maximum threat the wearer of an anti-stab garment is likely to face, for several reasons:

- the cross-section of volunteers used in the study, although covering a wide range of body types and sizes, was dominated by large, strong police officers trained in the skills of self-defence;

- In the calculation of total energy (and momentum), the energy of the torso was included but it is difficult to say whether all of this energy would be delivered to the target as the joints of the upper limb are not rigid;

- the instrumented knife, having a relatively large handle diameter and a padded hilt, allows for the production of higher forces than may be found with a more typical attack weapon;

- the target was rigidly mounted.

One factor that could work in the opposite direction, however, is the fact that none of the volunteers was in a state of fear, rage or excitement, which could tend to increase physical performance.

Mass (kg)	Impact velocity (m/s)	Energy (J)	Momentum (kg.m/s)	Peak Force* (N)
4.5	5.4	66.2	24.4	2116
4.5	7.0	110.4	31.5	2688
4.5	9.4	198.7	42.3	2979
1.9	5.4	28.0	10.3	869
1.9	7.0	46.6	13.3	1772
1.9	9.4	83.9	17.9	2515
1.0	5.4	14.7	5.4	511
1.0	7.0	24.5	7.0	882
1.0	9.4	44.1	9.4	996

Table 9.6 A summary of the force values measured in drop-tower tests at different levels of energy and momentum.

*Average of three trials

9.2 RESULTS OF DROP TOWER TESTS

Table 9.6 and Figures 9.25 to 9.27 present the results of the drop-tower tests. The combinations of velocity and mass to be used in the tests were chosen to try to replicate the range of values found in volunteer tests.

Although it is possible to replicate the magnitude of the axial force produced in human stab attacks with the drop-tower, the profile of the force-time curve is different. In most cases in the human attack, the force profile has two peaks (Figure 9.14). This may be due to the fact that there is some delay between the knife coming to rest and the soft tissue of the arm coming to rest. In the drop-tower test, there is only one peak (Figure 9.27) and this may be a serious shortcoming in terms of blade penetration. It is also very difficult to introduce cutting and lateral forces together with torque, with a simple drop-tower test.

With the current set-up, it can be seen that while the range of velocities, energies and momenta can be reproduced, it is impossible to match the combination of all three. It is possible to match only two of the three: energy and momentum, energy and velocity or momentum and velocity. This is because in the human stab the energy and momentum measured were made up of several different masses travelling at different velocities whereas the drop-tower has only one mass in motion. Due to the limitations of mass, the momentum values tended to be small compared with those seen in volunteer tests, for a given energy value.

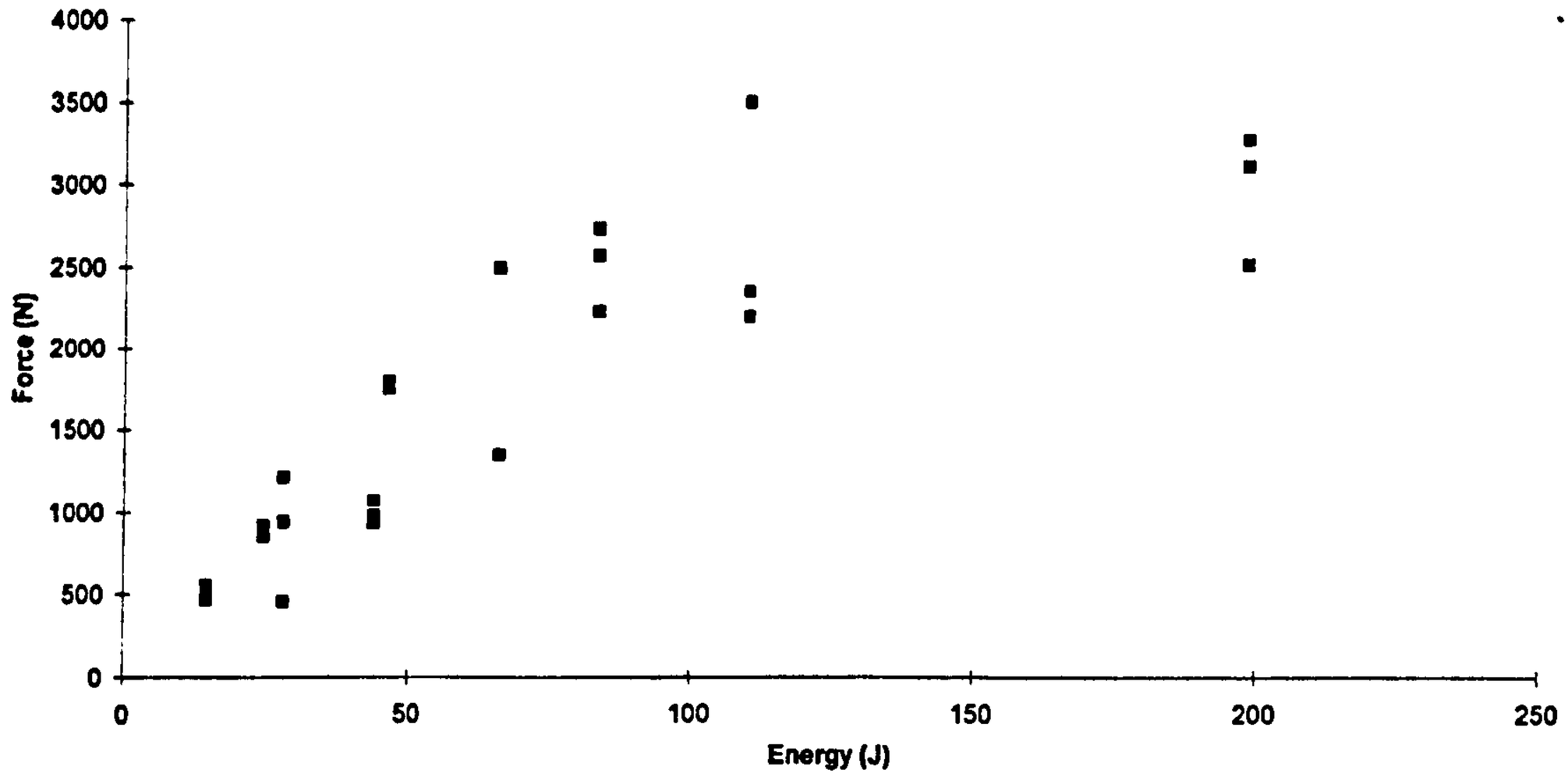

Figure 9.25 The relationship between force and approach energy during drop tower tests.

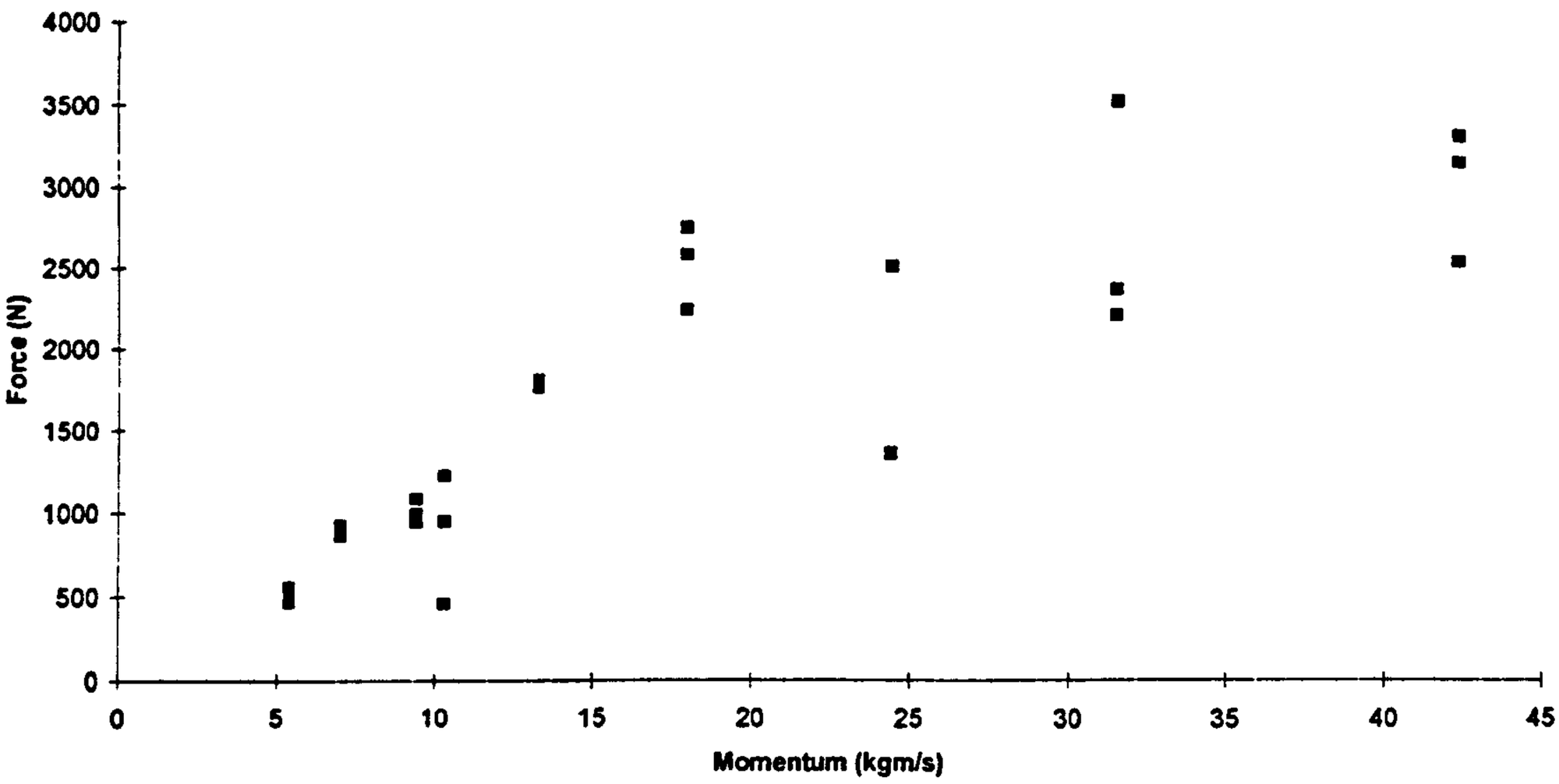

Figure 9.26 The relationship between force and approach momentum during drop tower tests.

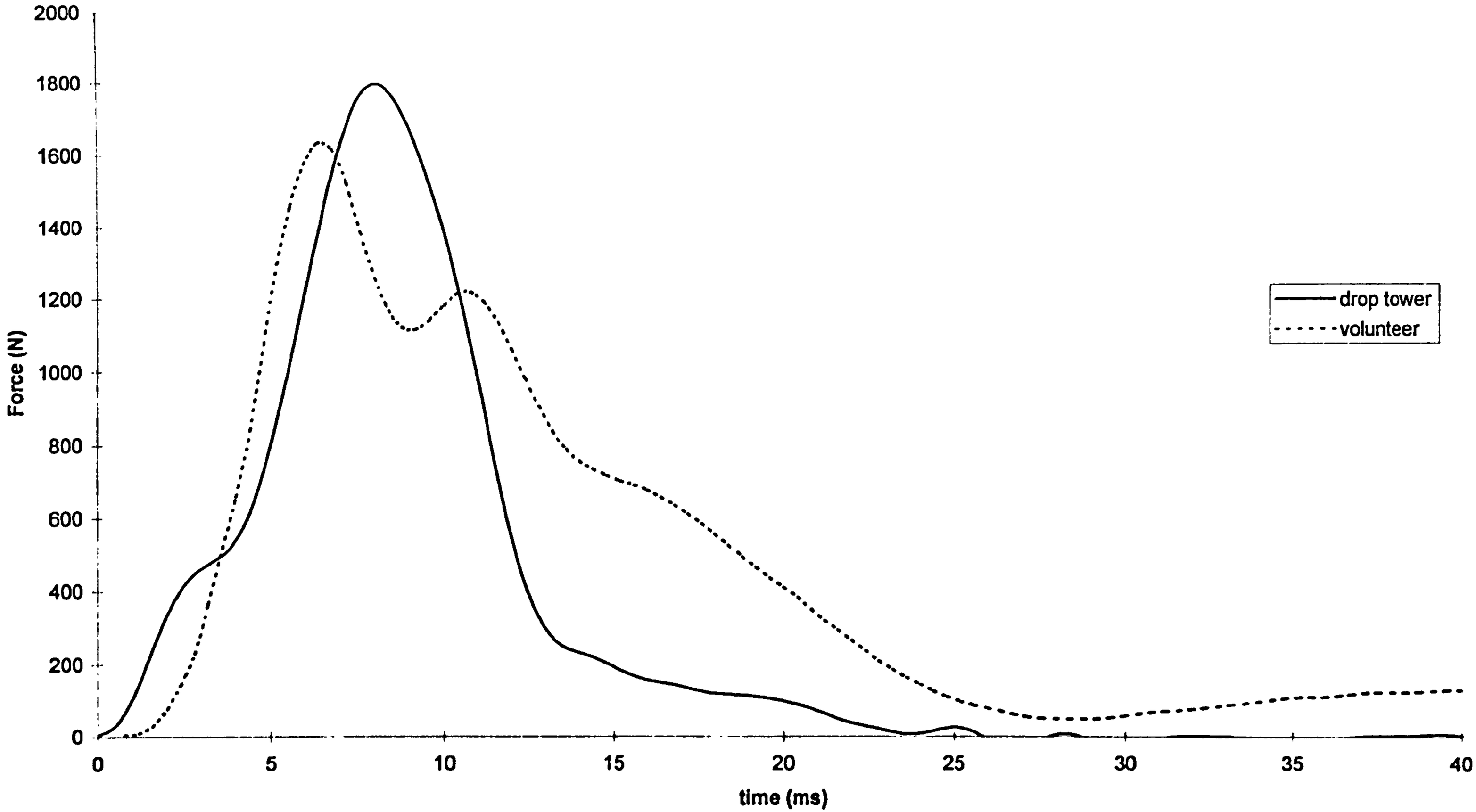

Figure 9.27 Drop tower test - mass 1.9kg, impact velocity 7.0m/s, energy 46.6J, momentum 13.3kg.m/s; Volunteer test - sweep, no foam, 8.6m/s, 56J, 53kg.m/s.

CHAPTER 10 CONCLUSIONS

The following table summarises the key findings from the volunteer stab measurements. The principal aim of the project was to provide such information, which could be used to formulate realistic simulations of human stab attacks for the testing of protective materials. It has also been shown that different combinations of mass and approach velocity in drop tower tests can come very close to simulating the magnitude of some of the parameters contained below. This represents a major step forward towards obtaining a standard method of testing protective materials, which will simulate real life stab attack actions. With the inclusion of work to characterise the high load-rate response of tissue and develop a more realistic backing material (flesh simulant), the author is confident that a fully verified test standard will be realised.

Property	Maximum	95th percentile	Mean	Median
Impact velocity (m/s)	9.2	8.4	5.8	-
Impact energy (J)	103	69	36	-
Impact momentum (kg.m/s)	104	68	40	-
Axial force (N)	2261	1885	-	1091
Cutting force (N)	869	465	-	146
Lateral force (N)	634	343	-	88
Torque (Nm)	9.4	6.6	-	2.6

REFERENCES

Amis, A.A. (1978) Biomechanics of the upper limb and design of an elbow prosthesis. PhD Thesis, University of Leeds.

Amis, A.A., Dowson, D. and Wright, V.(1979) Muscle strengths and musculo-skeletal geometry of the upper limb. *Engineering in Medicine* 8, 1, 41-48.

Amis, A.A., Dowson, D. and Wright, V. (1980a) Elbow joint force predictions for some strenuous isometric actions. *J. Biomechanics* 13, 765-775.

Amis, A.A., Dowson, D. and Wright, V. (1980b) Analysis of elbow forces due to high-speed forearm movements. *J. Biomechanics* 13, 825-831.

Amis, A.A., Miller, J.H., Dowson, D. and Wright, V. (1981) Biomechanical aspects of the elbow: joint forces related to prosthesis design. *Engineering in Medicine* 10, 2, 65-68.

An, K.N., Chao, E. Y. S. and Askew, L. J., (1980). Hand Strength Measurement Instruments. *Archives of Physical Medicine and Rehabilitation* 61, 366-368.

An, K.N., Hui, F.C., Morrey, B.F., Linscheid, R.L. and Chao, E.Y. (1981) Muscles across the elbow joint: a biomechanical analysis. *J. Biomechanics* 14, 10, 659-669.

An, K.N., Kwak, B.M., Chao, E.Y. and Morrey, B.F. (1984) Determination of muscle and joint forces: a new technique to solve the indeterminate problem. *Trans ASME J. Biomechanical Engineering* 106, 364-367.

An, K.N., Kaufman, K.R. and Chao, E.Y.S. (1989) Physiological considerations of muscle force through the elbow joint. *J. Biomechanics* 22, 11/12, 1249-1256.

An, K.N. and Chao, E. Y. S. (1991) Kinematic analysis. In An, K. N., Berger and Cooney, Biomechanics of the wrist joint. Springer-Verlag.

Andrews, J. G. and Youm, Y. (1979) A biomechanical investigation of wrist kinematics. *J. Biomechanics* 12, 83-93.

Atcheson, S. G., Ward, J. R. and Lowe, W. (1998) Concurrent medical disease in work-related carpal tunnel syndrome. *Archives of Internal Medicine* 158, 14, 1506-1512.

Bacis, M., Molinero, G., Cologni, L., Mosconi, G. and Seghizzi, P. (1996) Repetitive movements of the upper limbs: results of exposure assessment and clinical tests among workers sand papering timber products in the Province of Bergamo. *Medicina del Lavoro* 87, 6, 613-624.

Barbenel, J.C. (1972) The biomechanics of the temporomandibular joint: a theoretical study. *J. Biomechanics* 5, 251-256.

Barker, K.L. (1995) Repetitive strain injury. A review of the legal issues. *Physiotherapy* 81, 2, 1031-06.

Basmajian, J.V. and De Luca, C.J. (1985) Muscles alive – their functions revealed by EMG. 5th ed. Williams and Wilkins, Baltimore.

Bean, J.C., Chaffin, D.B. and Schultz, A.B. (1988) Biomechanical model calculation of muscle contraction forces: a double linear programming method. *J. Biomechanics* 21, 1, 59-66.

Bleetman, A., Perry, C. H., Crawford, R. and Swann, I.J. (1997) Effect of Strathclyde Police initiative 'Operation Blade' on accident and emergency attendances due to assault. *J. Accident and Emergency Medicine* 14, 3, 153-6.

Brand, P.W., Hollister, A. (1993) Clinical mechanics of the hand. Mosby Year Book, St. Louis.

Braus, H. (1954) Anatomie Des Menschen, Springer, Berlin.

Brooks, P. (1993) Repetitive strain injury. *BMJ* 307, 1298.

Brumbaugh, R.B., Crowninshield, R. D., Blair, W. F. and Andrews, J. G. (1982) An in-vivo study of normal wrist kinematics. *Trans ASME J. Biomech. Eng.* 104, 176-181.

Buchanan, T.S., Moniz, M.J., Dewald, J.P.A. and Rymer, W.Z. (1993) Estimation of muscle forces about the wrist joint during isometric tasks using an EMG coefficient method. *J. Biomechanics* 26, 4/5, 547-560.

Buchanan, T.S. and Shreeve, D. A. (1996) An evaluation of optimisation techniques for the prediction of muscle activation patterns during isometric tasks. Trans ASME J. Biomechanical Eng. 118, 565-574.

Buchanan, T.S. (1996) Personal communication.

Calvano, N. J. (1993) A study to determine the most important parameters for evaluating the resistance of soft body armour to penetration by edged weapons. Report no. NISTIR 4895. National Institute of Justice, Washington, DC 20531.

Cappozzo, A., Catani, F., Della Croce, U., and Leardini, A. (1995) Position and orientation in space of bones during movement: Anatomical frame definition and determination. *Clinical Biomechanics* 10, 4, 171-178.

Chadwick, E.K.J., McCormack, B., Nicol, A.C., Peterson, B. and Waide, V. (1996) Elbow joint standardisation proposal. ISB Standardisation Committee. Internet address: http://isb.ri.ccf.org//standards/elbow.html.

Chao, E.Y.S. and Morrey, B.F. (1978) Three-dimensional rotation of the elbow. *J. Biomechanics* 11, 57-73.

Cholewicki, J. and McGill, S.M. (1994) EMG assisted optimisation: a hybrid approach for estimating muscle forces in an indeterminate biomechanical model. *J. Biomechanics* 27, 10, 1287-1289.

Cole, G.K., Nigg, B.M., Ronsky, J.L. and Yeadon, M.R. (1993) Application of the joint co-ordinate system to three-dimensional joint attitude and movement representation: a standardisation proposal. *Trans. ASME J. Biomechanical Eng.* 115, 344-349.

Cross, M. (1996) Taking arms against the knife. *New Scientist* 9 March 1996, 31-33.

Crowninshield, R.D. and Brand, R.A. (1981) A physiologically based criterion of muscle force prediction in locomotion. *J. Biomechanics* 14, 11, 793-801.

Davy, D.T. and Audu, M.L. (1987) A dynamic optimisation technique for predicting muscle forces in the swing phase of gait. *J. Biomechanics* 20, 2, 187-201.

Drillis, R. and Contini, R. (1966) Body segment parameters. PB 174 945: Technical report 1166.03. New York: School of Engineering and Science, New York University.

Dul, J. (1986) The biomechanical prediction of muscle forces. *Clinical Biomechanics* 1, 1, 27-28.

Ejeskär, A. and Örtengren, R., 1981. Isolated finger flexion force - A methodological study. *The Hand* 13, 3, 223-229.

Finch, C.A. (1985) Estimation of body segment parameters of college age females using a mathematical model. (Thesis) Windsor: University of Windsor.

Fitzsimmons, A. (1995) Hip joint forces in hip replacement patients and normal subjects during activities of daily living. PhD Thesis, University of Strathclyde.

Fuss, F.K. (1991) The ulnar collateral ligament of the human elbow joint. Anatomy, function and biomechanics. *J. Anatomy* 175, 203-212.

Gerbeaux, M., Turpin, E. and Lensel-Corbeil, G. (1996) Musculo-articular modelling of the triceps brachii. *J. Biomechanics* 29, 2, 171-180.

Gonzalez, R.V., Hutchins, E.L., Barr, R.E. and Abraham, L.D. (1996) Development and evaluation of a musculoskeletal model of the elbow joint complex. *Trans ASME J. Biomech. Eng.* 118, 32-40.

Grood, E.S. and Suntay, W.J. (1983) A joint co-ordinate system for the clinical description of three-dimensional motions: applications to the knee. *J. Biomechanical Engineering* 105, 136-144.

Halls, A.A. and Travill, A. (1964) Transmission of pressures across the elbow joint. *Anatomical Record* 150, 243-248.

Hocking, M.A. (1989) Assaults in south east London. *J. Royal Society of Medicine.* 82, 5, 281-284.

Horii, E., An, K.N. and Linscheid, R.L. (1993) Excursion of prime wrist tendons. *J. Hand Surgery* 18 A, 1, 83-90.

Hunter, J.M., Mackin, E.J., Callahan, A.D. (1995) Rehabilitation of the hand: surgery and therapy. Mosby-Year Book, Inc., Missouri.4th edition.

Ireland, D.C.R. (1998) Australian repetition strain injury phenomenon. *Clinical Orthopaedics and Related Research* 351, 63-73.

Jackson, W.T., Hefzy, M.S. and Huqing Guo (1994) Determination of wrist kinematics using a magnetic tracking device. *Medical Engineering and Physics* 16, 123-133.

Jones, S., Nokes, L. and Leadbeatter, S. (1994) The mechanics of stab wounding. *Forensic Science International* 67, 59-63.

Kaufman, K.R., An, K.N., Litchy, W.J. and Chao, E.Y.S. (1991) Physiological prediction of muscle forces. 1. Theoretical formulation. *Neuroscience* 40, 3, 781-792.

Ketchum, L.D., Brand, P.W., Thompson, D. and Pocock, G.S. (1978) The determination of moments for the extension of the wrist generated by muscles of the forearm. *J. Hand Surgery* 3A, 3, 205-210.

Knight, B. (1975) The dynamics of stab wounds. *Forensic Science* 6, 249-255.

Koolstra, J.H., Van Eijden, T.M.G. and Weijs, W.A. (1988) An iterative procedure to estimate muscle lines of action in vivo. *J. Biomechanics* 22, 8/9, 911-920.

Lane, J.V. (1996) Calibration of knife transducer. Internal report, Bioengineering Unit, University of Strathclyde.

Lee, J.W. and Rim, K., (1991). Measurement of finger joint angles and maximum finger forces during cylinder grip activity. Journal of Biomedical Engineering 13, 152-161.

Lockhart, R.D., Hamilton, G.F. and Fyfe F.W. (1959) Anatomy of the human body. Faber and Faber Limited, London.

London, J.T. (1981) Kinematics of the elbow. *J. Bone and Joint Surgery* 63 A, 4, 529-535.

Lucchetti, L. (1995) Kinematics of the upper limb. Report for EC CAMARN project, University of Strathclyde.

Melhorn, J.M. (1998) Cumulative trauma disorders and repetitive strain injuries: the future. *Clinical Orthopaedics and Related Research* 351, 107-126.

Moore, J.A., Ellis, R.E., Pichora, D.R. and Hollister, A.M. (1993) A kinematic technique for describing wrist joint motion: analysis of configuration space plots. *Proceedings of the Institute of Mechanical Engineers* 207, 211-218.

Morrey, B.F., An, K.N. and Stormont, M.D. (1988) Force transmission through the radial head. *J. Bone and Joint Surgery* 70-A, 2, 250-256.

Morrey, B.F., Chao, E.Y., and Hui, F.C. (1979) Biomechanical study of the elbow following excision of the radial head. *J. Bone and Joint Surgery* 61A, 1, 63-68.

Morrey, B.F. (1993) The Elbow and its Disorders. W. B. Saunders Company, Philadelphia.

Murray, W.M., Delp, S.L. and Buchanan, T.S. (1995) Variation of muscle moment arm with elbow and forearm position. *J. Biomechanics* 28, 5, 513-525.

Nicol, A.C. (1977) Elbow joint prosthesis design: biomechanical aspects. PhD Thesis, University of Strathclyde.

Occhipinti, E. and Colombini, D. (1996) Musculo-skeletal disorders of the upper limbs due to mechanical overload: methods and criteria for the description and assessment of occupational overexposure. *Medicina del Lavoro* 87, 6, 491-525.

O'Driscoll, S. W., Bell, D. F. and Morrey, B. F. (1991) Posterolateral rotatory instability of the elbow. *J. Bone and Joint Surgery* 73A, 3, 440.

Pandy, M. G., Anderson, F. C. and Hull, D. G. (1992) A parameter optimisation approach for the optimal control of large-scale musculoskeletal systems. *Trans ASME J. Biomechanical Eng.* 114, 114-460.

Pearsall, D.J. and Reid, J.G. (1994) The study of human body segment parameters in biomechanics. An historical review and current status report. *Sports Medicine* 18, 2, 126-140.

Pigeon, P., Yahia, L'H. and Feldman A.G. (1996) Moment arms and lengths of human upper limb muscles as functions of joint angles. *J. Biomechanics* 29, 10, 1365-1370.

Press, W.H., Teukolsky, S.A., Vetterling, W.T. and Flannery, B.P. (1992) Numerical recipes in C. 2nd ed. Cambridge University Press.

Pronk, C.N.A. and Niesing, R., 1981. Measuring hand-grip force, using a new application of strain gauges. Medical & Biological Engineering & Computing 19, 127-128.

Quintner, J. (1991) The RSI syndrome in historical perspective. *International Disability Studies* 13, 99-104.

Raschke, U., Martin, B.J. and Chaffin, D.B. (1996) Distributed moment histogram: a neurophysiology based method of agonist and antagonist trunk muscle activity prediction. *J. Biomechanics* 29, 12, 1587-1596.

Regan, W.D., Korinek, S.L., Morrey, B.F. and An, K.N. (1989) Biomechanical study of ligaments around the elbow joint. *Clinical Orthopaedics and Related Research*, 271, 170-179.

Richards, L. and Palmiter-Thomas, P., (1996). Grip Strength Measurement: A Critical Review of Tools, Methods and Clinical Utility. *Critical Reviews in Physical and Rehabilitation Medicine* 8, 1/2, 87-109.

Rugg, S.G., Gregor, R.J., Mandelbaum, B.R. and Chiu, L. (1990) In Vivo moment arm calculations at the ankle using magnetic resonance imaging (MRI). *J. Biomechanics* 23, 5, 495-501.

Runciman, R.J. (1993) Biomechanical model of the shoulder joint. PhD Thesis, University of Strathclyde.

Sarrafian, S.K., Melamed, J.L. and Goshgarian, G.M. (1977) Study of wrist motion in flexion and extension. *Clinical Orthopaedics and Related Research* 126, 153-159.

Savelberg, H.H.C.M., Kooloos, J.G.M., Huiskes, R. and Kauer, J.M.G. (1993) An indirect method to assess wrist ligament forces with particular regard to the effect of preconditioning. *J. Biomechanics* 26, 11, 1347-1351.

Schuind, F., Garcia-Elias, M., Cooney, W.P.III., and An, K.N. (1992) Flexor tendon forces: In vivo measurements. *J. Hand Surgery* 17A, 2, 291-298.

Seireg, A. and Arvikar, R. (1989) Modeling of the musculoskeletal system for the upper and lower extremities. In Biomechanical analysis of the musculoskeletal structure for medicine and sports. Hemisphere Publishing Corporation, New York.

Sennwald, G. (1987) The Wrist. Springer-Verlag.

Shiba, R., Sorbie, C., Siu, D.W., Bryant, J.T., Cooke, D.V. and Wevers, H.W. (1988) Geometry of the humero-ulnar joint. *J. Orthopaedic Research* 6, 897-906.

Sjogaard, G. and Sjogaard, K. (1998) Muscle injury in repetitive motion disorders. *Clinical Orthopaedics and Related Research* 351, 21-31.

Swanson, A.B., Matev, I.B. and de Groot, G., (1970). The Strength of the Hand. *Bulletin of Prosthetics Research*, Fall 1970, 145-152.

Taleisnik, J. (1976) The ligaments of the wrist. *J. Hand Surgery* 1, 2, 110-118.

Tsirakos, D., Baltzopoulos, V. and Bartlett, R. (1997) Inverse optimisation: functional and physiological considerations related to the force-sharing problem. *Critical Reviews in Biomedical Engineering* 25, 4/5, 371-407.

Viegas, S.F., Patterson, R.M., Peterson, P., Roefs, J., Tencer, A., Choi, S. (1989) The effects of various load paths and different loads on the load transfer characteristics of the wrist. *J. Hand Surgery* 14A, 3, 458-465.

Viegas, S.F., Patterson, R.M., Todd, P.D. and McCarty, P. (1993) Load mechanics of the mid-carpal joint. *J. Hand Surgery* 18A, 1, 14-18.

Volz, R.G., Lieb, M. and Benjamin, J. (1980) Biomechanics of the wrist. *Clinical Orthopaedics and Related Research* 149, 112-117.

Wheeless, C.R. (1996) Wheeless textbook of orthopaedics. Internet address: http://www.worldortho.com/wheeless/med.htm.

Winters, J.M. and Kleweno, D.G. (1993) Effect of initial alignment on muscle contributions to isometric strength curves. *J. Biomechanics* 26, 143-153.

Wismans, J.A.C. (1980) A three-dimensional mathematical model of the human knee joint. Thesis (Doctoral) Technische Hogeschool, Eindhoven.

Wright, J., Kariya, A. (1997) Assault patients attending a Scottish accident and emergency department. *J. Royal Society of Medicine.* 90, 6, 322-326.

Yeo, B.P. (1976) Investigations concerning the principal of minimum total muscular force. *J. Biomechanics* 9, 413-416.

Youm, Y., McMurtry, R.Y., Flatt, A.E. and Gillespie, T.E. (1978) Kinematics of the wrist. 1. An experimental study of radial-ulnar deviation and flexion-extension. *J. Bone and Joint Surgery* 60 A, 4, 423-431.

Youm, Y. and Flatt, A.E. (1980) Kinematics of the wrist. *Clinical Orthopaedics and Related Research* 149, 21-32.

Young, J.W., Chandler, R.F., Snow, C.C. (1983) Anthropometric and mass distribution characteristics of the adult female. Technical report. Oklahoma City: FAA Civil Aeromedical Institute.

Young, W.C., (1989) Roark's Formulas for Stress and Strain. 6th edition. McGraw-Hill, New York.

Zatsiorsky, V.M. and Seluyanov, V.N. (1983) The mass and inertia characteristics of the main segments of the human body. In Matsui, H. and Kobayashi, K. (eds.), *Biomechanics VIII-B*, 1152-1159. Champaign: Human Kinetics Publishers.

APPENDIX A

This appendix contains detail and assembly drawings for the manufacture of the grip force transducer.

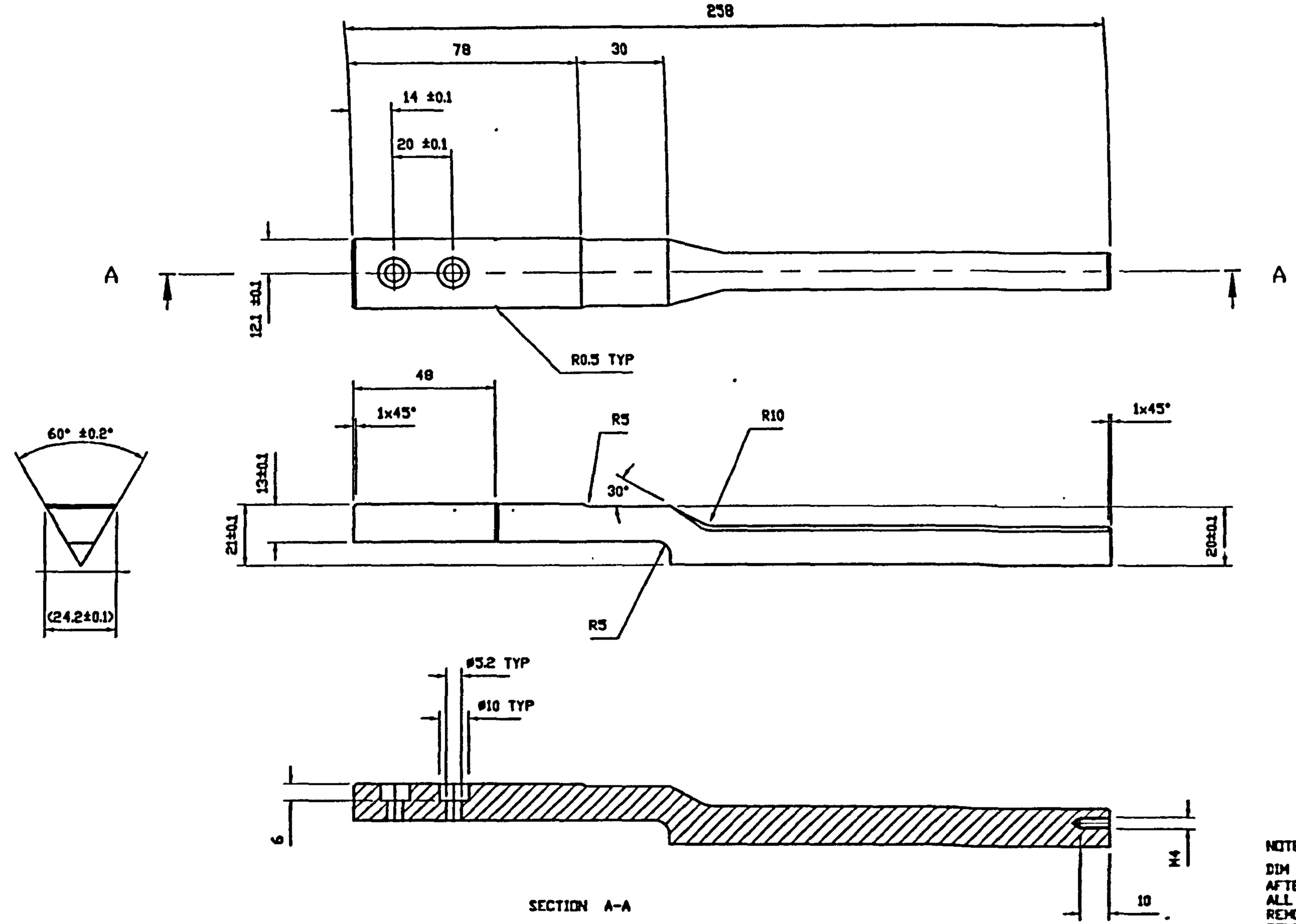

NOTES :

DIM MARKED THUS ≡ TO BE ACHIEVED AFTER ASSEMBLY.
ALL DIMS IN MM.
REMOVE ALL BURRS AND SHARP EDGES.
TOLERANCE : LINEAR ±0.25
ANGLES ±2°
UNLESS STATED.

25 / 01 / 95	MAT'L : STAINLESS STEEL 304	TRANSDUCER ARM	E.K.J. CHADWICK
	QUANTITY : 6 OFF	SCALE : NOT TO SCALE	DRG NO. 1

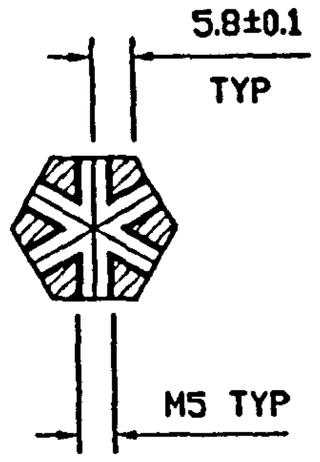

SECTION B-B

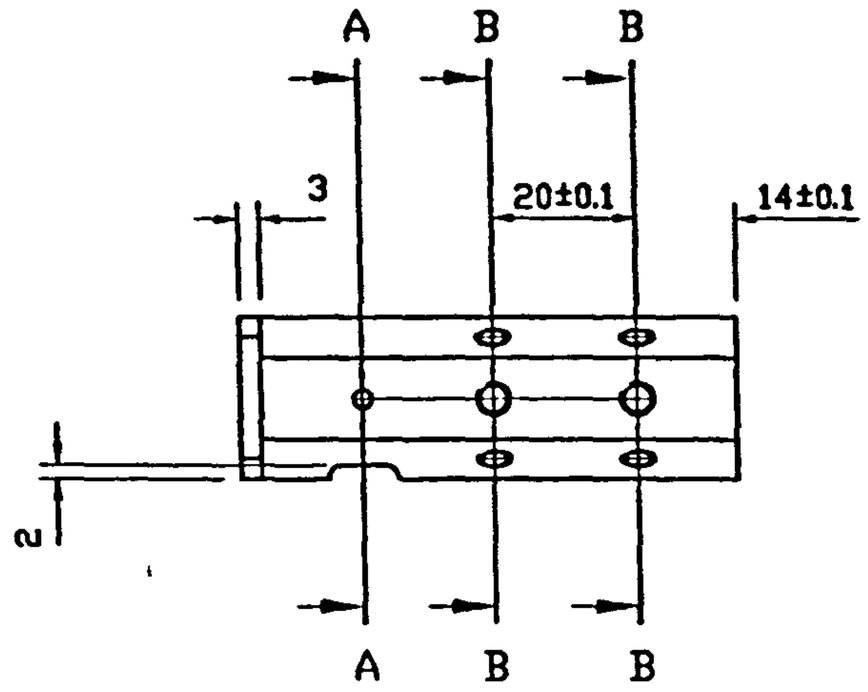

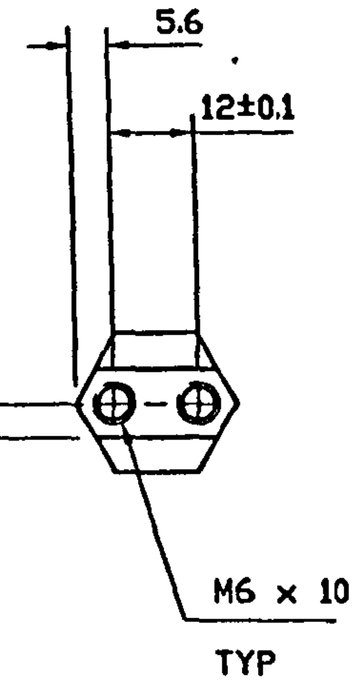

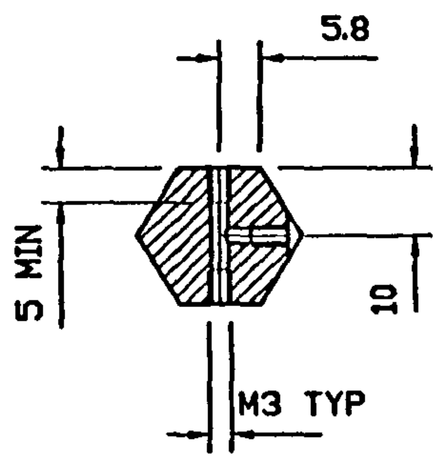

SECTION A-A

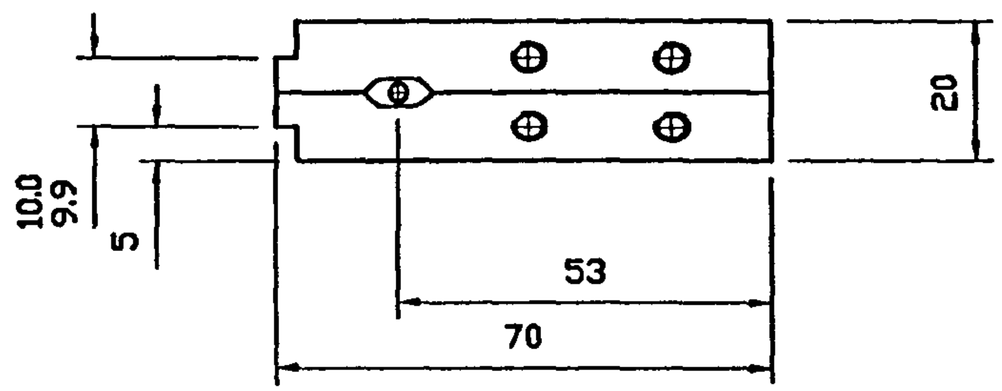

ALL DIMS IN MM.
REMOVE ALL BURRS AND SHARP EDGES.
TOLERANCE : LINEAR ±0.25
ANGULAR ±2°
UNLESS STATED.

25 / 01 / 95	MAT'L : STAINLESS STEEL 304	TRANSDUCER CORE	E.K.J. CHADWICK
	QUANTITY : 1 OFF	SCALE : 1 : 1.5 APPROX.	DRG NO. 2

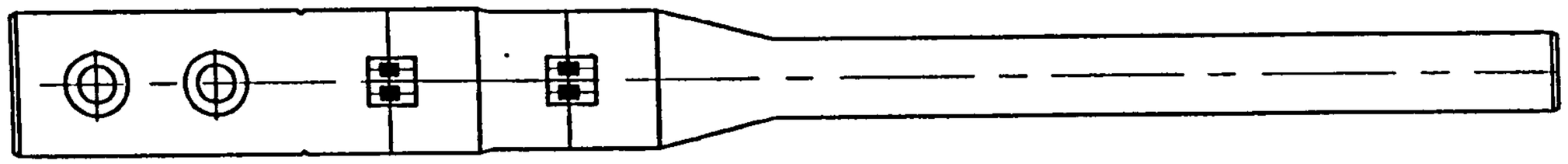

TOP VIEW

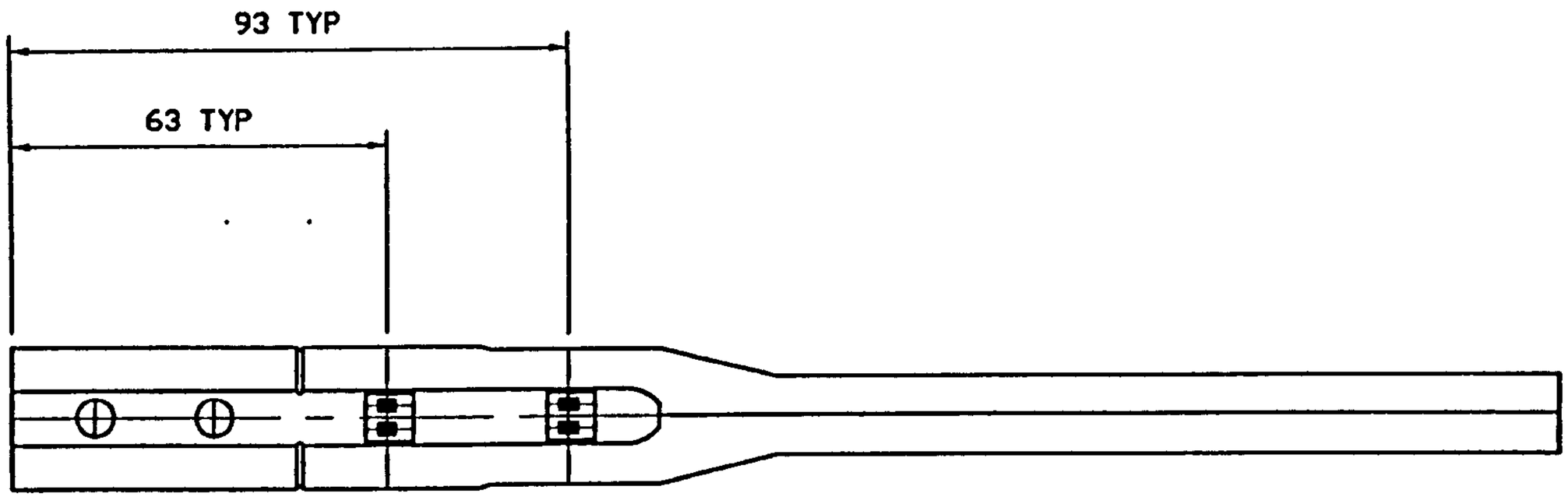

BOTTOM VIEW

25 / 01 / 95	MAT'L :	GAUGEING DIAGRAM	E.K.J. CHADWICK
	QUANTITY : 6 OFF	SCALE :	DRG NO. 5

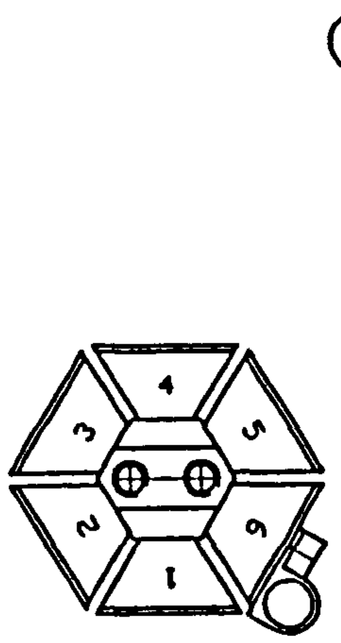

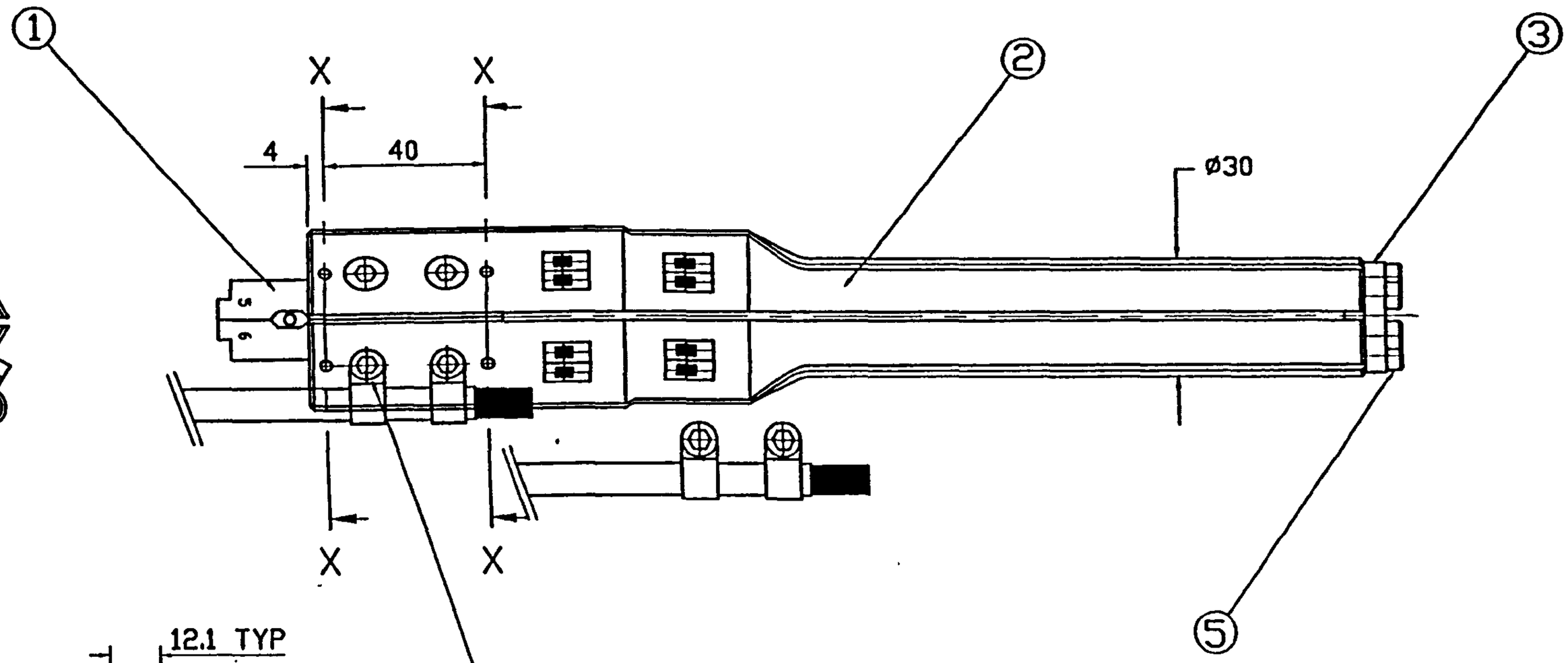

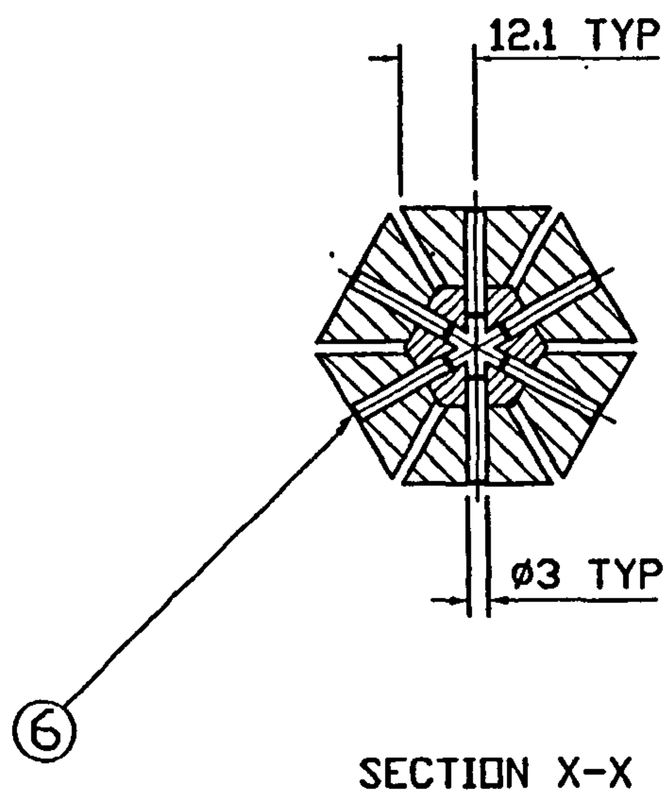

SECTION X-X

NOTES :
ALL DIMS IN MM.
REMOVE ALL BURRS AND SHARP EDGES.
TOLERANCE : ± 0.25.
STAMP I.D. NUMBERS WHERE SHOWN.

ITEM NO.	DESCRIPTION	DRG NO.	QTY
7	LOCTITE 242 OR SIMILAR	/	A/R
6	DOWEL PINS, ø3 X 20 LONG	/	12
5	SOCKET CAP HEAD SCREW, M4 X 12 LONG	/	6
4	SOCKET CAP HEAD SCREW, M5 X 12 LONG	/	12
3	END PLATE	3	1
2	TRANSDUCER ARM	1	6
1	TRANSDUCER CORE	2	1

03 / 02 / 95	MAT'L :	TRANSDUCER SUB-ASSEMBLY	E.K.J. CHADWICK
	QUANTITY :	SCALE :	DRG NO. 4

APPENDIX B

Figures B1 to B6 show the results of the linear regression analysis performed on the calibration data for the grip force transducer.

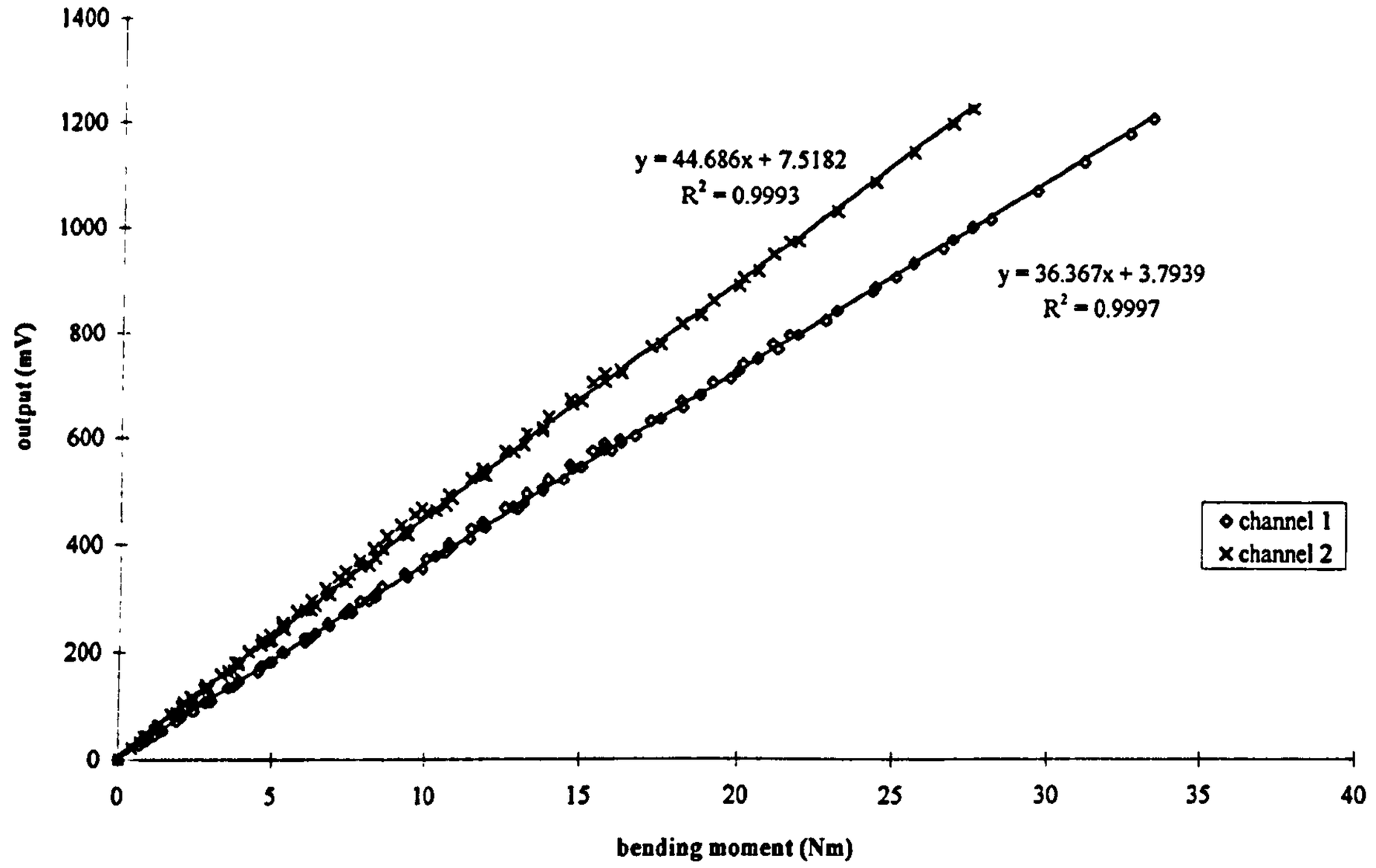

Figure B1 Results of calibration of beam 1.

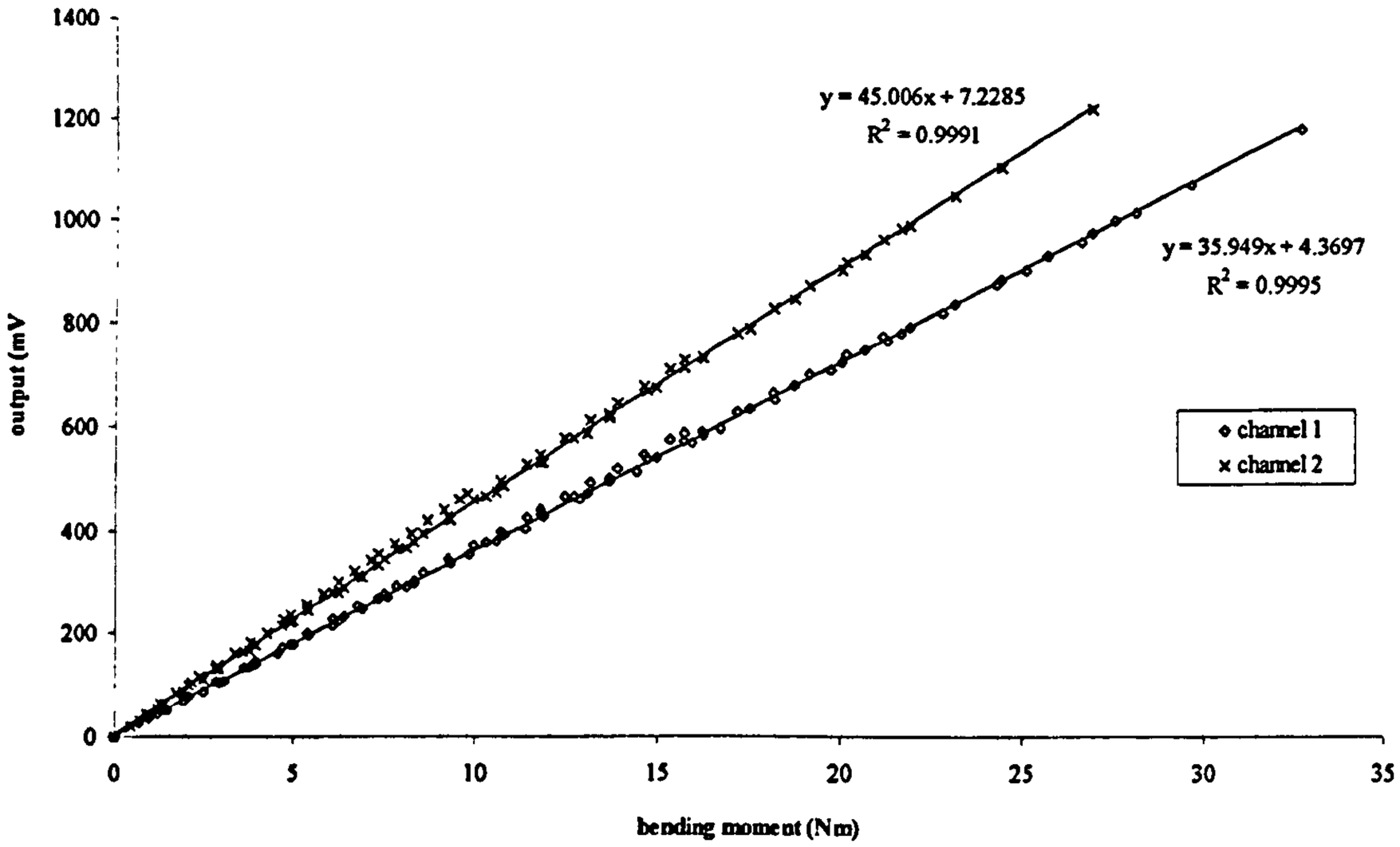

Figure B2 Results of calibration of beam 2.

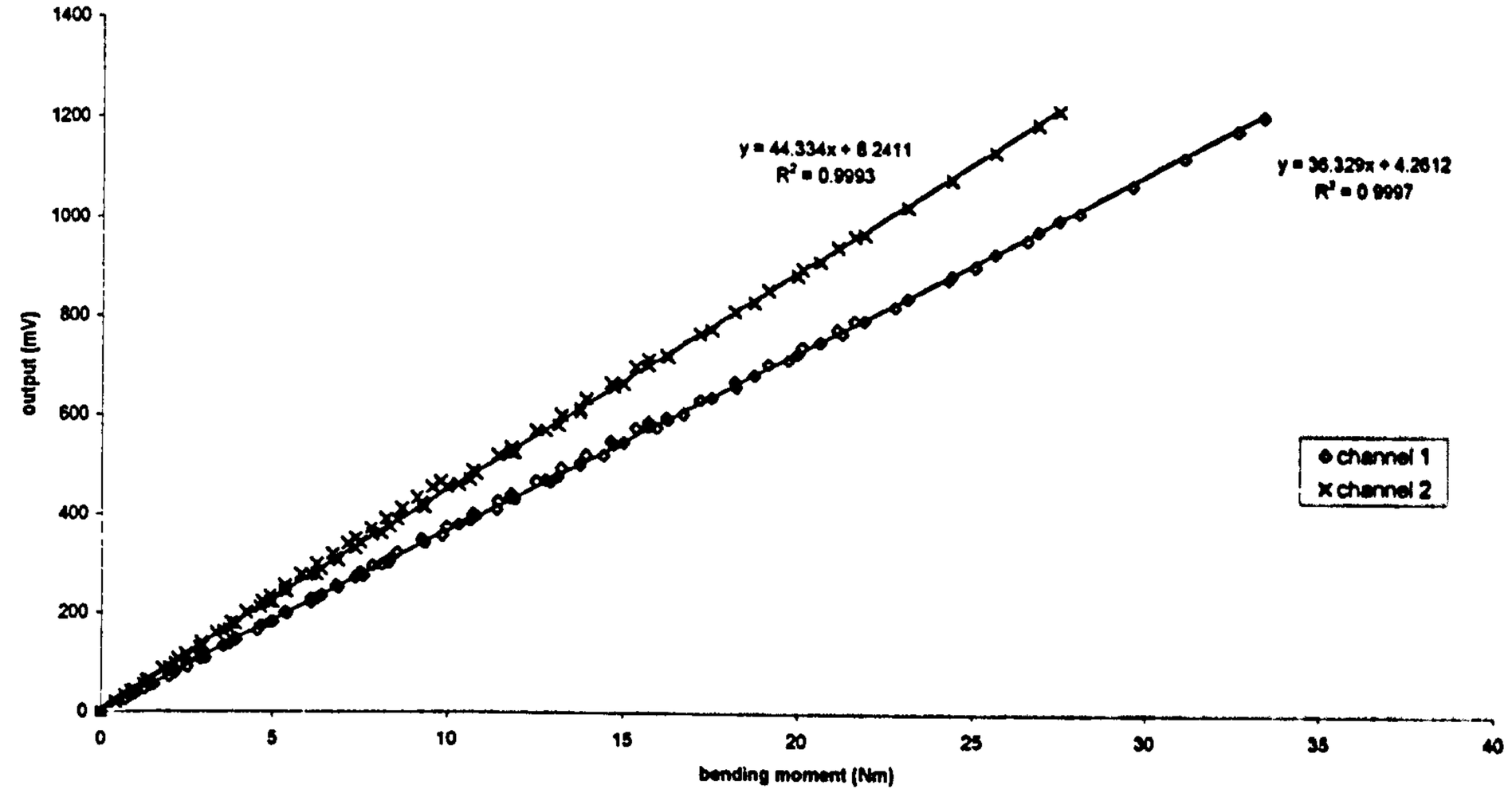

Figure B3 Results of calibration of beam 3.

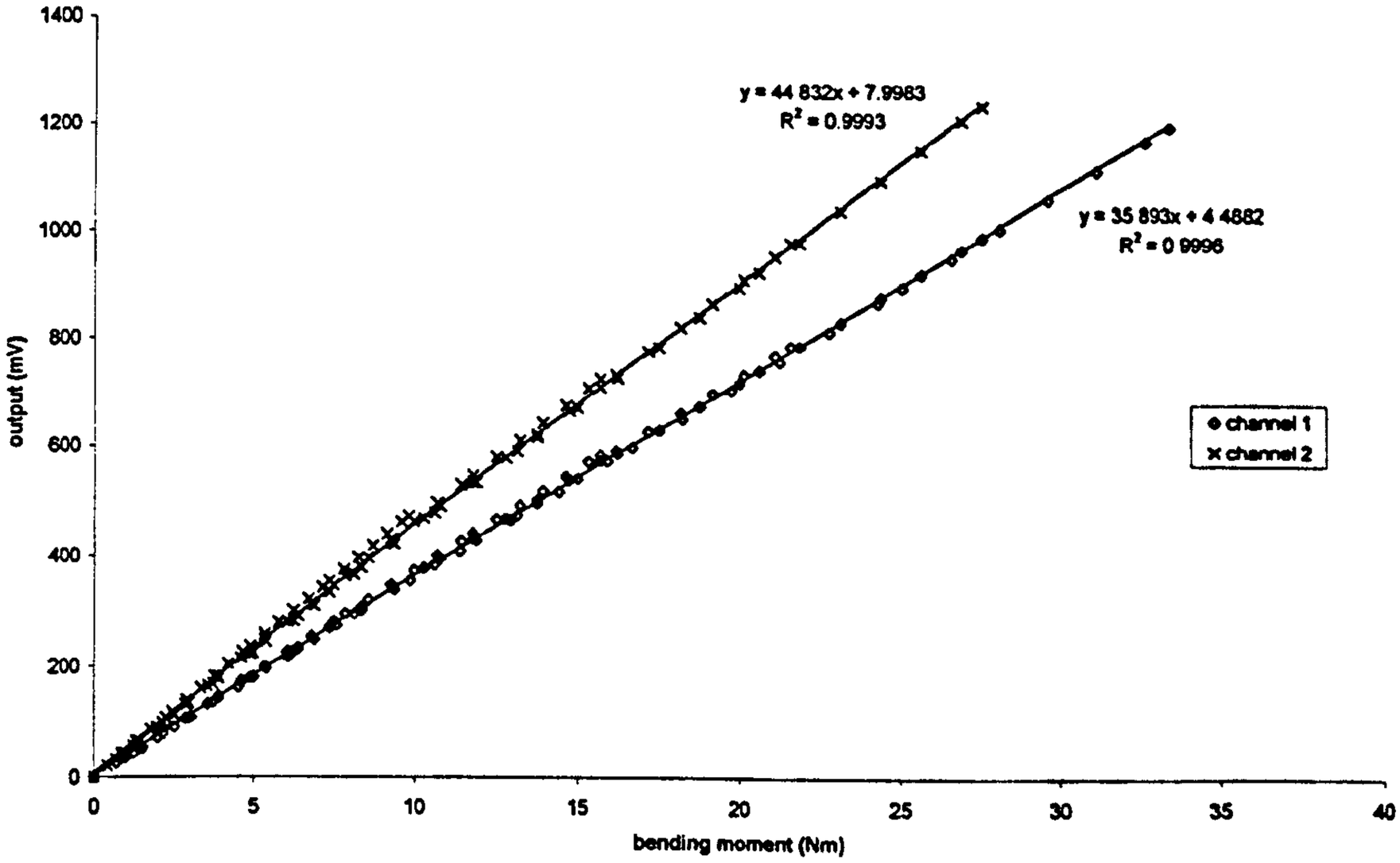

Figure B4 Results of calibration of beam 4.

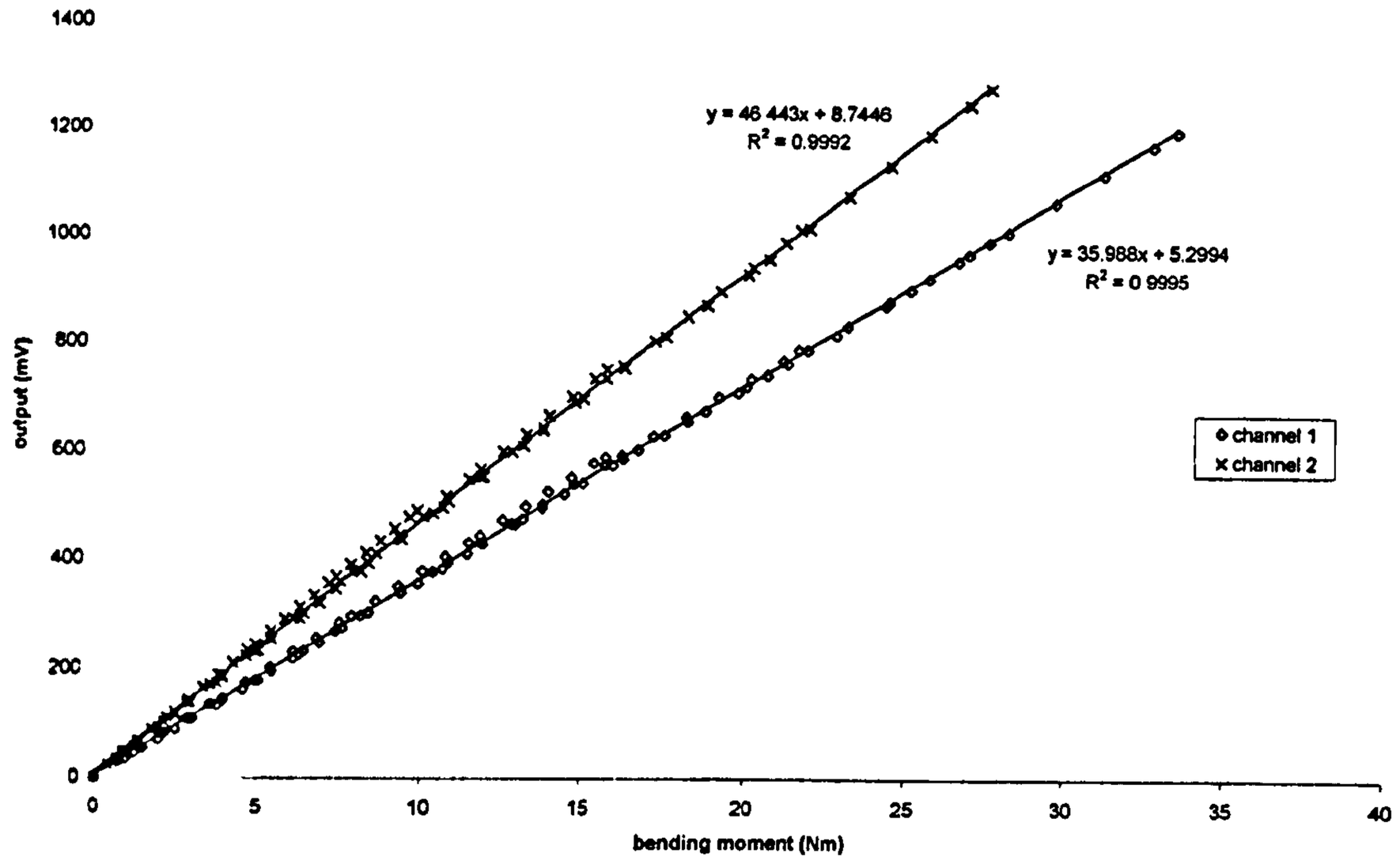

Figure B5 Results of calibration of beam 5.

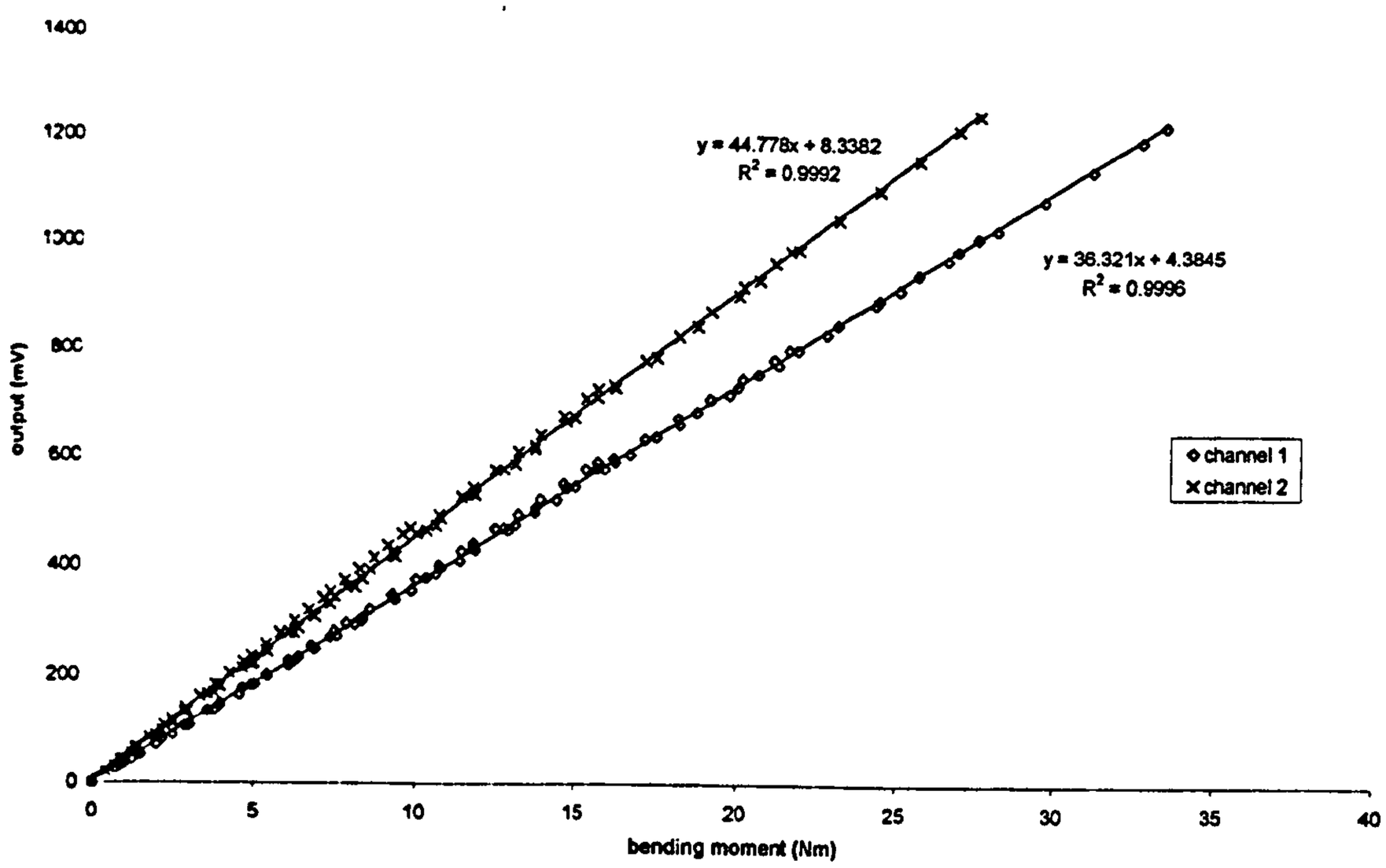

Figure B6 Results of calibration of beam 6.

APPENDIX C EXTERNAL FORCES AND MOMENTS

The following tables present the external force and moment data obtained during the grip study. The following abbreviations are used in the tables:

Fxe, Fye, Fze	Forces acting on the elbow in the ulnar axis system
Fxw, Fyw, Fzw	Forces acting on the wrist in the radial axis system
Mxe, Mye, Mze	Moments acting on the elbow in the ulnar axis system
Mxw, Myw, Mzw	Moments acting on the wrist in the radial axis system
MCP1	Moments tending to extend the thumb MCP joint
MCP2	Moments tending to extend the index finger MCP joint
MCP3	Moments tending to extend the middle finger MCP joint
MCP4	Moments tending to extend the ring finger MCP joint
MCP5	Moments tending to extend the little finger MCP joint
F1, 2, 3, 4, 5, 6	Forces measured on the grip transducer beams

trial	Mxe	Mye	Mze	Mxw	Myw	Mzw	Fxe	Fye	Fze	Fxw	Fyw	Fzw
1524	5.11	1.21	-8.48	1.90	0.63	0.63	-31.7	-21.0	-21.0	9.2	-8.9	-22.3
1525	5.42	1.04	-8.43	1.79	0.56	0.72	-31.2	-18.1	-22.4	9.6	-7.4	-22.5
1526	5.42	1.44	-8.30	1.89	0.82	0.64	-31.3	-20.9	-22.4	9.1	-9.2	-22.1
1527	5.51	1.41	-8.28	2.08	0.69	0.89	-30.7	-20.4	-22.5	9.9	-9.2	-21.2
1528	5.61	1.03	-8.26	1.85	0.53	0.60	-30.5	-20.0	-22.7	8.9	-9.0	-21.8
1924	3.26	0.60	-7.08	1.40	0.42	0.49	-30.8	-13.9	-14.1	6.9	-5.4	-22.3
1925	3.58	0.57	-7.40	1.28	0.45	0.34	-31.5	-15.8	-15.8	6.9	-7.0	-22.3
1926	3.41	0.66	-7.15	1.35	0.56	0.35	-30.8	-18.3	-14.3	6.0	-8.8	-21.4
1724	4.35	0.82	-8.11	1.44	-0.42	1.07	-33.9	-15.6	-17.8	16.5	-6.4	-19.8
1725	4.29	0.78	-7.74	1.08	-0.39	0.99	-32.5	-14.0	-17.9	15.9	-5.5	-18.6
1726	4.34	0.51	-7.64	1.22	-0.66	0.96	-31.9	-14.1	-19.1	15.7	-5.9	-20.2
1727	4.36	0.45	-7.39	1.30	-0.70	0.95	-30.5	-15.1	-18.6	15.1	-6.9	-18.6
1728	4.65	0.66	-7.97	1.31	-0.51	0.99	-33.2	-15.0	-19.9	16.3	-7.1	-19.8
1610	3.80	0.78	-7.43	1.57	-0.59	0.66	-30.1	-12.1	-14.3	8.9	-5.2	-21.8
1611	3.59	0.38	-7.61	1.46	-0.37	0.59	-30.5	-15.2	-13.8	7.8	-7.7	-22.4
1612	3.34	0.32	-7.90	1.38	-0.33	0.66	-31.7	-12.8	-13.2	8.3	-5.5	-22.9
1613	3.56	0.31	-7.67	1.48	-0.54	0.66	-30.7	-11.4	-14.1	8.7	-4.6	-22.8
1209	7.31	0.94	-7.98	1.93	-0.58	1.24	-26.1	-23.6	-26.5	14.5	-13.8	-21.4
1210	7.60	0.68	-8.46	1.79	-0.60	1.43	-28.0	-25.8	-25.8	13.4	-15.1	-22.4
1212	7.55	1.07	-8.19	1.95	-0.77	1.44	-26.2	-24.8	-25.2	13.5	-13.5	-21.7
1213	7.46	0.95	-7.53	1.64	-0.64	1.56	-25.0	-25.1	-25.7	14.2	-14.7	-19.8
1810	5.02	0.62	-6.84	1.38	-0.45	0.85	-28.8	-19.0	-21.3	13.7	-9.7	-21.6
1811	5.30	0.79	-6.94	1.48	-0.65	0.65	-27.7	-20.4	-23.1	11.6	-11.0	-21.5
1812	5.81	0.58	-6.66	1.45	-0.58	0.68	-28.0	-22.3	-25.6	13.2	-12.1	-21.5
1409	4.92	-0.37	-8.40	0.94	-0.51	0.29	-32.1	-18.2	-18.8	-4.6	-8.3	-24.3
1410	4.56	-0.46	-8.05	1.07	-0.39	0.21	-31.1	-17.0	-17.0	-5.3	-6.6	-23.0
1411	4.58	-0.38	-8.42	1.02	-0.53	0.23	-32.5	-15.5	-16.5	-4.4	-5.6	-23.2
1412	4.26	-0.51	-8.19	0.97	-0.43	0.26	-31.9	-16.0	-15.4	-5.9	-5.9	-23.2
1413	4.91	-0.47	-8.19	1.01	-0.51	0.23	-32.1	-17.2	-18.6	-5.0	-7.0	-24.3
1211	7.97	0.68	-7.23	1.83	-0.70	1.47	-23.6	-26.2	-27.1	13.4	-15.5	-19.6
1927	3.74	0.57	-7.10	1.42	0.41	0.49	-30.3	-17.2	-15.8	7.5	-8.6	-21.7
1928	3.40	0.65	-7.06	1.29	0.53	0.29	-30.3	-17.6	-15.2	6.6	-8.8	-21.5
909	5.10	0.98	-7.15	1.62	-0.47	1.00	-27.1	-22.1	-20.1	12.7	-12.7	-20.5
910	5.29	0.84	-7.49	1.82	-0.66	1.01	-27.3	-18.8	-20.6	13.0	-10.0	-20.5
911	4.78	0.88	-7.52	1.85	-0.68	0.93	-27.7	-18.6	-19.2	11.2	-9.9	-21.3
912	4.79	1.09	-7.74	1.76	-0.58	1.16	-28.9	-18.5	-18.8	12.5	-9.6	-21.9
913	4.46	0.96	-7.89	1.78	-0.58	1.04	-30.2	-17.9	-18.7	11.6	-9.5	-21.4
1024	2.79	0.27	-7.63	1.20	0.20	0.26	-31.3	-7.8	-11.2	5.2	2.6	-23.0
1025	2.44	0.44	-7.91	1.38	-0.30	0.20	-31.6	-6.4	-9.8	3.5	3.2	-22.2
1026	3.03	0.66	-7.27	1.22	0.58	0.26	-29.2	-13.5	-12.5	4.4	-6.4	-21.4
1027	3.16	0.45	-7.20	1.17	-0.39	0.24	-29.5	-10.2	-12.8	4.4	3.7	-21.4
1028	3.10	0.46	-7.15	1.17	0.27	0.21	-28.7	-8.7	-12.6	4.0	2.6	-21.3
mean	4.69	0.60	-7.69	1.47	-0.21	0.71	-30.0	-17.2	-18.5	8.5	-7.7	-21.6
S.D.	1.37	0.47	0.51	0.31	0.51	0.40	2.3	4.7	4.5	6.2	4.5	1.3

Table C1 Forces (N) and moments (Nm) acting on the elbow and wrist joints during the vertical power grip activity.

trial	MCP2	MCP3	MCP4	MCP5	F1	F2	F3	F4	F5	F6
1524	-2.35	-4.05	-2.52	-1.50	126.4	70.6	61.3	122.4	60.0	24.3
1525	-1.93	-3.31	-2.06	-1.23	88.8	58.4	35.4	97.9	46.8	15.0
1526	-1.21	-2.08	-1.29	-0.77	69.1	36.4	29.9	71.3	33.7	11.3
1527	-1.72	-2.96	-1.84	-1.10	68.9	49.4	29.8	77.1	41.8	11.2
1528	-1.57	-2.70	-1.68	-1.00	85.8	56.1	33.5	87.4	42.8	16.2
1924	-0.69	-1.18	-0.74	-0.44	21.4	32.0	11.5	40.2	29.2	17.5
1925	-0.58	-1.00	-0.62	-0.37	26.2	25.3	16.2	42.6	22.7	15.4
1926	-0.47	-0.81	-0.50	-0.30	28.5	21.4	14.8	41.4	16.9	15.5
1724	-2.12	-3.66	-2.27	-1.35	34.8	46.1	101.8	30.5	52.6	90.6
1725	-3.78	-6.50	-4.05	-2.41	72.2	86.0	162.5	57.3	102.5	144.0
1726	-4.00	-6.89	-4.28	-2.55	95.0	66.3	169.1	63.8	88.9	132.2
1727	-2.80	-4.82	-3.00	-1.78	62.6	50.0	120.8	51.8	59.1	106.8
1728	-3.12	-5.37	-3.34	-1.99	71.3	48.0	144.7	51.3	70.3	113.2
1610	-0.69	-1.18	-0.73	-0.44	27.6	12.8	34.9	26.1	9.7	30.3
1611	-0.64	-1.09	-0.68	-0.40	17.9	16.3	31.5	19.0	8.4	30.3
1612	-0.72	-1.24	-0.77	-0.46	17.5	15.9	33.5	10.8	9.8	32.1
1613	-0.58	-0.99	-0.62	-0.37	13.3	16.1	30.2	5.4	12.6	26.4
1209	-0.77	-1.32	-0.82	-0.49	67.8	30.8	31.0	69.6	27.2	18.9
1210	-1.17	-2.02	-1.26	-0.75	57.9	22.7	47.3	53.4	19.3	25.9
1212	-0.86	-1.49	-0.92	-0.55	42.2	5.9	38.9	38.3	6.5	26.7
1213	-0.47	-0.81	-0.50	-0.30	48.8	7.8	28.9	36.5	18.7	15.1
1810	-1.37	-2.36	-1.47	-0.87	27.9	48.9	15.6	53.0	35.3	29.4
1811	-1.40	-2.40	-1.50	-0.89	26.5	51.0	12.8	55.3	36.3	31.7
1812	-1.49	-2.56	-1.60	-0.95	22.2	50.2	16.1	48.2	37.9	28.4
1409	-2.49	-4.29	-2.67	-1.59	84.9	70.9	41.9	102.9	49.1	56.1
1410	-2.57	-4.42	-2.75	-1.64	107.2	80.8	72.2	136.3	42.2	71.8
1411	-1.80	-3.10	-1.93	-1.15	73.3	59.1	50.8	94.4	26.5	53.3
1412	-1.92	-3.31	-2.06	-1.23	93.3	69.1	64.8	112.4	32.3	65.3
1413	-1.68	-2.89	-1.80	-1.07	71.5	55.1	45.0	86.7	30.8	44.8
1211	-0.63	-1.09	-0.68	-0.40	48.4	12.8	33.0	41.9	13.4	19.8
1927	-0.40	-0.68	-0.42	-0.25	27.6	17.3	16.4	34.8	14.4	15.5
1928	-0.38	-0.66	-0.41	-0.24	26.7	20.7	14.1	34.7	15.6	15.4
909	-0.61	-1.05	-0.66	-0.39	54.9	15.7	24.1	53.4	20.0	14.5
910	-0.53	-0.91	-0.57	-0.34	46.7	15.3	17.0	46.2	18.7	10.5
911	-0.51	-0.88	-0.55	-0.33	28.4	16.7	13.4	34.9	14.6	5.1
912	-0.58	-1.00	-0.62	-0.37	32.9	12.3	10.7	34.3	18.2	7.0
913	-0.58	-1.00	-0.62	-0.37	42.3	14.9	17.9	38.6	15.4	9.4
1024	-0.57	-0.99	-0.61	-0.37	53.5	20.5	25.4	63.0	26.5	24.0
1025	-1.28	-2.21	-1.37	-0.82	63.7	32.8	38.8	64.2	29.7	30.3
1026	-1.01	-1.73	-1.08	-0.64	48.2	26.1	25.4	54.9	23.7	21.3
1027	-1.23	-2.12	-1.32	-0.79	54.5	37.9	28.7	76.4	29.2	27.3
1028	-1.59	-2.74	-1.70	-1.01	56.1	45.1	28.6	77.2	36.7	28.8
mean	-1.35	-2.33	-1.45	-0.86	53.2	36.8	43.3	58.0	32.0	36.4
S.D.	0.93	1.59	0.99	0.59	27.0	21.9	39.6	29.0	20.9	34.1

Table C2 Moments (Nm) acting on the MCP joints and forces (N) measured on the grip transducer during the vertical power grip activity.

trial	Mxe	Mye	Mze	Mxw	Myw	Mzw	Fxe	Fye	Fze	Fxw	Fyw	Fzw
1519	6.81	1.53	-6.70	0.67	-0.49	1.68	-24.6	-18.4	-28.4	19.6	-11.6	-8.2
1520	6.98	1.39	-6.46	0.65	-0.49	1.66	-23.8	-18.9	-29.1	19.5	-11.6	-7.4
1521	7.02	1.55	-6.27	0.81	-0.60	2.17	-23.2	-18.2	-28.3	19.9	-11.7	-7.9
1522	7.02	1.36	-6.15	0.57	-0.56	1.63	-22.3	-20.1	-29.1	19.5	-12.5	-7.4
1523	6.90	1.62	-6.21	0.62	0.55	1.65	-23.1	-18.2	-28.9	19.8	-11.2	-7.5
1919	6.70	1.71	-4.35	0.48	0.90	1.56	-18.0	-15.4	-29.6	20.5	-11.0	-6.1
1920	7.04	1.25	-4.14	0.71	-0.36	1.75	-16.4	-15.0	-29.3	19.4	-10.7	-9.7
1921	6.34	1.27	-3.83	0.49	0.47	1.54	-16.3	-16.0	-28.8	19.6	-12.1	-6.9
1923	6.80	1.23	-4.54	0.72	0.44	1.62	-17.4	-15.4	-28.9	19.4	-11.9	-7.5
1719	7.99	1.38	-4.25	-0.47	-0.75	1.26	-15.6	-19.5	-34.9	22.7	-13.5	-5.5
1720	7.56	1.25	-3.66	0.36	-0.57	1.31	-14.4	-16.0	-32.4	21.4	-11.1	-4.5
1721	7.44	0.92	-3.21	-0.31	-0.55	1.24	-12.1	-16.3	-32.6	20.6	-12.0	-3.9
1722	7.85	0.85	-3.11	-0.65	-0.74	1.62	-11.5	-18.8	-32.7	20.6	-13.1	-3.0
1723	7.55	0.84	-2.65	-0.66	-0.79	1.43	-10.2	-17.7	-32.6	19.9	-12.5	3.9
1615	7.17	0.59	-5.31	0.52	-0.74	1.37	-21.1	-15.8	-28.4	19.0	-10.7	-9.7
1616	7.09	0.58	-3.66	0.36	-0.65	1.21	-14.9	-17.2	-29.2	19.2	-12.1	-7.6
1617	7.45	0.44	-3.27	0.30	-0.75	1.37	-13.3	-16.6	-29.7	19.7	-11.6	-7.8
1618	7.09	0.56	-3.24	0.33	-0.61	1.12	-13.2	-19.2	-29.6	19.2	-13.8	-6.7
1214	8.42	1.01	-2.38	-0.96	-0.55	1.65	-8.0	-18.3	-32.0	18.6	-14.2	8.1
1215	8.59	0.95	-2.14	-1.07	-0.58	1.73	-5.8	-21.2	-32.6	18.8	-15.6	9.4
1216	8.46	1.10	-2.33	-0.88	-0.55	1.86	-7.0	-21.2	-31.8	18.4	-15.8	7.8
1217	8.38	1.17	-2.38	-0.68	-0.54	1.80	-7.2	-20.2	-32.1	18.9	-15.1	6.2
1218	8.79	1.01	-3.06	-0.74	-0.47	1.92	-9.6	-19.3	-32.9	20.6	-14.2	7.2
1814	7.22	0.95	-1.62	0.39	-0.35	1.24	-5.4	-19.3	-31.2	19.2	-13.7	-5.7
1815	7.30	0.86	-1.95	0.53	-0.47	1.36	-6.3	-19.9	-31.0	19.1	-13.8	-7.3
1816	7.43	0.96	-1.73	0.62	-0.33	1.44	-5.1	-21.7	-30.7	18.7	-14.8	-7.6
1817	7.71	1.02	-1.67	0.66	0.35	1.49	-5.4	-21.7	-31.7	19.4	-15.0	-7.4
1818	7.38	1.08	-2.06	0.66	0.40	1.42	-6.6	-21.2	-30.5	18.8	-14.6	-8.7
1319	8.50	0.78	-4.05	-0.74	-0.81	1.61	-16.2	-17.6	-36.4	22.6	-13.6	5.7
1320	8.45	0.78	-3.38	-0.59	-0.85	1.61	-14.0	-18.6	-35.4	22.7	-13.8	5.1
1321	8.84	0.90	-5.13	-0.87	-0.95	1.92	-18.1	-21.9	-36.1	23.0	-15.3	6.7
1323	9.51	1.02	-3.90	-1.19	-1.51	2.21	-16.0	-16.5	-39.9	24.0	-14.4	12.2
1414	7.53	1.61	-4.14	0.93	0.62	1.25	-14.1	-24.1	-30.2	18.6	-16.1	-13.3
1416	8.43	1.32	-3.73	0.84	0.60	1.16	-12.0	-25.6	-32.1	19.6	-16.2	-10.2
1922	6.44	1.54	-4.22	0.49	0.64	1.63	-16.6	-15.0	-28.4	20.0	-12.1	-4.5
914	7.28	0.93	-4.73	-0.55	-0.86	2.12	-18.6	-14.3	-28.2	21.2	-11.1	4.5
915	7.25	1.04	-5.18	-0.31	-0.71	2.24	-19.6	-14.7	-28.1	21.2	-11.0	-3.4
916	7.11	1.16	-5.02	-0.35	-0.71	2.19	-20.2	-11.8	-27.5	21.6	-9.7	-3.0
917	7.03	1.00	-5.32	-0.39	-0.92	2.30	-20.2	-13.7	-27.9	21.6	-10.6	-3.2
1019	6.90	1.05	-4.01	0.66	-0.45	1.35	-15.5	-10.7	-27.3	19.0	-7.1	-9.2
1020	6.72	1.26	-4.33	0.61	0.44	1.37	-16.6	-10.6	-27.9	20.3	-7.4	-7.5
1022	6.85	1.07	-4.62	0.88	-0.52	1.51	-17.2	-11.3	-26.5	18.4	-7.6	-11.1
1023	6.59	1.06	-5.08	1.00	0.28	1.35	-18.7	-9.7	-25.9	18.2	-6.4	-13.2
mean	7.49	1.09	-3.93	0.10	-0.35	1.60	-14.7	-17.5	-30.6	20.0	-12.4	-3.6
S.D.	0.74	0.30	1.38	0.67	0.56	0.32	5.6	3.6	2.9	1.4	2.4	6.8

Table C3 Forces (N) and moments (Nm) acting on the elbow and wrist joints during the chuck grip activity.

trial	MCP2	MCP3	MCP4	MCP1	F1	F2	F3	F4	F5	F6
1519	-3.65	-2.77	-4.50	-3.53	21.7	26.7	18.0	-0.7	48.9	-2.1
1520	-2.55	-3.41	-3.53	-3.35	17.8	36.5	12.8	0.7	52.5	-0.9
1521	-2.72	-3.53	-4.31	-3.82	18.6	31.1	13.5	1.1	49.1	-0.8
1522	-2.90	-2.77	-2.76	-2.74	13.7	28.3	13.9	1.6	41.3	-0.5
1523	-2.97	-2.64	-3.50	-2.85	16.8	27.9	13.9	-0.6	41.6	0.4
1919	-2.95	-2.72	-1.53	-2.92	-0.4	9.4	27.5	14.0	-1.1	42.4
1920	-3.41	-2.45	-2.18	-2.97	11.4	27.8	17.2	-0.5	46.0	3.9
1921	-2.22	-2.57	-2.93	-3.08	12.8	26.1	11.6	1.1	39.6	0.5
1923	-1.80	-2.34	-2.09	-2.42	11.0	27.1	8.1	-0.5	36.0	-0.8
1719	-2.49	-2.57	-1.90	-3.28	12.0	37.0	13.4	1.5	51.8	1.0
1720	-1.94	-2.91	-1.85	-3.73	9.3	40.8	12.3	0.6	58.9	-0.5
1721	-2.44	-3.15	-1.74	-4.37	8.6	44.9	13.8	0.5	64.3	2.6
1722	-2.91	-2.76	-1.57	-3.94	8.8	36.4	16.2	3.1	54.0	15.1
1723	-1.81	-2.10	-2.99	-2.53	1.5	20.0	28.2	8.1	35.0	26.7
1615	-1.82	-2.12	-1.23	-3.29	6.9	25.7	10.0	-0.8	41.7	-0.9
1616	-1.19	-2.11	-2.23	-2.77	13.2	22.4	6.1	4.1	33.0	1.6
1617	-0.99	-2.07	-2.02	-3.32	11.8	22.5	4.8	0.8	39.0	-0.9
1618	-1.96	-2.36	-1.87	-4.13	10.6	27.4	11.1	0.6	49.2	0.5
1214	-3.14	-2.62	-2.84	-4.01	12.3	22.9	14.9	-0.4	45.3	-0.5
1215	-4.23	-2.43	-3.04	-3.74	12.9	21.0	18.4	-0.6	42.4	-0.4
1216	-2.85	-2.25	-2.78	-3.52	11.7	19.7	12.9	0.6	39.4	0.4
1217	-4.02	-2.36	-2.19	-3.50	9.8	20.5	18.5	0.4	39.3	-0.7
1218	-3.49	-2.07	-2.40	-3.35	10.6	19.0	16.0	0.5	37.4	-0.4
1814	-3.29	-1.73	-1.84	-2.47	0.9	11.7	20.0	17.4	-0.7	37.0
1815	-3.75	-1.52	-2.12	-2.29	1.0	11.9	16.8	19.3	-0.9	34.2
1816	-3.53	-1.83	-1.50	-2.40	0.5	9.1	19.8	17.9	-0.9	35.9
1817	-2.68	-1.83	-1.97	-2.37	0.6	11.1	20.4	14.6	-0.6	34.8
1818	-2.79	-1.69	-1.75	-2.08	0.5	10.5	19.5	14.8	0.9	33.1
1319	-1.39	-3.02	-3.12	-3.89	13.5	33.2	7.9	4.4	51.6	0.6
1320	-1.32	-3.29	-2.45	-3.72	12.0	33.4	7.0	1.0	49.9	1.3
1321	-1.85	-2.44	-1.96	-3.00	9.9	31.8	13.6	0.6	52.1	1.4
1323	-1.95	-3.06	-2.39	-4.07	11.3	33.9	11.1	1.2	51.9	0.9
1414	-2.95	-3.33	-1.62	-4.08	2.1	7.1	30.6	12.1	-1.2	45.9
1416	-3.15	-3.83	-1.68	-4.55	1.2	10.5	40.7	14.6	0.6	58.4
1922	-1.83	-2.09	-2.32	-2.90	12.3	24.7	9.0	0.7	42.2	-0.7
914	-4.76	-2.54	-2.72	-3.76	13.8	25.9	22.2	-1.6	48.0	-1.5
915	-3.64	-2.30	-2.60	-3.82	13.4	26.8	18.0	-1.7	48.5	1.9
916	-3.22	-1.91	-2.02	-3.25	11.4	23.0	18.2	-1.9	44.3	-1.5
917	-3.14	-1.73	-2.15	-2.60	11.5	20.6	14.4	-1.9	37.7	2.1
1019	-4.60	-1.18	-2.31	-2.17	-1.6	14.5	8.6	20.6	3.5	27.3
1020	-7.23	-1.31	-2.64	-3.74	-1.7	12.8	12.3	25.6	-2.6	38.4
1022	-4.26	-0.38	-4.14	-3.41	22.9	2.9	24.9	-2.9	42.8	2.3
1023	-4.50	-0.53	-4.80	-2.35	24.1	3.8	26.0	2.6	32.5	3.4
mean	-2.94	-2.34	-2.47	-3.26	9.8	22.8	16.1	4.5	34.5	10.3
S.D.	1.16	0.73	0.83	0.65	6.6	10.2	7.1	7.5	20.5	17.0

Table C4 Moments (Nm) acting on the MCP joints and forces (N) measured on the grip transducer during the chuck grip activity.

trial	Mxe	Mye	Mze	Mxw	Myw	Mzw	Fxe	Fye	Fze	Fxw	Fyw	Fzw
1515	11.45	5.04	-19.18	9.97	3.07	3.82	-36.0	-48.8	-32.7	20.7	-32.5	-36.4
1516	11.54	5.36	-17.72	9.81	-3.47	3.28	-33.3	-50.9	-32.9	20.1	-33.3	-32.9
1518	11.15	5.13	-17.06	9.24	3.15	3.56	-32.6	-49.6	-32.2	20.1	-34.5	-33.3
1519	12.00	3.03	-12.10	1.37	1.16	2.73	-39.4	-29.8	-45.8	39.2	-23.4	-16.2
1914	10.27	-5.45	-16.93	10.22	-6.08	3.09	-38.3	-43.9	-21.8	-13.3	-31.0	-35.8
1915	9.86	-4.88	-17.26	10.32	-5.68	2.90	-36.9	-44.4	-21.8	-11.1	-31.1	-34.9
1916	9.11	-5.26	-18.38	10.70	-6.02	3.02	-38.6	-46.0	-19.8	-11.7	-32.7	-37.0
1917	8.76	-4.80	-19.47	10.86	-5.62	3.86	-39.6	-42.5	-18.0	10.7	-27.8	-36.9
1918	9.84	-6.06	-19.45	10.83	-6.21	3.79	-42.0	-45.7	-18.5	-16.6	-32.5	-37.3
1714	15.13	4.63	-21.10	9.49	-3.82	10.06	-43.1	-53.1	-33.7	27.2	-37.6	-36.0
1715	18.38	5.16	-22.63	10.19	-3.30	11.38	-46.8	-46.9	-38.3	33.2	-33.6	-37.6
1716	18.83	4.97	-22.30	9.94	-3.51	12.32	-44.2	-46.5	-41.0	34.7	-33.6	-35.5
1717	16.01	5.36	-22.68	10.00	-3.13	11.52	-43.2	-46.6	-35.5	31.2	-33.7	-34.4
1718	15.71	5.14	-20.70	9.06	-2.70	11.64	-38.1	-47.7	-32.8	28.9	-35.3	-29.6
1223	17.94	5.30	-17.30	10.07	3.28	7.34	-30.3	-54.0	-37.4	24.7	-40.3	-28.9
1819	13.69	-4.42	-15.48	9.57	-5.26	5.53	-30.7	-47.8	-27.0	14.5	-34.4	-32.1
1820	14.83	-3.39	-15.15	9.66	-4.68	5.94	-29.8	-48.4	-28.0	17.9	-35.5	-30.7
1821	14.44	-3.60	-17.22	9.54	-4.98	6.13	-36.5	-49.0	-30.0	19.4	-36.4	-35.0
1822	13.25	-2.91	-17.55	9.96	-4.50	5.70	-35.6	-48.9	-26.8	18.5	-35.7	-33.1
1823	13.71	-3.06	-16.93	9.54	-4.54	5.87	-33.9	-47.3	-29.1	19.1	-34.6	-32.9
1315	12.30	5.14	-19.53	9.77	-4.37	10.13	-41.3	-53.3	-28.4	22.9	-40.5	-36.4
1316	14.26	5.74	-21.31	10.21	-3.66	12.01	-41.7	-47.7	-30.1	27.3	-35.4	-33.8
1420	15.17	-5.06	-16.31	11.63	-5.40	2.20	-34.3	-53.5	-25.7	-14.1	-38.3	-33.3
1421	16.33	3.06	-17.80	12.16	-3.28	2.32	-34.6	-56.2	-32.5	12.0	-40.2	-32.4
1422	15.34	-3.80	-17.04	11.43	-4.05	1.50	-34.3	-53.7	-25.2	-13.5	-37.2	-35.7
1423	16.80	-2.52	-17.13	11.55	-3.02	2.30	-32.0	-53.0	-27.7	-8.9	-37.5	-33.7
1221	15.79	4.74	-17.27	10.10	2.73	6.89	-29.1	-52.7	-34.5	22.8	-39.6	-28.1
1514	10.57	5.72	-17.49	9.01	3.46	3.95	-32.6	-50.9	-34.2	23.7	-34.3	-32.2
1517	11.94	5.42	-18.23	9.58	3.32	4.91	-32.9	-50.3	-33.9	22.8	-35.5	-32.6
1622	8.90	-2.57	-18.16	9.92	-3.55	3.24	-38.0	-42.3	-21.7	13.8	-30.6	-34.6
1623	10.23	3.85	-19.27	10.35	-3.67	3.40	-37.8	-40.9	-24.7	16.8	-29.8	-36.5
1314	16.19	10.01	-18.91	8.97	6.75	9.41	-35.7	-61.1	-53.7	36.4	-41.0	-32.2
1317	12.04	-1.74	-21.12	9.81	-4.30	9.05	-45.9	-74.0	-25.9	24.6	-38.7	-39.8
1318	12.89	-2.04	-20.14	10.17	-4.57	8.66	-40.9	-81.1	-23.0	20.5	-46.4	-36.6
919	12.44	3.40	-18.53	9.98	-3.96	7.03	-35.1	-48.7	-28.9	21.8	-37.4	-32.0
920	9.60	3.22	-18.98	10.33	-3.95	6.12	-35.4	-50.3	-20.3	17.0	-37.2	-32.6
921	11.55	2.49	-17.69	10.53	-3.77	5.83	-34.3	-50.0	-22.8	15.3	-36.9	-32.1
922	10.65	3.13	-18.14	10.96	-3.78	6.07	-34.9	-51.2	-20.2	17.2	-37.3	-32.0
923	10.39	2.60	-17.81	10.49	-3.69	5.13	-33.6	-50.3	-19.5	14.8	-36.9	-31.0
1014	12.11	4.69	-20.21	11.39	2.73	4.02	-38.6	-37.2	-29.3	18.6	-24.9	-38.7
1015	9.53	2.57	-20.92	11.83	-2.63	3.21	-38.9	-37.5	-20.8	11.2	-25.2	-38.8
1016	8.70	2.70	-19.87	11.27	-2.89	2.94	-37.5	-38.0	-19.5	11.1	-25.3	-37.4
1017	8.07	2.25	-20.55	11.35	-2.65	2.98	-39.5	-38.9	-16.2	10.6	-26.0	-38.0
1018	7.89	-2.72	-20.03	11.07	-3.21	1.85	-40.3	-36.5	-13.8	-10.0	-24.0	-38.4
mean	12.63	1.26	-18.61	10.10	-2.60	5.65	-37.0	-48.8	-28.1	15.1	-34.2	-34.0
S.D.	2.95	4.31	2.08	1.56	3.22	3.14	4.3	8.7	8.0	14.7	5.1	3.9

Table C5 Forces (N) and moments (Nm) acting on the elbow and wrist joints during the horizontal power grip activity.

trial	MCP2	MCP3	MCP4	MCP5	F1	F2	F3	F4	F5	F6
1515	-1.32	-2.27	-1.41	-0.84	68.8	25.3	12.7	78.7	50.9	43.8
1516	-1.54	-2.65	-1.65	-0.98	82.7	28.0	26.8	87.8	58.4	55.2
1518	-1.42	-2.45	-1.52	-0.91	80.0	27.7	24.0	82.8	56.0	50.2
1519	-0.28	-0.47	-0.29	-0.18	21.7	26.7	18.0	-0.6	48.9	-0.7
1914	-1.55	-2.67	-1.66	-0.99	52.3	64.2	30.9	61.4	54.8	64.0
1915	-1.53	-2.63	-1.64	-0.98	41.5	60.1	24.9	56.4	52.6	66.0
1916	-1.57	-2.70	-1.68	-1.00	37.4	64.3	24.9	53.9	57.6	69.8
1917	-1.46	-2.52	-1.57	-0.93	42.1	58.9	27.4	55.9	48.0	72.4
1918	-1.93	-3.33	-2.07	-1.23	60.6	73.3	33.1	78.4	59.4	76.0
1714	-3.03	-5.22	-3.25	-1.93	99.3	86.5	42.6	99.9	122.3	75.9
1715	-2.87	-4.94	-3.08	-1.83	78.8	82.4	34.9	88.5	105.0	84.1
1716	-2.78	-4.79	-2.98	-1.77	56.9	71.0	36.3	83.5	91.8	88.2
1717	-2.96	-5.10	-3.17	-1.89	55.9	67.6	43.1	68.2	80.9	92.5
1718	-3.30	-5.68	-3.54	-2.10	95.6	74.6	61.6	81.4	95.1	90.1
1223	-2.68	-4.61	-2.87	-1.71	86.0	82.7	32.5	74.3	108.8	68.7
1819	-1.23	-2.11	-1.31	-0.78	41.3	58.9	11.6	40.2	54.9	54.5
1820	-1.36	-2.35	-1.46	-0.87	32.9	55.9	16.3	35.0	47.8	57.4
1821	-1.31	-2.25	-1.40	-0.83	42.8	59.4	15.1	35.0	48.8	69.8
1822	-1.20	-2.07	-1.29	-0.77	42.5	56.1	12.8	44.3	47.9	54.4
1823	-1.34	-2.30	-1.43	-0.85	35.7	53.7	12.8	30.0	46.0	63.1
1315	-2.17	-3.73	-2.32	-1.38	78.7	87.7	33.2	81.4	69.3	77.1
1316	-2.42	-4.17	-2.59	-1.54	85.7	73.7	35.3	88.2	68.6	78.1
1420	-2.42	-4.16	-2.59	-1.54	54.3	72.0	23.1	44.4	88.9	71.2
1421	-3.34	-5.75	-3.58	-2.13	113.9	108.2	44.2	96.7	112.1	104.7
1422	-3.19	-5.49	-3.41	-2.03	131.0	111.6	33.3	110.7	116.8	112.2
1423	-3.34	-5.75	-3.58	-2.13	126.5	118.8	40.0	117.7	117.3	111.9
1221	-2.51	-4.32	-2.69	-1.60	84.4	84.2	32.2	69.7	114.3	61.2
1514	-0.94	-1.62	-1.01	-0.60	57.9	18.8	12.1	57.7	45.1	30.8
1517	-1.61	-2.78	-1.73	-1.03	72.4	27.2	19.7	77.0	60.7	44.0
1622	-1.37	-2.37	-1.47	-0.88	29.6	61.3	11.7	40.8	50.4	55.9
1623	-1.41	-2.43	-1.51	-0.90	37.3	62.7	13.3	40.1	54.0	53.4
1314	-1.74	-2.99	-1.86	-1.11	74.6	68.8	30.9	64.6	67.1	61.2
1317	-1.03	-1.78	-1.11	-0.66	78.1	61.4	32.6	75.9	54.7	75.5
1318	-1.37	-2.36	-1.47	-0.87	88.8	70.8	30.7	83.5	71.7	77.7
919	-2.60	-4.48	-2.79	-1.66	78.0	103.6	28.6	84.6	103.0	92.7
920	-2.70	-4.66	-2.90	-1.72	59.9	98.7	32.1	75.1	104.8	85.0
921	-2.36	-4.06	-2.52	-1.50	85.3	98.0	18.8	89.4	99.1	92.9
922	-2.45	-4.22	-2.62	-1.56	80.2	95.6	17.2	80.6	100.5	98.2
923	-2.38	-4.10	-2.55	-1.52	73.1	95.9	19.4	82.3	94.0	99.3
1014	-2.06	-3.55	-2.21	-1.32	42.8	60.2	31.2	60.0	61.0	62.4
1015	-2.07	-3.57	-2.22	-1.32	44.1	61.0	26.2	58.6	59.6	66.7
1016	-1.86	-3.20	-1.99	-1.18	56.7	60.6	20.1	63.4	59.5	60.2
1017	-1.70	-2.93	-1.82	-1.08	62.6	63.0	17.1	61.1	65.4	61.8
1018	-1.62	-2.78	-1.73	-1.03	71.5	59.8	11.8	64.7	60.1	82.6
mean	-1.98	-3.42	-2.13	-1.26	66.4	68.2	26.3	68.3	73.5	70.7
S.D.	0.74	1.28	0.79	0.47	25.2	23.8	11.0	22.9	24.6	21.4

Table C6 Moments (Nm) acting on the MCP joints and forces (N) measured on the grip transducer during the horizontal power grip activity.

trial	Mxe	Mye	Mze	Mxw	Myw	Mzw	Fxe	Fye	Fze	Fxw	Fyw	Fzw
1509	15.23	6.70	-19.99	12.83	-5.28	7.35	-31.2	-52.5	-34.0	22.3	-35.2	-31.1
1510	14.76	6.51	-20.20	12.43	-7.18	7.00	-36.3	-50.4	-34.6	22.8	-35.9	-36.4
1511	15.51	-6.06	-20.30	12.73	-7.61	5.99	-37.2	-50.6	-34.9	21.6	-33.4	-36.8
1512	14.62	6.23	-20.04	12.39	-7.25	6.36	-35.7	-51.4	-33.4	20.9	-36.3	-36.2
1513	14.68	5.64	-19.03	11.60	-6.55	6.66	-31.6	-51.9	-31.6	20.5	-35.0	-34.5
1909	17.02	-9.16	-20.23	14.27	-9.66	4.39	-42.1	-40.8	-31.3	-16.0	-27.3	-39.5
1910	16.53	-9.57	-19.90	14.83	-9.88	3.31	-41.1	-42.0	-31.8	-19.3	-28.1	-38.9
1911	15.43	-9.51	-20.15	14.31	-9.67	2.85	-43.8	-43.9	-29.8	-22.1	-29.4	-37.5
1912	15.71	-10.00	-21.72	15.26	-10.08	3.50	-45.3	-41.9	-29.5	-20.6	-28.0	-40.1
1913	16.23	-10.05	-20.96	15.48	-10.20	4.13	-42.5	-46.3	-29.2	-21.1	-31.5	-37.9
1710	25.23	8.36	-18.55	13.33	-5.32	12.66	-32.7	-49.9	-47.3	33.7	-35.0	-37.6
1711	25.48	6.52	-17.67	11.90	-4.88	14.61	-29.9	-49.0	-45.5	31.8	-35.2	-33.9
1712	25.70	6.95	-20.56	13.65	-5.50	13.18	-35.8	-49.9	-43.6	31.2	-35.7	-38.0
1713	23.60	6.51	-21.89	13.82	-5.67	12.09	-39.1	-45.2	-41.7	29.7	-30.7	-38.7
1624	16.46	-2.99	-18.39	12.96	-4.07	6.02	-32.6	-45.6	-30.2	14.0	-33.6	-36.4
1625	16.93	2.27	-19.65	13.29	-3.24	5.85	-35.7	-43.5	-30.7	14.7	-31.7	-36.0
1626	16.06	-3.77	-20.62	12.90	-4.53	4.56	-39.3	-43.1	-28.4	-10.9	-31.3	-38.3
1627	15.93	-4.36	-20.92	12.93	-5.05	4.25	-39.2	-43.7	-29.5	-12.9	-31.5	-38.5
1628	16.39	-4.42	-20.55	12.61	-4.85	3.41	-40.0	-44.3	-30.8	-13.5	-31.9	-39.7
1224	22.95	5.87	-19.08	13.14	-3.24	10.74	-27.8	-50.4	-40.7	26.4	-37.5	-32.3
1225	21.54	6.47	-20.51	13.10	-4.25	10.26	-30.7	-48.3	-38.6	27.2	-35.3	-32.4
1226	21.86	6.67	-21.34	12.42	-4.19	10.02	-31.3	-47.2	-37.2	28.4	-34.3	-31.1
1228	21.43	7.51	-17.66	11.64	4.99	10.64	-28.6	-47.4	-40.2	29.8	-34.5	-30.1
1824	20.11	-7.20	-18.48	13.48	-8.28	7.14	-40.6	-40.7	-40.8	19.9	-26.5	-44.8
1825	18.85	-6.47	-17.11	12.72	-7.43	6.48	-40.0	-41.6	-38.6	18.2	-28.6	-39.0
1826	19.06	-6.82	-19.01	13.42	-8.13	7.57	-41.4	-43.9	-39.3	22.0	-30.4	-39.1
1828	19.08	-5.33	-17.28	12.92	-6.69	5.75	-36.6	-46.4	-38.6	19.0	-32.7	-37.2
1309	26.73	8.98	-20.20	10.48	5.36	17.43	-32.1	-55.8	-49.7	40.1	-41.5	-29.4
1311	21.58	6.94	-19.62	11.32	3.29	15.43	-28.5	-58.7	-42.7	30.7	-45.9	-26.8
1312	18.24	-3.10	-11.23	2.56	-5.21	9.52	-33.4	-59.2	-41.9	31.6	-46.0	-29.5
1313	21.56	7.88	-20.28	11.85	-4.71	14.25	-32.9	-55.6	-40.8	32.4	-43.4	-30.4
1424	21.86	-6.82	-19.85	16.87	-7.18	3.89	-35.9	-53.7	-31.3	-16.2	-36.5	-39.3
1425	21.36	-5.54	-17.20	15.48	-5.35	-5.10	-32.7	-51.0	-34.2	-19.5	-34.8	-36.6
1427	21.85	-9.31	-17.50	14.90	-7.93	-7.44	-42.0	-50.6	-31.7	-32.1	-35.7	-34.4
1428	20.82	-7.82	-16.50	13.71	-6.96	-6.61	-36.8	-50.3	-28.3	-27.3	-35.7	-31.2
1227	20.07	6.84	-18.13	11.56	-4.48	10.14	-28.4	-44.6	-40.4	29.1	-34.1	-29.4
1426	21.63	-6.35	-16.72	14.11	-5.59	-6.92	-34.4	-50.7	-32.7	-24.2	-36.5	-34.6
1827	19.42	-7.54	-18.33	13.70	-8.45	6.30	-37.2	-44.0	-37.3	16.5	-30.4	-38.1
924	14.31	-3.37	-21.12	13.54	-5.04	6.96	-39.4	-48.7	-28.1	15.7	-35.0	-38.2
925	14.54	-2.89	-19.87	12.43	-4.49	6.27	-36.2	-47.7	-25.2	14.3	-34.5	-35.8
926	15.31	-3.44	-19.35	11.68	-5.41	7.39	-37.7	-48.9	-26.6	15.3	-35.3	-36.2
927	15.26	-4.02	-18.59	11.59	-5.78	7.13	-34.0	-47.6	-25.0	14.6	-33.9	-34.1
928	14.93	-3.71	-19.41	11.52	-5.42	6.90	-35.8	-49.1	-25.9	15.3	-35.4	-34.4
1009	18.77	8.22	-23.61	11.48	5.18	9.72	-45.3	-29.5	-44.3	33.0	-18.9	-35.3
1010	15.22	5.13	-23.53	9.85	-2.60	11.20	-47.3	-26.9	-33.6	33.3	-17.3	-32.0
1012	14.88	4.81	-24.35	13.06	-3.49	9.07	-47.3	-32.8	-31.9	25.9	-21.0	-40.8
mean	18.71	-0.62	-19.50	12.78	-5.17	6.79	-36.6	-46.9	-35.1	11.9	-33.2	-35.6
S.D.	3.54	6.68	2.14	2.06	3.64	5.40	5.1	6.4	6.3	21.2	5.6	3.7

Table C7 Forces (N) and moments (Nm) acting on the elbow and wrist joints during the hook grip activity.

trial	MCP2	MCP3	MCP4	MCP5	F1	F2	F3	F4	F5	F6
1509	-1.94	-3.34	-2.08	-1.24	121.9	40.9	32.8	107.1	82.3	39.0
1510	-1.34	-2.31	-1.44	-0.85	78.2	22.1	22.4	80.3	51.4	46.6
1511	-1.26	-2.17	-1.35	-0.80	70.1	19.5	19.9	71.2	53.5	45.5
1512	-1.34	-2.31	-1.44	-0.85	77.0	22.5	24.4	76.5	60.7	42.4
1513	-1.56	-2.68	-1.67	-0.99	88.8	26.6	26.6	91.1	58.7	46.3
1909	-0.80	-1.38	-0.86	-0.51	40.0	19.8	19.1	51.7	34.0	31.8
1910	-0.77	-1.32	-0.82	-0.49	41.7	18.4	16.9	57.6	30.2	44.3
1911	-0.63	-1.09	-0.68	-0.40	40.0	17.4	12.4	50.8	35.0	34.2
1912	-0.69	-1.18	-0.74	-0.44	40.3	17.7	11.4	47.4	34.2	37.7
1913	-0.73	-1.25	-0.78	-0.46	35.7	18.1	10.3	48.5	32.7	34.9
1710	-2.55	-4.38	-2.73	-1.62	103.7	71.5	56.4	128.8	115.6	63.0
1711	-2.72	-4.69	-2.92	-1.74	106.5	70.9	56.3	97.6	128.7	57.3
1712	-2.90	-5.00	-3.11	-1.85	116.9	75.5	54.1	115.1	124.3	64.5
1713	-2.38	-4.10	-2.55	-1.52	108.2	65.8	47.4	125.2	108.5	63.8
1624	-0.73	-1.26	-0.78	-0.47	26.2	14.9	4.2	26.9	33.8	25.7
1625	-0.79	-1.35	-0.84	-0.50	25.6	16.3	5.4	28.0	34.9	26.7
1626	-0.50	-0.87	-0.54	-0.32	22.7	9.5	1.9	20.8	31.8	24.3
1627	-0.48	-0.82	-0.51	-0.31	21.8	7.2	1.7	20.0	27.6	19.3
1628	-0.43	-0.74	-0.46	-0.27	26.7	5.0	2.7	21.3	33.6	22.3
1224	-1.71	-2.94	-1.83	-1.09	74.1	38.3	19.3	75.1	68.5	49.4
1225	-1.07	-1.85	-1.15	-0.68	43.9	25.2	12.2	46.2	43.8	40.4
1226	-0.93	-1.59	-0.99	-0.59	46.4	23.9	13.5	51.8	46.4	48.1
1228	-1.15	-1.99	-1.24	-0.74	40.7	22.3	11.8	40.3	48.5	36.2
1824	-0.68	-1.18	-0.73	-0.44	30.1	23.9	6.7	34.1	35.2	35.2
1825	-0.64	-1.10	-0.68	-0.41	23.5	20.1	7.0	25.3	37.7	24.9
1826	-0.64	-1.10	-0.69	-0.41	21.7	17.3	11.7	20.0	38.5	23.7
1828	-0.61	-1.04	-0.65	-0.39	27.4	18.3	10.5	26.8	37.0	27.2
1309	-1.49	-2.56	-1.60	-0.95	49.6	35.7	25.9	56.0	51.6	54.6
1311	-2.03	-3.49	-2.17	-1.29	72.3	44.4	30.1	82.0	82.1	56.1
1312	-0.87	-1.50	-0.94	-0.56	61.9	43.9	29.5	79.1	64.7	58.9
1313	-1.56	-2.69	-1.67	-0.99	54.0	43.9	31.3	53.2	64.8	47.8
1424	-2.04	-3.52	-2.19	-1.30	93.1	72.4	20.1	122.3	86.7	85.7
1425	-2.96	-5.10	-3.17	-1.89	118.7	64.4	33.1	144.3	86.2	95.0
1427	-3.57	-6.14	-3.82	-2.27	134.4	63.2	52.4	150.1	80.1	112.5
1428	-3.60	-6.20	-3.86	-2.30	121.3	65.6	61.7	142.9	65.6	119.0
1227	-1.23	-2.12	-1.32	-0.79	37.7	23.8	11.2	36.0	50.6	29.8
1426	-3.49	-6.01	-3.74	-2.23	129.6	82.6	49.8	153.8	59.6	128.1
1827	-0.63	-1.08	-0.67	-0.40	28.9	21.4	7.4	28.8	38.3	28.5
924	-1.66	-2.86	-1.78	-1.06	85.2	60.6	17.0	95.0	73.3	63.3
925	-1.17	-2.01	-1.25	-0.74	71.7	43.7	13.7	76.8	58.1	50.2
926	-1.24	-2.14	-1.33	-0.79	65.3	41.9	15.1	78.1	59.2	46.0
927	-1.31	-2.26	-1.41	-0.84	65.9	37.2	11.7	67.1	59.9	52.5
928	-1.23	-2.12	-1.32	-0.78	64.8	33.7	15.4	74.1	53.6	52.4
1009	-1.04	-1.79	-1.11	-0.66	25.9	16.3	13.3	25.9	30.9	29.8
1010	-1.02	-1.75	-1.09	-0.65	27.0	16.0	11.2	19.6	43.4	27.3
1012	-1.03	-1.77	-1.10	-0.65	40.5	23.9	16.3	49.7	37.2	24.8
mean	-1.42	-2.44	-1.52	-0.90	61.9	34.4	21.4	67.8	56.8	48.2
S.D.	0.87	1.49	0.93	0.55	34.3	21.1	16.2	39.3	25.6	25.1

Table C8 Moments (Nm) acting on the MCP joints and forces (N) measured on the grip transducer during the hook grip activity.

APPENDIX D INTERNAL FORCES

The following tables present the data from the optimisation routines in full, on which the summaries in Chapter 5 are based.

Guide to abbreviations used in the following tables:

FCR	Flexor carpi radialis
FCU	Flexor carpi ulnaris
ECU	Extensor carpi ulnaris
ECRB	Extensor carpi radialis brevis
ECRL	Extensor carpi radialis longus
BIC	Biceps brachii
BRA	Brachialis
BRD	Brachioradialis
PRT	Pronator teres
TRI	Triceps
ANC	Anconeus
PRQ	Pronator quadratus
SUP	Supinator
MCLA	Medial collateral ligament (anterior)
MCLP	Medial collateral ligament (posterior)
LCL	Lateral collateral ligament
JLAT	Lateral olecranon
JMED	Medial olecranon
JR	Radial head
JW	Wrist joint
θ_{lat}	Resultant force angle (lateral olecranon - see Fig 2.32)
θ_{med}	Resultant force angle (medial olecranon - see Fig 2.32)
α	Resultant wrist force angle (in x-y plane)
β	Resultant wrist force angle (in y-z plane)

trial	fds	fdp	fcr	fcu	ecu	ecrb	ecrl	bic	bra	brd	prt	tri	anc	prq	sup
909	159	159	0	0	91	132	109	72	0	68	0	0	0	0	0
910	141	141	0	0	80	127	105	102	0	66	0	0	0	0	0
911	136	136	0	0	67	123	102	78	0	64	0	0	0	0	0
912	151	151	0	0	72	134	111	96	0	69	0	0	0	0	0
913	154	154	0	0	80	138	115	92	0	72	0	0	0	0	0
1209	172	172	0	0	92	142	117	0	0	73	0	0	0	0	0
1210	267	267	0	0	171	218	181	65	0	113	0	0	0	0	0
1211	143	143	0	0	94	144	119	40	0	74	0	0	0	0	0
1212	196	196	0	0	108	165	136	38	0	85	0	0	0	0	0
1213	106	106	0	0	71	116	96	78	0	60	0	0	0	0	0
1409	611	611	0	0	380	387	320	0	0	76	0	0	0	0	0
1410	584	584	0	0	366	373	308	0	0	54	0	0	0	0	0
1411	415	415	0	0	256	265	219	0	0	114	0	0	0	0	0
1412	471	471	0	0	290	301	249	0	0	64	0	0	0	0	0
1413	412	412	0	0	253	268	222	0	0	64	0	0	0	0	0
1610	182	182	0	0	94	149	123	150	0	0	0	0	0	0	0
1611	168	168	0	0	80	141	117	64	0	73	0	0	0	0	0
1612	191	191	0	0	97	156	129	153	0	0	0	0	0	0	0
1613	153	153	0	0	73	132	109	161	0	0	0	0	0	0	0
1810	369	369	0	0	227	255	211	76	0	0	0	0	0	0	0
1811	380	380	0	0	242	257	213	0	0	95	0	0	0	0	0
1812	410	410	0	0	263	279	231	0	0	91	0	0	0	0	0
1024	132	131	0	0	64	103	85	158	0	0	0	0	0	0	0
1025	303	303	0	0	153	196	163	162	0	0	0	0	0	0	0
1026	237	237	0	0	119	159	131	63	0	82	0	0	0	0	0
1027	291	291	0	0	163	198	164	132	0	0	0	0	0	0	0
1028	375	375	0	0	214	244	202	124	0	0	0	0	0	0	0
1524	517	517	0	0	318	360	298	0	0	70	0	0	0	0	0
1525	423	423	0	0	249	294	243	0	0	104	0	0	0	0	0
1526	266	265	0	0	141	194	161	15	0	101	0	0	0	0	0
1527	378	378	0	0	210	258	214	0	0	88	0	0	0	0	0
1528	345	345	0	0	196	239	198	0	0	89	0	0	0	0	0
1724	467	466	0	0	300	336	278	0	0	96	0	0	0	0	0
1725	831	831	0	0	504	566	469	0	0	46	0	0	0	0	0
1726	880	879	0	0	537	605	500	0	0	13	0	0	0	0	0
1727	616	615	0	0	362	439	363	0	0	41	0	0	0	0	0
1728	686	686	0	0	398	476	394	0	0	12	0	0	0	0	0
1924	191	191	0	0	101	136	112	64	0	70	0	0	0	0	0
1925	160	160	0	0	81	123	102	79	0	64	0	0	0	0	0
1926	130	130	0	0	63	105	87	91	0	55	0	0	0	0	0
1927	109	109	0	0	47	97	81	97	0	50	0	0	0	0	0
1928	106	106	0	0	39	84	69	107	0	43	0	0	0	0	0
mean	319	319	0	0	186	229	189	56	0	57	0	0	0	0	0
S.D.	201	201	0	0	128	127	105	56	0	35	0	0	0	0	0

Table D1 Muscle forces (Newtons) encountered at maximum joint force, during the vertical power grip activity.

trial	mcla	mclp	lcl	jlat	jmed	jr	jw	θ_{lat}	θ_{med}	α	β
909	0	0	0	196	278	20	640	56.5	56.5	4.2	-1.6
910	0	0	0	190	257	35	586	58.7	49.7	4.4	-1.4
911	0	16	0	174	248	0	556	59.0	46.2	4.2	-1.1
912	0	0	0	197	260	27	611	58.6	49.1	4.1	-1.2
913	0	0	0	207	275	15	634	57.8	49.7	4.3	-1.2
1209	0	72	0	148	282	0	690	56.8	51.9	4.0	-2.0
1210	0	0	0	279	367	163	1002	60.2	59.5	3.8	-30.0
1211	0	47	0	163	281	0	576	60.4	52.8	4.5	-30.0
1212	0	0	0	237	321	16	793	60.8	57.2	3.7	-2.0
1213	0	70	0	115	251	0	442	56.6	44.1	5.1	-30.0
1409	0	0	0	502	634	315	2305	58.5	60.4	3.1	-2.9
1410	0	0	0	478	594	298	2211	58.3	58.9	3.0	-2.9
1411	0	0	0	377	469	200	1565	60.2	58.3	3.1	-2.5
1412	0	0	0	406	509	205	1778	57.7	58.6	3.0	-2.8
1413	0	0	0	376	493	127	1563	57.9	59.8	3.2	-2.7
1610	0	91	0	167	329	0	726	64.3	21.6	4.0	-1.6
1611	0	42	0	187	283	0	668	58.1	43.7	4.0	-1.4
1612	0	57	0	196	320	0	761	60.7	27.1	3.9	-1.7
1613	0	98	0	135	306	0	617	65.1	12.9	4.2	-1.2
1810	0	0	0	355	465	68	1429	55.5	53.2	3.4	-2.7
1811	0	0	0	341	445	179	1462	58.0	61.7	3.5	-2.6
1812	0	0	0	358	460	213	1582	57.8	61.4	3.4	-2.7
1024	0	82	0	119	273	0	515	62.0	12.9	4.0	-0.9
1025	0	0	0	306	381	62	969	58.2	39.1	-30.0	-2.2
1026	0	0	0	252	327	57	880	56.9	53.7	3.3	-1.9
1027	0	0	0	307	400	18	1107	55.4	45.6	3.4	-2.3
1028	0	0	0	349	430	120	1411	57.0	45.8	3.1	-2.6
1524	0	0	0	446	575	232	2006	55.9	61.0	3.2	-2.7
1525	0	0	0	364	464	228	1626	55.7	62.1	3.2	-2.5
1526	0	0	0	264	358	77	1021	53.6	62.5	3.4	-2.0
1527	0	0	0	333	437	152	1430	55.9	62.7	3.3	-2.6
1528	0	0	0	305	394	159	1318	55.1	62.2	3.2	-2.5
1724	0	0	0	381	459	345	1694	58.3	61.2	3.4	-30.0
1725	0	0	0	619	739	578	2943	59.7	60.9	3.1	-30.0
1726	0	0	0	675	830	514	3127	58.2	60.5	3.2	-30.0
1727	0	0	0	504	640	302	2200	58.8	61.0	3.3	-30.0
1728	0	0	0	546	698	316	2425	58.8	60.8	3.3	-30.0
1924	0	0	0	215	292	26	727	54.6	55.2	3.8	-1.5
1925	0	0	0	199	276	3	621	56.8	53.7	4.0	-1.3
1926	0	13	0	165	241	0	508	59.3	46.8	4.1	-0.8
1927	0	52	0	121	225	0	435	60.3	36.6	4.5	-0.4
1928	0	62	0	101	216	0	395	54.9	33.5	4.6	-0.1
mean	0	17	0	294	400	121	1204	58	51	3	-7
S.D.	0	30	0	143	151	146	711	2	13	5	11

Table D2 Ligament and joint forces (Newtons), and joint force angles (degrees), encountered at maximum joint force, during the vertical power grip activity.

trial	fpl	fds	fdp	fcr	fcu	ecu	ecrb	ecrl	bic	bra	brd	prt	tri	anc	prq	sup
914	256	606	552	0	0	684	583	420	0	0	33	0	0	0	0	0
915	255	485	433	0	0	631	538	325	0	0	66	0	0	0	0	0
916	236	427	383	0	0	578	493	310	0	0	86	0	0	0	0	0
917	171	407	369	0	0	507	432	322	0	0	64	0	0	0	0	0
1214	251	431	383	0	0	596	508	192	0	0	48	0	0	0	0	0
1215	235	457	410	0	0	601	512	195	0	0	14	0	0	0	0	0
1216	220	384	346	0	0	520	443	162	0	0	44	0	0	0	0	0
1217	219	444	397	0	0	551	470	221	0	0	38	0	0	0	0	0
1218	211	378	337	0	0	526	449	175	0	0	42	0	0	0	0	0
1414	275	426	360	0	0	537	458	181	65	0	0	0	0	0	0	0
1416	303	467	394	0	0	578	493	169	112	0	0	0	0	0	0	0
1615	238	305	261	0	0	470	401	223	51	0	0	0	0	0	0	0
1616	202	303	266	0	0	447	382	245	0	0	7	0	0	0	0	0
1617	242	289	253	0	0	478	408	209	0	0	29	0	0	0	0	0
1618	299	382	334	0	0	609	519	259	0	0	39	0	0	0	0	0
1814	189	449	406	0	0	562	480	268	0	0	0	0	0	0	0	0
1815	175	466	429	0	0	566	483	307	0	0	0	0	31	0	0	0
1816	184	446	399	0	0	539	460	267	0	0	0	0	44	0	0	0
1817	181	398	357	0	0	504	430	245	0	0	0	0	43	0	0	0
1818	158	401	360	0	0	483	412	255	0	0	0	0	44	0	0	0
1019	122	411	384	0	0	504	430	317	0	0	0	0	74	0	0	0
1020	232	540	510	0	0	1129	963	631	0	0	0	0	156	0	0	0
1022	222	441	432	0	0	601	513	295	34	0	0	0	0	0	0	0
1023	148	522	509	0	0	563	499	413	4	0	0	0	0	0	0	0
1319	209	318	276	0	0	488	416	241	0	0	27	0	0	0	0	0
1320	229	317	274	0	0	499	426	206	0	0	79	0	0	0	0	0
1321	185	324	285	0	0	459	391	269	0	0	110	0	0	0	0	0
1323	251	319	269	0	0	512	436	210	0	0	33	0	0	0	0	0
1519	211	543	498	0	0	607	524	433	0	0	68	0	0	0	0	0
1520	189	441	391	0	0	554	473	364	0	0	92	0	0	0	0	0
1521	232	537	482	0	0	628	536	432	0	0	102	0	0	0	0	0
1522	158	381	343	0	0	506	432	322	0	0	87	0	0	0	0	0
1523	166	406	367	0	0	558	476	364	0	0	87	0	0	0	0	0
1719	178	312	270	0	0	546	466	276	0	0	8	0	0	0	0	0
1720	226	318	272	0	0	567	483	238	0	0	85	0	0	0	0	0
1721	242	328	277	0	0	554	473	219	0	0	56	0	0	0	0	0
1722	238	353	306	0	0	539	460	223	0	0	17	0	0	0	0	0
1723	152	349	317	0	0	509	434	284	0	0	35	0	0	0	0	0
1919	221	462	400	0	0	575	490	237	0	0	101	0	0	0	0	0
1920	227	512	458	0	0	617	526	260	0	0	103	0	0	0	0	0
1921	234	460	411	0	0	591	504	259	0	0	109	0	0	0	0	0
1922	192	320	290	0	0	462	394	230	0	0	136	0	0	0	0	0
1923	178	387	341	0	0	493	420	218	0	0	87	0	0	0	0	0
mean	213	411	367	0	0	559	477	277	6	0	45	0	9	0	0	0
S.D.	40	77	77	0	0	104	89	90	21	0	41	0	28	0	0	0

Table D3 Muscle forces (Newtons) encountered at maximum joint force, during the chuck grip activity.

trial	mcla	mclp	lcl	jlat	jmed	jr	jw	θ_{lat}	θ_{med}	α	β
914	0	0	0	497	573	726	2850	53.6	57.5	3.2	-30.0
915	0	0	0	425	496	630	2451	50.8	57.3	3.3	-30.0
916	0	0	0	384	440	619	2231	51.7	57.9	3.4	-30.0
917	0	0	0	370	434	534	2027	54.3	58.9	3.4	-30.0
1214	0	0	0	317	363	625	2171	55.8	62.2	3.2	-30.0
1215	0	0	0	321	370	613	2216	57.6	62.5	3.2	-30.0
1216	0	0	0	280	340	520	1904	53.8	66.2	3.3	-30.0
1217	0	0	0	317	367	605	1453	58.5	64.1	60.0	60.0
1218	0	0	0	292	349	516	1312	55.1	62.4	60.0	60.0
1414	0	0	0	386	483	345	2048	37.6	53.0	3.3	-30.0
1416	0	0	0	404	496	422	2203	41.5	47.1	3.3	-30.0
1615	0	0	0	316	391	346	1739	45.6	50.8	3.5	-30.0
1616	0	0	0	298	372	357	1690	49.0	57.1	3.5	-30.0
1617	0	0	0	290	356	384	1722	45.6	55.6	3.5	-30.0
1618	0	0	0	331	373	619	2207	48.8	55.6	3.3	-30.0
1814	0	0	0	363	449	504	2158	47.9	59.6	3.3	-30.0
1815	0	0	0	393	484	522	2225	44.8	59.1	3.3	-30.0
1816	0	0	0	387	480	449	2101	40.6	58.2	3.3	-30.0
1817	0	0	0	344	429	438	1936	41.0	59.3	3.4	-30.0
1818	0	0	0	347	437	418	1895	42.0	59.6	3.4	-30.0
1019	0	0	0	461	550	293	1994	37.4	55.5	3.4	-30.0
1020	0	0	0	655	572	1238	3687	23.7	49.1	3.2	-30.0
1022	0	0	0	433	515	447	2300	42.1	53.2	3.3	-30.0
1023	0	0	0	507	622	428	2442	49.3	58.0	3.3	-30.0
1319	0	0	0	280	329	492	1791	49.7	55.2	3.4	-30.0
1320	0	0	0	283	336	508	1790	51.1	57.0	3.5	-30.0
1321	0	0	0	300	346	547	1756	51.7	62.4	3.6	-30.0
1323	0	0	0	264	294	553	1839	43.0	58.0	3.2	-30.0
1519	0	0	0	406	447	845	2586	53.6	65.3	3.3	-30.0
1520	0	0	0	341	371	780	2215	51.4	66.0	3.3	-30.0
1521	0	0	0	407	440	902	2615	53.5	66.6	3.3	-30.0
1522	0	0	0	317	354	662	1968	50.5	64.1	3.4	-30.0
1523	0	0	0	316	338	802	2147	48.9	67.7	3.3	-30.0
1719	0	0	0	256	272	639	1883	49.3	54.7	3.3	-30.0
1720	0	0	0	272	296	671	1935	45.8	59.4	3.4	-30.0
1721	0	0	0	267	297	623	1923	46.7	57.9	3.4	-30.0
1722	0	0	0	288	344	532	1945	44.5	58.1	3.3	-30.0
1723	0	0	0	277	309	620	1878	54.8	61.3	3.4	-30.0
1919	0	0	0	356	419	649	2190	49.5	65.2	3.3	-30.0
1920	0	0	0	384	431	725	2388	55.8	63.9	3.3	-30.0
1921	0	0	0	349	391	727	2262	52.0	64.6	3.3	-30.0
1922	0	0	0	267	291	628	1737	51.9	67.5	3.5	-30.0
1923	0	0	0	312	369	545	1871	51.1	64.6	3.4	-30.0
mean	0	0	0	350	405	583	2086	48.4	59.5	6.0	-25.8
S.D.	0	0	0	79	84	172	391	6.5	4.9	12.1	19.2

Table D4 Ligament and joint forces (Newtons), and joint force angles (degrees), encountered at maximum joint force, during the chuck grip activity.

trial	fds	fdp	fcr	fcu	ecu	ecrb	ecrl	bic	bra	brd	prt	tri	anc	prq	sup
920	718	718	0	0	292	734	607	22	0	380	0	0	0	0	0
921	626	626	0	0	243	683	566	46	0	354	0	0	0	0	0
922	650	650	0	0	233	690	571	26	0	357	0	0	0	0	0
923	633	633	0	0	219	660	546	18	0	341	0	0	0	0	0
1221	569	568	0	0	295	661	547	0	0	190	0	0	0	0	0
1223	608	608	0	0	282	679	562	0	0	147	0	0	0	0	0
1420	593	593	0	0	103	522	432	0	0	207	0	0	0	0	0
1421	819	819	0	0	249	663	549	0	0	176	0	0	0	0	0
1422	772	772	0	0	201	635	525	0	0	200	0	0	0	0	0
1423	819	819	0	0	185	661	547	0	0	221	0	0	0	0	0
1622	350	350	49	0	0	444	368	130	0	230	0	0	0	0	0
1623	330	330	108	0	0	443	366	117	0	229	0	0	0	0	0
1819	327	327	0	0	117	465	385	121	0	241	0	0	0	0	0
1820	369	369	0	0	182	521	431	95	0	270	0	0	0	0	0
1821	360	360	0	0	188	518	429	84	0	268	0	0	0	0	0
1822	327	327	0	0	109	484	401	132	0	250	0	0	0	0	0
1823	370	370	0	0	159	516	427	60	0	267	0	0	0	0	0
1014	487	487	2	0	0	497	412	143	0	257	0	0	0	0	0
1015	483	483	53	0	0	492	407	171	0	255	0	0	0	0	0
1016	429	429	88	0	0	455	376	206	0	235	0	0	0	0	0
1017	402	401	172	0	0	433	358	233	0	224	0	0	0	0	0
1018	379	378	209	0	0	413	342	203	0	214	0	0	0	0	0
1314	410	411	0	0	219	628	520	37	0	325	0	0	0	0	0
1315	511	511	0	0	327	741	613	65	0	383	0	0	0	0	0
1316	572	571	0	0	273	751	621	0	0	376	0	0	0	0	0
1317	201	201	0	0	190	497	412	266	0	257	0	0	0	0	0
1318	324	323	0	0	84	510	422	108	0	264	0	0	0	0	0
1514	203	203	0	0	114	393	325	321	0	203	0	0	0	0	0
1515	248	248	0	0	163	428	355	217	0	222	0	0	0	0	0
1516	305	305	0	0	200	507	419	140	0	262	0	0	0	0	0
1517	322	321	0	0	194	491	406	144	0	254	0	0	0	0	0
1518	287	287	0	0	133	457	378	189	0	236	0	0	0	0	0
1714	667	666	0	0	521	800	662	0	0	313	0	0	0	0	0
1715	631	631	0	0	481	838	694	0	0	391	0	0	0	0	0
1716	611	610	0	0	514	850	703	0	0	335	0	0	0	0	0
1717	651	651	0	0	533	841	696	0	0	347	0	0	0	0	0
1718	682	682	0	0	521	854	706	0	0	382	0	0	0	0	0
1914	390	391	72	0	0	418	346	251	0	216	0	0	0	0	0
1915	423	423	0	0	47	442	366	129	0	229	0	0	0	0	0
1916	433	433	27	0	0	454	375	239	0	235	0	0	0	0	0
1917	388	388	82	0	0	439	363	179	0	227	0	0	0	0	0
1918	536	536	0	0	125	563	466	125	0	291	0	0	0	0	0
mean	481	481	21	0	183	576	476	100	0	268	0	0	0	0	0
S.D.	167	167	48	0	158	140	116	92	0	64	0	0	0	0	0

Table D5 Muscle forces (Newtons) encountered at maximum joint force, during the horizontal power grip activity.

trial	mcla	mclp	lcl	jlat	jmed	jr	jw	θ_{lat}	θ_{med}	α	β
920	0	0	0	689	801	593	3034	60.1	64.6	3.2	-2.8
921	0	0	0	694	817	381	2708	62.8	61.9	3.2	-2.7
922	0	0	0	715	841	346	2759	63.2	61.8	3.2	-2.7
923	0	0	0	693	822	305	2655	63.2	61.9	3.2	-2.7
1221	0	0	0	645	814	199	2601	59.6	64.7	3.3	-2.9
1223	0	0	0	701	983	0	2485	53.3	67.6	3.4	-30.0
1420	0	350	0	424	808	0	2212	74.0	37.5	3.1	-2.5
1421	0	0	0	828	1044	15	3066	64.6	61.1	3.0	-2.9
1422	0	154	0	703	993	0	2875	67.1	52.7	3.0	-2.7
1423	0	177	0	718	1034	0	2994	66.1	52.9	3.0	-2.8
1622	0	164	0	396	644	0	1531	62.7	41.7	3.4	-2.0
1623	0	274	0	345	694	0	1548	67.6	31.7	3.4	-1.9
1819	0	0	0	553	657	13	1587	68.7	52.8	3.3	-2.2
1820	0	0	0	559	653	173	1839	68.7	56.8	3.3	-2.4
1821	0	0	0	516	641	201	1822	60.9	62.3	3.4	-2.5
1822	0	1	0	546	692	0	1613	62.5	57.1	3.5	-2.2
1823	0	0	0	560	698	60	1809	62.1	60.7	3.4	-2.4
1014	0	300	0	403	774	0	1860	66.0	34.8	3.4	-2.1
1015	0	283	0	446	818	0	1895	67.6	33.3	3.2	-2.1
1016	0	259	0	443	804	0	1753	68.6	31.8	3.2	-2.1
1017	0	266	0	459	853	0	1510	69.4	29.2	-30.0	-2.0
1018	0	423	1	372	919	0	1475	80.0	18.5	-30.0	-2.0
1314	0	0	0	582	692	273	1977	61.8	60.5	3.6	-30.0
1315	0	0	0	578	665	691	2448	55.7	66.5	3.4	-30.0
1316	0	0	0	671	767	469	2759	62.1	62.2	3.4	-2.7
1317	0	0	0	425	508	369	1345	57.0	50.6	4.2	-30.0
1318	0	0	0	528	587	103	1632	69.2	48.4	3.6	-2.0
1514	0	0	0	295	447	441	1105	30.7	70.0	4.1	-30.0
1515	0	0	0	306	450	472	1296	37.2	73.4	3.9	-30.0
1516	0	0	0	354	471	521	1704	44.5	72.5	3.6	-2.4
1517	0	0	0	339	437	549	1701	48.4	70.1	3.5	-2.5
1518	0	0	0	348	482	400	1511	45.9	68.4	3.7	-2.3
1714	0	0	0	715	835	682	3018	57.8	64.8	3.4	-30.0
1715	0	0	0	752	918	611	2979	55.6	67.1	3.6	-30.0
1716	0	0	0	749	949	557	2994	51.7	67.9	3.6	-30.0
1717	0	0	0	711	864	737	3072	52.4	69.0	3.5	-30.0
1718	0	0	0	712	825	831	3138	55.8	67.9	3.4	-30.0
1914	0	64	0	523	740	0	1590	66.2	46.2	3.2	-2.1
1915	0	75	0	513	678	0	1673	69.8	47.5	3.1	-2.3
1916	0	0	0	551	722	43	1695	60.6	53.9	3.3	-2.1
1917	0	60	0	517	702	0	1637	65.1	46.1	3.3	-2.0
1918	0	0	0	622	771	186	2193	61.7	59.5	3.2	-2.6
mean	0	68	0	552	746	243	2121	60.7	55.5	1.8	-9.6
S.D.	0	120	0	145	159	262	624	9.4	13.6	7.2	12.3

Table D6 Ligament and joint forces (Newtons), and joint force angles (degrees), encountered at maximum joint force, during the horizontal power grip activity.

trial	fds	fdp	fcr	fcu	ecu	ecrb	ecrl	bic	bra	brd	prt	tri	anc	prq	sup
924	441	441	0	0	51	602	499	141	0	312	0	0	0	0	0
925	279	279	43	0	0	482	399	364	0	249	0	0	0	0	0
926	329	329	0	0	124	550	456	73	0	285	0	0	0	0	0
927	348	349	0	0	121	560	464	2	0	290	0	0	0	0	0
928	324	325	0	0	92	539	446	108	0	279	0	0	0	0	0
1224	378	378	0	0	312	688	569	0	0	121	0	0	0	0	0
1225	237	237	0	0	105	572	473	220	0	296	0	0	0	0	0
1226	197	197	0	0	126	554	458	268	0	287	0	0	0	0	0
1227	273	272	0	0	236	616	510	118	0	318	0	0	0	0	0
1228	257	257	0	0	246	598	495	167	0	309	0	0	0	0	0
1424	407	407	341	0	0	494	409	61	0	256	0	0	0	0	0
1425	607	607	237	0	0	519	430	0	0	183	0	0	0	0	0
1427	871	870	0	25	66	594	492	0	0	0	0	16	136	0	0
1624	107	107	316	288	0	458	379	1	0	237	0	0	0	0	0
1625	131	131	318	168	0	461	381	110	0	238	0	0	0	0	0
1626	118	118	341	180	0	494	409	67	0	256	0	0	0	0	0
1627	72	72	339	546	0	492	407	34	0	254	0	0	0	0	0
1628	82	82	361	497	0	524	434	326	0	0	0	0	0	0	0
1824	186	186	215	0	0	432	358	110	0	224	0	0	0	0	0
1825	150	149	109	0	0	381	315	44	0	197	0	0	0	0	0
1826	167	167	277	0	0	419	347	153	0	217	0	0	0	0	0
1827	124	125	171	0	0	374	309	103	0	193	0	0	0	0	0
1828	132	132	227	0	0	364	302	99	0	188	0	0	0	0	0
1009	133	133	258	0	0	417	345	72	0	216	0	0	0	0	0
1010	126	126	185	0	0	402	332	65	0	208	0	0	0	0	0
1012	243	242	0	0	175	616	510	108	0	319	0	0	0	0	0
1309	228	228	0	0	338	636	526	50	0	329	0	0	0	0	0
1311	238	238	0	0	62	573	474	227	0	296	0	0	0	0	0
1312	351	351	0	0	723	839	695	0	0	95	0	0	0	0	0
1313	454	453	0	0	416	822	680	0	0	406	0	0	0	0	0
1509	197	197	0	0	432	480	397	35	0	248	0	0	0	0	0
1510	355	355	0	0	434	815	674	41	0	421	0	0	0	0	0
1511	427	427	0	0	289	708	586	187	0	366	0	0	0	0	0
1512	224	224	0	0	138	500	414	184	0	259	0	0	0	0	0
1513	277	277	0	0	18	438	362	230	0	226	0	0	0	0	0
1710	248	248	0	0	91	492	407	210	0	254	0	0	0	0	0
1711	335	334	0	0	294	629	521	135	0	326	0	0	0	0	0
1712	539	539	0	0	331	833	690	0	0	223	0	0	0	0	0
1713	594	593	0	0	512	853	706	0	0	0	0	95	0	0	0
1909	624	624	0	0	516	856	709	0	0	0	0	67	0	0	0
1910	476	476	0	0	268	784	649	0	0	341	0	0	0	0	0
1911	179	179	368	0	0	341	442	145	0	276	0	0	0	0	0
1912	208	208	259	0	0	399	330	303	0	206	0	0	0	0	0
1913	68	68	476	126	0	0	571	0	0	217	0	0	0	0	0
Mean	284	284	123	40	142	541	472	100	0	239	0	4	3	0	0
S.D.	171	171	157	119	182	169	115	98	0	97	0	17	20	0	0

Table D7 Muscle forces (Newtons) encountered at maximum joint force, during the hook grip activity.

trial	mcla	mclp	lcl	jlat	jmed	jr	jw	θ_{lat}	θ_{med}	α	β
924	0	0	0	631	793	60	2002	63.8	58.9	3.3	-2.5
925	0	0	0	552	769	34	1448	64.3	52.8	3.4	-2.1
926	0	0	0	518	649	133	1756	61.8	63.2	3.5	-2.5
927	0	0	0	565	691	22	1811	64.4	62.7	3.4	-2.5
928	0	0	0	517	654	102	1694	60.1	60.9	3.5	-2.4
1224	0	0	0	587	811	54	2109	53.3	69.3	3.7	-30.0
1225	0	0	0	504	688	150	1457	51.3	63.0	3.9	-30.0
1226	0	0	0	462	632	244	1375	46.5	63.1	4.1	-30.0
1227	0	0	0	485	656	366	1723	44.8	71.8	3.9	-30.0
1228	0	0	0	456	602	446	1673	46.1	69.4	3.9	-30.0
1424	0	511	180	458	1059	0	1758	72.8	27.8	-30.0	-2.3
1425	0	537	211	467	1055	0	2057	72.9	28.7	-30.0	-2.6
1427	0	614	131	506	1083	0	2493	80.0	26.0	-30.0	-2.9
1624	0	474	115	259	842	0	1443	56.1	26.3	3.4	-1.8
1625	0	411	0	292	848	0	1484	67.8	25.3	3.4	-1.9
1626	0	374	0	374	934	0	1686	64.5	30.1	3.3	-2.0
1627	0	346	0	373	919	0	1654	60.0	32.1	3.2	-1.9
1628	0	401	0	402	1154	0	1679	61.1	18.7	-30.0	-2.2
1824	0	447	199	360	882	0	1173	78.6	16.6	-30.0	-1.4
1825	0	351	178	282	650	0	932	80.0	18.7	-30.0	-1.3
1826	0	434	226	404	941	0	1173	76.6	17.1	-30.0	-1.3
1827	0	387	183	280	738	0	1082	72.6	15.4	3.5	-1.1
1828	0	377	189	296	768	0	1142	65.9	15.6	3.5	-1.2
1009	0	431	178	273	783	0	1263	54.3	23.2	3.5	-1.5
1010	0	415	138	214	689	0	1148	54.4	23.4	3.6	-1.4
1012	0	0	0	569	746	77	1626	46.3	64.2	4.1	-30.0
1309	0	0	0	535	651	328	1784	45.1	64.2	4.0	-30.0
1311	0	45	0	543	723	0	1564	57.0	50.4	4.0	-1.9
1312	0	0	0	606	798	590	2703	37.9	75.6	3.7	-30.0
1313	0	0	0	568	667	787	2565	52.9	73.4	3.5	-30.0
1509	0	0	0	360	362	584	1526	66.0	60.6	4.0	-30.0
1510	0	0	0	564	638	767	2385	53.6	69.5	3.6	-30.0
1511	0	0	0	472	587	823	2208	50.3	71.0	3.5	-30.0
1512	0	0	0	378	520	337	1472	44.0	69.1	3.8	-2.2
1513	0	115	0	481	652	0	1341	80.0	34.0	3.3	-1.8
1710	0	0	0	392	551	279	1456	45.9	67.0	3.7	-2.2
1711	0	0	0	399	487	750	1912	48.1	73.5	3.5	-30.0
1712	0	0	0	725	946	196	2667	56.7	66.2	3.5	-30.0
1713	0	0	0	703	937	336	2974	48.5	67.1	3.4	-30.0
1909	0	0	0	718	947	322	3040	51.3	66.1	3.4	-30.0
1910	0	0	0	715	902	200	2631	59.0	64.5	3.6	-2.5
1911	0	341	0	415	897	0	1486	71.7	33.4	3.2	-1.7
1912	0	199	136	582	903	0	1198	80.0	28.1	-30.0	-1.7
1913	0	204	38	620	935	0	1126	80.0	32.7	-30.0	-1.6
Mean	0	182	46	467	781	174	1737	60.7	47.1	-3.0	-11.7
S.D.	0	214	78	134	169	249	525	12.0	21.1	13.5	13.5

Table D8 Ligament and joint forces (Newtons), and joint force angles (degrees), encountered at maximum joint force, during the hook grip activity.

APPENDIX E

This appendix contains detail drawings for the manufacture of the handheld and telemetry force measuring knives.

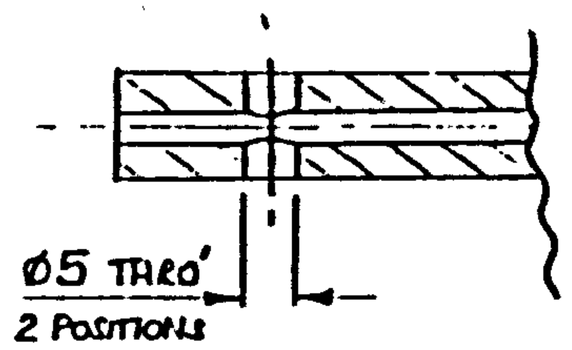

PARTIAL SECTION D-D

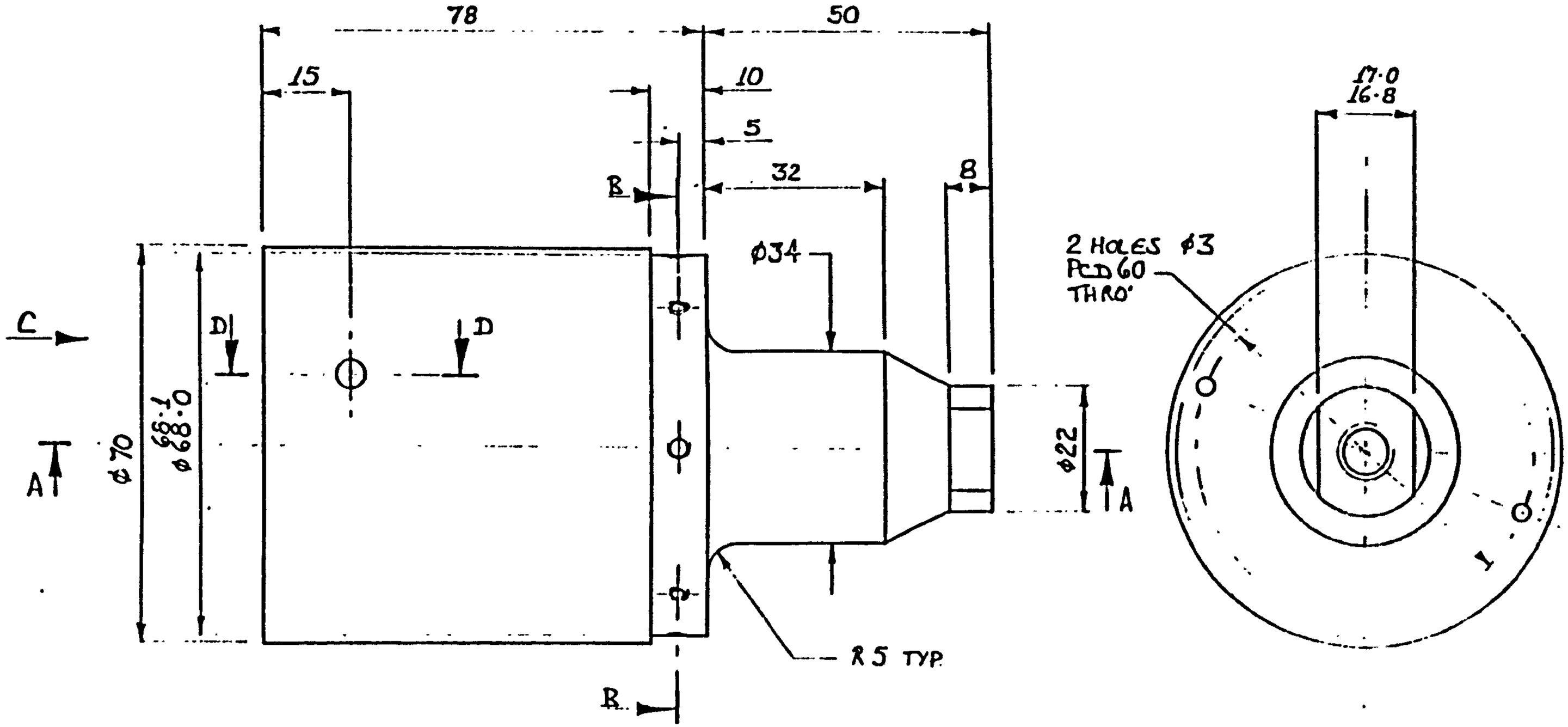

130 A

E.K.J. Chadwick 04/02/97 TELEMETRY KNIFE BODY MAT'L: HE30 SCALE 1:1

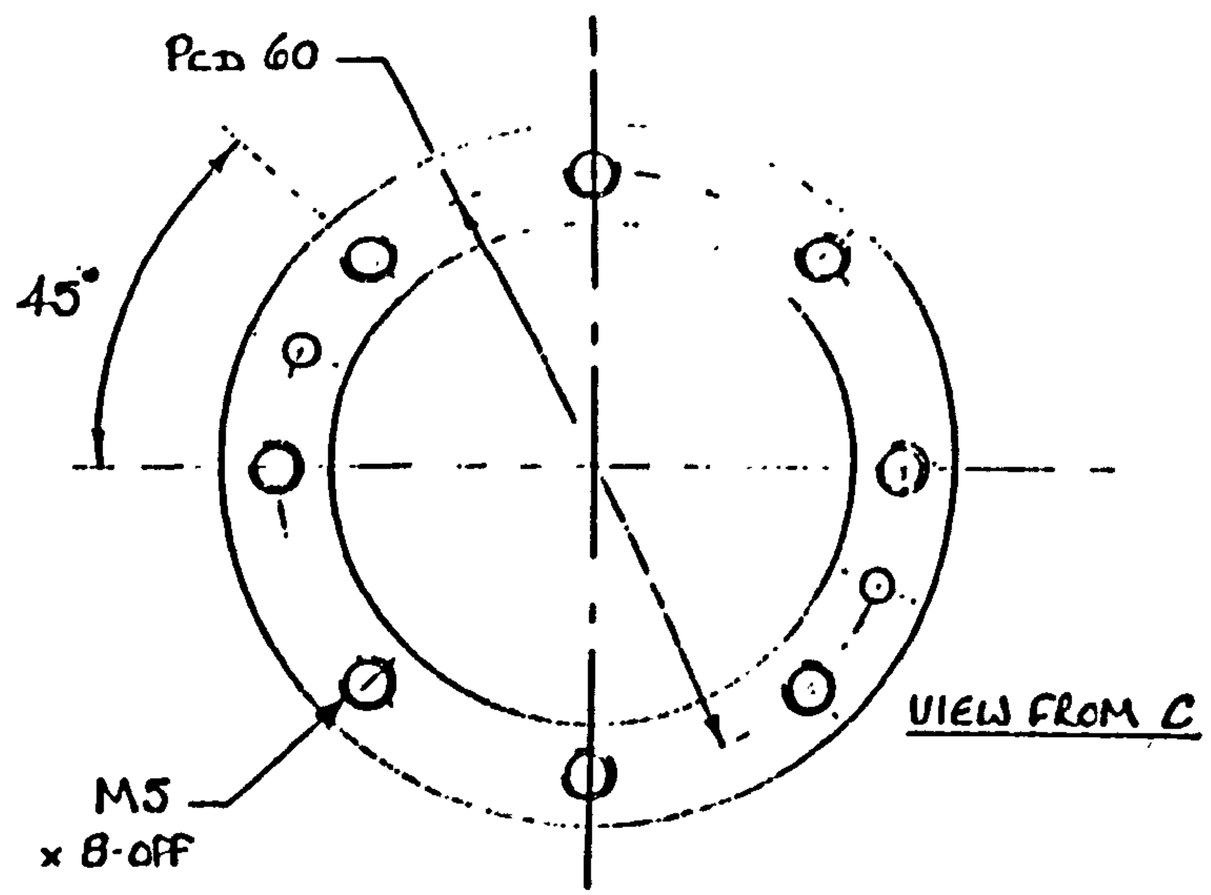

VIEW FROM C

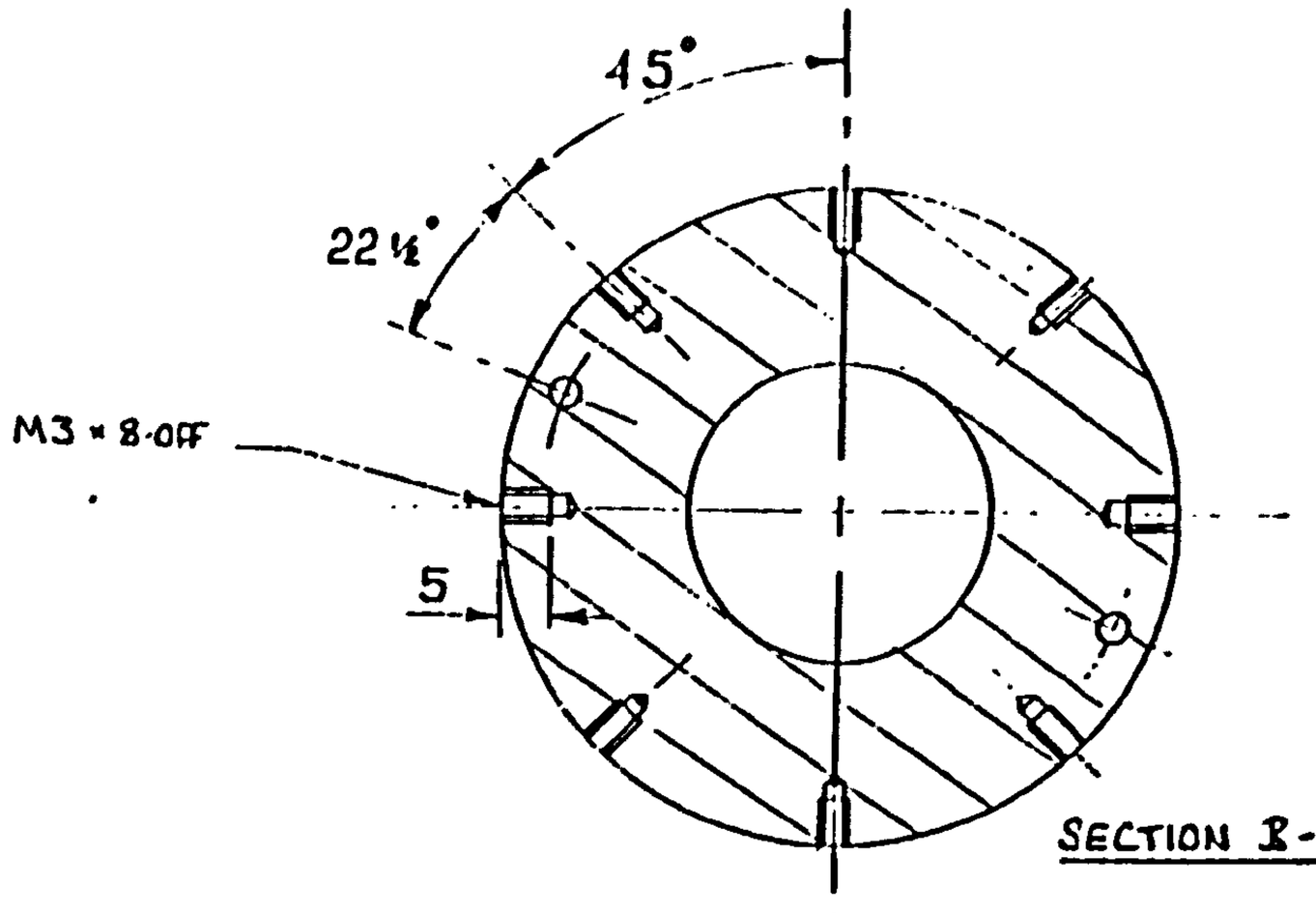

SECTION B-B

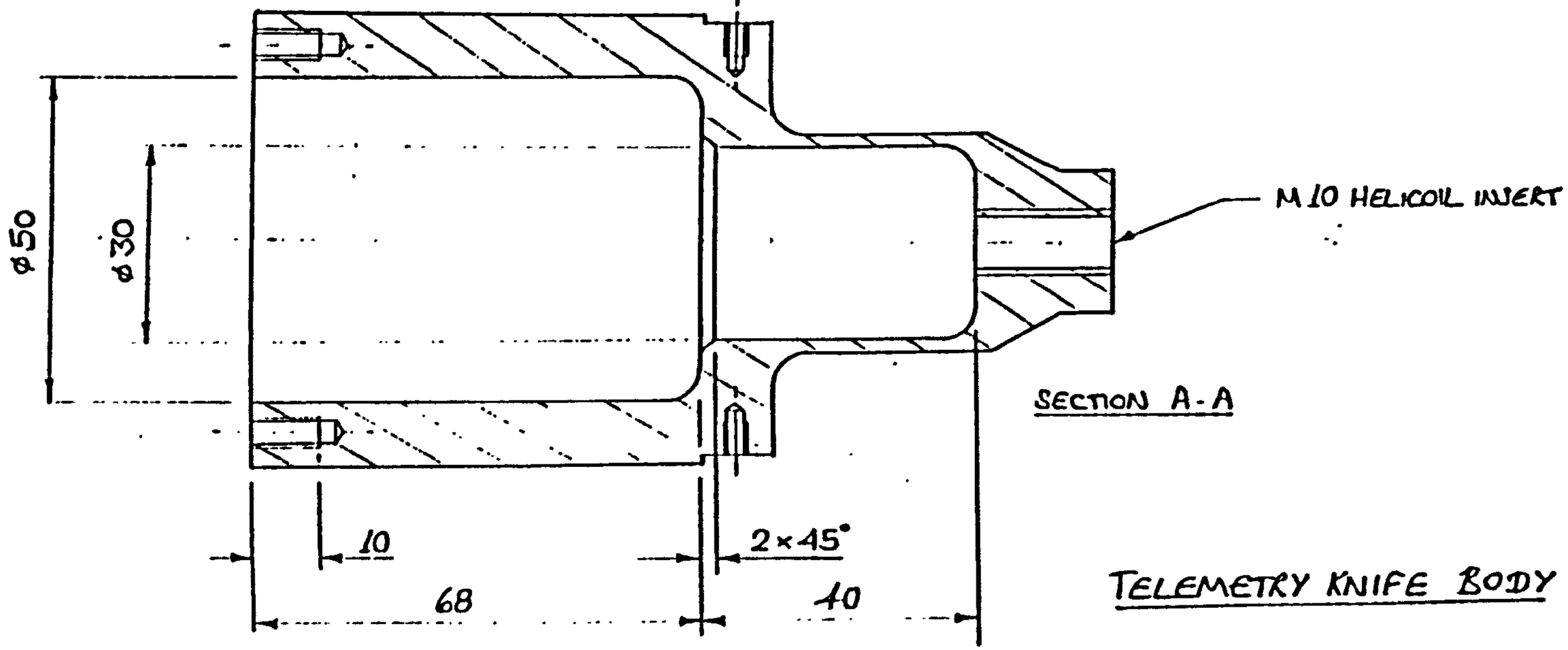

SECTION A-A

TELEMETRY KNIFE BODY

130

131 A

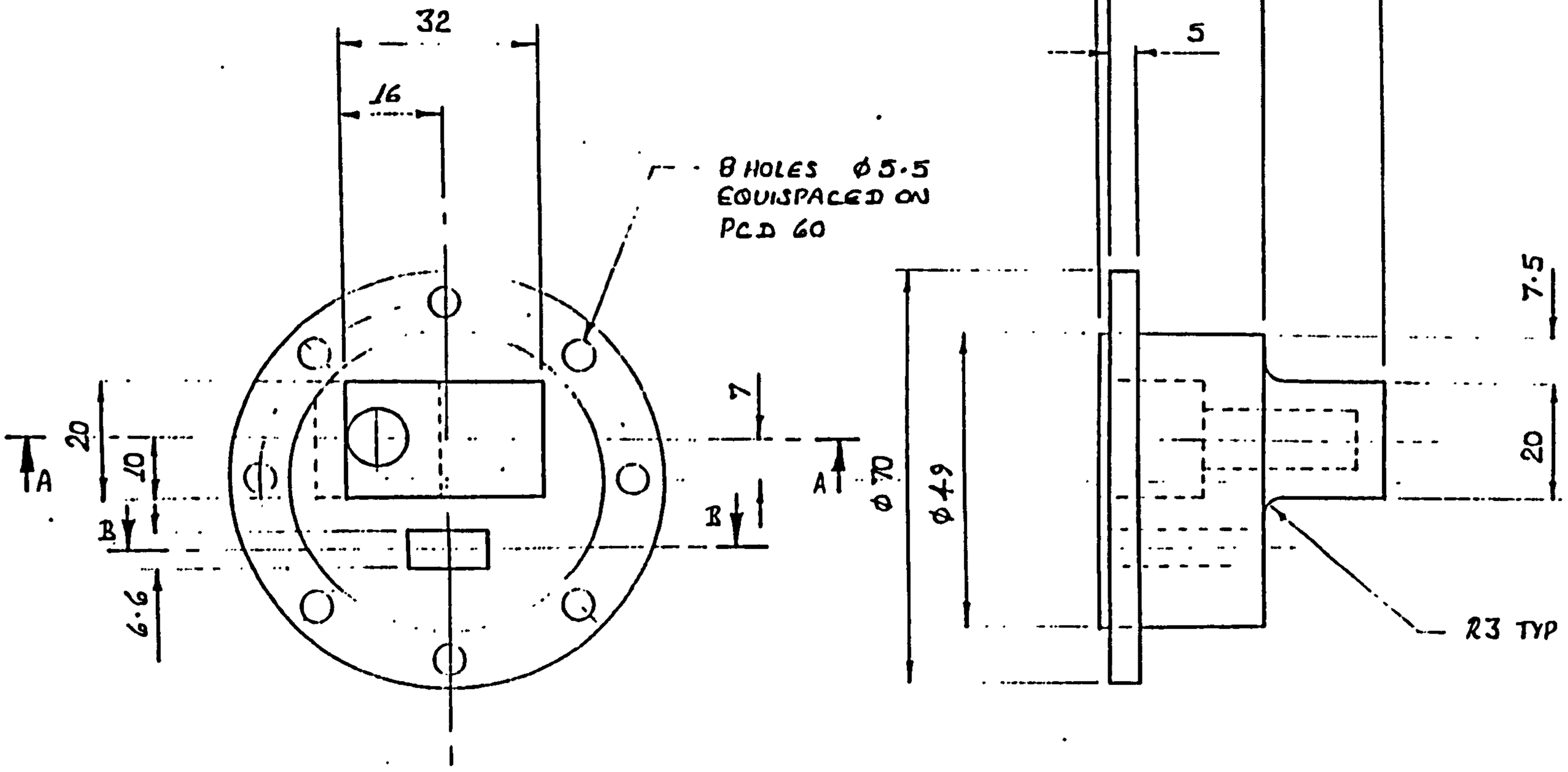

E.K. Chadwick 24/2/97 END CAP MATL: ACETATE SCALE 1:1

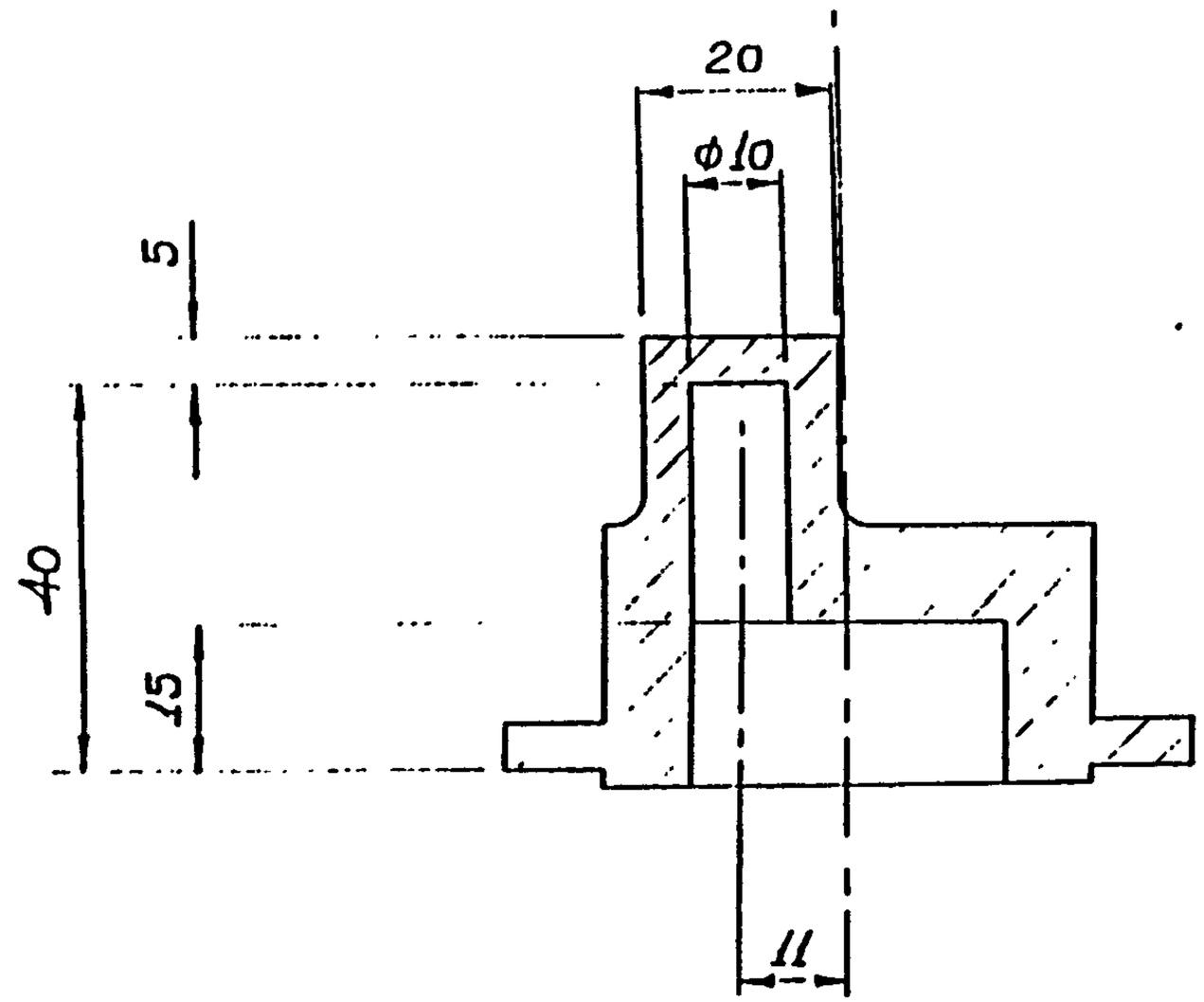

SECTION AA

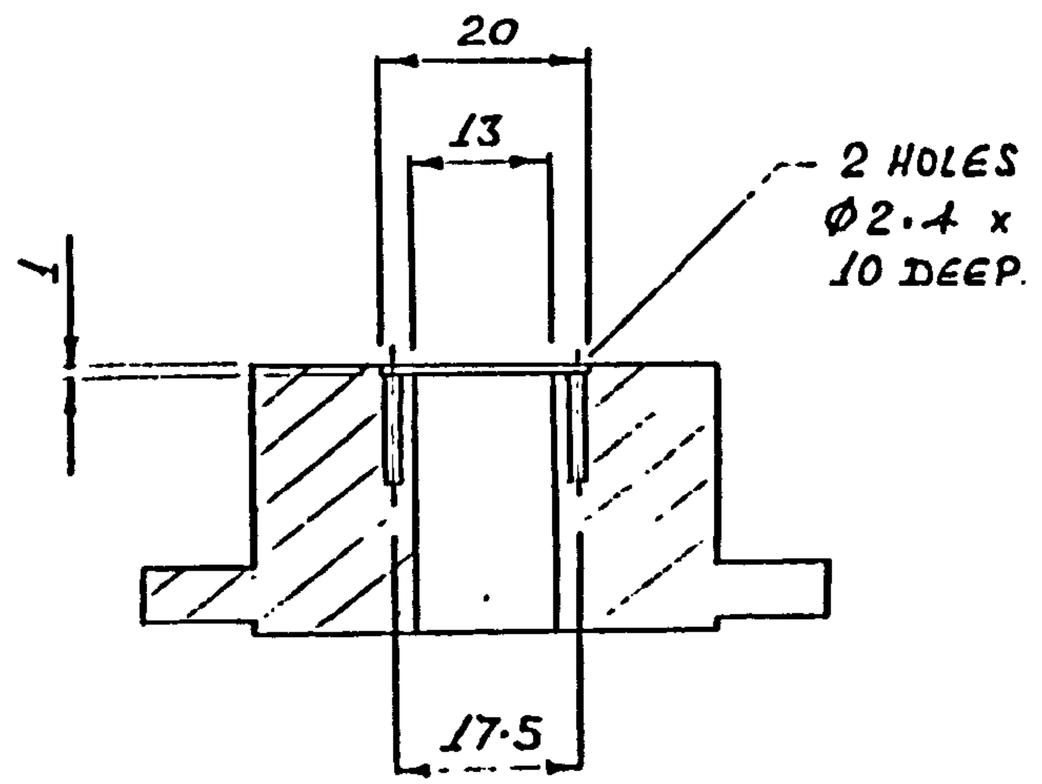

SECTION B-B

END CAP

132A

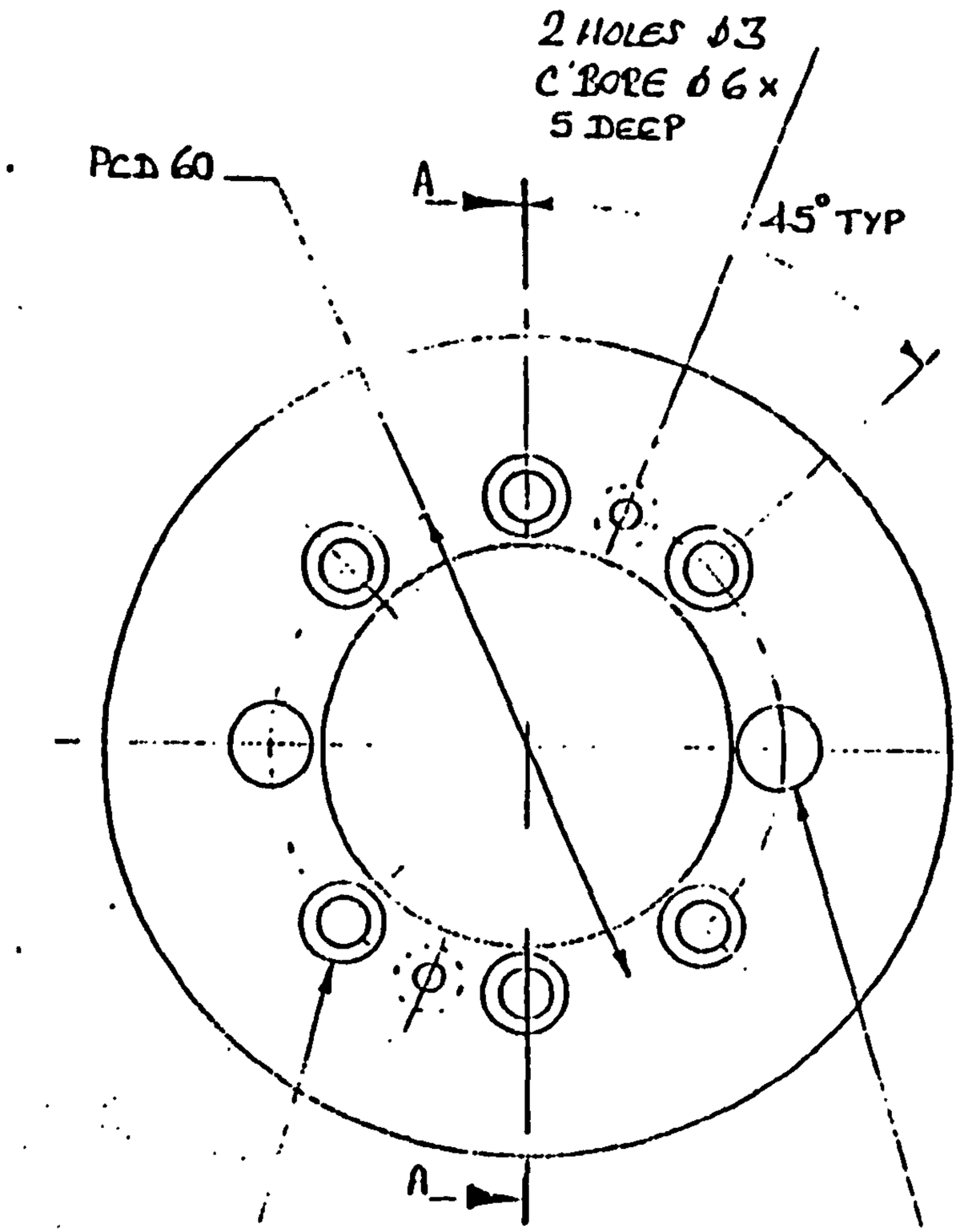

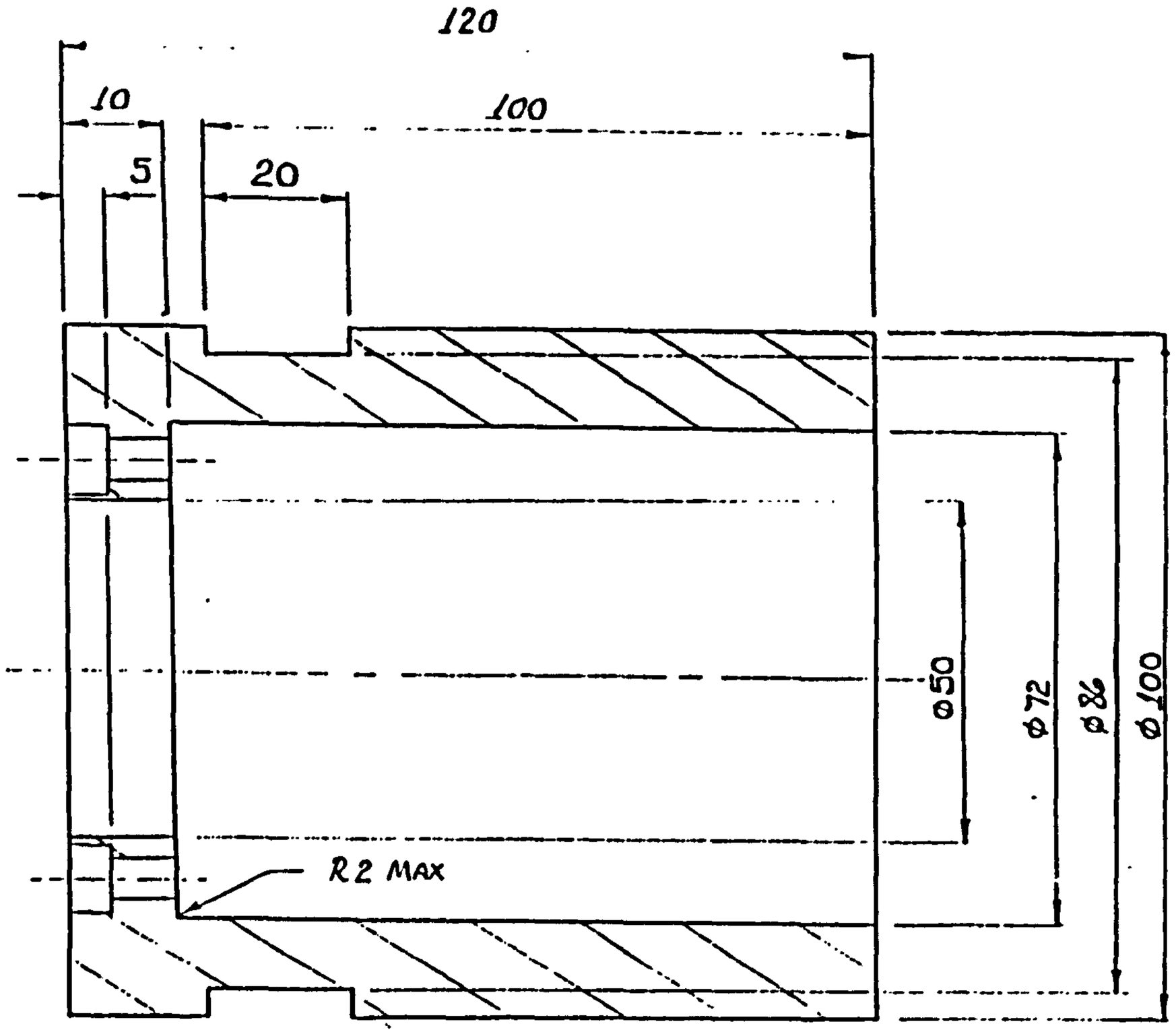

SECTION A-A

EKJ. Chadwick 7/2/97 SLEEVE MAT'L: VARIOUS SCALE 1:1

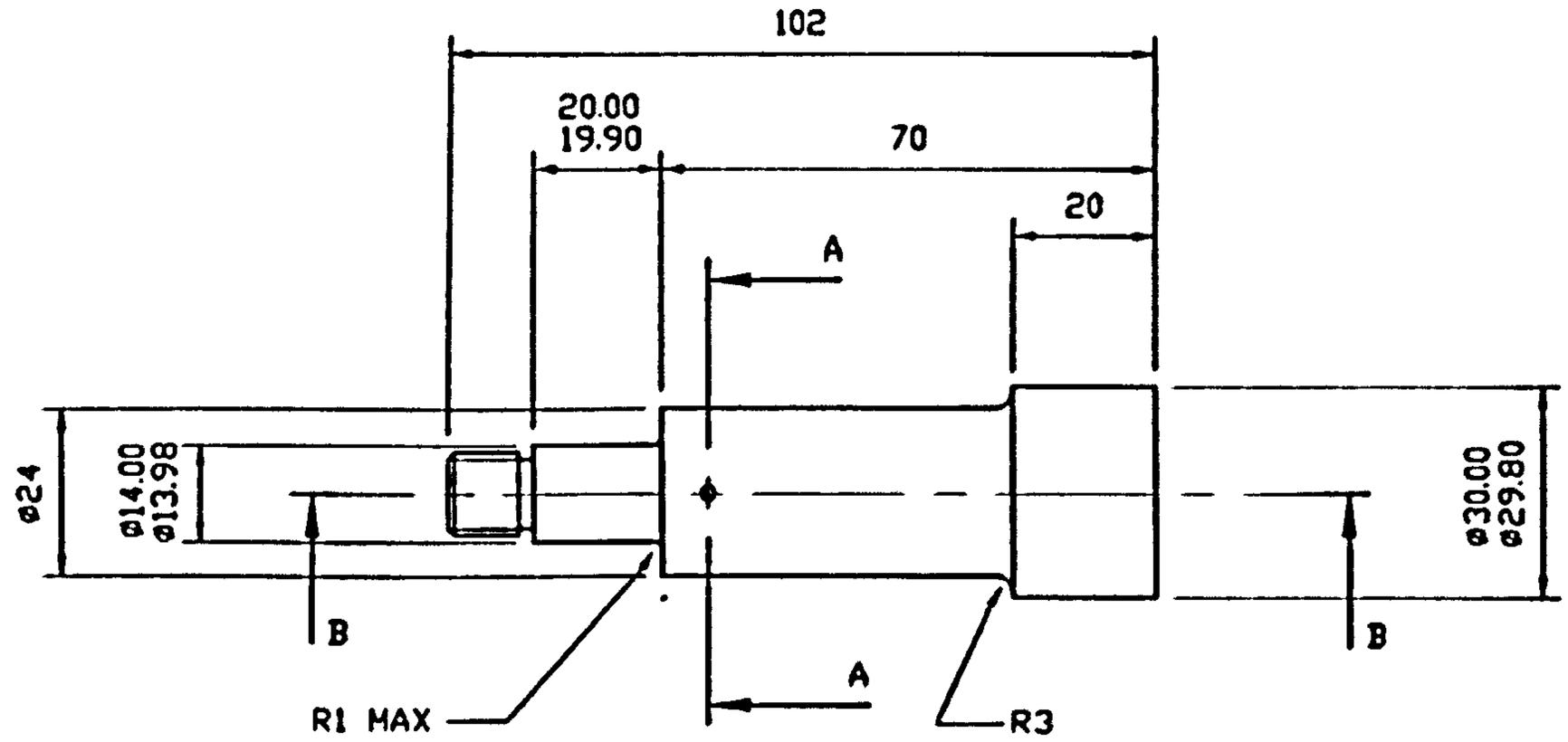

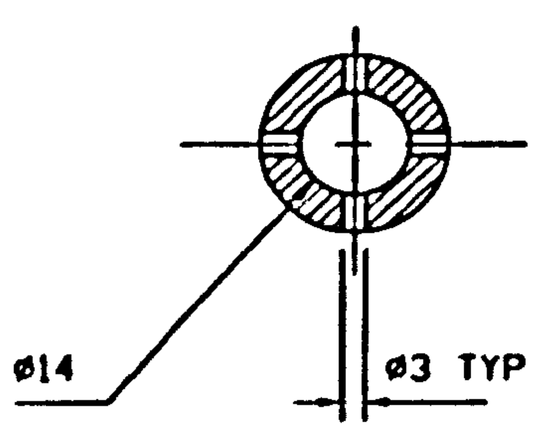

SECTION A-A

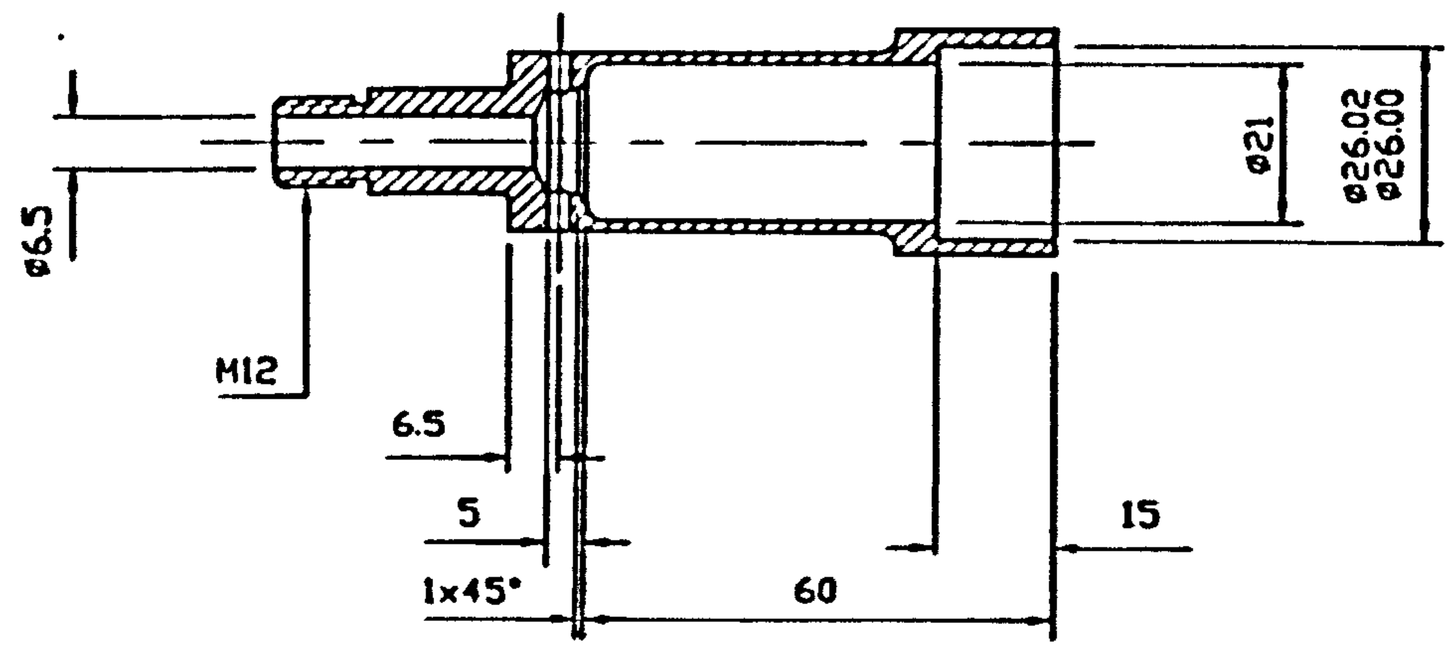

SECTION B-B

NOTES :

ALL DIMS IN MM.
REMOVE ALL BURRS AND SHARP EDGES.
TOLERANCE : LINEAR ±0.25
ANGLES ±2°
UNLESS STATED.

	⊕◁	MAT'L : ALUMINIUM ALLOY HE30 WP	KNIFE HANDLE : INNER	E.K.J. CHADWICK
		QUANTITY : 1 OFF	SCALE : NOT TO SCALE	DRG NO. 1

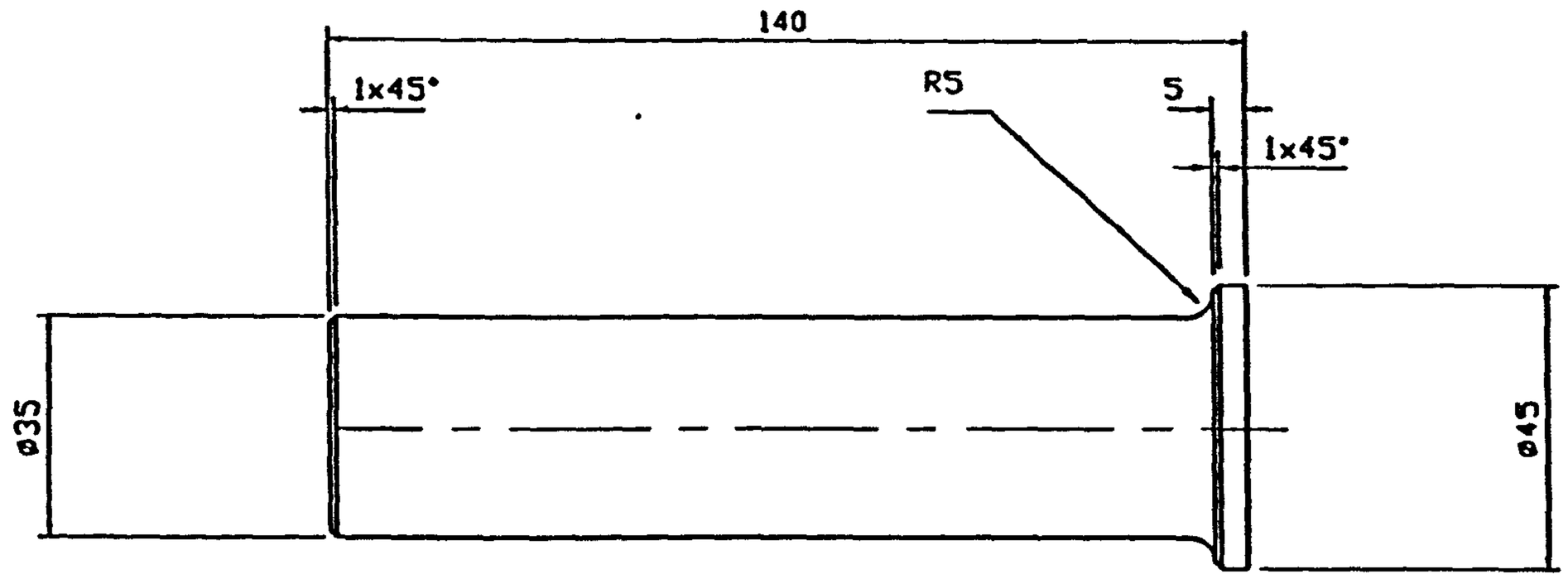

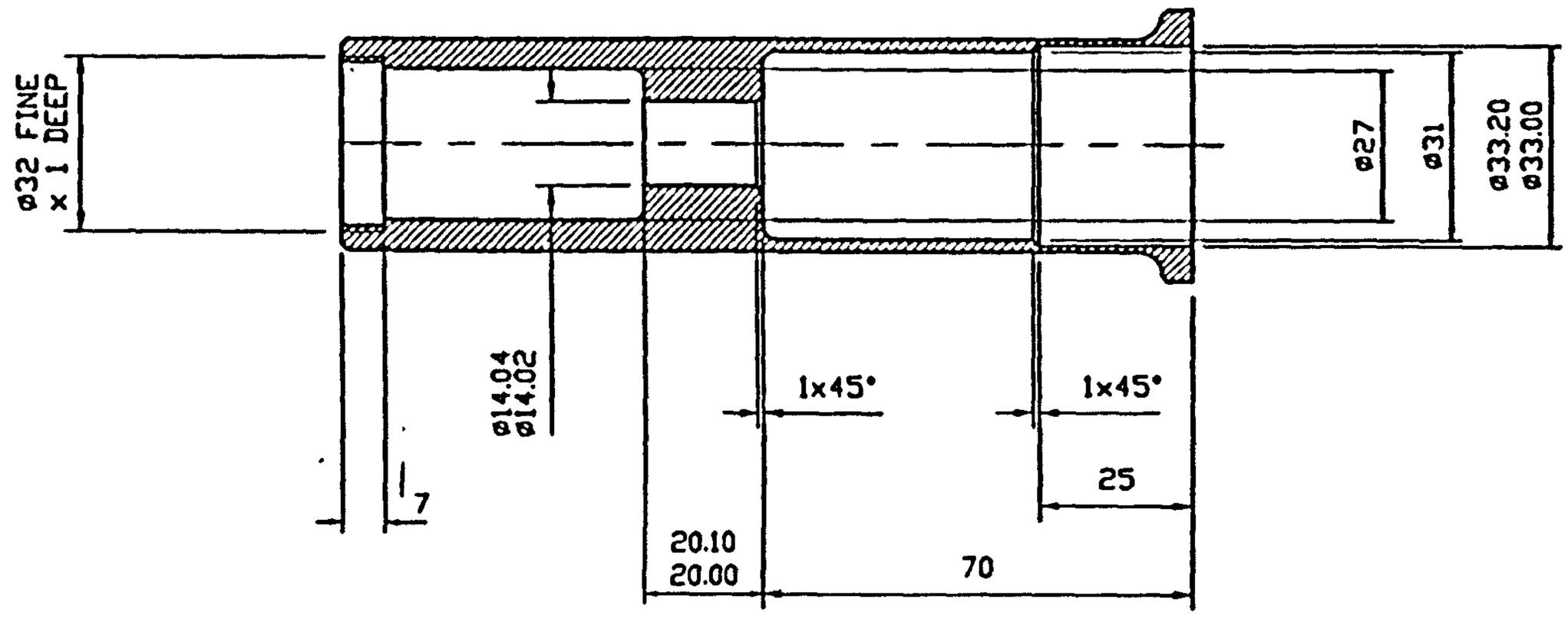

NOTES :

ALL DIMS IN MM.
REMOVE ALL BURRS AND SHARP EDGES.
TOLERANCE : LINEAR ±0.25
ANGLES ±2°
UNLESS STATED.

	MAT'L : ALUMINIUM ALLOY HE30 WP	KNIFE HANDLE : OUTER	E.K.J. CHADWICK
	QUANTITY : 1 OFF	SCALE : NOT TO SCALE	DRG NO. 2